

# On the Thermal Budget of Pahoehoe Lava Flows

Thesis by  
László P. Keszthelyi

In Partial Fulfillment of the Requirements  
for the Degree of  
Doctor of Philosophy

California Institute of Technology

Pasadena, California

1994

(Defended Friday, May 13, 1994)

## ACKNOWLEDGMENTS

It is unfortunately impractical for me to acknowledge by name everyone who has helped me complete this thesis. However, there are some people who I simply must single out for special thanks. I would like to thank those who got me as far as Caltech, especially my mother, sister, and father. I also thank my ex-housemates (Don, Bryan, Bob, Stuart, Rich and Lydia, Dave, Jeremy, and Blair) and my officemates (Steve and Rich) for both the good times and the lessons in the vagaries of life. And Nicole who has been a friend from Hawai'i to Germany and all points between.

I must also take this time to thank those without whom this thesis simply never would have happened. I will forever thank my advisor, Bruce Murray for insisting that I go to Hawai'i to see some real lava. And I will also be in perpetual debt to all the staff of the Hawaiian Volcano Observatory and the USGS Volunteer Program. Without their help, experience, and equipment, I would not have been able to accomplish even 10% of the research in this thesis. I am especially grateful Jim, Maggie, Tari, and Christina. Without their guidance I would now either be a very dumb volcanologist or a very dead volcanologist. "Thank you" just doesn't say enough.

I would also like to thank Dave Pieri for sicking me onto the Carrizozo flow field and assisting me through a sometimes painful first paper. For Chapter 2, Dave and I thank the staff of HVO, especially Margaret Mangan, Tari Mattox, Christina Heliker, James Kauahikaua, and Tom Wright for their kind hospitality and for their generosity in sharing their experience, ideas, and unpublished data. We also thank Elsa Abbott and Vince Realmuto with their help in processing the remote sensing data, Linda Rowan and Nicole Stroncik-Treue for their assistance in the field work and useful discussions, and the aircrews of the NASA Aircraft Research Program based at Stennis Research Center, Bay St. Louis, Mississippi (May 1988 flight with NASA LearJet) and at the Ames Research

Center, Moffett field, California (September 1989 flight with Lockheed C-130B). Chapter 2 also benefited from generous reviews by Harry Pinkerton and Steve Self.

For Chapter 3, I would like to thank Alun Jones for introducing me to this interesting problem and providing some of the raw data in his thesis. Steve Leroy's suggestions were more than helpful. This chapter also benefited greatly from comments by James Kauahikaua, Margaret Mangan, Joy Crisp, Bruce Murray, Duane Mulhleman, Eugene Robertson, and James Zimbelman.

I would like to thank Roger Denlinger for his data and helpful discussions on Chapter 4. Roger and I would also like to thank James Foster, Jean Hsieh and Bruce Murray for assistance in the various field experiments. I would also like to thank Ken Hon and James Kauahikaua for providing data from their earlier work on sheet flows.

The lava lance in Appendix C could never have been built, operated, or maintained without the supreme engineering skills of George Powell, then a student at Utah State University. For that project, George and I would like to thank Dr. Louis Friedman of the Planetary Society for permitting us to use the Society's video camera, Dr. Frank Redd for permitting us to use, without his expressed consent, the USU CR-10 datalogger, CNES and USU for funding the construction of the load cell (for other purposes), Burrow Brown Inc. for donating several amplifying chips, and Redd Supply in helping us select the proper plumbing materials. We would especially like to thank Dr. Dave Pieri for paying for our transportation costs from unidentified funds and Dr. Bruce Murray for the housing costs.

I would also like to thank my thesis committee (Hugh Taylor, Bruce Murray, Arden Albee, Roger Denlinger, Joann Stock, and Ed Stolper) and Dave Stevenson for their many helpful comments.

And last, but most definitely not least, I would like to thank the radiant Pele.

## ABSTRACT

In this thesis I investigate some aspects of the thermal budget of pahoehoe lava flows. This is done with a combination of general field observations, quantitative modeling, and specific field experiments. The results of this work apply to pahoehoe flows in general, even though the vast bulk of the work has been conducted on the lavas formed by the Pu'u 'O'o - Kupaianaha eruption of Kilauea Volcano on Hawai'i. The field observations rely heavily on discussions with the staff of the United States Geological Survey's Hawaiian Volcano Observatory (HVO), under whom I labored repeatedly in 1991-1993 for a period totaling about 10 months.

The quantitative models I have constructed are based on the physical processes observed by others and myself to be active on pahoehoe lava flows. By building up these models from the basic physical principles involved, this work avoids many of the pitfalls of earlier attempts to fit field observations with "intuitively appropriate" mathematical expressions. Unlike many earlier works, my model results can be analyzed in terms of the interactions between the different physical processes. I constructed models to: (1) describe the initial cooling of small pahoehoe flow lobes and (2) understand the thermal budget of lava tubes.

The field experiments were designed either to validate model results or to constrain key input parameters. In support of the cooling model for pahoehoe flow lobes, attempts were made to measure: (1) the cooling within the flow lobes, (2) the amount of heat transported away from the lava by wind, and (3) the growth of the crust on the lobes. Field data collected by Jones [1992], Hon *et al.* [1994b], and Denlinger [Keszthelyi and Denlinger, in prep.] were also particularly useful in constraining my cooling model for flow lobes. Most of the field observations I have used to constrain the thermal budget of lava tubes were collected by HVO (geological and geophysical monitoring) and the Jet Propulsion Laboratory (airborne infrared imagery [Realmuto *et al.*, 1992]). I was able to

assist HVO for part of their lava tube monitoring program and also to collect helicopter-borne and ground-based IR video in collaboration with JPL [Keszthelyi *et al.*, 1993].

The most significant results of this work are (1) the quantitative demonstration that the emplacement of pahoehoe and 'a'a flows are fundamentally different, (2) confirmation that even the longest lava flows observed in our Solar System could have formed as low effusion rate, tube-fed pahoehoe flows, and (3) the recognition that the atmosphere plays a very important role throughout the cooling of history of pahoehoe lava flows. In addition to answering specific questions about the thermal budget of tube-fed pahoehoe lava flows, this thesis has led to some additional, more general, insights into the emplacement of these lava flows. This general understanding of the tube-fed pahoehoe lava flow as a system has suggested foci for future research in this part of physical volcanology.

# On the Thermal Budget of Pahoehoe Lava Flows

## TABLE OF CONTENTS

### CHAPTER 1: INTRODUCTION

1.1	Scientific context.....	1
1.2	The 1983-present Pu'u 'O'o - Kupaianaha eruption of Kilauea Volcano, Hawai'i.....	4
1.2.1	Geologic Setting.....	4
1.2.2	Eruption Chronology.....	7
1.3	Idealized example of a pahoehoe lava flow.....	10
1.5.1	Lava Distribution System.....	10
1.5.2	Flow Lobes.....	12
1.5.3	Inflation Zone.....	14
1.5.4	Lava Tubes.....	16
1.4	Overview.....	18

### CHAPTER 2: THE EMPLACEMENT OF THE 75-KM LONG CARRIZOZO FLOW FIELD, SOUTH CENTRAL NEW MEXICO

2.0	Abstract.....	20
2.1	Introduction.....	21
2.2	Morphology of the Carrizozo flow field.....	23
2.3	Estimate of the rheology of the Carrizozo lava.....	31
2.4	Comparison with the 1986-1992 Kupaianaha flow field.....	36
2.5	Quantitative estimates of emplacement parameters.....	39
2.6	Discussion.....	44
2.7	Conclusions.....	47

### CHAPTER 3: CALCULATED EFFECT OF VESICLES ON THE THERMAL PROPERTIES OF COOLING BASALTIC LAVA FLOWS

3.0	Abstract.....	48
3.1	Introduction.....	49
3.2	Conduction in vesicular basalt.....	53

3.3 Convection within vesicles.....	61
3.4 Thermal radiation across vesicles.....	62
3.5 Effect of vesicles on effective thermal diffusivity.....	65
3.6 Discussion.....	66
3.7 Conclusions.....	72

## CHAPTER 4: MODELING THE COOLING OF PAHOEHOE FLOW LOBES: THE FIRST FIVE MINUTES

4.0 Abstract.....	67
4.1 Introduction.....	68
4.2 Physical phenomena affecting cooling.....	71
4.2.1 Radiative Processes.....	75
4.2.2 Atmospheric Convective Processes.....	76
4.2.3 Motion of the Lava.....	85
4.2.4 Phase Changes.....	88
4.3 Thermal model.....	90
4.3.1 Basic Equations.....	90
4.3.2 Numerical Methods.....	91
4.4 Comparison to field measurements.....	91
4.5 Comparison to other cooling models.....	96
4.5.1 Simple Conductive Model.....	97
4.5.2 Simple Radiative Model.....	97
4.5.3 Model of Head and Wilson [1986].....	101
4.5.4 Empirical Model of Hon <i>et al.</i> , [in press].....	101
4.6 Model Predictions.....	102
4.6.1 Initial Lava Temperature.....	104
4.6.2 Porosity.....	106
4.6.3 Atmospheric Convective Cooling.....	109
4.7 Applications of the model.....	109
4.7.1 Field Measurements.....	109
4.7.2 Chill Crust Formation.....	111
4.7.3 Future Modeling.....	114
4.8 Conclusions.....	115

## CHAPTER 5: THERMAL BUDGET OF LAVA TUBES

5.0 Abstract.....	117
-------------------	-----

<b>5.1 Introduction</b> .....	<b>118</b>
<b>5.2 Observations from Kilauea lava tubes</b> .....	<b>119</b>
<b>5.3 Terms in the thermal budget of lava tubes</b> .....	<b>126</b>
5.3.1 Conduction Through the Walls.....	127
5.3.2 Radiation out of Skylights.....	127
5.3.3 Rain.....	129
5.3.4 Air Circulation.....	132
5.3.5 Volcanic Gasses.....	134
5.3.6 Release of the Latent Heat of Crystallization.....	137
5.3.7 Viscous Dissipation.....	139
5.3.8 Thermal Erosion.....	139
5.3.9 Cooling of the Lava Inside the Tube.....	141
<b>5.3 Application to the Wahaula lava tube</b> .....	<b>141</b>
<b>5.5 Application to the cooling-limited length of tube-fed lava flows</b> .....	<b>150</b>
<b>5.4 Conclusions</b> .....	<b>161</b>

## CHAPTER 6: CONCLUSIONS AND DISCUSSION

<b>6.0 Executive summary</b> .....	<b>162</b>
<b>6.1 Summary of conclusions</b> .....	<b>162</b>
<b>6.2 Pahoehoe vs. 'a'a</b> .....	<b>164</b>
<b>6.3 Some future field experiments</b> .....	<b>167</b>
<b>6.4 Planetary applications</b> .....	<b>169</b>
<b>6.5 Continental flood basalts</b> .....	<b>175</b>

## APPENDIX A: TEMPERATURE DEPENDENCE OF THERMAL AND PHYSICAL PROPERTIES

<b>A.1 Properties of basalt</b> .....	<b>178</b>
A.1.1 Thermal Conductivity.....	178
A.1.2 Heat Capacity.....	178
A.1.3 Density.....	179
<b>A.2 Properties of gasses</b> .....	<b>179</b>
A.2.1 Viscosity.....	179
A.2.2 Density.....	180
A.2.3 Heat Capacity.....	180

A.2.4 Thermal Conductivity.....	180
---------------------------------	-----

**APPENDIX B: COMPUTER CODE FOR, AND TESTING OF,  
NUMERICAL MODEL FOR THE INITIAL COOLING OF PAHOEHOE  
FLOW LOBES**

<b>B.0 Executive summary.....</b>	<b>181</b>
<b>B.1 Code.....</b>	<b>181</b>
B.1.1 General Comments.....	181
B.1.2 Code.....	181
<b>B.2 Testing.....</b>	<b>187</b>
<b>B.3 Additional model runs.....</b>	<b>188</b>

**APPENDIX C: FIELD MEASUREMENTS OF THE RHEOLOGY OF  
PAHOEHOE FLOW LOBES, OCTOBER 1991, KILAUEA, HAWAII**

<b>C.0 Abstract.....</b>	<b>194</b>
<b>C.1 Introduction.....</b>	<b>194</b>
C.1.1 Previous Work.....	195
<b>C.2 Instrument design.....</b>	<b>197</b>
C.2.0 Introduction.....	197
C.2.1 Structure.....	197
C.2.2 Instruments.....	199
C.2.3 Instrument Mounts.....	203
C.2.4 Power Systems.....	204
C.2.5 Data Collection.....	204
C.2.6 Total System.....	204
<b>C.3 Field procedure.....</b>	<b>205</b>
C.3.1 Standard Operating Procedure.....	205
C.3.2 Log of Actual Operations.....	208
<b>C.4 Data.....</b>	<b>208</b>
C.4.1 Format.....	208
C.4.2 Quality Check.....	209
C.4.3 Processing Algorithm.....	210
<b>C.5 Interpretation.....</b>	<b>215</b>
C.5.0 Conceptual Model.....	215
C.5.1 Strength of the Crust.....	215
C.5.2 Growth of the Chill Crust.....	218

C.5.3 Viscosity.....	223
<b>C.6 Conclusions.....</b>	<b>224</b>
C.6.1 Lava Rheology.....	224
C.6.2 Field Measurements.....	228

#### **APPENDIX D: TERMINOLOGY AND SYMBOLS**

D.1 Lava Flow.....	230
D.2 Pahoehoe.....	230
D.3 'A'a.....	231
D.4 Parts of Pahoehoe Lava Flows.....	232
<b>Symbols.....</b>	<b>234</b>

#### **APPENDIX E: VHS VIDEO LOG**

E.0 Introduction.....	237
E.1 Tour of the Episode 50-53 Pu'u 'O'o Flow Field.....	238
E.2 My field experiments.....	240
E.3 Some other interesting footage.....	244

<b>REFERENCES.....</b>	<b>246</b>
------------------------	------------

LIST OF FIGURES

<b>Figure 1-1:</b> Map of the island of Hawai'i and its five volcanoes.....	5
<b>Figure 1-2:</b> Structural map of Kilauea Volcano.....	6
<b>Figure 1-3:</b> Map of the Pu'u 'O'o - Kupaianaha Flow Field.....	8
<b>Figure 1-4:</b> Map view of an idealized tube-fed pahoehoe flow field.....	11
<b>Figure 1-5:</b> Two end members of pahoehoe flow lobe motion.....	13
<b>Figure 1-6:</b> Cross-section through an active tumulus.....	15
<b>Figure 1-7:</b> Cartoon of the various possible fates for an embryonic lava tube forming in the inflation zone.....	17
<b>Figure 2-1:</b> Location of the Carrizozo flow field and the Tularosa Basin with respect to the Rio Grande Rift.....	22
<b>Figure 2-2:</b> Main physiographic sections of the Carrizozo flow field.....	24
<b>Figure 2-3a:</b> Photograph of the surface of the Carrizozo flow field.....	26
<b>Figure 2-3b:</b> Aerial photograph of the surface of the Carrizozo flow field.....	27
<b>Figure 2-4:</b> Aerial photograph showing the long, linear tumuli overlying the inferred lava tube in the neck region of the Carrizozo flow field.....	28
<b>Figure 2-5a:</b> TIMS data from around the Carrizozo flow field.....	29
<b>Figure 2-5b:</b> TIMS data from the Carrizozo flow field.....	30
<b>Figure 2-6a:</b> Photograph of the surface of the Kupaianaha flow field.....	37
<b>Figure 2-6b:</b> Aerial Photograph of the surface of the Kupaianaha flow field.....	38
<b>Figure 2-7:</b> Hypothetical emplacement history of the Carrizozo flow field based on the Kupaianaha flow field.....	46
<b>Figure 3-1:</b> Field measurements of cooling pahoehoe flow lobes showing the effect of porosity.....	50
<b>Figure 3-2:</b> Idealized cross-section of cooling pahoehoe flow lobe.....	51
<b>Figure 3-3:</b> Plot of conditions necessary for convection within vesicles.....	56
<b>Figure 3-4:</b> Model of vesicle for radiative heat transfer.....	68
<b>Figure 3-5:</b> Thermal conductivities of vesicular basalt.....	62
<b>Figure 3-6:</b> Effective thermal diffusivity of vesicular basalt.....	63
<b>Figure 3-7:</b> Calculated thermal inertia of vesicular basalt.....	65
<b>Figure 4-1a,b:</b> Photograph of active pahoehoe flow lobes.....	72

<b>Figure 4-1c:</b> Photograph of inactive pahoehoe flow lobes.....	<b>73</b>
<b>Figure 4-2:</b> Cartoon of the thermal budget of a pahoehoe flow lobe.....	<b>74</b>
<b>Figure 4-3:</b> Comparison of radiative and convective heat loss.....	<b>78</b>
<b>Figure 4-4:</b> Free atmospheric convective heat transfer coefficient.....	<b>79</b>
<b>Figure 4-5:</b> Simple experiment to determine the heat transfer coefficient for forced convection over Hawaiian pahoehoe flow lobes.....	<b>81</b>
<b>Figure 4-6:</b> Rayleigh Numbers inside lava flows.....	<b>87</b>
<b>Figure 4-7a:</b> Field measurements from cooling pahoehoe flow lobes.....	<b>93</b>
<b>Figure 4-7b:</b> Field measurements from cooling pahoehoe flow lobes.....	<b>94</b>
<b>Figure 4-8:</b> Comparison of field data with model results.....	<b>95</b>
<b>Figure 4-9:</b> Comparison of numerical cooling model to simple analytic model.....	<b>98</b>
<b>Figure 4-10:</b> Model predictions for depths of isotherms.....	<b>99</b>
<b>Figure 4-11:</b> Comparison of numerical cooling model to simple radiative cooling model.....	<b>100</b>
<b>Figure 4-12:</b> Comparison of numerical cooling model to empirical fit.....	<b>103</b>
<b>Figure 4-13:</b> Predicted effect of changing the initial lava temperature.....	<b>105</b>
<b>Figure 4-14:</b> Predicted effect of changing porosity.....	<b>107</b>
<b>Figure 4-15:</b> Predicted temperature profiles through flow lobes of different porosities.....	<b>108</b>
<b>Figure 4-16:</b> Predicted effect of changing the atmospheric convective heat transfer coefficient.....	<b>110</b>
<b>Figure 4-17:</b> Predicted average cooling rates through the glass transition.....	<b>113</b>
<b>Figure 5-1:</b> Location of the Wahaula lava tube, Kilauea Volcano, Hawai'i.....	<b>121</b>
<b>Figure 5-2a:</b> Photograph of lava tube monitoring.....	<b>122</b>
<b>Figure 5-2b:</b> Photograph of lava tube hunting.....	<b>123</b>
<b>Figure 5-2c:</b> Photograph of lava tube monitoring.....	<b>124</b>
<b>Figure 5-3:</b> Conductive heat losses as a function of tube diameter and roof thickness.....	<b>128</b>
<b>Figure 5-4:</b> Radiative heat loss out of skylights.....	<b>130</b>
<b>Figure 5-5:</b> Estimated heat loss from rainfall.....	<b>131</b>
<b>Figure 5-6:</b> Idealized lava lake temperature profile.....	<b>133</b>
<b>Figure 5-7:</b> Heat lost by air convecting in the wall rocks.....	<b>135</b>
<b>Figure 5-8:</b> Heat loss by air blowing out of skylights.....	<b>136</b>
<b>Figure 5-9:</b> Heat released by the latent heat of crystallization.....	<b>138</b>
<b>Figure 5-10:</b> Heat input from viscous dissipation.....	<b>140</b>

<b>Figure 5-11:</b> Detailed breakdown of the Wahaula tube into 5 segments.....	<b>143</b>
<b>Figure 5-12:</b> Relative magnitudes and uncertainties of the terms in the thermal budget of the Wahaula lava tube.....	<b>147</b>
<b>Figure 5-13:</b> Relative magnitudes of the heat transfer mechanisms plotted by tube segment.....	<b>149</b>
<b>Figure 5-14:</b> Computed relative viscosities.....	<b>154</b>
<b>Figure 5-15:</b> Relative magnitudes of each term in the thermal budgets of the six model lava tubes.....	<b>155</b>
<b>Figure 5-16a:</b> Cooling-limits for the three terrestrial model lava tubes.....	<b>158</b>
<b>Figure 5-16b:</b> Relative cooling-limited lengths of model lava tubes on the different planets.....	<b>159</b>
<b>Figure 5-17:</b> Calculated effusion rates for the model lava tubes.....	<b>160</b>
<b>Figure 6-1:</b> Free convective heat transfer coefficients for Venus, Earth, and Mars..	<b>170</b>
<b>Figure 6-2a:</b> Model surface cooling curves for pahoehoe flow lobes on different planets.....	<b>173</b>
<b>Figure 6-2b:</b> Blow-up of model surface cooling curves for pahoehoe flow lobes on different planets.....	<b>174</b>
<b>Figure B-1:</b> Analytic and numerical solutions for fixed temperature conductive cooling problem.....	<b>190</b>
<b>Figure B-2:</b> Analytic and numerical solutions to fixed heat transfer coefficient conductive cooling problem.....	<b>191</b>
<b>Figure B-3:</b> Conservation of energy test of numerical model.....	<b>192</b>
<b>Figure B-4:</b> Comparison of model runs with different expressions for thermal conductivity.....	<b>193</b>
<b>Figure C-1:</b> Balance of forces on penetrometer.....	<b>198</b>
<b>Figure C-2:</b> Instruments on the Lava Lance.....	<b>198</b>
<b>Figure C-3:</b> Calibration curves for the load cell.....	<b>200</b>
<b>Figure C-4:</b> Calibration curves for linear potentiometers.....	<b>201</b>
<b>Figure C-5:</b> Calibration curve for the inclinometer.....	<b>202</b>
<b>Figure C-6:</b> Photograph of Lava Lance in the field.....	<b>206</b>
<b>Figure C-7a:</b> Typical position vs. time data from Lava Lance.....	<b>211</b>
<b>Figure C-7b:</b> Typical force vs. time data from Lava Lance.....	<b>212</b>
<b>Figure C-7c:</b> Typical angle vs. time data from Lava Lance.....	<b>213</b>

<b>Figure C-7d:</b> Typical velocity vs. time data from Lava Lance.....	<b>214</b>
<b>Figure C-8:</b> Plot of hardening of the crust of a single lobe with time.....	<b>216</b>
<b>Figure C-9:</b> Combined data for all 7 lobes.....	<b>217</b>
<b>Figure C-10:</b> Model predictions for thickness of chill crust.....	<b>218</b>
<b>Figure C-11:</b> Fits to yield strength field data.....	<b>219</b>
<b>Figure C-12:</b> Prediction of pahoehoe crust strength based on laboratory data and thermal modeling.....	<b>221</b>
<b>Figure C-13:</b> Predicted yield strengths for a fractured crust.....	<b>222</b>
<b>Figure C-14:</b> Stress vs. strain rate diagrams for lobe 7.....	<b>225</b>
<b>Figure C-15:</b> Apparent viscosity vs. depth for lobe 7.....	<b>226</b>
<b>Figure C-16:</b> Stress vs. strain for lobe 7.....	<b>227</b>
<b>Figure D-1:</b> Photograph of some exceptionally well formed pahoehoe flow lobes, Kupaianaha flow field, Hawai'i.....	<b>233</b>
<b>Figure D-2:</b> Photograph of a typical tumulus.....	<b>233</b>

LIST OF TABLES

<b>Table 2-1:</b> Bulk chemistry of Carrizozo and Kilauea lavas.....	<b>31</b>
<b>Table 2-2:</b> Comparison of calculated viscosities of the Carrizozo lava with a Kilauea and an Etna lava.....	<b>34</b>
<b>Table 2-3:</b> Results from the simple Bingham plastic model.....	<b>40</b>
<b>Table 4-1:</b> Results of simple field experiment to measure cooling by wind.....	<b>81</b>
<b>Table 4-2:</b> Comparison between field measurements and predictions from micro- meteorological models.....	<b>84</b>
<b>Table 5-1:</b> Estimates for the input parameters for the Wahaula lava tube.....	<b>144</b>
<b>Table 5-2:</b> Predicted cooling inside the Wahaula lava tube.....	<b>145</b>
<b>Table 5-3:</b> Input for the 6 hypothetical tube-fed flows.....	<b>151</b>
<b>Table 5-4:</b> Bulk compositions for different basalts.....	<b>152</b>
<b>Table 6-1:</b> Input parameters for cooling model.....	<b>171</b>
<b>Table C-1:</b> Results of quality check of raw data.....	<b>209</b>

## CHAPTER 1: INTRODUCTION

### 1.1 Scientific context

Large basaltic lava flows make up a major part of the surface of the Earth and the other terrestrial planetary bodies. In the last few years a revolutionary new hypothesis has been put forward for the formation of these large lava flows.

It has been generally assumed that large lava flows require high effusion rates. This view is supported by three lines of reasoning. First, there is an empirical correlation between the length of historical lava flows and their observed effusion rates [Walker, 1973; Kilburn and Lopes, 1991]. Second it has been argued that a lava flow must reach its final dimensions quickly to avoid freezing [e.g., Swanson *et al.*, 1975]. This statement is quantified by the observation that lava flows tend to stop when the non-dimensional Grätz Number (is a ratio of advective and conductive heat fluxes) reaches a critical value of about 300 [Walker, 1973]. For a constant Grätz Number, a longer flow requires a higher effusion rate (see Chapter 2). Third, large lava flows are quite thick. Simple flow models clearly indicate that thick basaltic lava flows flow very quickly.

However, observations from the Kupaianaha flow field on Kilauea Volcano, Hawai'i, in 1990-1991 have led to the realization that large lava flows can be formed by low effusion rate eruptions [Hon and Kauahikaua, 1991; Self *et al.*, 1991; Hon *et al.*, 1994a]. The key insight leading this new hypothesis is the observation and understanding of the "inflation" process. "Inflation" refers to the continued injection of lava underneath the solid, stationary crust of a lava flow. This process has only been observed for pahoehoe lava flows which are characterized by an essentially continuous solid crust. In Hawai'i, inflation converts fans of 20-50 cm thick lobes into a single, 2-5 m thick, sheets.

Because the final thickness of inflated pahoehoe flows is often an order of magnitude thicker than the moving lobes, simple flow models greatly over estimate the flow velocity. Also, because most of the lava flows beneath a solid, insulating, crust, the

lava can reach great distances even at these slow flow velocities. Finally, it is known (but often ignored) that the observed empirical correlation between effusion rate and flow length breaks down for tube-fed lava flows [*e.g.*, Malin, 1980]. The inflation process usually leads to the formation of lava tubes within the inflated lava flow. Thus, inflated tube-fed pahoehoe flows circumvent all the reasoning behind the generally accepted rule that large lava flows require high effusion rates.

There is good reason to suspect that many large basaltic lava flows are indeed inflated pahoehoe flows. First, pahoehoe flows are common wherever basaltic volcanism occurs. In the case of Kilauea Volcano, more than 90% of its surface is pahoehoe. The longest well-preserved terrestrial subaerial flows are tube-fed pahoehoe [*e.g.*, Stephenson and Griffin, 1967; Keszthelyi and Pieri, 1993]. Large submarine flows also show inflated pahoehoe surface morphologies [*e.g.*, BVSP, 1981; Appelgate and Embley, 1992; Bryan *et al.*, 1994]. And the Columbia River flood basalts show clear signs of inflation [*e.g.*, Finnemore *et al.*, 1993].

This new hypothesis for the emplacement of large pahoehoe lava flows has important implications. The effusion rates for the eruptions that formed these flows has probably been overestimated by 2-4 orders of magnitude (and eruption durations underestimated by the same factor) [Keszthelyi and Pieri, 1993]. For example, it was previously suggested that the  $1.5 \times 10^3 \text{ km}^3$  Roza member of the Columbia River Basalts was emplaced in about a week with "paroxysmal environmental impacts [Swanson *et al.*, 1975]. It is now suggested that the eruption may have gone on for decades or centuries [Hon and Kauahikaua, 1991] and may not have been much more dramatic than historical eruptions on Iceland or even Hawai'i [Self *et al.*, 1991]. However, the largest historical Icelandic eruptions have had substantial local and regional impact on climate [Thordarson *et al.*, 1992; Thordarson and Self, 1993]. Such climatic effects may become important on a global scale if the eruption continues for decades or centuries.

Changing an eruption's effusion rate by orders of magnitude also has repercussions on the plumbing system required to feed it. Geodynamic and geochemical studies as well as K-Ar dating indicate that the source region for flood basalts produced on the order of  $1 \text{ km}^3/\text{year}$  of lava [Renne and Basu, 1991; Arndt and Christensen, 1992]. Given a high effusion rate model for the formation of flood basalts, the difficulty is in storing up magma over thousands of years and then suddenly venting it in a single cataclysmic event. In contrast, if flood basalts were fed by low effusion rate eruptions, then one must explain how an efficient plumbing system was preserved for decades or centuries.

In this thesis I concentrate on the thermal aspects of this new hypothesis for the emplacement of large pahoehoe lava flows. I divide pahoehoe flows into 3 parts: flow lobes, the "inflation zone," and lava tubes. In Chapter 4, I investigate the cooling of flow lobes on the time scale of minutes. I rely on the published work of Hon *et al.* [1994a] to describe the inflation zone and time scales of hours to days. In Chapter 5, I examine the thermal budgets of mature lava tubes on the time scale of months to years. Thus, combined with the work on Hon *et al.* [1994a], this thesis describes the thermal budget of the entire pahoehoe lava flow. While more work on the thermal aspects of pahoehoe flows is still important, it is now possible to begin to address the petrologic, rheologic, and dynamic aspects of large pahoehoe lava flows.

In the remainder of this introductory chapter, I will discuss the observations from Hawai'i that have led to the new insights into pahoehoe lava flows and then provide an overview of the rest of the thesis.

## 1.2 Pu'u 'O'o - Kupaianaha eruption Kilauea Volcano, Hawai'i

This is not a thesis on Hawaiian volcanism. However, given the key role this particular eruption has played in all aspects of this thesis, a brief description is necessary. I will begin with a short review of the geologic setting of the island of Hawai'i before describing the Pu'u 'O'o - Kupaianaha eruption. In this section all chapter references refer to chapters in USGS Professional Paper 1350 [Decker *et al.*, 1987].

### 1.2.1 Geologic setting

Hawai'i is the last of a long chain of islands and seamounts that are thought to have formed by the passage of the Pacific Plate over a mantle hotspot. The volcanoes making up this chain are remarkably systematic, not just in their geographic progression, but also in their evolutionary sequence. Each volcano appears to have undergone a series of stages from submarine to shield-building to atoll. There is a distinct suite of lavas and style of eruption associated with each stage of the active volcano's evolution [Ch 1, 12]. The island of Hawai'i is built up of five volcanoes: green and weathered Kohala, towering Mauna Kea crowned with cinder cones and astronomical domes, Hualalai with its xenoliths, majestic Mauna Loa, and hyperactive Kilauea (Fig. 1-2). Kohala and Mauna Kea are considered dormant and last erupted about 60 Ka and 3.5 Ka respectively [Ch 22]. Hualalai last erupted in 1801 [Ch 20], Mauna Loa in 1984 [Ch 18, 19]. The Pu'u 'O'o - Kupaianaha eruption at Kilauea, which started in 1983, continues as of this writing.

By most measures, Kilauea is the most active volcano on the world. This fact and accessibility of Kilauea has made it the world's premier laboratory for basaltic volcanism. This level of activity has also caused changes at a staggering rate. The present Kilauea Caldera formed in the 18th century and the Halemaumau Pit Crater in 1924 [Ch 12]. Because of the quantity and quality of the work done on them, several eruptive events have become renown across the globe. Kilauea Iki (1959) and Makaopuhi (1965) Lava Lakes have yielded the some of the most valuable data on the petrologic evolution of cooling basaltic melts [Ch 23]. They have also produced the first *in situ* measurements of

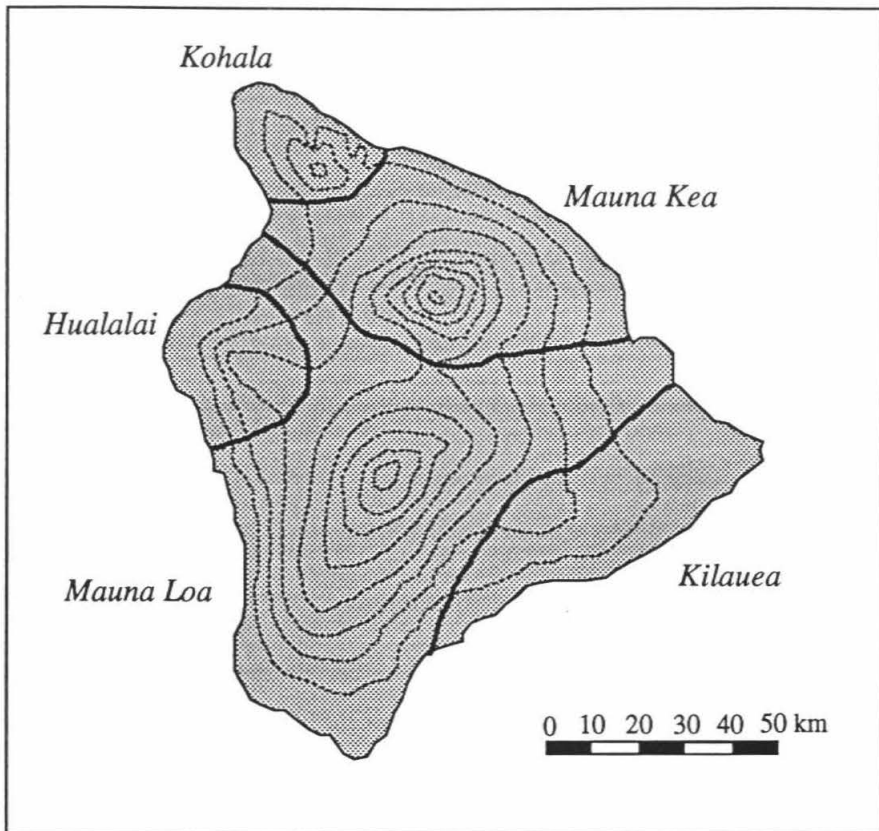


**Figure 1-1: Map of the island of Hawai'i and its five volcanoes.** Contour interval is 500 m.

[From USGS Prof. Paper 1350]

lava viscosity and cooling rates [Shaw *et al.*, 1968; Hardee, 1980]. The Mauna Ulu Flow Field (1969-1974) produced key insights into the formation of lava tubes [Ch 16, 59].

Kilauea Volcano is broken into five major structural subdivisions: Summit, East Rift Zone, Southwest Rift Zone, South Flank, and North Flank (Fig. 1-2). The orientations of these major structures appear to be controlled by the adjacent and much larger Mauna Loa. There also seems to be a roughly 100 year cycle between having activity dominantly at the summit versus at the rift zones. In the last few decades the majority of the lava has erupted from the East Rift Zone [Ch 12]. Based mostly on seismic and petrologic evidence, it is believed that Kilauea's lava is first brought up from about 60-90 km depth to an irregular shaped, 3-7 km deep, magma chamber under the

southwest corner of the caldera. Deformation studies have shown that the East Rift Zone is a 4-6 km wide zone of dikes that reaches from a depth of about 8 km to the surface [Ch 12, 42]. The relationship between the spreading at the rift zones and the seaward sliding of the South Flank of Kilauea is at present a subject of intense interest, in part because of the structure's potential for giant landslides.

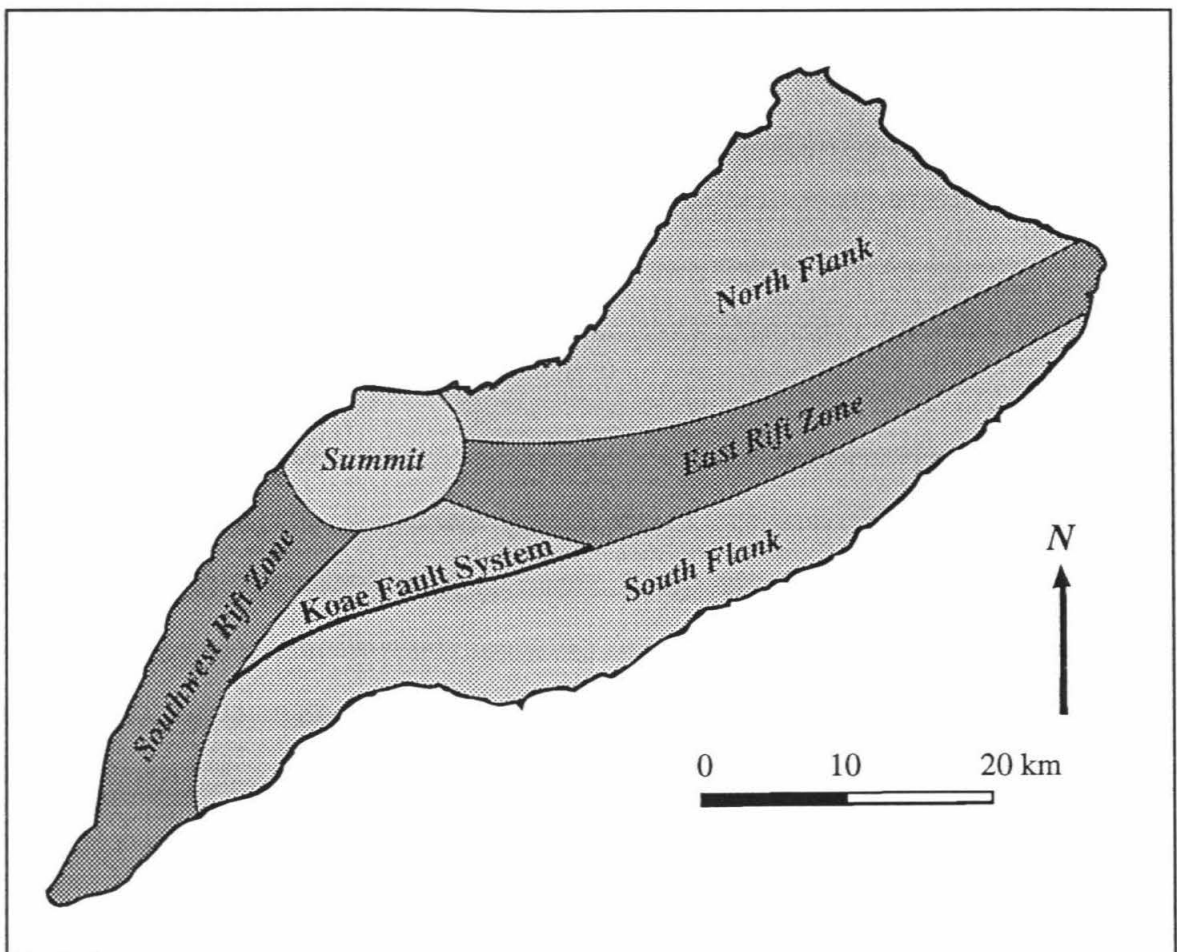


**Figure 1-2: Structural map of Kilauea Volcano.** The entire South Flank is sliding seaward under some combination of gravitational slumping and widening of the rift zones. The Pu'u 'O'o - Kupaianaha eruption is located about halfway down the East Rift Zone. [after USGS Prof. Paper 1350]

### 1.2.2 Eruption Chronology

The Pu'u 'O'o eruption started on January 3, 1983 with fire curtains opening up along the central part of Kilauea's East Rift Zone. By February the eruption had focused to a single point and a new cinder cone, Pu'u 'O'o, was forming (Fig. 1-3) [Ch 17]. Pu'u 'O'o continued to grow through a series of 47 high fountaining events that would throw lava as high as 400 meters into the air. Each of these fountaining events would flare up for a few days or weeks and then the eruption would pause for a similar length of time. This was a rather orderly pattern of eruption with rapid deflation at the summit of Kilauea followed by a steady reinflation until the next fountaining event. These fountaining events were christened "episodes" by HVO. The lava fountains also sent 'a'a flows toward the sea several times during 1983 and 1984, partially destroying the community of Royal Gardens. The details of the first 20 episodes are thoroughly documented in USGS Professional Paper 1463.

On July 20, 1986 the style of the eruption changed dramatically with the start of Episode 48. Lava was transported about 3 km further downrift from Pu'u 'O'o and quickly formed a new lava pond, Kupaianaha. Large tube-fed pahoehoe flows were fed from Kupaianaha, eventually reaching the sea and destroying the Wahaula Visitor Center in 1986 and the town of Kalapana in 1990 [Weisel and Heliker, 1990; Moulds *et al.*, 1990; Mattox *et al.*, 1993]. During 1991 and early 1992, the Kupaianaha lava lake died, the tube system began to break down, and an active lava pond reappeared in Pu'u 'O'o. Episode 48 was crippled by a new fissure vent that opened up between Pu'u 'O'o and Kupaianaha on November 8, 1991. This 10 day eruptive event (Episode 49) produced a large 'a'a flow which reached the top of Royal Gardens. Episode 48 was finally officially declared dead the 6th of February, 1992 though lava continued to drain from the tube system for a few more days.

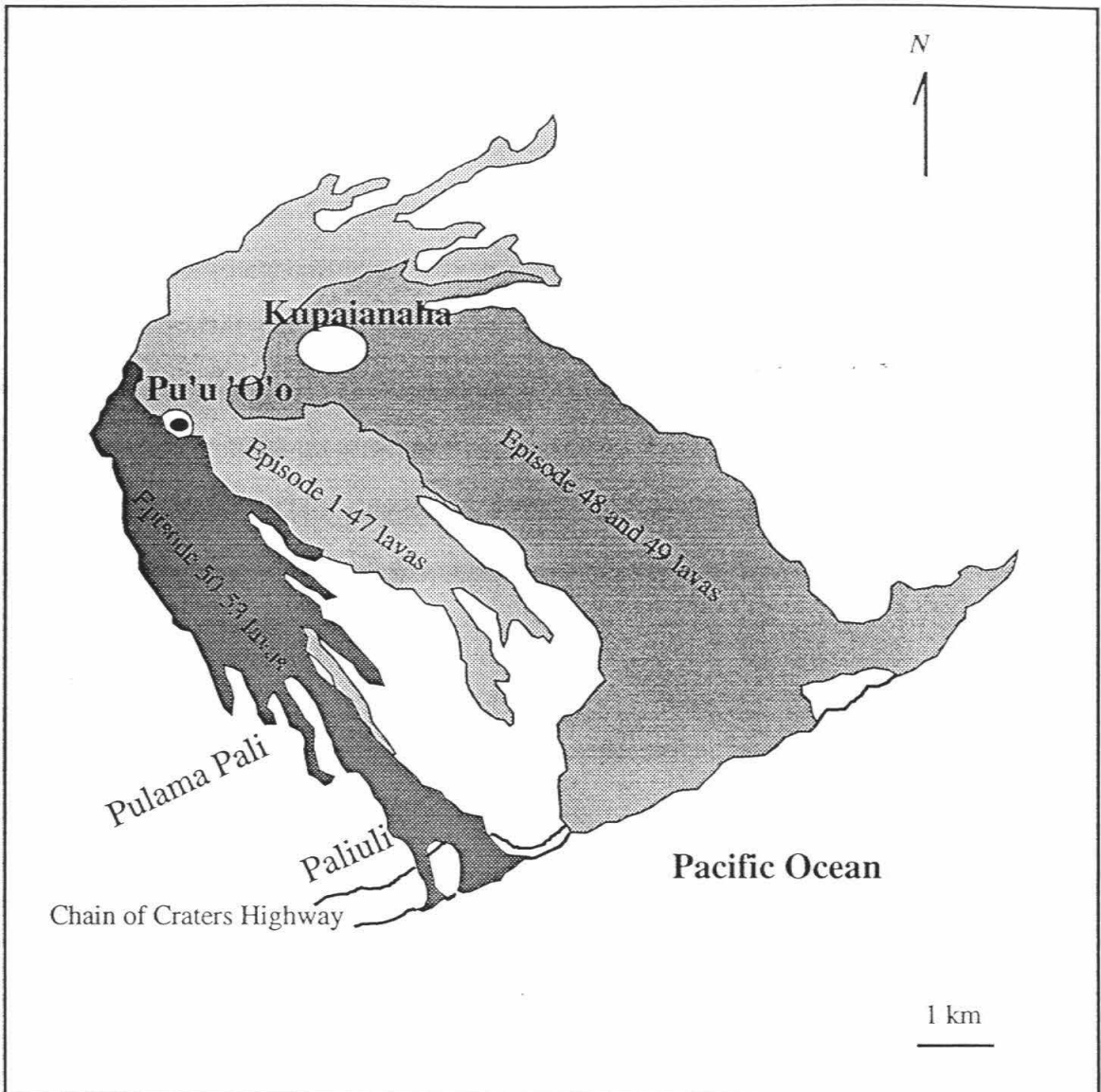


**Figure 1-3: Map of the Pu'u 'O'o - Kupaianaha Flow Field.** [Courtesy of USGS]

It did not take long for the lava to create another path to the surface. On February 17 Episode 50 erupted with a new fissure on the uprift side of Pu'u 'O'o. This vent immediately sent out shelly pahoehoe flows and began building up a perched lava pond. After a brief respite related to an Upper East Rift Zone intrusive event, the eruption continued as Episode 51. This latest incarnation of the Pu'u 'O'o - Kupaianaha eruption

has had a number of short pauses, with none lasting much over a week. Two of the pauses ended with new episodes when lava erupted from new vents on the south flank of Pu'u 'O'o. Episode 52 started on September 2, 1992 and Episode 53 on February 20, 1993. Both fed lava flows that reached a few kilometers before their vents shut down. After each of these new episodes, activity gradually returned to the Episode 50/51 vent.

In November 1992 the episode 51 lavas reached the sea at Kamoamoia, destroyed the scenic black sand beach there, and built a lava bench which moved the coastline 300m makai (seaward). This lava bench is very unstable and a collapse on April 19, 1993 resulted in the death of one visitor to the national park. These lavas continue to extend the bench in the Kamoamoia and Lae Apuki area as of this writing.

### 1.3 Idealized pahoehoe lava flow

From the observations in Hawai'i, a general picture for pahoehoe lava flows has arisen. The idealized lava flow I describe in the following incorporates what I have seen on Mt. Etna and the Southwestern United States, as well as the Pu'u 'O'o - Kupaianaha flow field. Appendix E (video) is intended to supplement this section.

The idealized tube-fed pahoehoe lava flow can be broken into 4 major zones: (1) active flow lobes, (2) inflation zone, (3) the tube system, and (4) vent (Fig. 1-4). I have not interested myself in the vent processes, which have been extensively studied by others [*e.g.*, Wilson and Head, 1983] and are not unique to pahoehoe lava flows. In the following I briefly describe the flow field as a system, then examine the three zones of interest in some detail.

#### 1.3.1 Lava Distribution System

The transport and distribution of lava within a tube-fed pahoehoe flow field is somewhat analogous to an inefficient irrigation system. The well (vent) pours out liquid with no significant hydraulic head. Gravity must provide the driving force for all the flow. The main tube system is an anastomosing pipe system with open "relief valves" (skylights). The system usually runs with the tubes only partially full. Blockages in a tube or sudden increases in effusion rate can be accommodated by spill-overs through skylights.

In the region I have termed the "inflation zone," smaller feeder pipes are plugged into the main tube system. The details of how the branching from larger to smaller pipes is achieved is not perfectly clear. In Figure 1-4, I have tried to schematically reproduce my impressions of this branching based on helicopter-borne IR imaging. In this figure I suggest that the distribution is more akin to pipes connected in series than to a dendritic pattern. In fact, the inflation zone does not appear to be made of well defined, discrete tubes. Instead, it appears to be a zone of small storage reservoirs that are interconnected

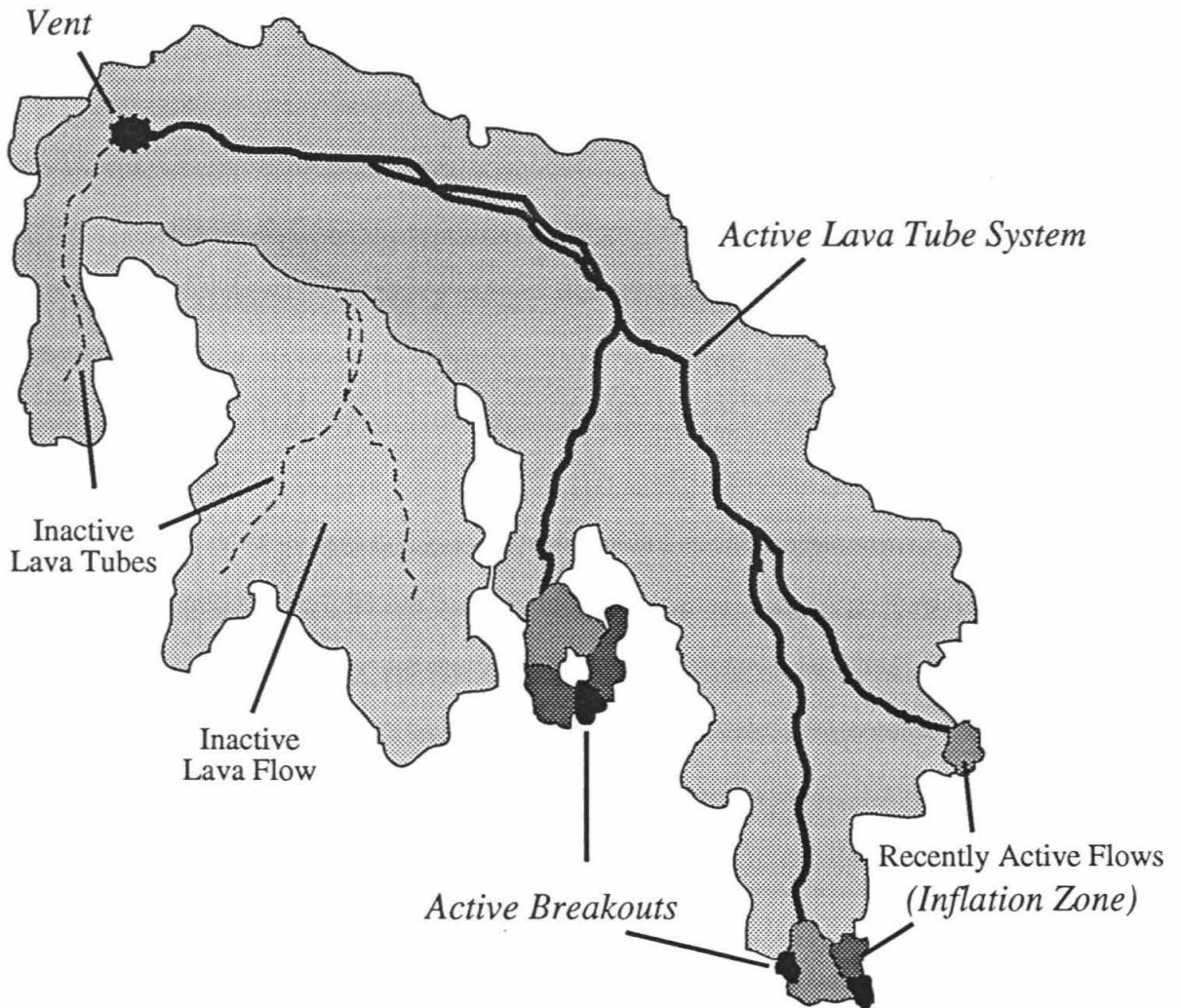


**Figure 1-4: Map view of an idealized tube-fed pahoehoe flow field.** There are four main zones within the active part of the flow field: (1) vent, (2) lava tubes, (3) inflation zone, and (4) breakouts. The anastomosing nature of the lava tubes is derived from airborne IR imaging. The inflation zone corresponds to the recently active parts of the flow field. This zone is characterized by pockets of molten lava interconnected by a network of fluid filled conduits. The hydrostatic head in this zone serves to both feed breakouts and to “inflate” the pockets of melt. The active breakouts are the only area on the flow field where red lava is exposed.

by a network of irregular, liquid filled, conduits. While this region is somewhat "leaky," substantial pressure can build up in the inflation zone. The storage reservoirs (tumuli) are able to raise their roofs in order to accommodate this pressure.

The front of the inflation zone is riddled with leaks where small breakouts form. These breakouts move much like water balloons being filled by a garden hose. Typically the "hose" has enough pressure to allow the lobes to climb small topographic obstacles. Roadcuts of cooled pahoehoe flows suggest that as these lobes coalesce, they may remelt their walls.

### 1.3.2 Flow Lobes:

The first zone considered here in more detail is the region where breakouts and active flow lobes occur. There are several reasons to study the flow lobes. Most importantly, these flow lobes are the vanguard of the entire lava flow. If incursions by small flow lobes can be continuously halted in an area, that area cannot be overrun by even the largest pahoehoe flow field. Flow lobes are also the only place where red lava is exposed directly to the "cold" ground and air. This is also where the distinctive mm - 10 cm scale pahoehoe surface textures are formed.

Flow lobes range from tens of centimeters in diameter to sheet flows hundreds of meters across. While there may be no upper limit to the size of what might be called a single flow lobe, there does seem to be a distinct lower limit of about 10 cm in diameter. The size and shape of the lobe is controlled by the competition between the growth of the chill crust and the flux of hot lava into the breakout. Ten cm seems to be the smallest size for an orifice that can extrude lava fast enough to overcome the cooling at the surface. Typical flow lobes are a few tens of centimeters thick and a few meters long and wide. They usually move at a speed of several cm/s though some exceptional flows can race forward at about a meter per second.

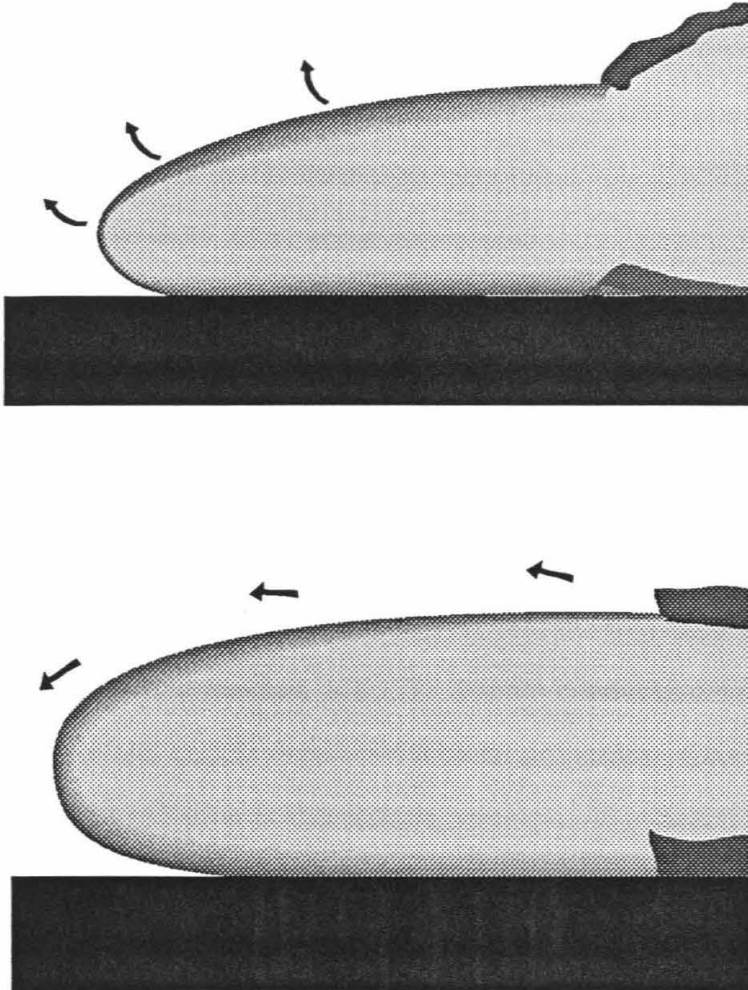


**Figure 1-5: Two end members of pahoehoe flow lobe motion.** In the upper lobe, the crust is thinnest at the front of the flow and the motion is similar to an inflating balloon. In the lower lobe, the crust is thinnest on the top at the breakout point. In this case the crust flows over the lobe.

In watching flow lobes, I have noticed two end members in the style of motion and crust formation (Fig. 1-5). The distinction derives from where red incandescent lava is exposed (*i.e.*, where the crust is the thinnest). In the first type of motion the crust is the thinnest at the very front of the flow lobe. This kind of motion typically forms entrail or billowy pahoehoe. The other end member has new crust only forming at the initial breakout point. This often leads to a smooth rolling caterpillar tread motion. Shelly

pahoehoe usually moves in this fashion. Sometimes the sides of the lobe will become stagnant and a central (covered) channel will form. This kind of motion is required to form pahoehoe ropes.

With regard to the thermal budget of flow lobes, which after all is one of the main thrusts of this thesis, 17 physical phenomena were examined. These phenomena are (1) thermal radiation at the surface, (2) enhanced thermal radiation through cracks in the crust, (3) radiative heat transfer within a flow lobe, (4) air circulating in the outer solid crust, (5) forced atmospheric convection, (6) free atmospheric convection, (7) forced convection of the lava, (8) free convection of the lava, (9) bubble rise within the flow lobe, (10) viscous dissipation, (11) rain, (12) latent heat of crystallization, (13) spalling of the crust, (14) gas exsolution and escape, (15) thermal radiation across vesicles, (16) gas convection within vesicles, and (17) thermal conduction within the lobe including the temperature and vesicle dependent thermal properties. Chapters 3 and 4 will show that only thermal radiation at the surface, atmospheric convection, and thermal conduction within the flow lobe are important in the initial few minutes of cooling. Over longer time scales many more phenomena become significant.

### 1.3.3 Inflation Zone:

The most distinctive aspect of the inflation zone is the presence of inflation features. Lava inflation features are multiple-meter scale topographic highs on the surface of pahoehoe lava flows. The basic process involved in their formation is the upheaval of crack bounded blocks of cold crust by the intrusion of fresh lava underneath the solid crust. Observational data on the formation and growth of tumuli and more complex inflation features were only collected within the last few years [Walker, 1991; Hon *et al.*, 1994a].

The significance of lava inflation features was not fully recognized before the emplacement of the Pu'u 'O'o - Kupaianaha Flow Field. A large portion of the lava that is

erupted is never exposed to the surface. This intrusive behavior provides a way to thicken flows that is not taken into account in previous flow emplacement models. The lava inflation features also form a set of 10-100 meter morphologic features that can be used to identify pahoehoe lava flows remotely in moderate spatial resolution images.

The same 17 physical processes involved in the cooling of flow lobes can be examined for the case of the growth of lava inflation features. While radiative cooling is now a minor term, processes such as the release of the latent heat of crystallization, air circulating in cracks, and the flow of lava become very significant. Another major difference is that the crust is too thick to deform ductily. Instead, the surface blocks are rotated and translated by the intruding lava (Fig. 1-6). The relative amounts of these two motions are probably controlled by the shape of the intruding lava body and the distribution of pre-existing surface cracks. Despite all these complications, Hon et al. [1994a] appears to have successfully described the cooling of inflating sheet flows with a simple conductive cooling model.

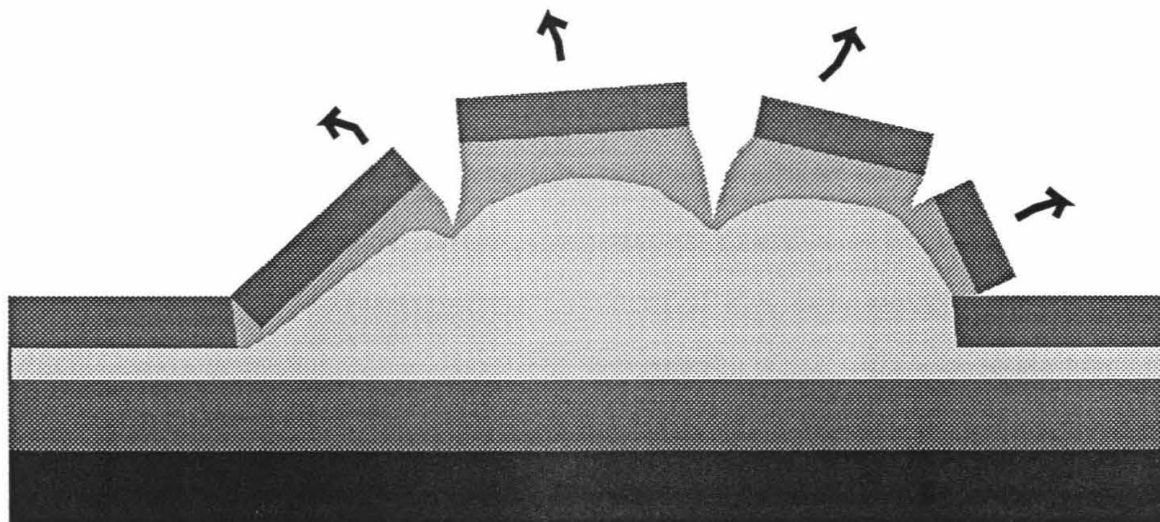


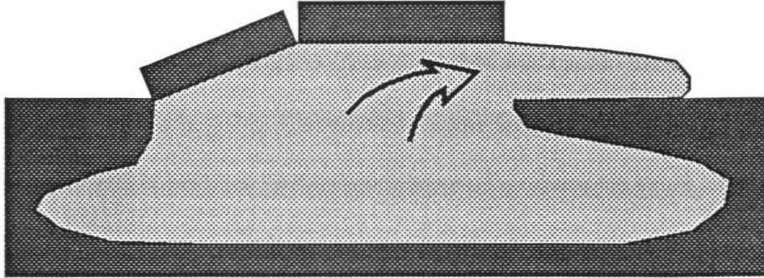
**Figure 1-6: Cross-section through an active tumulus.** Lighter shades represent hotter material. The old, cold crust is moved with a combination of translations and rotations as fresh melt is injected into the tumulus. There should be enhanced cooling at the cracks. The crack-bounded blocks are typically a few meters across.

#### 1.3.4 Lava tubes:

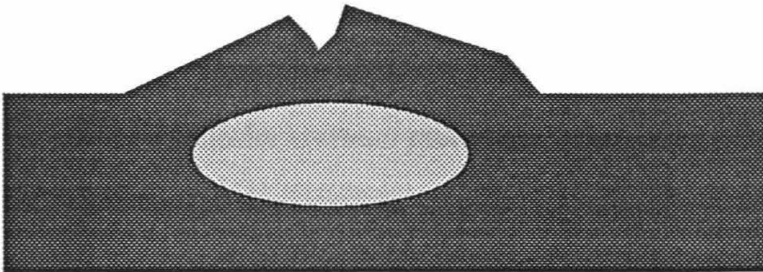
The importance of lava tubes in a large pahoehoe lava flow is obvious. They are the structures that allow lava to travel many kilometers from their sources. Without tubes pahoehoe flows would be short, squat, insignificant stacks of flow lobes, choking off their own vents.

Lava tubes form in a variety of ways, several of which have been carefully described by previous workers [*e.g.*, Peterson and Swanson, 1974; Greeley, 1972]. However this previous work has concentrated on channelized flows which are relatively uncommon in pahoehoe flow fields. A perhaps more important mode of tube formation has been repeatedly observed during the emplacement of the Pu'u 'O'o - Kupaianaha Flow Field. This process starts with the emplacement of a larger flow lobe or a sheet flow. Under certain conditions the continued flux of lava under the growing crust is concentrated into a single stream. This concentrated flow can develop into a tube as the surrounding stagnant lava solidifies. The volumetric flux of lava underneath the sheet flow is one of the critical parameters. If this rate is too low, the flow will simply freeze. If it is too high, breakouts will form and the lava will be diverted from the embryonic tube (Fig. 1-7).

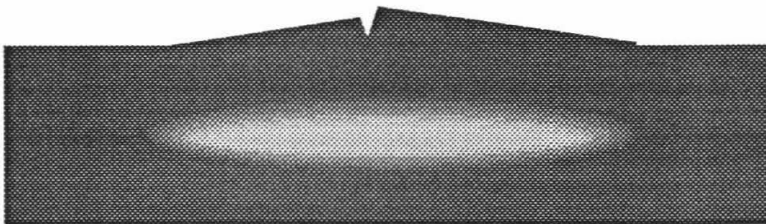
The thermal budget of a lava tube involves the same physical processes that operate on inflation features. In fact, the formation of a tube in the manner described above is simply a special case of the formation of lava inflation features. A major simplification is that there is no significant deformation of the surface once the tube has been established. Furthermore, a long-lived lava tube will reach a near steady-state thermal condition. These simplifications are sufficient to allow a simple, but quantitative, description of the thermal budget of lava tubes to be drawn up (Chapter 5 of this thesis).



(a) If inflation is too rapid relative to the growth of the solid crust, breakouts will form, diverting lava from the embryonic tube



(b) If the flux of fresh lava matches the heat lost through the walls, a stable lava tube can form.



(c) If the volumetric flux of lava is too low, the embryonic tube will simply freeze.

**Figure 1-7: Cartoon of the various possible fates for an embryonic lava tube forming in the inflation zone.** I suggest that the volumetric flux of fresh lava relative to the cooling is the parameter that separates these cases.

## 1.4 Overview

In the remainder of this thesis, I examine several aspects of the emplacement of pahoehoe lava flows, concentrating on their thermal budgets. In Chapter 2, I examine the emplacement of the 75-km long Carrizozo flow field in New Mexico. Based on its pahoehoe surface texture and its inflation features, I argue that the Carrizozo flow field was emplaced by a steady, low effusion rate eruption that lasted 2-3 decades. I also show that applying any of the available techniques for quantifying the effusion rates of inactive lava flows overestimates the effusion rate by 2-5 orders of magnitude. These techniques fail because (1) they assume that the entire lava flow was emplaced at one time (*i.e.*, do not recognize inflation) or (2) because they do not take into account the insulation that lava tubes provide. Having shown the failure of previous work to quantitatively describe the emplacement of large pahoehoe flows, I proceed to fill parts of this hole with the rest of my thesis.

Before being able to discuss the thermal budget of lava flows, it is necessary to understand the effect of temperature and porosity on the thermal properties (thermal conductivity, thermal diffusivity, density, heat capacity, and thermal inertia) of the lava. While the effect of temperature has been extensively studied in the laboratory, the effect of porosity has only been investigated at low temperatures. However, there is field data suggesting that porosity has a strong effect on the cooling of pahoehoe flow lobes [Jones, 1992]. In Chapter 3, I quantify the effect of porosity (in the form of vesicles and bubbles) on the thermal properties of basaltic lava at high temperatures. This work also provides a qualitative explanation for the field data of Jones [1992].

In Chapter 4, I construct a theoretical model for the initial cooling of pahoehoe flow lobes. This model is constructed from the physics controlling the significant physical processes and is solved numerically. This model is the first to incorporate the temperature and porosity dependent thermal properties of lava. The model results agree very well with field data collected by myself and others. In Chapter 5, I describe the

thermal budget of mature lava tubes. This model is relatively crude, but is still a useful tool. Chapters 4 and 5, combined with the work of Hon *et al.* [1994a] span the entire pahoehoe lava flow. Perhaps the most surprising result from my work is the important role that the atmosphere plays at all time scales in the cooling of subaerial pahoehoe flows. I apply these results to extra-terrestrial lava flows as well as discuss future work in Chapter 6. Appendix C describes my initial attempt to investigate the rheology and dynamics of pahoehoe flow lobes. The results in Appendix C should be taken as an indication of what is now possible rather than as a completed investigation.

## CHAPTER 2: EMPLACEMENT OF THE 75-KM-LONG CARRIZOZO LAVA FLOW FIELD, SOUTH CENTRAL NEW MEXICO

LASZLO P. KESZTHELYI and DAVID C. PIERI

This chapter is essentially identical to the paper published in the *Journal of Volcanology and Geothermal Research*, 59: 59-75 (1993). Dr. Pieri (Earth and Space Science Division, Jet Propulsion Laboratory), had the airborne remote sensing data collected, suggested this problem to me, and provided invaluable discussions, especially regarding Mt. Etna. The rest of the work is my own.

### 2.0 Abstract

The Carrizozo lava flow field is a young, 75-km-long, compound tube-fed pahoehoe flow field located in south-central New Mexico. Topographic channeling, unusually low viscosity, and fissure vents are ruled out as possible explanations for the length of the flow field. Effusion rates are estimated using: (1) a Bingham plastic model; (2) correlations between flow morphology and effusion rate; and (3) comparison with Hawaiian pahoehoe flows. The Bingham plastic model placed no useful restrictions on the effusion rate, while empirical and theoretical correlations gave estimates between 300 and  $3 \times 10^5 \text{ m}^3 \text{ s}^{-1}$  for the effusion rate. The striking morphological similarity of the Carrizozo flow field to the compound tube-fed pahoehoe Kupaianaha flow field on Kilauea Volcano suggests an effusion rate of about  $5 \text{ m}^3 \text{ s}^{-1}$  and an eruption duration of nearly 3 decades. This long eruption duration and a long-lived lava tube system are interpreted to be the most important factors responsible for the length of the Carrizozo flow field. Furthermore, we conclude that the Bingham plastic model does not apply to tube-fed pahoehoe flow fields and that the correlation techniques grossly overestimate their effusion rates. This indicates that effusion rates may also have been overestimated for extra-terrestrial lava flows where it has not been possible to distinguish between pahoehoe and 'a'a.

## 2.1 Introduction

The 75-km-long Carrizozo lava flow field provides a valuable opportunity to examine the factors that produce long basaltic lava flows on the Earth and elsewhere. While investigating the factors responsible for the great length of the Carrizozo flow field, this paper also examines a variety of techniques used to determine effusion rate, eruption duration, and lava rheology from remote sensing data from inactive lava flows. Thus, in addition to understanding the emplacement of the Carrizozo flow field itself, we also wish to test the usefulness of these techniques in studying the emplacement of the several hundred kilometers long lava flows that are seen on Venus, the Moon, and Mars.

The Carrizozo flow field is particularly well suited for this study because of its great length, simple planimetric form, and well preserved primary morphology. Many lava flows of comparable length are less well suited. For example, the 160-km-long Undara flow in Queensland, Australia [Stephenson and Griffin, 1967] and the 103-km-long Tappen Wash flow in Arizona [M. Malin, *pers. comm.*, 1989] are extensively weathered and are confined by narrow river channels. In other cases, such as the 52-km-long 1859 Mauna Loa flow, the lava flows have ended in the sea and their total length is indeterminate.

The Quaternary Carrizozo flow field is located in the Tularosa Basin in south-central New Mexico (Fig. 2-1). Previous work on the flow field includes general description during geologic mapping [Allen, 1952; Weber, 1964; Smith, 1964], major- and trace-element analyses [Renault, 1970; Farris, 1980] and morphological description [Theilig, 1986]. The lavas are intermediate in composition between alkalic and tholeiitic basalts and are part of the volcanism associated with the Rio Grande rift [Renault, 1970]. The flow field has a maximum length of 75 km and a surface area of 330 km<sup>2</sup> [Allen, 1952].

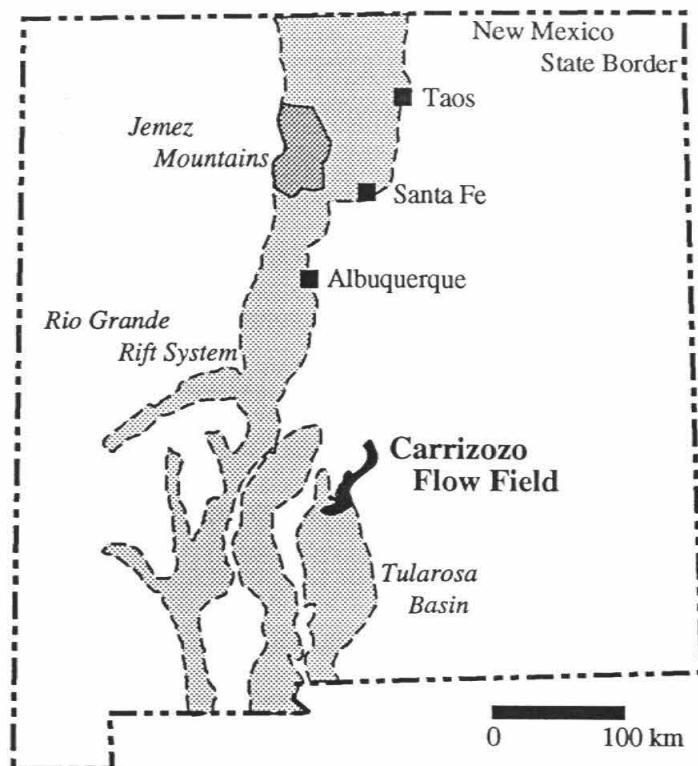


**Figure 2-1: Location of the Carrizozo flow field and the Tularosa Basin with respect to the Rio Grande Rift (after Clemons et al., 1982).**

Both airborne remote sensing and ground truth data were collected for this study. The Carrizozo flow field was overflown by NASA aircraft in May 1988 and September 1989 with the Thermal Infrared Multispectral Scanner (TIMS), NS-001 Landsat Thematic Mapper Simulator, and a Zeiss color photometric camera. The TIMS instrument has 6 channels covering the 8-13 micron wavelength region and a spatial resolution of 11-19 m/pixel [NASA-Ames Research Center, 1989]. The NS-001 instrument has 7 channels similar to the Landsat Thematic Mapper in the 0.45-2.3 micron region and an additional thermal infrared channel at 10.4-12.5 microns and a spatial resolution the same as that of TIMS [NASA-Ames Research Center, 1989]. The air photos provide stereoscopic coverage over the entire flow with sub-meter spatial resolution. Ground truth data consist

of four days of field work involving still photography, magnetometer surveys, and collecting rock samples.

## 2.2 Morphology of the Carrizozo flow field

The single most striking feature about the Carrizozo flow field is its 75 km length. It covers 330 km<sup>2</sup> to an estimated depth of 10-15 m, for a total erupted volume of about 4.3 km<sup>3</sup> [Allen, 1952]. The flow field is 1-5 km wide and runs down the center of the Tularosa Basin (Fig. 2-2). USGS 7.5' quadrangle topographic maps show that the nearly planar basin floor dips at an angle of 0.2 - 0.4° toward the south. For a fraction of its length, the Carrizozo flow field abuts the mountains at the edge of the basin. The flow field is also diverted around some local topographic highs, but has surrounded others, forming kipukas (islands) of the underlying sedimentary rocks. Overall, topography did not play a major role in the shape of the flow field except that most of the lava flowed directly down slope from the vent.

The only identifiable source for the Carrizozo flow field is the 27-m-tall Little Black Peak (Fig. 2-2). This small cone sits on the center of a 2-5 km diameter, 30-40 m high, topographic swell of the Carrizozo flow field. This swell has radiating flow patterns, suggesting a very shallow shield-like structure. Little Black Peak itself consists of 3 nested cinder cones and a frozen lava pond. There are no signs of a vent (*i.e.*, spatter ramparts, lava ponds, cinder cones, lava shields, or radiating flow patterns) anywhere else on the flow field. While it is impossible to rule out a fissure source during the earliest stages of the emplacement of the Carrizozo flow field, by the time the final lava surface was formed, the vent was concentrated at the northern end of the flow field.

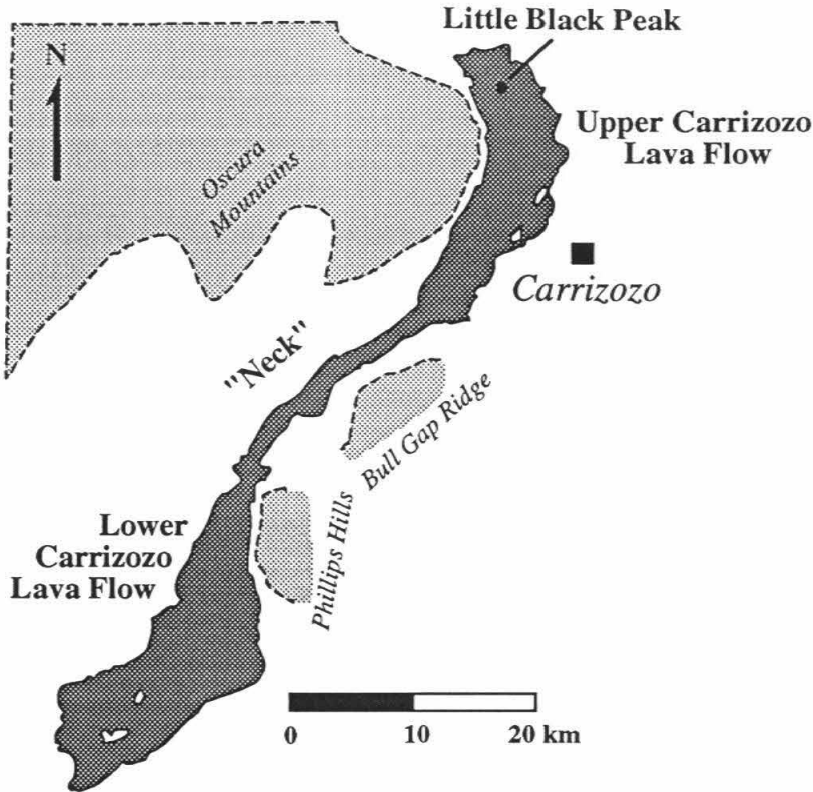


**Figure 2-2: Main physiographic sections of the Carrizozo flow field.** The flow field is topographically constrained only along the northern half of the western side of the Upper Carrizozo Lava Flow and the southeast side of the "neck" region.

The surface textures of the Carrizozo flow field show that it is a compound, tube-fed, pahoehoe flow field. At the 10-100 centimeter scale, the surface is built up of ropes, smooth sheets, and toes (Fig. 2-3a). At the 10-100 meter scale, the flow field consists of inflation features such as tumuli, pressure ridges, and lava-rise pits (Fig. 2-3b). Inflation features are diagnostic of tube-fed pahoehoe and form when relatively thin (<1 m thick) flows are inflated by continued injection of lava under the initial crust [Walker, 1991; Hon *et al.*, 1994a].

The air photos show several small patches of darker, rough areas that were initially suspected to be 'a'a. Ground observations of some of these patches found that they consist of slabby pahoehoe or broken-up tumuli. Given that the inflation features are typically 2-5

meters tall, it is clear that the flow field must be completely pahoehoe to at least 5 meters depth. While it is not possible to categorically reject the possibility of some 'a'a underneath the pahoehoe surface, it seems extremely unlikely that significant volumes of 'a'a lava are hidden without a trace.

Lava tubes capable of transporting the bulk of the erupted lava are expected in the Carrizozo flow field. Such tubes are common in large pahoehoe lava flows and may even be necessary for their formation [Greeley, 1987]. There is strong, but indirect, morphological evidence for a large lava tube in the narrow "neck" region just south of the end of the Upper Carrizozo Flow (Fig. 2-2). Careful examinations of the aerial photographs, ground observations, and a magnetometer survey have confirmed that the necking of the flow field is a primary feature and is not caused by either erosion, alluvial cover, or topographic constriction. The narrowness of the flow field in this region, with no concomitant increase in thickness, implies that lava was efficiently transported through this region to the apron of flows to the south. A large tube or channel with few spillovers would provide such an efficient transport mechanism. However, since no channel is seen, a major tube is favored. The long line of tumuli in this region is also very suggestive of a tube (Fig. 2-4). Similar features are commonly observed over Hawaiian tubes and can be part of the tube forming process [Kauahikaua *et al.*, 1990].

The morphologic features of the Carrizozo flow field suggest that it was built up of many small outpourings of lava both directly from the vent and from the tube system. The TIMS data support this suggestion. TIMS has consistently demonstrated an ability to distinguish different lithologies in various geologic environments [*e.g.*, Kahle and Rowan, 1980; Gillespie *et al.*, 1984; Lang *et al.*, 1987] and the ability to separate basaltic lava flows on the basis of age and surface textures [Kahle *et al.*, 1988; Realmuto *et al.*, 1992]. Spectra from the processed TIMS data clearly distinguish the major lithologies in the Carrizozo area (Fig. 2-5a). However, the spectra do not show distinguishable flow units within the Carrizozo flow field itself. Instead of any systematic spatial variation, the

spectra show slight variations among 100 pixel scale patches (Fig. 2-5b). This generally homogeneous (albeit mottled) TIMS image leads us to conclude that there are no strong compositional or age contrasts exposed. Clearly, some of the observed variations in the spectra are caused by inhomogeneities in the scattered vegetation and eolian material trapped in the cracks in the lava. However, the spectra are also consistent with the patchwork of slightly different age and composition lavas expected from a single long-lived eruption.



**Figure 2-3a** Photograph of the surface of the Carrizozo flow field.

Photograph from the top of a 4 m tall tumulus. Note large ropes and individual pahoehoe toes at the center of the picture. Pole is 2 m long.



**Figure 2-3b: Aerial photograph of the surface of the Carrizozo flow field.**

Medium altitude vertical aerial photograph of the northern Carrizozo flow field from NASA C-130. The mottled topography evident in the photo is caused by inflation features such as tumuli, lava-rise pits, and pressure ridges.

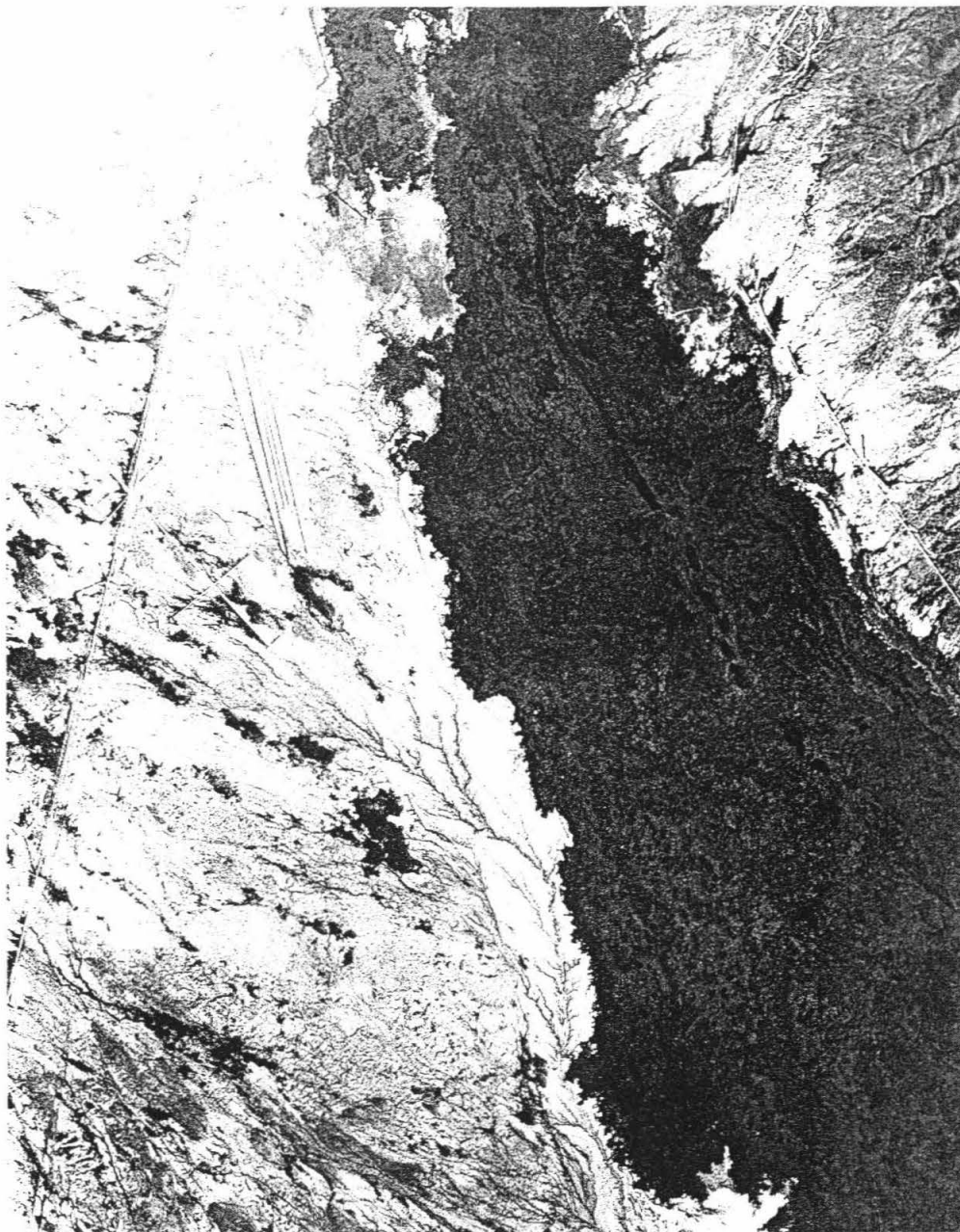


**Figure 2-4:** Aerial photograph showing the long, linear tumuli overlying the inferred lava tube in the neck region of the Carrizozo flow field. The runway to the left of the lava flow is about 1 km long and oriented toward  $010^{\circ}$ . The discontinuous dark linear feature in the center of the lava flow is a line of large tumuli which are very suggestive of a lava tube underneath them.

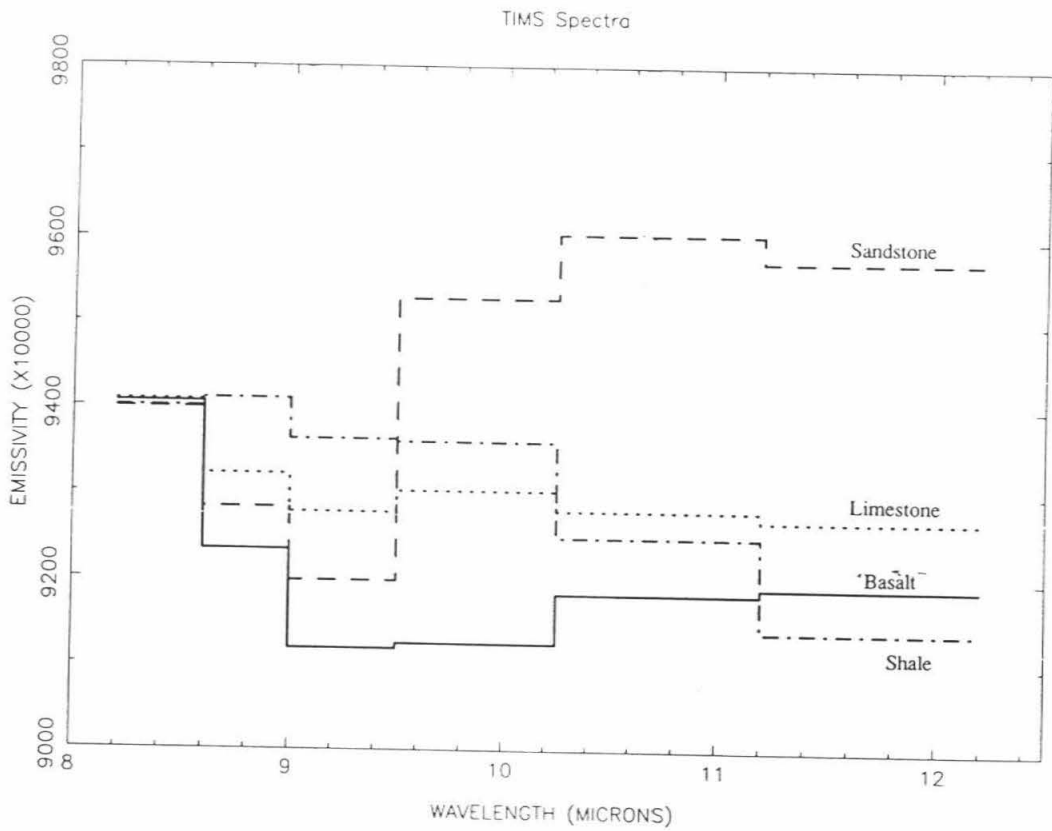


**Figure 2-5a: TIMS data from around the Carrizozo flow field.** TIMS spectra from different lithologies in the Carrizozo area. These spectra show that TIMS very clearly distinguishes the major lithologies it observed in this flight.

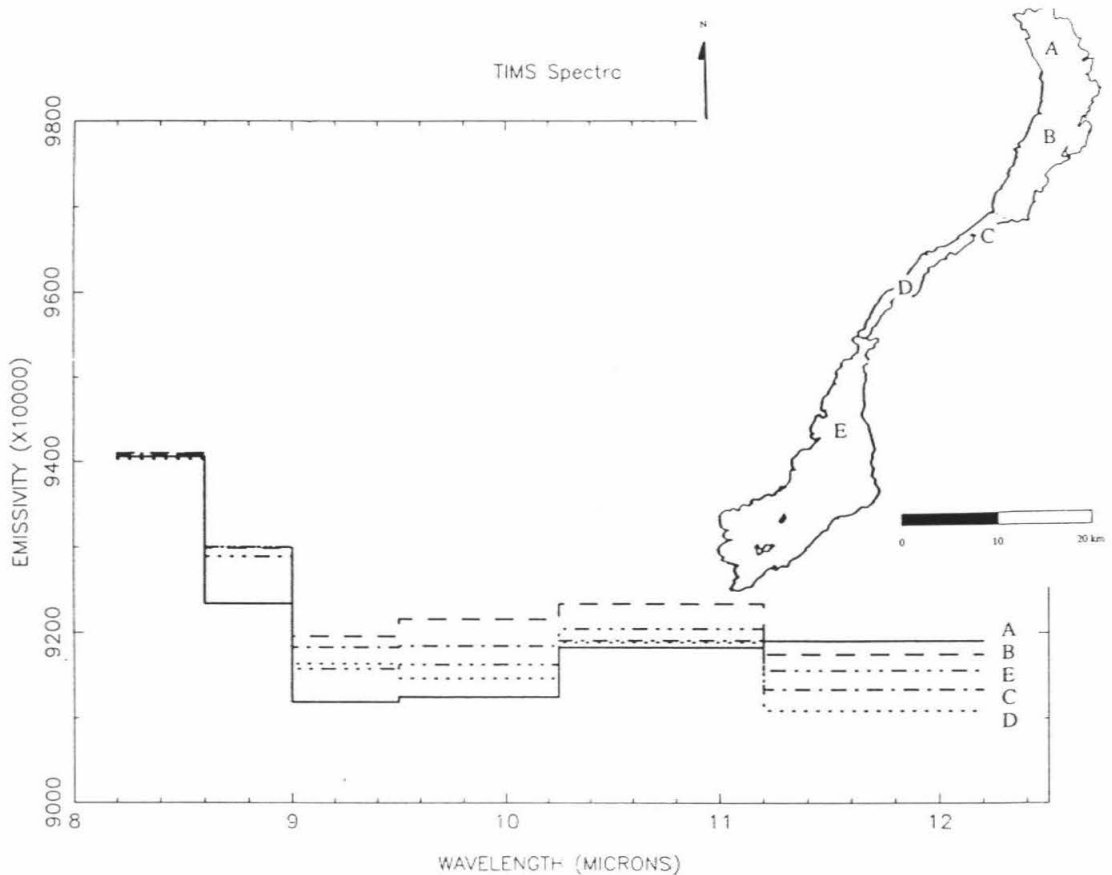


**Figure 2-5b: TIMS data from the Carrizozo flow field.** Examples of TIMS spectra from parts of the Carrizozo Flow Field and location map for the spectra. Each plotted spectrum represents the average over an approximately 20 pixel x 20 pixel area. The spectra show no systematic variation with distance from the vent or between the Upper and Lower Carrizozo Flows. These data are consistent with a patchwork of lavas of slightly different compositions and ages. However, the scattered vegetation and eolian cover also contribute to the variations in the spectra.

### 2.3 Estimate of the rheology of the Carrizozo lava

Estimating the rheology of the Carrizozo lava is an important first step in understanding its emplacement. In general, lower viscosity lavas (such as basalts) tend to form longer lava flows than more viscous lavas (such as andesites or rhyolites). Unusually low viscosity in basaltic melts can be caused by a number of factors such as: (1) high dissolved water content; (2) unusual major element composition (*e.g.*, high titanium or alkali content); and (3) high temperature. The chemical analyses (Table 2-1) and rock samples show no unusual bulk chemistry, vesicularity, crystal content, mineralogy, or mineral textures when compared to other basaltic lava flows.

**Table 2-1: Bulk Chemistry of Carrizozo and Kilauea lavas.**

Oxide	Lower Carrizozo Flow		Upper Carrizozo Flow		Kilauea
	Wt.%	standard dev.	Wt.%	standard dev.	Wt.%
SiO <sub>2</sub>	49.85	0.86	51.60	0.86	50.40
Al <sub>2</sub> O <sub>3</sub>	16.84	0.40	17.21	0.54	12.90
FeO*	9.71	0.18	9.66	0.31	11.50
MgO	6.83	0.44	6.30	0.53	8.92
CaO	8.77	0.29	8.26	0.11	10.90
Na <sub>2</sub> O	3.51	0.19	3.71	0.15	2.17
K <sub>2</sub> O	1.38	0.13	1.28	0.18	0.40
TiO <sub>2</sub>	1.75	0.09	1.71	0.07	2.43
MnO	0.16	0.01	0.15	0.01	0.17
Total	98.80		99.88		99.79

\* all Fe reported as FeO

Standard deviations based on 11 samples for the Lower Carrizozo Flow, 7 samples for the Upper Carrizozo Flow [Renault, 1970]. The Kilauea composition is for a typical sample from the Kupaianaha flow field [M. Mangan, USGS, HVO, *personal communication*]

The mineral texture of a lava provides some information about its initial temperature and cooling rate. The Carrizozo lava flows contain coarse-medium grained subhedral phenocrysts of olivine and plagioclase within a glassy to microcrystalline groundmass. The near vent sample that is interpreted to best record the initial lava contains 5.5 vol.% olivine phenocrysts, 4.9 vol.% plagioclase phenocrysts, 18.6 vol.% vesicles, and 71.0 vol.% glass. Modes were obtained by point counts on thin sections. Other samples collected along the length of the flow field contain more fine-grained plagioclase (up to 30 vol.%) but show no significant variation with distance from the vent. This observation is consistent with the Carrizozo flow field being fed by insulating lava tubes.

Lofgren [1983] conducted an extensive set of experiments on basalts from further north in the Rio Grande rift in order to derive quantitative information from their mineral textures. The composition of the lavas used in his study are similar to that of the Carrizozo lava. He finds that both plagioclase and olivine are on the liquidus below 1187 °C and pyroxene would come in at 1133 °C. This suggests that the Carrizozo lava was erupted between these temperatures. Furthermore, Lofgren [1983] reports that the intersertal texture and the absence of pyroxene that we observe in the Carrizozo samples develops when the lava is cooled at 2-5 °C/hr. Kouchi *et al.* [1986] suggest that intersertal texture is indicative of crystallization without vigorous stirring. While some samples of the Carrizozo lava have pilotaxitic textures with the plagioclase showing flow alignment, we interpret the largely intersertal texture of the Carrizozo lava to indicate that it was emplaced at low velocities and strain rates.

There is no direct measurement of the composition or abundance of volatiles in the Carrizozo lava. However, a magma with a high initial volatile content would be expected to de-gas on ascent and produce observable pyroclastic constructs (*e.g.*, tephra fields, cinder cones, spatter ramparts) around the vent. The only pyroclastic materials on the flow field are the small cinder cones at Little Black Peak. This limited explosive activity and the low vesicularity of the Carrizozo lava suggests a low volatile content in the erupting

magma. Thus the water content of the Carrizozo lava should not have led to it having an unusually low viscosity.

Our first estimate of the viscosity of the Carrizozo lava is made using two laboratory derived empirical formulae [Bottinga and Weill, 1972; Shaw, 1972] and bulk-rock major-element analyses [Renault, 1970]. The estimated viscosities are similar for both sets of calculations but Shaw's technique is easier to extrapolate down to typical lava temperatures. The laboratory experiments were conducted at super-liquidus temperatures while eruption temperatures are usually sub-liquidus. Chill margins, vesicles, crystals, and non-Newtonian effects combine to raise the effective viscosity of real lava flows [Shaw, 1969; Murase and McBirney, 1973; McBirney and Murase, 1984; Ryerson *et al.*, 1988; Pinkerton and Stevenson, 1992]. At the crystallinity of the initial Carrizozo lava it is appropriate to use the Einstein-Roscoe equation to correct for the effect of the crystals on the lava viscosity [Pinkerton and Stevenson, 1992]. The Einstein-Roscoe equation is given by

$$\eta_e = \eta_m (1-R\phi)^{-2.5}$$

where  $\eta_e$  is the effective viscosity of the liquid crystal mixture,  $\eta_m$  is the viscosity of the pure melt,  $R$  is a constant, and  $\phi$  is the crystallinity of the liquid [Roscoe, 1952]. Using the recommended value for  $R$  of 1.67 [Pinkerton and Stevenson, 1992] and the 10 vol.% crystals observed in the initial Carrizozo lava, we find that the crystals would increase viscosity by a factor of 1.6. The effect of vesicles on the viscosity of lavas is not certain, but Shimozuru [1978] would suggest that the effect of the 15-20% vesicularity of the Carrizozo lava would be insignificant. Thus our best estimate for the viscosity of the Carrizozo lava is 54 - 160 Pa s.

**Table 2-2: Comparison of calculated viscosities of the Carrizozo lava with a Kilauea and an Etna lava.**

	Carrizozo		Kilauea	Etna
Crystallinity (vol%)	10.4		0.5	not provided
Vesicularity (vol%)	18.6		60	not provided
Temperature (°C)	1130	1180	1170	1070
Calculated Viscosity (Pa s)	96-160	54-110	42	630-890

The Kilauea lava is the same Kupaianaha sample as in Table 2-1 and the Etna lava is from the 1989 eruption. The viscosities of the Carrizozo and Kilauea lava were calculated using Shaw [1972], corrected for crystallinity [Pinkerton and Stevenson, 1992] and vesicularity [Shimozuru, 1978]. Range of viscosities for the Carrizozo lava comes from the compositional range of the Carrizozo samples and from the uncertainty in the water content. Water content was assumed to be between zero and the average water content of Kilauea basalts (0.3 wt.% [Greenland, 1987]). Viscosity of Etna lava from Bertagnini *et al.* [1990] was calculated in a similar fashion. These calculations suggest that the Carrizozo lavas were only slightly more viscous than the Kilauea lava.

Similar calculations for a Kilauea lava and an Etna lava are shown in Table 6-2. This comparison suggests that the viscosity of the Carrizozo lava was between that of the lavas from Hawaii and Etna, but more akin to Hawaiian lavas. It is also important to note that the calculated viscosity for the Kilauea lava (42 Pa s) is somewhat lower than those obtained from direct observations of Kilauea lavas: 50-800 Pa s from lava lakes [Shaw *et al.*, 1968],  $0.2-8.2 \times 10^6$  Pa s from 'a'a flows [Fink and Zimbelman, 1986], and 85-140 Pa s from channelized pahoehoe [Heslop *et al.*, 1989]. Nevertheless, the calculated viscosities should be useful for comparing the relative viscosities of the different lavas.

The simplest, and only widely used, rheological model that attempts to account for the non-Newtonian behavior of lavas is the Bingham plastic model [Hulme, 1974]. This

model introduces a yield strength which must be overcome before the fluid flows as a Newtonian fluid. Assuming a Bingham Plastic rheology, it is possible to retrieve a lava flow's yield strength from its final dimensions. Two of the methods described in Moore *et al.* [1978] were used:

$$\sigma_y = \rho g H^2 / W \quad (2.1)$$

and

$$\sigma_y = \rho g H \sin(\alpha) \quad (2.2)$$

where  $\sigma_y$  is the yield strength,  $\rho$  the density,  $g$  the gravitational acceleration,  $\alpha$  the slope on which the flow stopped,  $H$  the flow height, and  $W$  the flow width. Values of  $2300 \text{ kg/m}^3$  for  $\rho$  and  $9.8 \text{ m/s}^2$  for  $g$  were used. The value for the density of the melt was derived from Lange and Carmichael [1987] and 15% vesicularity. The flow height for the Carrizozo flow field varies from 10 to 15 meters and the width from 1 to 5 km. The slope at the southern end of the flow field is about  $0.2^\circ$ . The resulting yield strengths range from 450 - 5100 Pa from equation (2.1) and 790 - 1200 Pa from equation (2.2). These fall within the range of values reported for Kilauea basalts: 70-120 Pa [Shaw *et al.*, 1968], 300-11,000 Pa [Moore *et al.*, 1978] and 1500 - 50,000 Pa [Fink and Zimbelman, 1986].

It will be pointed out later that it is not appropriate to use this Bingham plastic model for pahoehoe lava flows which shows signs of inflation. However, the above calculations do show that the Carrizozo lava was not radically different from other basaltic lava flows. Combining this with the fact that there is nothing unusual about the chemistry or petrography of these lavas, it seems reasonable to rule out unusual rheology as a factor in the length of the Carrizozo flow field.

#### 2.4 Comparison with the 1986-1992 Kupaianaha flow field

Further insights can be gained by comparing the Carrizozo flow field with similar flow fields whose emplacement styles are known. By far the most closely studied example of a large tube-fed pahoehoe flow field is the Kupaianaha flow field on Hawaii. The Kupaianaha flow field was formed between July 20, 1986 and February 6, 1992 by Episode 48 of the Pu'u 'O'o - Kupaianaha eruption of Kilauea Volcano. This flow field has a subaerial length of 11 km and has covered 41 km<sup>2</sup> of land with about 0.5 km<sup>3</sup> of lava [T. Mattox, USGS, HVO, *pers. comm.*, 1993]. While no other lava flow is as well suited for comparison to the Carrizozo flow field, other long pahoehoe flow fields, such as the 1619-1629 pahoehoe eruption of Mount Etna [Chester *et al.*, 1985], also support the following conclusions.

Except for the inhospitable vegetation and slight weathering on the Carrizozo flow field, the surfaces of the two flow fields are essentially indistinguishable. The Kupaianaha flow field exhibits the same convoluted stacking of small toes with larger smooth and ropy sheets (Fig. 2-6a). Both flow fields exhibit the same inflation features (tumuli, pressure ridges, and lava-rise pits) (Fig. 2-6b) though some of those on the Carrizozo flow field are larger than those seen on the Kupaianaha flow field. It is noteworthy that the largest inflation features on the Hawaiian flow field formed on the coastal flats where slope angles are similar to those of the Tularosa Basin. The Kupaianaha flow field was fed by several major tube systems, some of which survived for well over a year [Heliker and Wright, 1991].

Because of the morphological similarities between the two flow fields, we expect that they were emplaced in similar fashions. Direct measurements of the effusion rate feeding the Kupaianaha flow field are somewhat sparse but indicate an average effusion rate of 3.5 m<sup>3</sup> s<sup>-1</sup> (dense rock equivalent) [Jackson *et al.*, 1988]. During times of sustained activity, the lava inundated land at a rate of 3.5x10<sup>4</sup> m<sup>2</sup>/day [Mattox *et al.*, 1993]. The eruption had 12 pauses lasting from 1 to 4 days [Heliker *et al.*, 1991]. Some



**Figure 2-6a: Photograph of the surface of the Kupaianaha flow field.**

Photograph from the surface of the flow field. Note the jagged tumulus on the skyline, large ropes, and smooth pahoehoe lobes. Photo courtesy of USGS.

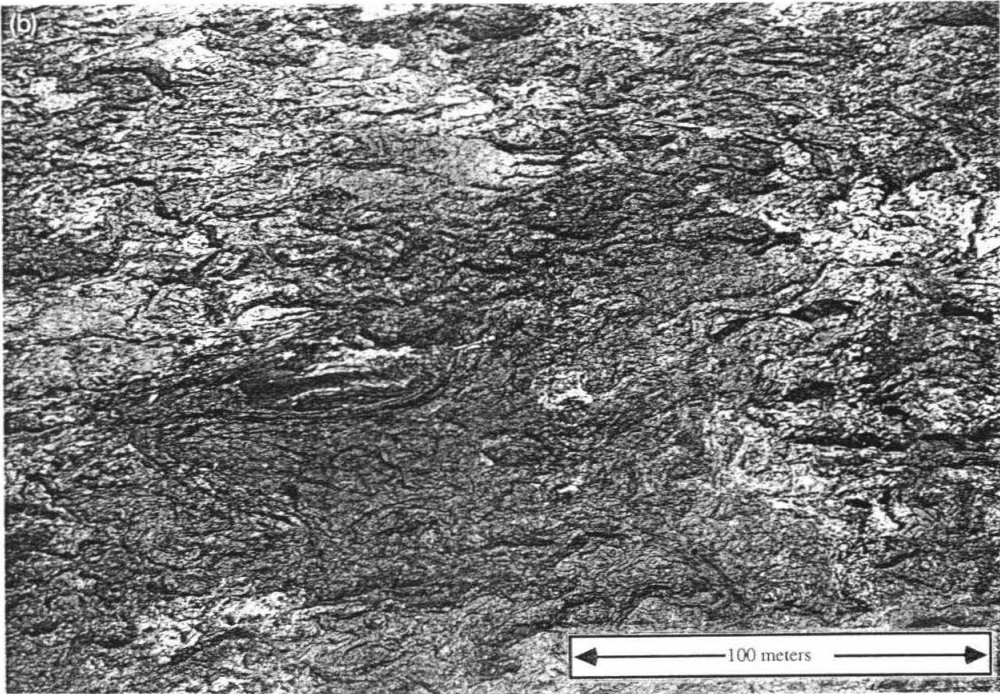


**Figure 2-6b:** Aerial photograph of the surface of the Kupaianaha flow field. Low altitude oblique of the Kupaianaha flow field. Surface is mottled by tumuli, pressure ridges, and lava-rise pits. (Note helicopter in center for scale.) Also note the similarity to the Carrizozo flow field (Fig. 2-4a,b). Photo courtesy of USGS.

of these pauses were long enough to allow the main tube system to degrade to the point that it could not be fully reoccupied when activity resumed [Kauahikaua *et al.*, 1990; Mattox *et al.*, 1993]. We conclude that the Carrizozo flow field was emplaced in a similar steady, long-duration, low effusion rate eruption.

## 2.5 Quantitative estimates of emplacement parameters

Given this qualitative understanding of the emplacement of the Carrizozo flow field, a more quantitative analysis is now attempted. So far we have rejected unusual rheology, topographic channeling, multiple vents, a long fissure vent, and steep slopes as possible explanations for the length of the Carrizozo flow field. Next we apply a number of published techniques relating lava flow dimensions to eruption characteristics. These techniques have typically been used for both pahoehoe and 'a'a flows. In the following, we demonstrate that caution should be used when applying these techniques without careful evaluation of the flow morphology.

Hulme [1974] modeled lava as a Bingham plastic fluid and calculated the flux of lava through a cross-section of a flow. For a Bingham plastic fluid flowing down an inclined plane

$$\Psi = \langle v \rangle WH$$

$$\langle v \rangle = [\sigma_y H_c^2 / (3\eta H)] [(H/H_c)^3 - (3/2)(H/H_c)^2 + 1/2]$$

$$H_c = \sigma_y / (\rho g \sin(\alpha))$$

where  $\Psi$  is the volumetric effusion rate,  $\langle v \rangle$  is the average velocity of the flow,  $H_c$  is the thickness of the undefining plug,  $\eta$  is the kinematic viscosity,  $\alpha$  is the slope of the plane, and the other terms are defined as in equations (2.1) and (2.2) [Hulme, 1974; Dragoni *et al.*, 1986].

The results are presented in Table 2-3. They show that this simple Bingham plastic model places no useful constraints on the emplacement of the Carrizozo flow field. It

allows one to conclude that either the Carrizozo lavas should not have been able to flow or that the average flow velocity was more than 100 m/s or anything in between.

**Table 2-3: Results from the simple Bingham plastic model.**

	Maximum for $\Psi$	Best Estimate for $\Psi$	Minimum for $\Psi$
Flow height (H)	15 m	12m	10m
Flow width (W)	5 km	2 km	1 km
Viscosity ( $\eta$ )	60 Pa s	150 Pa s	160 Pa s
Yield strength ( $\sigma_y$ )	800 Pa	1000 Pa	1200 Pa
Slope ( $\alpha$ )	0.4°	0.3°	0.2°
Average velocity ( $\langle v \rangle$ )	100 m/s	4.5 m/s	0 m/s
Effusion rate ( $\Psi$ )	$8 \times 10^6 \text{ m}^3/\text{s}$	$1 \times 10^5 \text{ m}^3/\text{s}$	$0 \text{ m}^3/\text{s}$

Results show the enormous range of flow velocities and effusion rates allowed by the uncertainty in input parameters. Even though the result for the best estimate for effusion rate seems plausible, we conclude that this model provides no useful constraints on the emplacement of the Carrizozo flow field. Other inputs into the model are  $2300 \text{ kg/m}^3$  for density and  $9.8 \text{ m/s}^2$  for gravitational acceleration.

It is worthwhile to examine why the Bingham plastic model fails when applied to the Carrizozo flow field. The problem is greater than can be explained by the previously described difficulties in determining the actual viscosity of the lava. The uncertainties in  $\sigma_y$  and  $\alpha$  have the greatest effect on the calculated effusion rate. Given the low slopes of the floor of the Tularosa Basin, small errors in the value of the slope will cause large errors in the estimated effusion rate.

Two factors make the estimate of yield strength for the Carrizozo lavas highly suspect. First, the errors in estimating the slope also affect the values for  $\sigma_y$  determined by

equation (2.2). Second, the Carrizozo flow field exhibits abundant inflation features. These features suggest that the thickness of the flow field has increased, perhaps even by a factor of 5 - 10, since the time the lava initially flowed down the slope. Such inflation was routinely observed on the Kupaianaha flow field in Hawaii [Hon *et al.*, 1994a]. Inflation affects the estimates derived from both equations (2.1) and (2.2).

Having determined the unsuitability of the Bingham plastic model, a number of published empirical correlations between eruption characteristics and flow dimensions are used. Walker [1973] challenged the long-held assumption that viscosity controlled the length of lava flows and argued instead that effusion rate was the single most important factor. Using his plot of flow length versus average effusion rate, one would estimate that the Carrizozo flow field was fed by an eruption with an effusion rate of about  $2000 \text{ m}^3 \text{ s}^{-1}$ . Malin [1980] investigated the apparent correlation between flow length and effusion rate proposed by Walker [1973] and suggested that there was a better correlation between flow length and total erupted volume. Malin's plots would suggest a flow volume of  $0.4 \text{ km}^3$  for a 75-km-long lava flow. This is an order of magnitude less than the actual volume of the Carrizozo flow field. Pieri and Baloga [1986] suggested that the correlation is improved if one plots planimetric area instead of length against effusion rate. Their work showed that the  $\Psi/A$  ratio varied greatly from volcano to volcano but was reasonably consistent for a given edifice. Also, in the lava flows examined, the ratio remained between 1 and  $120 (\text{m}^3 \text{ s}^{-1})/\text{km}^2$ . Thus one would expect an effusion rate between 300 and  $4 \times 10^4 \text{ m}^3 \text{ s}^{-1}$  for the Carrizozo flow field which covers  $330 \text{ km}^2$ .

Given the likelihood that no single parameter controls the lengths of lava flows, several more sophisticated, but purely empirical, correlations between morphology and eruption characteristics have been developed [Kilburn and Lopes, 1991; Pinkerton and Wilson, 1992; Pinkerton and Wilson, in press] Unfortunately, only the correlation described in Kilburn and Lopes [1991] does not require information gathered while the flow is active. They obtain the formula

$$b\kappa\tau = W_{\max} H^2 \sin(\alpha) / L_{\max}$$

where  $\kappa$  is the thermal diffusivity,  $H$  is the thickness of the flow,  $W_{\max}$  and  $L_{\max}$  are the maximum width and length respectively,  $b$  is a non-dimensional number equal to 3 for flows with  $H \ll W$ , and  $\tau$  is the emplacement time. Using  $0.3^\circ$  for the slope, 5 km for  $W_{\max}$ , 75 km for  $L_{\max}$ ,  $7 \times 10^{-7} \text{ m}^2 \text{ s}^{-1}$  for  $\kappa$ , and 10-15 m for  $H$ , this formula produces an eruption duration of less than a day and an effusion rate of  $1 \times 10^5 - 3 \times 10^5 \text{ m}^3 \text{ s}^{-1}$ . The caveat for this estimate is that this correlation was developed specifically for simple (single lobe) 'a'a flows while the Carrizozo flow field is both compound and pahoehoe.

Another simple correlation, derived from the assumption that conductive cooling stops lava flows, is called the Grätz number correlation. The dimensionless Grätz number is defined as

$$G_z = \Psi H / (\kappa L W)$$

where  $\Psi$  is the volumetric effusion rate, and  $H$ ,  $L$ , and  $W$  are the height, length and width of the flow. It has been empirically observed that lava flows stop when the  $G_z$  is about 300 [Walker, 1973]. Thus, using  $7 \times 10^{-7} \text{ m}^2 \text{ s}^{-1}$  for  $\kappa$ , 10-15 m for  $H$ , and 1-5 km for  $W$ , an effusion rate of 1000-8000  $\text{m}^3 \text{ s}^{-1}$  is obtained.

The Grätz number correlation can be improved by using the theoretical channel width calculated from the Bingham plastic model in place of the actual width of the lava flow [Wilson and Head, 1983]. The resulting expression is

$$L = Q^{2/3} (\sin(\alpha))^{2/3} H (\sigma_y / \eta)^{1/3} / [24^{1/3} G_z \kappa] \quad (2.3)$$

where  $\sigma_y$  is the yield strength and  $\eta$  is the viscosity of the lava [Pinkerton and Wilson, 1988]. Pinkerton and Wilson [1988] cite field measurements suggesting that  $\sigma_y / \eta$  remains

between 0.2 and 0.6 s<sup>-1</sup> for basaltic flows. Using the same input values as before, the resulting effusion rates are 1300 - 4200 m<sup>3</sup> s<sup>-1</sup>.

Expressions have also been derived for the case that a lava flow's length is limited by the volume of the eruption [Guest, *et al.*, 1987; Pinkerton and Wilson, 1988; Pinkerton and Wilson, 1992]. These flows should obey the following expression:

$$L = \Psi^{2/3} \tau (\sin(\alpha))^{2/3} (\sigma_y/\eta)^{1/3} / [24^{1/3} H] \quad (2.4)$$

where  $\tau$  is the emplacement time [Pinkerton and Wilson, 1988]. Since the total volume of the lava flow (V) equals the product of the effusion rate and eruption duration,

$$L = V (\sin(\alpha))^{2/3} \tau (\sigma_y/\eta)^{1/3} / [24^{1/3} \Psi^{1/3} H]$$

and

$$\Psi = (1/24) (V/LH)^3 (\sin(\alpha))^2 (\sigma_y/\eta)$$

Using 0.3° for  $\alpha$ , 0.2-0.6 for  $\sigma_y/\eta$ , 4.3 km<sup>3</sup> for V, 75 km for L, and 10-15 m for H yields effusion rates between 1.2 x 10<sup>4</sup> and 1.3 x 10<sup>5</sup> m<sup>3</sup> s<sup>-1</sup>. Again, caution must be used because both (2.3) and (2.4) were derived from the consideration of channelized flows, not tube-fed lava flows.

Even more sophisticated mathematical models have been produced for channelized flows [Pinkerton and Wilson, in press]. However applying these to tube-fed flows completely violates key assumptions of the models. Ignoring these violations again results in unreasonably high effusion rates. Thus, we find that none of the quantitative techniques for estimating flow emplacement characteristics produce values for the Carrizozo flow field that are consistent with the simple morphological comparison to the Kupaianaha flow field.

## 2.6 Discussion

This study has highlighted some of the difficulties in deciphering the emplacement of lava flows, especially compound tube-fed pahoehoe flow fields. For example, it was not possible to determine the input parameters for the Bingham plastic model with sufficient accuracy for the model to be of any practical use. This was despite high resolution aerial photographs, observations from the ground, detailed chemical analyses, and good topographic maps. In any case, the Bingham plastic model is probably not valid for lava flows such as the Carrizozo and Kupaianaha flow fields which have abundant inflation features. This is because the final flow thickness bears little resemblance to the thickness of the active flow lobes. The Bingham model should work better for simple (single lobe) 'a'a flows.

Our work also demonstrates that the existing empirical and theoretical correlations between flow morphology and effusion rate grossly overestimate the effusion rate for the Carrizozo flow field. These methods for estimating effusion rates from flow dimensions produce a range of values ( $300\text{--}3 \times 10^5 \text{ m}^3 \text{ s}^{-1}$ ) for the Carrizozo flow field. This translates to eruption durations between 4 hours and nearly half a year. These high effusion rates are not consistent with the pahoehoe surface of the Carrizozo flow field. In Hawaii, it has been observed that 'a'a flows are produced by eruptions with effusion rates over  $15 \text{ m}^3 \text{ s}^{-1}$  (or average flow velocities above 35 m/hr) [Rowland and Walker, 1990]. Since the Carrizozo lavas were probably marginally more viscous than the Hawaiian lavas, the transition to 'a'a should have taken place at marginally lower effusion rates [Peterson and Tilling, 1980]. Given the differences in their styles of cooling and motion, it may be unreasonable to expect one correlation between flow dimensions and eruption style to hold for both 'a'a and pahoehoe lava flows.

Our work on the Carrizozo flow field seems to underline the importance of identifying a lava flow as a simple (*i.e.*, single lobe) 'a'a flow before existing techniques can be used with confidence. This casts some doubt on the high effusion rates estimated

for large lava flows such as continental flood basalts and long extra-terrestrial lava flows. Overestimating effusion rates by one or more orders of magnitude may lead to erroneous conclusions about possible climatic impacts of the eruptions and the nature of the source region for the lavas.

If one accepts the Kupaianaha eruption as a model, an emplacement history for the Carrizozo flow field can be hypothesized (Figure 2-7). Using an effusion rate of  $5 \text{ m}^3 \text{ s}^{-1}$  (including vesicles), it would take 27 years to erupt the  $4.3 \text{ km}^3$  of the Carrizozo flow field. Using the  $3.5 \times 10^4 \text{ m}^2/\text{day}$  rate of surface coverage implies an eruption duration of 26 years. This suggests that the single most important factor in the great length of the Carrizozo flow field was an exceptionally long eruption duration. The suggestion of an inverse correlation between long duration and effusion rate is supported by the behavior of pahoehoe lavas on Mount Etna. There, for instance, the 1614-1624 eruption produced a large (approximately  $36 \text{ km}^2$ ) pahoehoe flow field on the north slope of the volcano, distinguished by large tumuli and lava tubes [Chester *et al.*, 1985]. The average effusion rate for this 10-year eruption was about  $4.5 \text{ m}^3 \text{ s}^{-1}$ .

A long eruption duration in itself is probably not sufficient to produce a long pahoehoe lava flow. In addition, we believe that a long lava tube system must be maintained throughout most of the eruption. This suggestion is supported by the general observation that most large pahoehoe flow fields contain large lava tubes. It has been observed that fluctuating effusion rates inhibit lava tube formation [Greeley, 1987]. A long pause, or a sustained drop in effusion rate, allows the tube to cool off, making it difficult to re-occupy when the eruption resumes [Mattox *et al.*, 1993]. A significant increase in the effusion rate would cause large breakouts from the tube which could permanently divert the lava from the tube. Therefore, the long eruption must also be reasonably steady and continuous to produce an unusually long flow. Such an observation may have some implications with regard to the regional tectonics.

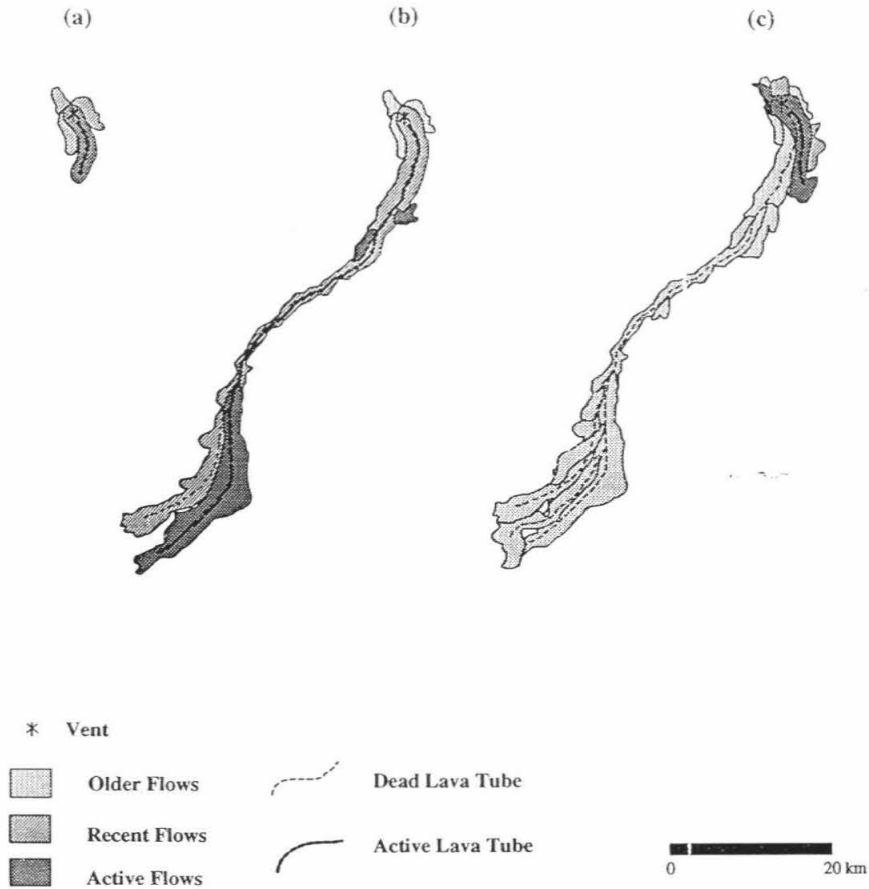


**Figure 2-7: Hypothetical emplacement history of the Carrizozo flow field based on the Kupaianaha flow field.** (a) The initial eruption was probably centered around the present location of Little Black Peak. Lava flows may have attempted to advance in all directions from the source, but found motion down the shallow slope preferable. (b) For some length of time a large, stable, tube system developed through the narrow "neck" region of the flow field. This tube fed a series of sub-parallel, abutting flows to the south. (c) At some later point in time, this tube system broke down (possibly due to a longer pause in the eruption) and further flows built up around Little Black Peak, producing the topographic swell and radiating flow patterns observed in the present flow surface.

Part of our current research is focused on understanding the conditions under which a lava tube can be maintained for a time scale of years to decades. Further research in this area may allow narrow bounds to be placed on the flux of lava through a long-lived lava tube. We are also planning further work to examine the formation of inflation features. The identification of the 1-100 meter scale inflation features is important, because they are diagnostic of pahoehoe and because they invalidate the use of simple Bingham plastic flow models. There are hints of pressure ridges, tumuli, and other inflation features on Mars [Theilig and Greeley, 1986]. In late 1993, the Mars Observer Camera will begin returning images approaching 1.5 m/pixel resolution. These images hold out the possibility of positively identifying some Martian flow fields as pahoehoe and permitting more realistic constraints to be placed on their effusion rates.

## **2.7 Conclusions**

The Carrizozo flow field was most probably emplaced by a 2-3 decade-long, steady, low effusion rate eruption. The single most important factor governing the length of the flow field appears to have been the long, undisturbed eruption duration. This provides a counter-example to the notion that long lava flows require high effusion rates. This raises questions about the high effusion rates estimated for the continental flood basalts and long extra-terrestrial lava flows.

Present models for lava flows and empirical correlations between flow dimensions and effusion rate are only reliable when applied to simple 'a'a flows. This suggests caution in the use of these techniques where it has not been possible to determine whether a lava flow is pahoehoe or 'a'a. This also indicates the need for further research on the emplacement mechanisms of pahoehoe lava flows.

## CHAPTER 3: CALCULATED EFFECT OF VESICLES ON THE THERMAL PROPERTIES OF COOLING BASALTIC LAVA FLOWS

### 3.0 Abstract

This chapter is essentially identical to a single author paper that I have in press with the Journal of Volcanology and Geothermal Research. These results lay some important groundwork for the next chapter: the modeling of the cooling of pahoehoe flow lobes.

In this chapter, I investigate the effects of porosity, in the form of vesicles and bubbles, on the transfer of heat within basaltic lava. This study was undertaken to provide input for realistic cooling models of basaltic lava flows and to help explain some recent field measurements by Jones [1992, 1993]. These field observations indicate that the surfaces of vesicular pahoehoe flows cool significantly more rapidly than that of dense flows. It has been suggested that thermal radiation across vesicles is responsible for this enhanced cooling rate.

It is shown here that, for vesicles in typical pahoehoe flows, radiation across vesicles may enhance the effective thermal conductivity and thermal diffusivity, but only at high temperatures ( $T > 800^{\circ}\text{C}$ ) and high vesicularities ( $\phi > 40\%$ ). It is also found that convection of the gas phase within bubbles will not occur unless the cavities are larger than about 1 cm. Furthermore, previous work has demonstrated that porosity greatly reduces the thermal conductivity and thermal inertia of cold lava. It is shown here that this should also be true at high temperatures.

Examining only radiation across vesicles severely understates the effect of porosity on the cooling of the surface of lava flows. Thermal inertia, developed to describe diurnal surface temperature variations, is the most appropriate thermal parameter in this case. Thermal inertia is a measure of how quickly surface temperature responds to heating or cooling, with low thermal inertia materials responding more quickly. It is shown here that

porosity greatly reduces thermal inertia at all temperatures and that this provides a more general explanation for the field observation.

### 3.1 Introduction

The main goal of this chapter is to estimate the effect of vesicles and bubbles on the thermal properties of basaltic lava in order to (1) interpret recent observations of the effect of porosity on the cooling of pahoehoe flow lobes and (2) provide an input for more realistic thermal models for lava flows, especially pahoehoe flow lobes.

Recent field data from the Pu'u 'O'o - Kupaianaha eruption of Kilauea Volcano have provided some surprising results. Using hand held radiometers, Jones [1992, 1993] found that the surface of more vesicular (porous) lavas cool more rapidly than that of denser lavas. Lobes with 20-25% porosity cooled to only about 600 °C in about the time that lobes with 50-60% porosity cooled to 500 °C (Fig. 3-1). Porosity is the only parameter that has been shown to have such a dramatic effect on the cooling rate of pahoehoe flows.

The observed relationship between surface cooling rate and porosity appears stronger than any possible difficulties with the measurements of Jones [1992, 1993]. His data were collected in the evening to reduce the effect of reflected sunlight and two radiometers were used to cover the range of observed temperatures. Slow-moving or stagnant lobes were selected to minimize the flux of fresh hot lava into the cooling lobe. Flynn *et al.*, [1993] demonstrated that hot cracks account for less than 10% of the radiated energy from active lava surfaces and this translates to a minimal correction for the radiance temperature. The notion that vesicularity affects the cooling of pahoehoe lobes is also supported by Wilmoth and Walker [1993] who found that the thickness of the solid crust on highly vesicular pahoehoe lobes is twice as thick as that on dense lobes. However, it is likely that this latter observation has more to do with the effect of vesicles on the rheology of lava than on its cooling.

### Field Measurements of Cooling Pahoehoe Lobes

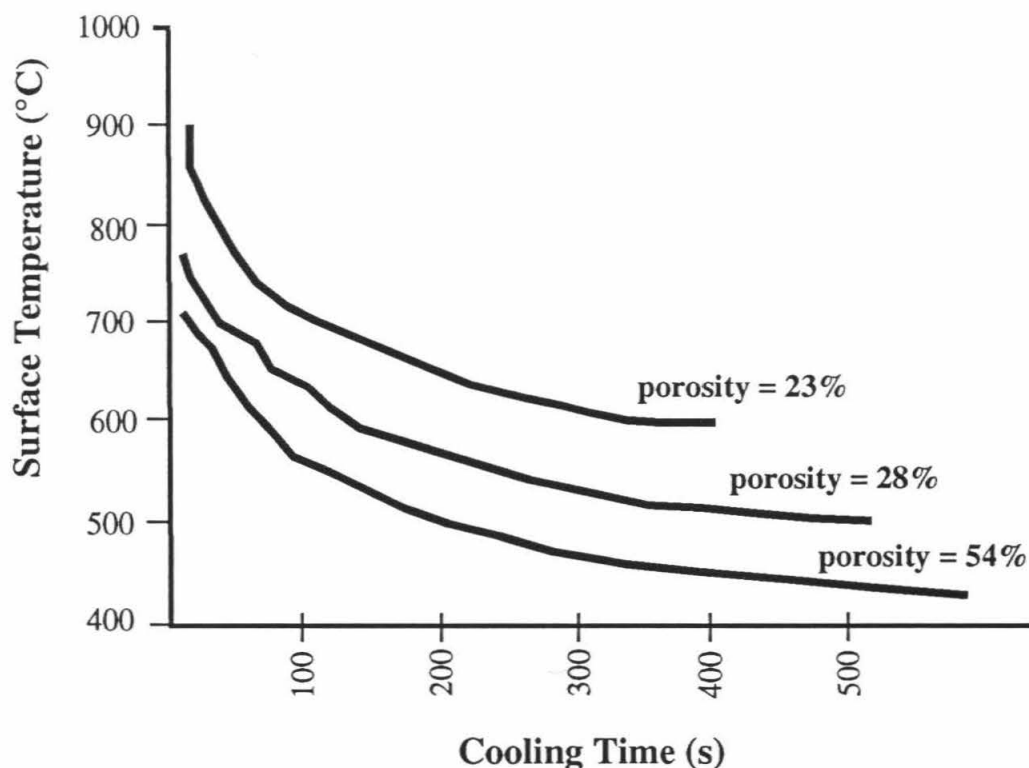


**Figure 3-1: Field measurements of cooling pahoehoe flow lobes showing the effect of porosity.** After Jones [1992]. This plots shows the observed effect of porosity on the cooling rate of pahoehoe surfaces. After 400 seconds of cooling, there is more than a 150 °C difference in the surface temperature of a dense (23% porosity) lobe and a vesicular (54% porosity) flow lobe. The largest uncertainty in this data is in determining the time of the initial breakout ( $t=0$ ).

Both Jones [1993] and Wilmoth and Walker [1993] suggest that these differences in cooling rates may arise from enhanced heat transport caused by radiation across vesicles. In the following, this suggestion will be quantified and shown to be plausible in the extremes of high temperature and high porosity. However, it will also be shown that porosity will significantly affect the cooling of lava flow lobes even when radiation across vesicles is not important.

Before continuing, it is useful to briefly examine a cooling pahoehoe flow lobe (Fig. 3-2). The flow lobe can be divided into 3 parts: (1) the brittle outer chill crust, (2) a plastic transitional “mush” zone, and (3) molten lava. Within the molten and plastic lava, all porosity will be in the form of gas bubbles. In the brittle crust, porosity consists of both microfractures and air-filled vesicles. Even though vesicles make up the bulk of the pore space in the chilled crust, microfractures have a significant effect on the thermal conductivity of cold basalt. Neglecting microfractures can lead one to overestimate the thermal conductivity of fractured basalt by as much as 50% [Horai, 1991].

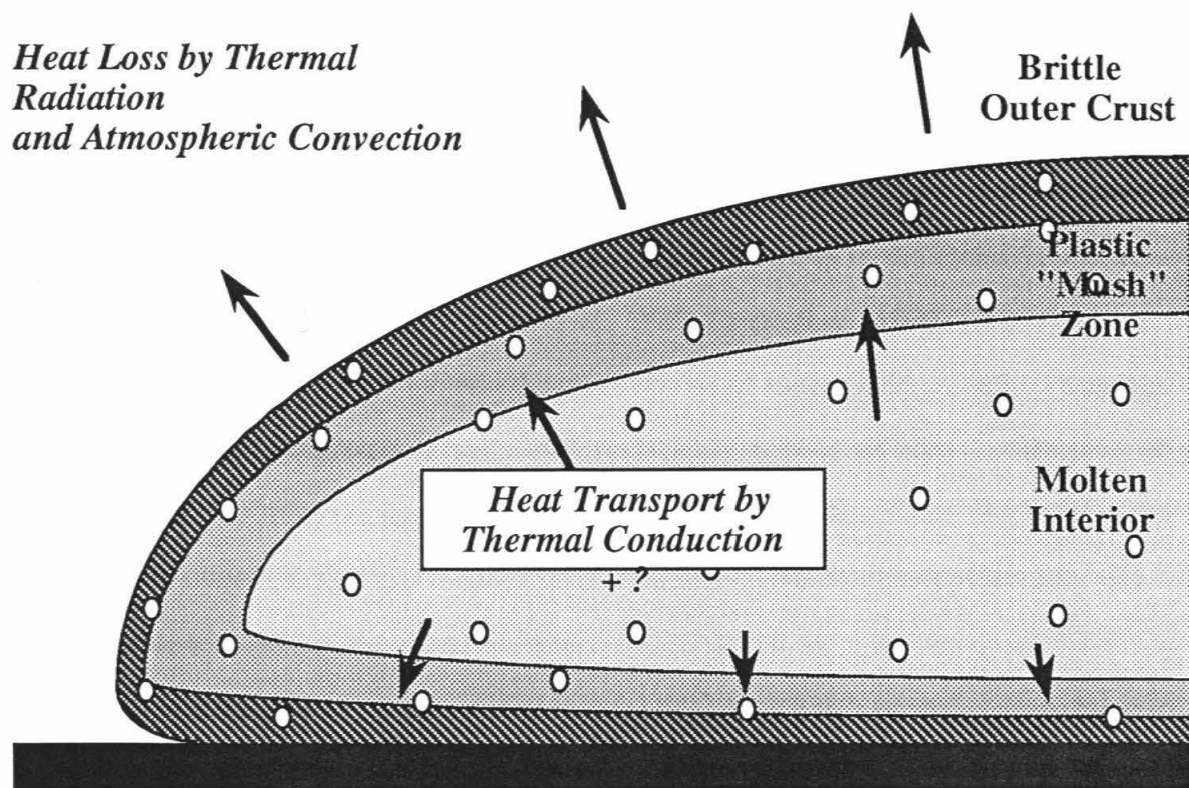


**Figure 3-2:** Idealized cross-section of cooling pahoehoe flow lobe. This cartoon shows the three major parts of a cooling pahoehoe flow lobe: (1) brittle outer crust, (2) plastic “mush” zone, and (3) the molten interior. Heat is lost at the surface through a combination of thermal radiation and atmospheric convection. Within the flow lobe, heat is transported primarily by conduction and possibly other heat transport mechanisms which could operate across bubbles and vesicles.

While the effect of porosity on the thermal properties of cold basalt has been examined in some detail [Robertson and Peck, 1974; Horai, 1991], similar data are not presently available at high temperatures. In this study I extrapolate across this gap. I also ignore the effects of fractures and only examine porosity in the form of vesicles and bubbles. Thus this work is precisely correct only in the molten and plastic portions of a lava flow. However, for many properties the shape of the pore space is irrelevant and the results are valid for the cold chill crust as well. I will also apply the term "vesicle" to both bubbles within the molten lava and air-filled vesicles in the frozen lava. This seems excusable since whether the gas is surrounded by liquid or solid does not affect the following discussions.

Returning to the problem of the cooling pahoehoe flow lobes, there is no obvious mechanism by which porosity can significantly increase the rate at which heat is extracted from the surface of a lava flow. For example, the differences in the emissivity of lava caused by surface textures [*e.g.*, Kahle *et al.*, 1988; Crisp *et al.*, 1990; Ondrusek *et al.*, 1993] are not large enough to explain the observations of Jones [1992, 1993]. Therefore, any variation of the surface cooling rate with vesicularity must come from the rate at which heat is transported from the interior of the flow to its surface. In a thick, fast moving 'a' flow, it is possible to argue that convection of lava will be the dominant process by which heat is transported within the flow. However, inside slow moving and stagnant pahoehoe flow lobes, such as the ones observed by Jones [1992, 1993], it is probably reasonable to ignore the motion of the lava. Thus I will only consider heat transfer mechanisms that can operate in stagnant lava: conduction, thermal radiation across vesicles, and the convection of gasses within a vesicle.

Vesicles can modify the heat transfer within lava by changing both the thermal properties controlling the conduction of heat and by introducing cavities in which convective and radiative heat transport can take place. The overall heat flux through lava will be a sum of the heat carried by each of these processes:

$$q_{\text{tot}} = q_{\text{cond}} + q_{\text{rad}} + q_{\text{conv}} \quad (3.1)$$

If one assumes that each of the heat fluxes are independent of the others, they can be described by an effective thermal conductivity such that

$$k_{\text{eff}} = k_{\text{cond}}(T, \phi) + \phi k_{\text{rad}}(T, r) + \phi k_{\text{conv}}(T, r) \quad (3.2)$$

where  $\phi$  is porosity,  $T$  is temperature,  $r$  is the radius of the vesicle,  $k_{\text{eff}}$  is the combined effective thermal conductivity,  $k_{\text{cond}}$  is the bulk thermal conductivity of the vesicular basalt,  $k_{\text{rad}}$  is the effective radiative thermal conductivity and  $k_{\text{conv}}$  is the effective convective thermal conductivity. I will now examine each of the three terms in the effective thermal conductivity.

### 3.2 Conduction in vesicular basalt

There are several techniques for calculating the bulk thermal conductivity of mixtures such as a lava containing vesicles. Maxwell's Formula, developed for a homogeneous matrix with randomly distributed spherical inclusions, seems most appropriate for vesicles in the molten or plastic portion of a lava flow and will be used here. However, it must be noted that Horai [1991] reviewed the measurements of the thermal conductivity of cold vesicular Hawaiian basalts made by Robertson and Peck [1974] and concluded that, in the case of fractured basalt, Maxwell's formula only provides an upper bound for the thermal conductivity. Thus the following may somewhat overestimate the thermal conductivity in the chill crust but should be accurate for the warmer parts of the flow lobe. Maxwell's formula is given by

$$k_{\text{cond}} = \frac{k_{\text{bas}} [2(1 - \phi)k_{\text{bas}} + (1 + 2\phi)k_{\text{gas}}]}{[(2 + \phi)k_{\text{bas}} + (1 - \phi)k_{\text{gas}}]} \quad (3.4)$$

where  $k_{\text{cond}}$  is the bulk thermal conductivity of the mixture,  $k_{\text{bas}}$  is the thermal conductivity of the basalt and  $k_{\text{gas}}$  is the thermal conductivity of the gas filled inclusions [Robertson and Peck, 1974]. The original magmatic gas is typically about 80 vol.% H<sub>2</sub>O for Kilauea East Rift Zone eruptions [Gerlach, 1986] and is eventually replaced by air. The expressions used in this study to describe the temperature dependence of  $k_{\text{gas}}$  and  $k_{\text{bas}}$  are listed in Appendix A.

The values for  $k_{\text{bas}}$  deserve some discussion. I have primarily relied on data in Touloukian *et al.* [1989] which are compiled from numerous works that used several different techniques. These data are in good agreement with the laboratory measurements of Murase and McBirney [1973] and have the thermal conductivity of basalt decrease with increasing temperature. However, there are data which suggests that  $k_{\text{bas}}$  increases with temperature [*e.g.*, Birch and Clark, 1940; Peck *et al.*, 1977; Robertson, 1988]. Peck *et al.* [1977] find that an increase in  $k_{\text{bas}}$  of 0.19 % per °C provides the best fit between numerical modeling and field measurements from the cooling of Alae lava lake. However, the thermal properties from Touloukian *et al.* [1989] yield a thermal diffusivity of 5.0-3.5 x 10<sup>-7</sup> m<sup>2</sup>/s for T > 300°C which is in agreement with the thermal diffusivity of pahoehoe flows calculated from *in situ* measurements of the cooling of active pahoehoe lava flows (4.5 x 10<sup>-7</sup> m<sup>2</sup>/s) [Hon *et al.*, 1994a]. In the final analysis, the exact value or form of the thermal conductivity of the basalt is not critical to the conclusions of this work. To demonstrate this, data from Birch and Clark [1940] for a diabase is used as an example where  $k_{\text{bas}}$  increases with temperature.

### 3.3 Convection within vesicles

Convection will only start when the Rayleigh number exceeds a value of at least 1000 [e.g., Bejan, 1984]. The Rayleigh number (Ra) is defined as

$$Ra = \frac{\rho^2 g \beta \Delta T C_p D^3}{k \eta} \quad (3.4)$$

where  $\rho$  is the density,  $\beta$  is the coefficient of thermal expansion,  $C_p$  is the specific heat,  $k$  is the thermal conductivity, and  $\eta$  is the viscosity of the gas inside the vesicle,  $g$  is gravitational acceleration,  $\Delta T$  is the temperature difference between the top and bottom of the vesicle, and  $D$  is the diameter of the vesicle.

In order to properly evaluate the Rayleigh number, the temperature dependence of the physical properties of the gas within the vesicle (water vapor or air) must be included. It was found that for the purposes of this study, the differences in the properties of water vapor and air are negligible (Fig. 3-3). The pressure dependence of these properties is also relatively small and has been ignored. The data used are given in Appendix A. Figure 3-3 shows that, even with temperature gradients as high as 1000 °C/cm, convection will not occur unless vesicles are larger than a centimeter. Vesicles this large are exceedingly rare in pahoehoe lava flows [Walker, 1989; Mangan *et al.*, 1991; and Wilmoth and Walker, 1993] and thus convection within vesicles can usually be ignored. However, this analysis also suggests that convection of the gas phase should be important inside partially drained lava tubes and perhaps even shelly pahoehoe. The latter commonly contains gas blisters tens of centimeters in size.

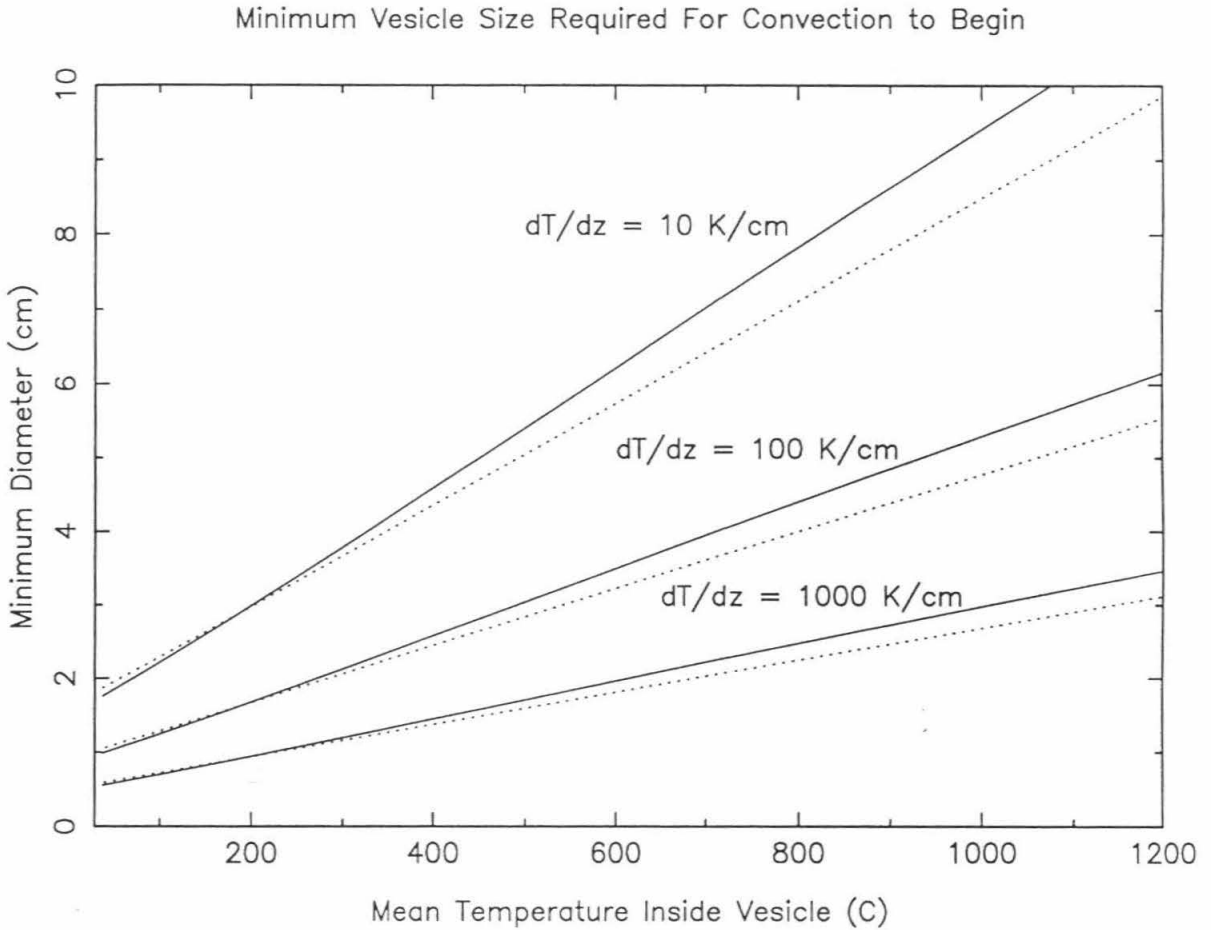


**Figure 3-3: Plot of conditions necessary for convection within vesicles.**

This figure plots the minimum diameter required to reach the critical Rayleigh number of 1000 as a function of mean vesicle temperature, temperature gradient across the vesicle, and the gas composition within the vesicle. Solid lines calculated using the properties of water vapor, dotted lines for air. Note that even at extreme temperature gradients convection will not occur in vesicles smaller than about 1 cm. Such large vesicles are very rare in basaltic lava flows.

### 3.4 Thermal radiation across vesicles

Radiative heat transfer across vesicles is modeled by a hollow sphere within a block with a linear temperature gradient (Fig. 3-4). The heat flux between any two points on the sphere can be calculated by

$$dQ_{12} = \frac{\epsilon\sigma}{\pi} (T_2^4 - T_1^4) \frac{\cos^2\alpha}{d_{12}^2} dA_1 dA_2 \quad (3.5)$$

where  $\epsilon$  is emissivity,  $\sigma$  is the Stephan-Boltzmann constant,  $T_1$  and  $T_2$  are the temperatures at point 1 and 2 respectively,  $dA_1$  and  $dA_2$  are area elements, and  $\alpha$  and  $d_{12}$  are geometric constructs defined in Figure 3-4.

Equation (3.5) can be integrated to obtain the net heat flux between the upper, cooler, half of the sphere and the lower, warmer, half. It can be shown that  $d_{12} = 2r\cos\alpha$ , where  $r$  is the radius of the sphere. It is also helpful to describe the temperature at any point on the sphere by

$$T(\theta, \phi) = T_0 (1 + \gamma \sin\theta) \quad \text{where} \quad \gamma = r(\partial T / \partial z) / T_0 .$$

The net heat flux to point "1" in Figure 3-4 is

$$\begin{aligned} Q_1 &= \int_0^{2\pi} \int_{-\pi/2}^{\pi/2} Q_{12} r^2 \cos\theta_2 d\theta_2 d\phi_2 \\ &= \epsilon\sigma \left[ T_0^4 (1 + 2\gamma^2 + \gamma^2/5) - T_1^4 \right] \end{aligned} \quad (3.6)$$

The heat transported between the cooler upper half and the warmer lower half of the sphere is given by

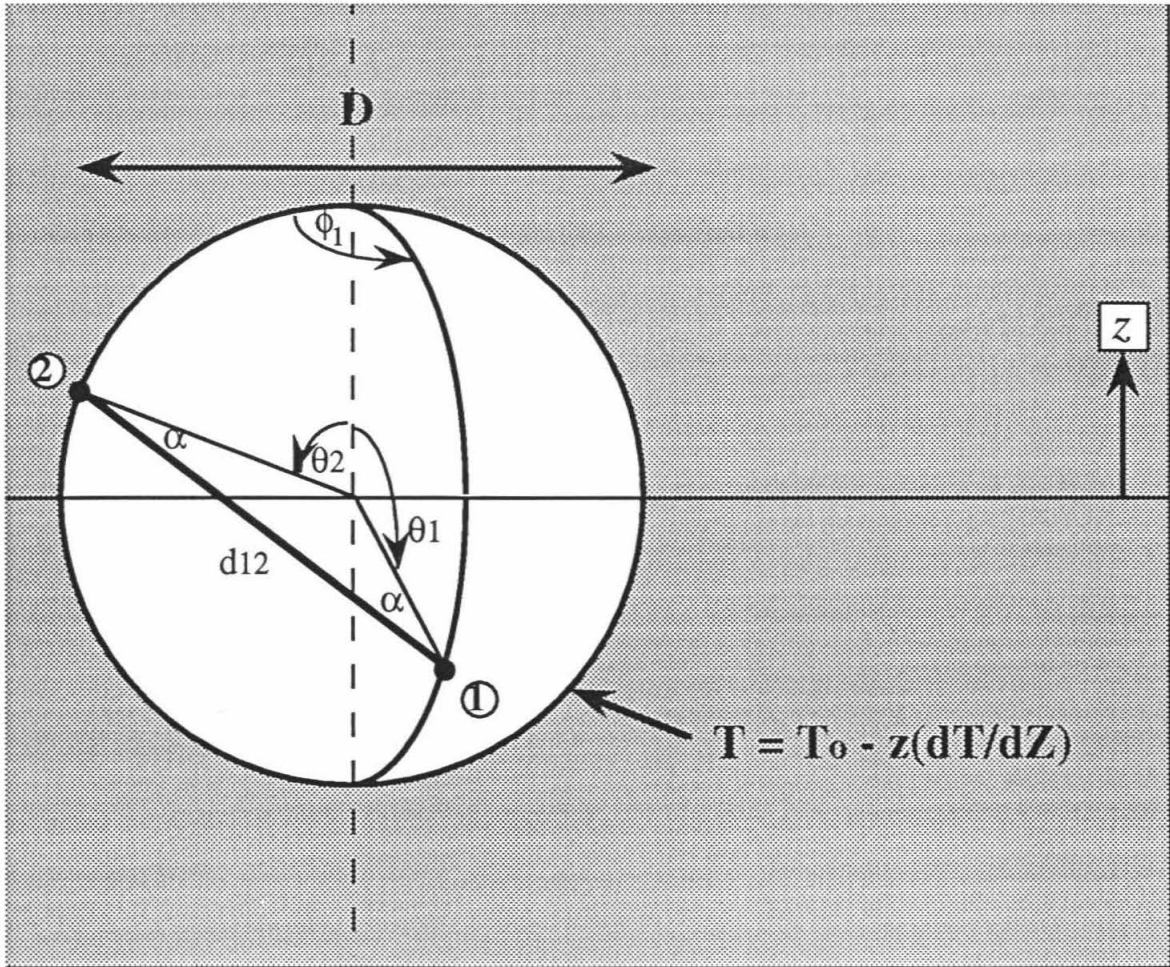


**Figure 3-4: Model of vesicle for radiative heat transfer.** Vesicles are modeled as a hollow sphere of diameter ( $D$ ). The temperature of the wall of the sphere decreases linearly with  $z$ . The heat flux is calculated by integrating the heat transported between all points such as those labeled (1) and (2).

$$\begin{aligned}
Q_{\text{rad}} &= \int_0^{2\pi} \int_0^{\pi/2} Q_1 r^2 \cos \theta_1 d\theta_1 d\phi_1 \\
&= -4\pi r^2 \epsilon \sigma T_0^4 \gamma \left(1 - \frac{\gamma^2}{2}\right)
\end{aligned} \tag{3.7}$$

In realistic cases  $|\gamma| \ll 1$  and this can be further simplified to

$$Q_{\text{rad}} = 4\pi r^2 \epsilon \sigma T_0^4 \gamma. \tag{3.8}$$

In order to obtain the heat flux ( $q_{\text{rad}}$ ), one divides by the cross-sectional area of the sphere

$$q_{\text{rad}} = Q_{\text{rad}}/\pi r^2 = 4\epsilon \sigma T_0^4 \gamma = 4r\epsilon\sigma(\partial T/\partial z)T_0^3 \tag{3.9}$$

and therefore,

$$k_{\text{rad}} = 4r\epsilon\sigma T_0^3 \tag{3.10}$$

This  $T^3$  dependence for  $k_{\text{rad}}$  is the usual result for porous materials [Wechsler *et al.*, 1972]. Upon evaluating equation (3.10) it is apparent that radiative heat transport across vesicles dominates over conduction only for vesicles about a centimeter in diameter or larger. For typical lava flows with vesicles on the order of 1 mm, radiation across vesicles becomes a significant correction to pure conduction only at high temperatures and high vesicularities (see Fig. 3-5).

### 3.5 Effect of vesicles on effective thermal diffusivity

We have so far quantified the heat flux through the lava but not how this affects temperatures. One should recall that it is thermal diffusivity ( $\kappa = k/\rho C_p$ ), and not thermal conductivity, that controls the rate at which temperature changes inside a conductively cooling body. Vesicles influence the thermal diffusivity of a lava not only through the effective thermal conductivity, but also through the density and heat capacity of the lava. The effective thermal diffusivity of vesicular basalt ( $\kappa_{\text{eff}}$ ) can be written as

$$\kappa_{\text{eff}} = \frac{k_{\text{eff}}(T, \phi)}{(1 - \phi)\rho_{\text{bas}}(T) C_{p_{\text{bas}}}(T) + \phi\rho_{\text{gas}}(T) C_{p_{\text{gas}}}(T)} \quad (3.11)$$

where  $k_{\text{eff}}$  is the effective thermal conductivity of the vesicular lava,  $\phi$  is the porosity,  $\rho_{\text{bas}}$  and  $C_{p_{\text{bas}}}$  are the temperature dependent density and heat capacity of pure basalt and  $\rho_{\text{gas}}$  and  $C_{p_{\text{gas}}}$  are the density and heat capacity of the gas within the vesicle. Again, the expressions for the temperature dependence of each of these properties is listed in Appendix A. It should be noted that it is the product of  $\rho$  and  $C_p$  (*i.e.*, the heat capacity per unit volume) that is of interest in the governing partial differential equation and not  $\rho$  or  $C_p$  individually. This explains the form of the denominator in equation (3.11).

Since  $\rho_{\text{gas}} \ll \rho_{\text{bas}}$  while  $C_{p_{\text{gas}}} \approx C_{p_{\text{bas}}}$ , this equation can be simplified to

$$\kappa_{\text{eff}} = \frac{k_{\text{eff}}(T, \phi)}{(1 - \phi)\rho_{\text{bas}}(T) C_{p_{\text{bas}}}(T)} \quad (3.12)$$

### 3.6 Discussion

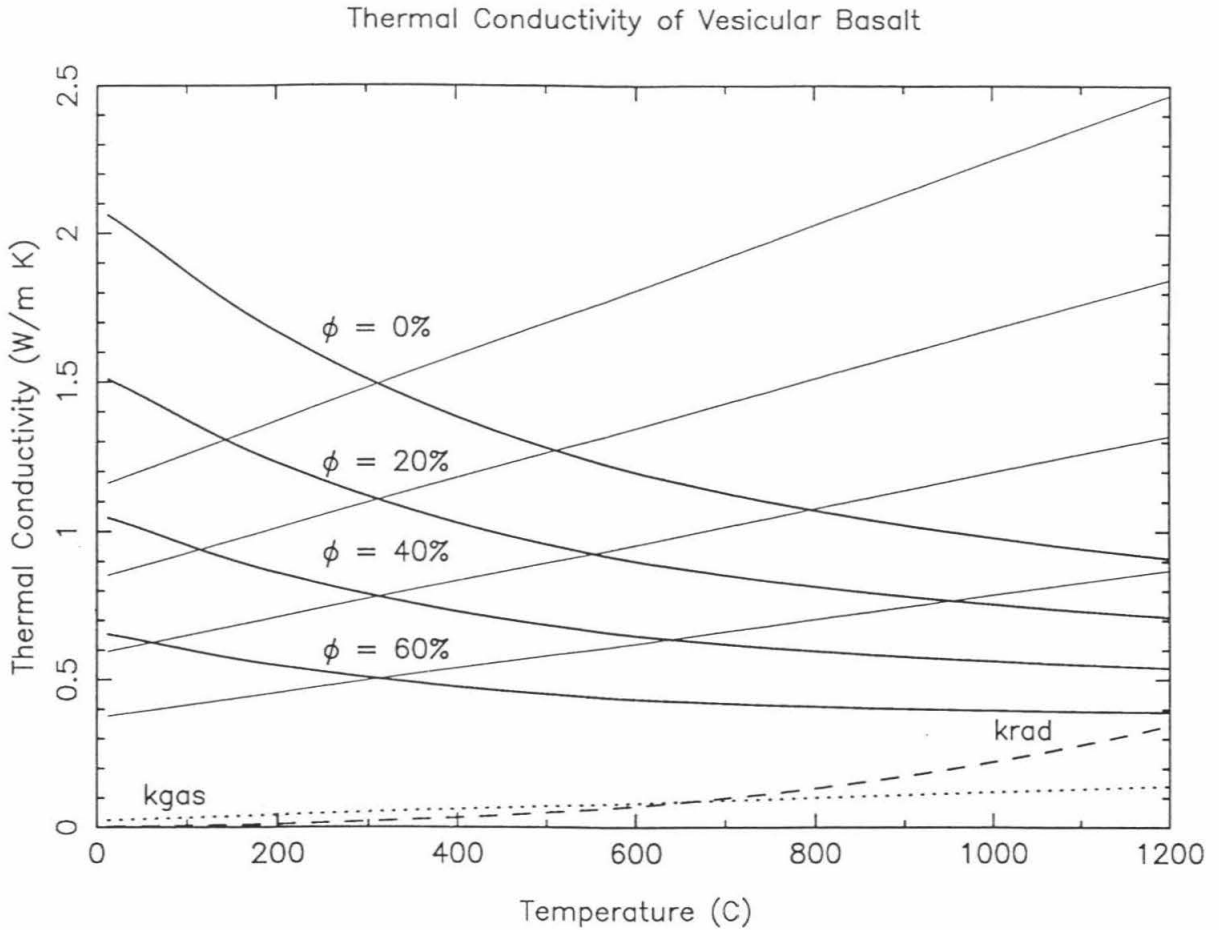
Figure 3-5 shows the various thermal conductivities as functions of temperature and porosity. The primary effect of adding vesicles is to monotonically lower the thermal conductivity toward the value of the gas phase ( $k_{\text{gas}}$ ). Radiation across 1 mm diameter vesicles ( $k_{\text{rad}}$ ) never dominates over conduction. However, it can become a significant contribution at high temperature and high vesicularity, especially when using the data from Touloukian *et al.* [1989].

Figure 3-6 shows the effective thermal diffusivity as a function of temperature and porosity. Because of the effects of temperature and porosity on density and heat capacity, thermal diffusivity need not exactly mimic thermal conductivity. However, thermal diffusivity does generally behave like thermal conductivity except that thermal diffusivity is significantly less sensitive to porosity. There are also some interesting, although sometimes subtle, effects of vesicles. At temperatures below about 500 °C porosity slightly reduces the thermal diffusivity. In the temperature range of 700 °C to 900 °C, radiation across vesicles begins to assert itself on thermal diffusivity and at a temperature of 1100 °C a highly vesicular lava may have a thermal diffusivity more than twice that of dense lava.

Increased thermal diffusivity in vesicular lavas would imply more rapid cooling of more vesicular flow lobes. However, the effect of vesicles on the cooling of a flow lobe is more profound than is evident from just examining thermal diffusivity. This problem of a cooling lava flow is in many ways similar to the problem of diurnal surface temperature variations [Carslaw and Jaeger, 1959]. In this latter problem it is thermal inertia, and not thermal diffusivity, that describes the magnitude and rate of the temperature changes [*e.g.*, Jaeger and Harper, 1950; Palluconi and Kieffer, 1981]. Thermal inertia ( $I$ ) is defined as

$$I = (k\rho C_p)^{1/2} \quad (3.13)$$

where the thermal conductivity, density, and heat capacity are those of the vesicular basalt.



**Figure 3-5: Thermal conductivities of vesicular basalt.** Thermal properties are calculated for 1 mm diameter vesicles filled with water vapor. Using air as the gas phase does not cause any notable changes in the plotted curves. Porosities much above 60% are not relevant to lava flows and have not been plotted. Dark lines use thermal conductivities from Touloukian *et al.* [1989] while the thin lines use Birch and Clark [1940]. Solid lines show the effective thermal conductivity of basalt as calculated by equation (3.3). Dotted line is the thermal conductivity of the gas phase ( $k_{gas}$ ) and the dashed line is the effective radiative thermal conductivity ( $k_{rad}$ ) calculated using equation (3.10). This plot shows that, for typical lava flows, vesicles significantly and systematically decrease the effective thermal conductivity of basalt. The effect of radiation across vesicles is only notable at high temperatures and high vesicularities.

## Effective Thermal Diffusivity of Vesicular Basalt

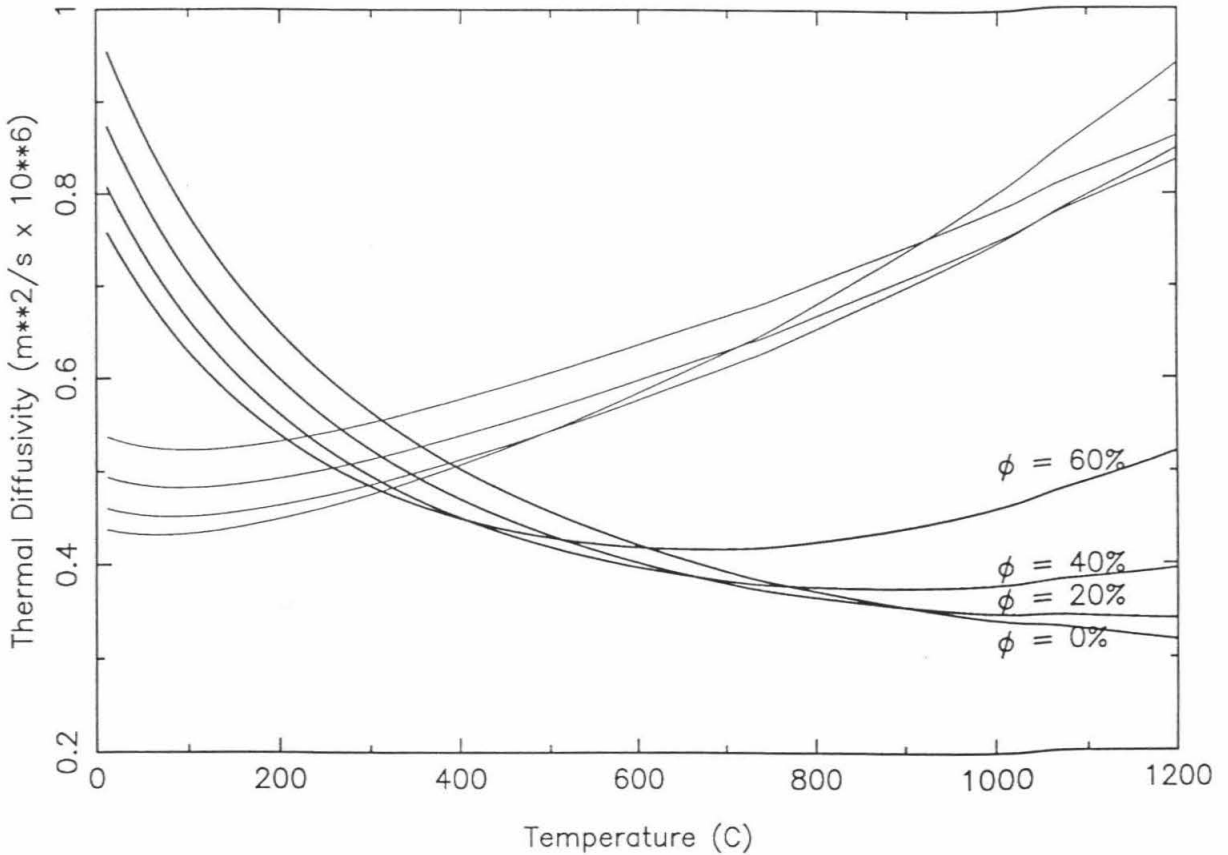


**Figure 3-6: Effective thermal diffusivity of vesicular basalt.** Solid lines show the effective thermal diffusivity for several vesicularities as calculated by equation (3.12). Dark lines use thermal conductivities from Touloukian *et al.* [1989] while the thin lines use Birch and Clark [1940]. Note that the effect of vesicles on thermal conductivity is less marked than the effect of vesicles on thermal conductivity and that thermal diffusivity is enhanced for highly vesicular lavas at high temperatures.

Thermal inertia can be thought of as the heat capacity per unit area of a surface. Thermal conductivity provides a measure of the thickness of the thermal skin depth and  $\rho C_p$  is the heat capacity per unit volume. The higher the thermal inertia of a material, the more it “resists” changes in surface temperature. This is because a high thermal inertia material will have a thick layer cooled slightly during the same time in which a low thermal inertia material will have a thin layer cooled greatly.

This would seem to contradict the observations of Wilmoth and Walker [1993]. However, I suspect that the thicker solid layer in the more vesicular lavas is a consequence of the effect of bubbles on the rheology of the lava and not a result of cooling. It is known that bubbles produce yield strength in lava and greatly increase its effective viscosity [*e.g.*, Pinkerton and Stevenson, 1992]. This increases “stiffness” of the vesicular lava should be more than sufficient to explain the observed relative thicknesses of the solid crusts.

Increasing vesicularity significantly decreases two of the properties that control thermal inertia. Figure 3-7 plots thermal inertia versus temperature and porosity. Using either data set for  $k_{bas}$ , thermal inertia drops by a factor of two between 20 and 60% porosity. Thus a moderate increase in the vesicularity of a lava flow will produce a detectable increase in the cooling rate of its surface. This effect is not confined to high temperatures or high vesicularities. Furthermore, a very weak dependence of the cooling rate on vesicle size is expected because vesicle size only very weakly affects one of the properties (effective thermal conductivity) controlling thermal inertia. These results agree with an empirical study of the effect of porosity on the thermal inertia of cold basalt [Zimbelman, 1986].

A more complete thermal model that calculates temperature profiles within flow lobes is necessary to properly quantify the differences in the cooling of vesicular and dense pahoehoe lobes. Such a thermal model is presented in the following chapter.

## Calculated Thermal Inertia of Vesicular Basalt

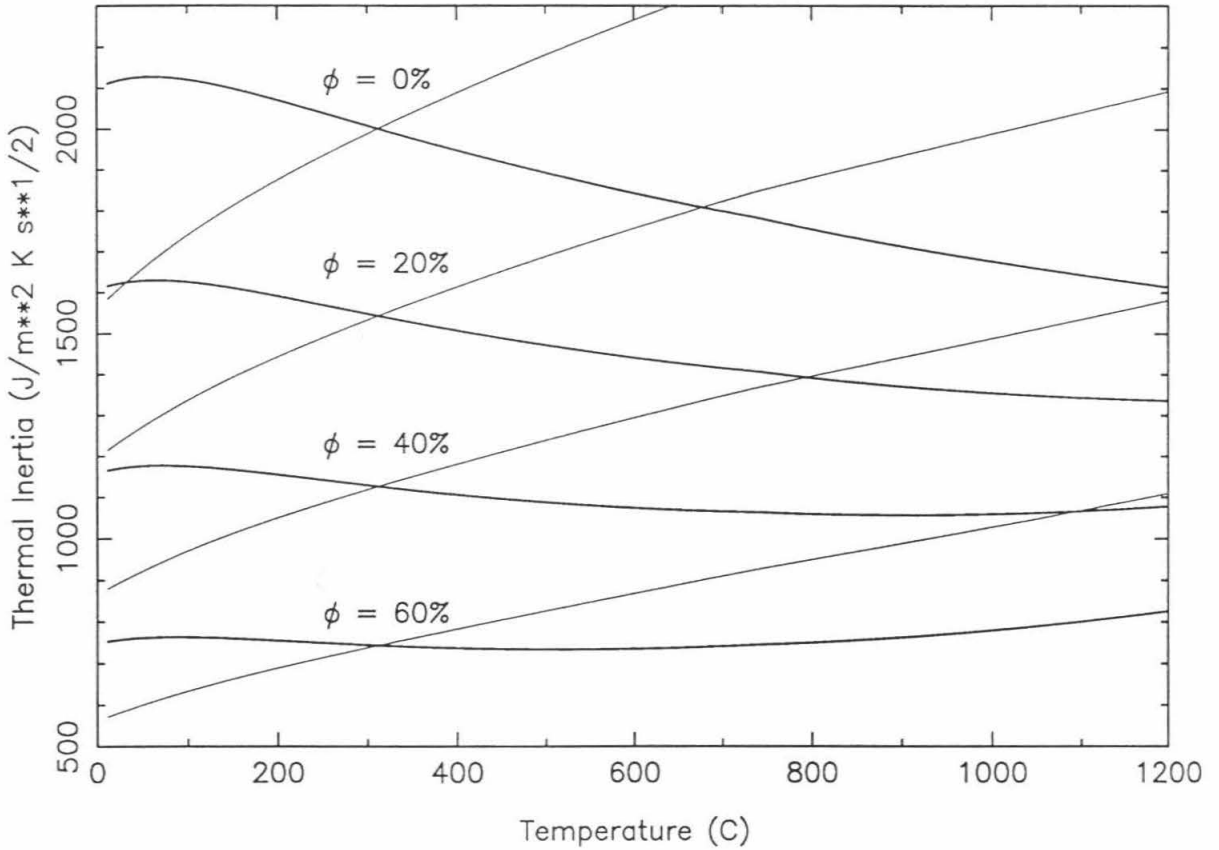


**Figure 3-7: Calculated thermal inertia of vesicular basalt.** Dark lines use thermal  $k_{\text{bas}}$  from Touloukian *et al.* [1989] and thin lines use Birch and Clark [1940]. Note that thermal inertia is greatly depressed by increased porosity at all temperatures.

### 3.7 Conclusions

Based on available laboratory data and some simple calculations, the following conclusions can be drawn about the effect of vesicles (or bubbles) on the thermal properties of most pahoehoe lava flows: (1) convection of the gas phase within vesicles does not take place; (2) radiation across vesicles can transport significant heat only at high temperatures; (3) porosity significantly lowers the bulk thermal conductivity and density of lava; (4) thermal diffusivity is relatively insensitive to porosity except in the limit of high temperature ( $T > 800$  °C) and high vesicularity ( $\phi > 40\%$ ) where radiation across vesicles may boost the thermal diffusivity of lava; and (5) thermal inertia is significantly depressed by porosity.

The effect of porosity on thermal diffusivity is consistent with the faster cooling of more porous lava flows, but is rather subtle. Thermal inertia provides a better explanation for the observations of Jones [1992, 1993] because thermal inertia is significantly decreased by porosity at any temperatures. Thus, the surface of a porous flow is always expected to cool more quickly than that of a dense flow.

## CHAPTER 4: MODELING THE COOLING OF PAHOEHOE FLOW LOBES: THE FIRST FIVE MINUTES

A modified version of this chapter will be submitted this summer to the Journal of Geophysical Research with Roger Denlinger (Hawaiian Volcano Observatory, United States Geological Survey) as my co-author. Dr. Denlinger provided the 1989 field measurements, has reviewed my numerical model, and has provided valuable discussions. The rest of the work is my own.

### 4.0 Abstract

In this chapter I produce a new thermal model that describes the first five minutes of the cooling of pahoehoe lava flows. This model is built from the physics of the physical phenomena that control the initial cooling of pahoehoe flows and is not an empirical fit to field data. The model output is validated against published field measurements, those collected by Dr. Denlinger, and data I collected myself. The model includes (1) cooling by thermal radiation, (2) cooling by atmospheric convection, and (3) heat transport within the flow by conduction with temperature and porosity dependent thermal properties.

Other physical phenomena, such as the latent heat of crystallization and the motion of the lava, are shown to be negligible. However, because of these simplifications the model is strictly valid only for the first few minutes of the cooling of a pahoehoe flow. I show that, within these first few minutes, the model is able to very accurately reproduce the field measurements and that it does so significantly better than previous cooling models for lava flows.

By adjusting one parameter at a time, the sensitivity of the cooling rate to each of the input parameters was determined. I find that: (1) large changes in initial temperature result in only small differences in surface temperature, (2) more porous flows have their

surfaces cool more quickly than dense flows, and (3) the cooling rate is very sensitive to the efficiency of atmospheric convective cooling.

These model results have some immediate applications. It quantitatively supports the explanation for the recently observed relationship between the surface cooling rate of pahoehoe lobes and the porosity of those lobes that was described in the previous chapter. The model also allows some suggestions to be put forward regarding the formation of the glassy rind on flow lobes. The differences in the growth of this rind may explain some of the features of shelly pahoehoe and blue-glassy (P-type) lobes. The fact that the model cooling rate is sensitive to atmospheric cooling leads to the recommendation of a specific field experiment to verify this prediction.

#### 4.1 Introduction

Pahoehoe lava flows are an extremely common aspect of basaltic volcanism. Pahoehoe flows cover about 96% of Kilauea Volcano [Holcomb, 1987] and 50% of Mauna Loa [Lockwood and Lipman, 1987]. Essentially all observed submarine lava flows can be classified as some form of pahoehoe [*e.g.*, BVSP, 1981; Appelgate and Embley, 1992; Bryan *et al.*, 1994]. It has also been argued that Continental Flood basalt flow units are actually inflated pahoehoe sheet flows [*e.g.*, Hon and Kauahikaua, 1991; Self *et al.*, 1991; Finnemore *et al.*, 1993]. Pahoehoe flows may also have been detected on Mars [Theilig and Greeley, 1986] and Venus [Bruno *et al.*, 1992].

Small pahoehoe flow lobes deserve attention primarily because they are the front of the entire pahoehoe lava flow. Without understanding flow lobes, the "initial" conditions for the formation of inflation features and lava tubes would be uncertain. To put it another way, the cooling of pahoehoe flows on a time scale of second to minutes is an important step in understanding processes which act on time scales of hours, days, or years.

Another reason to concentrate on pahoehoe flows is the wealth of new field data collected from pahoehoe flows on the Pu'u 'O'o - Kupaianaha flow field on Kilauea

Volcano. These recent field data include temperature measurements using radiometers [Jones, 1992, 1993], a spectroradiometer [Flynn *et al.*, 1992], and thermocouples [Hon *et al.*, 1994b; Keszthelyi and Denlinger, this study]. In related work, Wilmoth and Walker [1993] measured the growth of the chill crust on flow lobes and there have been several unpublished attempts to make *in situ* measurements of the rheology of these Kilauea lavas [S. Rowland, pers. comm., 1991; M. Coltelli, pers. comm., 1992; and Keszthelyi and Powell, Appendix C]. Perhaps the most interesting result to date from these various field data is the suggestion that porosity plays an important role in the cooling of pahoehoe flow surfaces. Jones [1992, 1993] shows that the surfaces of more porous flows cool significantly more rapidly than those of denser flows. All of these field data require an accurate thermal model to assist in their interpretation.

However, despite the importance of pahoehoe lava flows and the wealth of field data from them, neither their dynamics nor their cooling has been properly modeled. For example, nearly all available flow models for lava flows are based on the Bingham plastic model [*e.g.*, Hulme, 1974; Moore *et al.*, 1978; Wilson and Head, 1983; Dragoni *et al.*, 1986; Young and Wadge, 1990; Pinkerton and Wilson; *in press*]. However, inflating pahoehoe flows do not behave like a simple fluid flowing down an inclined plane. Models based on an inflating skin confining a viscous liquid (such as those that have been used to model lava domes [*e.g.*, Iverson, 1990; Denlinger, 1990]) seem more appropriate for pahoehoe flow lobes. However, such a model has only recently been applied to large pahoehoe sheet flows [Hon *et al.*, 1994a].

As with the flow models, most earlier works on the cooling of lava flows use assumptions (such as a well-mixed hot interior that is at least partially exposed at the surface) that are valid only for large channelized or 'a'a flows [*e.g.*, Danes, 1972; Dragoni, 1989; Crisp and Baloga, 1990; Dragoni and Tallarico, 1994; Crisp and Baloga, *in press*].

Another group of thermal models is based on the dimensionless Grätz number correlation and the empirical suggestion that lava flows stop when the Grätz number reaches a critical value of about 300 [*e.g.*, Pinkerton and Sparks, 1976; Wilson and Head, 1983; Pinkerton and Wilson, 1988; Pinkerton and Wilson, in press]. However, the Grätz number was developed for pipe flow with purely conductive cooling. Since the cooling of lava flows is arguably controlled by a combination of thermal radiation and convective processes, it is not clear that the Grätz number is applicable. This is especially true in the first few minutes of cooling, while the surface temperature of the flow is changing rapidly.

The thermal model presented in Head and Wilson [1986] would appear to be directly applicable to pahoehoe lava flows. However, as is explained later in this chapter, their model contains mathematically unjustifiable steps. Recently, more appropriate thermal models have been constructed. For time scales of hours to days, Hon *et al.* [1994a] have been able to accurately fit observed cooling rates with a conductive cooling model that includes the release of latent heat (Stefan Problem). The work most similar to that presented here is the numerical model accompanying the wax modeling of lava flows by Griffiths and Fink [1992a, 1992b].

It is also significant that even the most recent cooling models for lava flows have not included the effect of vesicles or temperature dependent thermal properties. This is despite laboratory data [*e.g.*, Birch and Clark, 1940; Murase and McBirney, 1973; and Robertson and Peck, 1974], thermal models for dikes [*e.g.*, Delaney, 1988; Carrigan, 1992], thermal models for lava lakes [*e.g.*, Peck, 1978; Hardee, 1980], field observations [Jones, 1992, 1993], and theoretical calculations (Chapter 3) which all suggest that these effects may be important. Therefore previous works on the dynamics and cooling of lava flows are probably inadequate to study the emplacement of pahoehoe lava flows.

Before continuing, I would like to briefly describe pahoehoe flow lobes. Flow lobes are typically 10-40 cm tall, 0.2-1 m wide, and advance at a few cm/s to a final length of 0.5-3 m (see Fig. 4-1a for some typical lobes). However, much larger lobes do

occasionally occur . Because of their relatively small size and slow motion, it is not difficult to conduct *in situ* studies (see Fig. 4-1b). In general, lobes grow as an inflating, stretching sack. The lobe halts when the crust cools and hardens to the point that the pressure driving the lobe is no longer able to bend the crust. However, this pressure is able to lift crack-bounded blocks long after the lobe has stopped advancing (Fig. 4-1c). The dynamics and inflation of flow lobes is outside the scope of this chapter and I now return to their thermal budget.

The main goal of this chapter is to present a realistic thermal model that can be used to study the initial cooling of pahoehoe lava flows. I will first examine the physical processes which play a role in the cooling of pahoehoe flow lobes, then describe the significant processes in terms of the relevant physics. The resulting set of equations are used to construct a numerical model. It is important to note that, unlike many previous studies, the model is derived directly from the physics describing the key processes and is not an empirical fit to field data. The model is then validated by comparing its output to field data collected by ourselves and others. My model is also compared to earlier cooling models to show that it is a significant improvement. Afterward the sensitivity of the model to each of the input parameters is investigated and some preliminary suggestions are drawn about specific field observations. I end by discussing future field experiments and further modeling efforts suggested by this work.

## **4.2 Physical phenomena affecting cooling**

I have determined that of the veritable cornucopia of physical phenomena associated with the cooling of lava flows, only three processes are significant (Fig. 4-2). These phenomena are (1) radiative cooling at the surface, (2) atmospheric convective cooling at the surface, and (3) conduction of heat within the flow including temperature and vesicle dependent thermal properties. I justify the dismissal of the other phenomena, but these simplifications limit the model to the first few minutes of cooling.



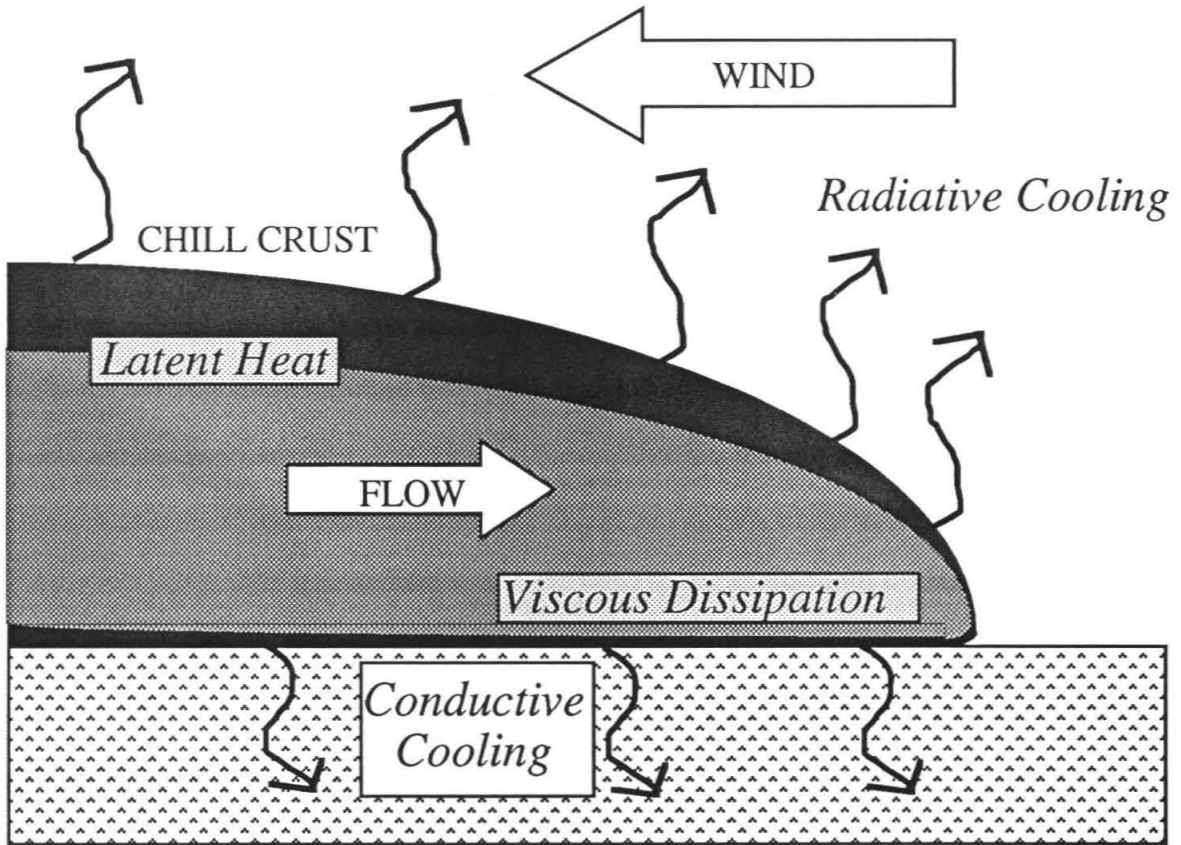
**Figure 4-1a: Photograph of active pahoehoe flow lobes.** The mass of smooth shiny lobes in the center of the photo is active. Note incandescent lobe fronts. Lobes are about 20 cm tall. October, 1991, Kupaianaha flow field. [Photo courtesy of USGS]



**Figure 4-1b: Photograph of active pahoehoe flow lobes.** Geologist collecting a sample for scale. Note that most flow lobes are 20-30 of cm tall, 30-70 cm wide, and 0.5-2 m long. January, 1991, Kupaianaha flow field. [Photo courtesy of USGS]



**Figure 4-1c: Photograph of inactive pahoehoe flow lobes.** The metal stake in the center of the photo is painted in 10 cm strips. The stake was originally 1 m tall. Photo taken a few days after the flows advanced through this area. Note the ropy texture on the right. October, 1991 Kupaianaha flow field. [Photo courtesy of USGS]

*Convective Cooling*

**Figure 4-2: Cartoon of the Thermal Budget of a Pahoehoe Flow Lobe.** This cartoon describes the key physical processes involved in the cooling of a pahoehoe flow lobe. The upper surface of a pahoehoe flow lobe is cooled by both thermal radiation and atmospheric convection while the bottom loses heat by conduction into the ground. In the first few minutes, the heat added to the lobe by processes such as the advection of additional hot lava, viscous dissipation, and the release of latent heat are negligible. Heat conduction within the lobe is controlled by the temperature and porosity dependent thermal properties.

#### 4.2.1 Radiative Processes

Initially, thermal radiation from the surface is the dominant heat loss mechanism from a lava flow (Fig. 4-3). The radiative heat flux ( $q_{\text{rad}}$ ) is given by

$$q_{\text{rad}} = \varepsilon F \sigma_b (T_s^4 - T_a^4) \quad (4.1)$$

where  $\varepsilon$  is emissivity,  $F$  is a geometric view factor,  $\sigma_b$  is the Stefan-Boltzmann constant,  $T_s$  is the surface temperature of the flow lobe, and  $T_a$  is the ambient temperature. Basaltic lavas are close to blackbodies and have emissivities that vary between 0.80-1.0 with wavelength. 0.95 is a median value [Kahle *et al.*, 1988; Crisp *et al.*, 1990]. For a flat plate radiating into an infinite half-space, the view factor has a value of unity.

The other radiative processes examined are (1) enhanced radiation from hot cracks, (2) radiative heat transport directly through the lava, and (3) radiative heat transport across vesicles and bubbles. Cracks formed by thermal contraction should radiate most efficiently normal to the cooling surface (*i.e.*, straight up). However, multispectral infrared measurements have shown that, even in this most favorable geometry, hot cracks enhance the radiant energy flux by only about 1-10% [*e.g.*, Pieri *et al.*, 1990; Oppenheimer, 1991; Flynn *et al.*, 1993]. Therefore the effect of cracks on the total radiative heat loss is taken to be negligible.

In theory, at very high temperatures, radiative heat transfer directly through minerals can transport a significant amount of heat within rocks [Clark, 1957]. In fact, Murase and McBirney [1973] found a steep increase in the apparent thermal conductivity of basaltic melts above 1200 °C. They attribute this increase to radiative heat transfer through the molten lava. However, since eruptive temperatures are typically below 1200 °C, I have ignored this process. Finally, in the previous chapter I showed that radiation across vesicles can be significant but only in the limits of high temperature and high vesicularity.

In my model, this process has been incorporated into the temperature dependence of the effective thermal conductivity of the basalt and is not treated as a separate physical process.

#### 4.2.2 Atmospheric Convective Processes

The heat flux due to atmospheric convection ( $q_{\text{conv}}$ ) is typically described by an expression of the form

$$q_{\text{conv}} = \mathbf{h} (T_s - T_a) \quad (4.2)$$

where  $\mathbf{h}$  is the heat transfer coefficient,  $T_s$  is the temperature of the solid surface, and  $T_a$  is the ambient atmospheric temperature. The heat transfer coefficient usually must be determined by experiments or extensive numerical modeling because it is highly dependent on the geometry of the problem [*e.g.*, Bejan, 1984]. The temperature dependence of  $\mathbf{h}$  can be explicitly shown by having  $(T_s - T_a)$  raised to some power other than 1. The non-dimensional Nusselt number ( $\text{Nu}$ ), the ratio of the convective and conductive heat fluxes, is particularly useful in evaluating  $\mathbf{h}$ . The  $\text{Nu}$  is defined as

$$\text{Nu} = \mathbf{h}H/k \quad (4.3)$$

where  $\mathbf{h}$  is the heat transfer coefficient,  $H$  is the height of the plume of hot air, and  $k$  the thermal conductivity of air [*e.g.*, Bird *et al.*, 1960].

In the following, I examine both free (natural) convection and forced convection. For cooling by free convection the following formula from Turcotte and Schubert [1982] was used

$$\text{Nu} = 0.225 \text{Ra}^{1/3} \quad (4.4)$$

where 0.225 is an empirically determined factor and Ra is the dimensionless Rayleigh number defined by

$$Ra = \rho g \beta \Delta T H^3 / \eta \kappa \quad (4.5)$$

where  $g$  is the gravitational acceleration,  $\beta$  the coefficient of thermal expansion of air,  $\Delta T$  is the temperature difference between the ambient air and the lava surface,  $H$  is the height of the plume of hot air,  $\eta$  is the viscosity of the air, and  $\kappa$  the thermal diffusivity of air. The 1/3 power on the Rayleigh number can be derived theoretically [*e.g.*, Turcotte and Schubert, 1982].

By plugging equations (4.4) and (4.5) into equation (4.3), one can solve for  $h$ . [*e.g.*, Bejan, 1984]. Note that this allows  $H$  to be algebraically canceled when solving for the heat transfer coefficient. Because  $H$  is never determined, I have not computed values for the Ra. Thus I have not formally demonstrated that the Ra exceeds the critical value of about 1000 for free convection to occur. However, based on direct field observations, I have no doubt that atmospheric convection does indeed occur over active flows.

It is important to incorporate the temperature dependence of the atmospheric properties in these calculations. Between 1000 to 300 K, air density varies by more than a factor of three, and viscosity and thermal conductivity a factor of two. The mathematical expressions for the physical properties of air as a function of temperature are listed in Appendix A. Taking these effects into account, the free convective heat transfer coefficient is about 11 W/m<sup>2</sup>K. This value for  $h$  does not change significantly with surface temperature until the flow has cooled to near ambient temperatures (Fig 4-4). While trivial early on, free convection does become a non-negligible as the surface cools below 500 °C (Fig. 4-3).

## Comparison of Radiative and Convective Heat Transport

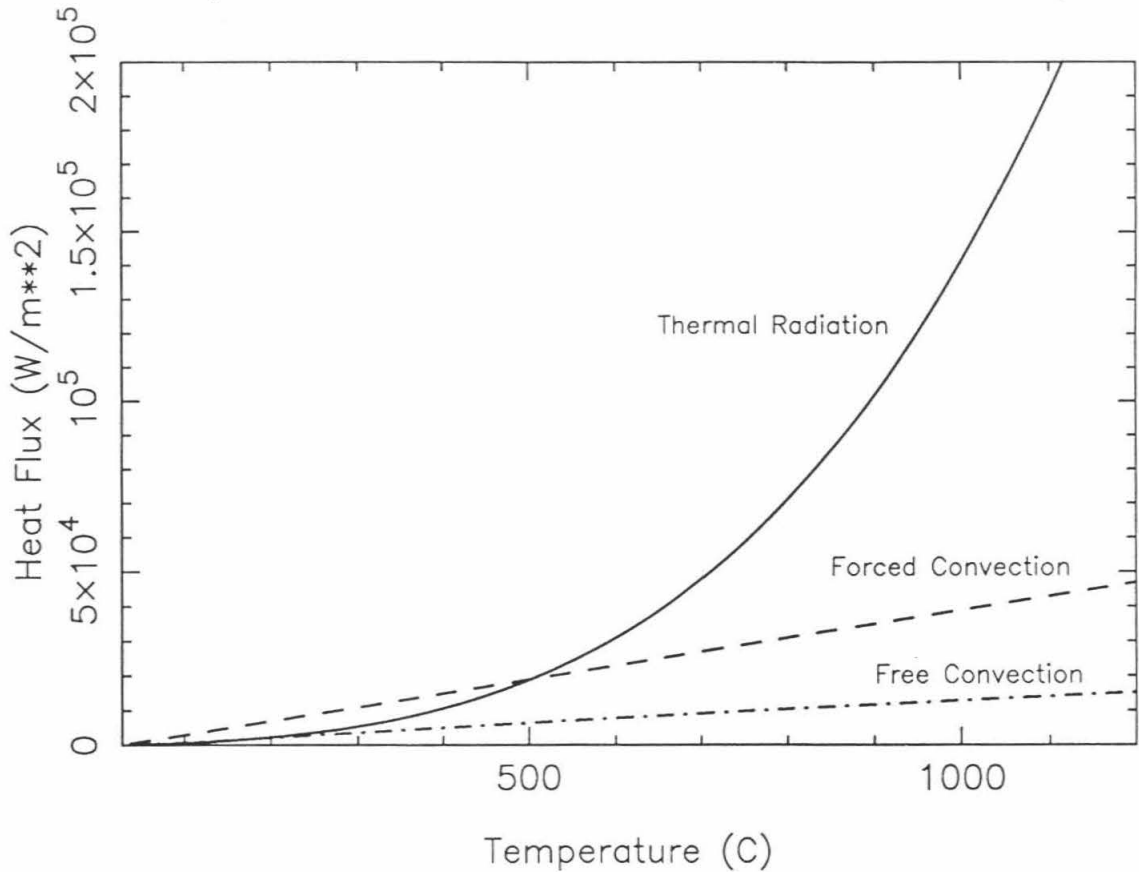


**Figure 4-3: Comparison of Radiative and Convective Heat Loss.** This plots the amount of heat transported by thermal radiation, forced convection, and free convection as a function of surface temperature. A heat transfer coefficient of  $40 \text{ W/m}^2\text{K}$  was assumed for the forced convection and  $13 \text{ W/m}^2\text{K}$  for free convection. Note that, if there is sufficient wind blowing, thermal radiation is the dominant heat loss mechanism only till about  $500^\circ\text{C}$ .

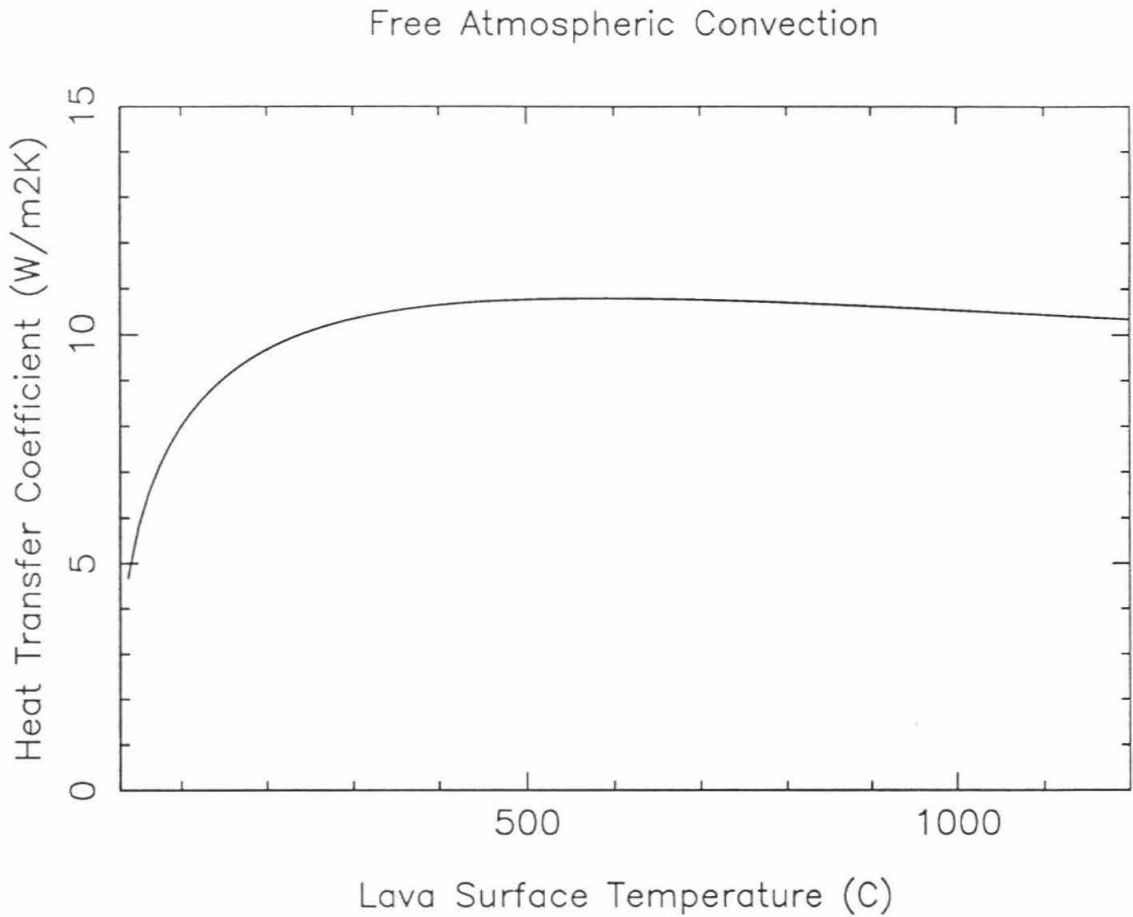


**Figure 4-4: Free atmospheric convective heat transfer coefficient.** Heat transfer coefficient calculated using equations (4.3-4.5) and the properties of air listed in Appendix A. Note that the value for the heat transfer coefficient is nearly constant at about 10-11 W/m<sup>2</sup>K until the lava surface cools below about 300 °C.

Describing cooling by forced atmospheric convection (*i.e.*, the wind) has proven difficult. The forced convective heat transfer coefficient cannot be accurately determined without extensive laboratory experiments and/or numerical simulations. The forced convective heat transfer coefficient is also found to be very sensitive to the geometry of the problem [*e.g.*, Bejan 1984]. Such issues as whether the flow is laminar or turbulent and the growth of the viscous boundary layer have a strong influence on the amount of heat transported by forced convection.

In their cooling model, Head and Wilson [1986] use an unreferenced formula that appears to be derived from experiments involving turbulent flow over a flat plate. Unfortunately, this particular formula gives negative heat transfer coefficients for meter-scale lava flows. Since I found no other more suitable formula, a simple field experiment was conducted.

My method for estimating the forced atmospheric heat transfer coefficient was to measure the heat flux carried by the wind, the ambient temperature, and the lava surface temperature and then solve for  $h$  using equation (4.2). The heat flux from the lava surface into the overlying air ( $q_{\text{conv}}$ ) can be determined by measuring how much air is heated, to what degree, how quickly. In terms of a heat flux per unit surface area of hot lava, this can be written as

$$q_{\text{conv}} = \rho_{\text{air}} C_{p\text{air}} U H \Delta T / L \quad (4.6)$$

where  $\rho_{\text{air}}$  is the density of the air,  $C_{p\text{air}}$  is the heat capacity of the air,  $U$  is the wind velocity,  $H$  is the height of the thermal boundary layer,  $\Delta T$  is the amount by which the air in the thermal boundary layer was heated above the ambient temperature, and  $L$  is the length of the lava flow (see Fig. 4-5).

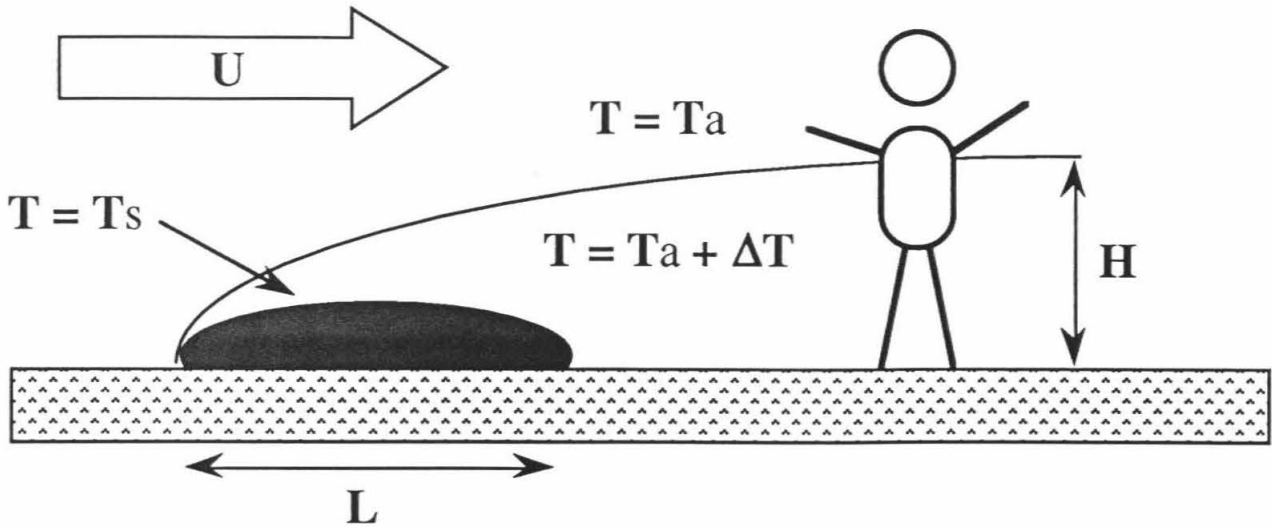


**Figure 4-5: Simple experiment to determine the heat transfer coefficient for forced atmospheric convection over Hawaiian pahoehoe flow lobes.** This figure describes the simple field experiment carried out in March 1993 to constrain the cooling of pahoehoe lobes by the wind. By measuring the wind speed ( $U$ ), thickness of the thermal boundary layer ( $H$ ), and the amount by which the air within the thermal boundary layer is heated ( $\Delta T$ ), one can estimate the amount of heat being carried away from the lava. Note that this geometry is not easy to find in the field since active flow lobes are rarely found in isolation. While the experiment was very crude, the heat transfer coefficient was determined to within a factor of two.

**Table 4-1: Results of simple field experiment to measure cooling by wind.**

	$T_s$	$T_a$	$\Delta T$	$L$	$H$	$U$	$h$
<b>first run</b>	450 °C	30 °C	20 °C	1 m	0.5 m	3 m/s	75 W/m <sup>2</sup> K
<b>second run</b>	120 °C	30 °C	7 °C	6 m	1.5 m	4 m/s	70 W/m <sup>2</sup> K

Tabulation of measurements derived from the experiment described in Figure 4-5. Uncertainties are about  $\pm 10$  °C for surface temperature,  $\pm 2$  °C for ambient temperature and  $\Delta T$ ,  $\pm 10$  cm for  $L$  and  $H$ , and  $\pm 0.5$  m/s for  $U$ . The resulting formal uncertainty in  $h$  is about 20-25 W/m<sup>2</sup>K.

Figure 4-5 sketches how the field experiment was carried out to measure the factors in equation (4.6). A hand-held thermoanemometer was used to measure air temperature and wind speed while a thermocouple was used to measure surface temperatures. The height of the thermal boundary layer was measured by finding the lowest height at which the thermometer consistently found the air temperature to be essentially ambient. Smoke grenades were used to visualize the airflow in order to help locate the boundary layer. This experiment was carried out successfully twice in March of 1993 and the measurements are tabulated in Table 4-1. The raw heat transfer coefficients that were derived are approximately 75 and 70 W/m<sup>2</sup>K. In the second case enough data were collected to conservatively estimate the uncertainty to be  $\pm 30$  W/m<sup>2</sup>K. It is interesting that the value for **h** appears similar for runs with the lava surface at 120 °C and 450 °C, suggesting that **h** has only a weak dependence on surface temperature. This is not surprising since previous workers have used  $T^{4/3}$  [R. Denlinger, written comm., 1993] or  $T^{5/4}$  [Griffith and Fink, 1992a] to describe the temperature dependence for the forced convective heat transfer coefficient.

Despite the retrieval of a heat transfer coefficient, there are a great many deficiencies in my simple field experiment. For example, I was not able to determine the dependence of the heat transfer coefficient on such clearly important factors as wind speed and atmospheric density. Perhaps the most serious problem with my simple experiment is that it could not distinguish between radiative and convective heating of the atmosphere. Since I have already taken into account the radiative heat loss from the surface of the flow, I am only interested in the additional heat being removed by the wind. Using an atmospheric radiative heat transport model, it has been shown that absorption of thermal radiation by H<sub>2</sub>O bands in the atmosphere leads to a few °C/s of atmospheric heating above active flows [M. Gerstell, pers. comm., 1993]. This is about half the measured atmospheric heating. Therefore the measured  $\Delta T$  is only an upper bound on the additional convective heating of the air and this experiment provides only a rough upper bound on **h**. Because of this, I

select 40 W/m<sup>2</sup>K as a nominal value for the forced atmospheric heat transfer coefficient. This value is consistent with the general rule of thumb that forced convection transports 3-5 times more heat than free convection.

However, it must also be noted that my field measurements are inconsistent with micrometeorological models for the internal thermal boundary layer (ITBL). An ITBL forms when air passes over a sharp change in surface temperature, such as passing from a large lake onto the shore [e.g., Stunder and Sethuraman, 1985; Taylor, 1971]. The most sophisticated ITBL models require inputs (such as the stability of the atmosphere) which I did not measure [e.g., Garratt, 1990]. However, Arya [1988] does provide three readily applicable formulas:

$$q_{\text{conv}} = 2 \times 10^{-3} \rho C_p U (T_s - T_a) \quad (4.7)$$

$$q_{\text{conv}} = \rho C_p U \gamma h^2 / (2.25 x) \quad (4.8)$$

$$q_{\text{conv}} = C_H \rho C_p U (T_s - T_a) \quad (4.9)$$

where  $\rho$  is air density,  $C_p$  the heat capacity of air,  $U$  the mean wind speed,  $T_s$  the surface temperature,  $T_a$  the unheated air temperature,  $\gamma$  the adiabatic lapse rate,  $H$  the thickness of the ITBL,  $x$  the downwind distance from the front of the lava, and  $C_H$  is roughly  $(U^*/U)^2$ , where  $U^*$  is the friction wind speed (the theoretical slip speed of the wind across the ground). The quantity  $(U^*/U)$  has been measured as about 0.06 at the Amboy flow field in the Mojave Desert [Greeley and Iverson, 1987]. The Amboy flow field consists of pahoehoe flows that are morphologically similar to those on Hawai'i. Rough input values for Hawaii are  $\rho = 1 \text{ kg/m}^3$ ,  $C_p = 1 \text{ kJ/kgK}$ , and  $\gamma = 0.01 \text{ K/m}$ . When the predictions based on equations (4.7), (4.8), and (4.9) are compared to my field measurements (Table 4-2), it is clear that these expressions seriously underestimate the atmospheric heat transfer. The discrepancy is larger than can be explained by the radiative heating of the atmosphere. I can only speculate that the large heating rate over lava flows drives atmospheric

**Table 4-2: Comparison between field measurements and predictions from micrometeorological models.**

	Measured	Eq. (4.7)	Eq. (4.8)	Eq. (4.9)
<b><math>q_{\text{conv}}</math> (W/m<sup>2</sup>)</b>				
1st run	30 000	2500	3	4500
2nd run	7 000	700	7	1300
<b><math>h</math> (W/m<sup>2</sup>K)</b>				
1st run	75	6	0.008	11
2nd run	70	8	0.07	14

This table shows the heat fluxes and heat transfer coefficients calculated using equations (4.7), (4.8), and (4.9) from micrometeorological models presented in Arya [1988]. Measured values from Table 4-1. The observed heat fluxes and heat transfer coefficients should be divided by about 2 if one wishes to remove the effect of radiative heating of the atmosphere. Note that the forced convective heat transfer coefficients computed using equations (4.7) and (4.9) are roughly equivalent to the calculated free convective heat transfer coefficient. Equation (4.8) appears to be completely inappropriate for this problem. In all cases the predicted heat transfer is significantly less than that which was measured.

convection into a different regime than that investigated by meteorologists.

The final atmospheric convective process to consider is that of air circulating in the fractured solid upper crust of the flow lobe. Cooling by circulating gasses within the solidified lava is important for the cooling of lava lakes [*e.g.*, Hardee, 1982] and lava tubes (see Chapter 5). One estimate of the heat flux by this process is given by Lai and Kulack [1991]. In experiments on porous beds they find the following relationship between the Nusselt number and Rayleigh number:

$$\text{Nu}_D = 0.516 \text{Ra}_D^{0.357} \quad \text{Ra}_D \geq 40 \quad (4.10)$$

$$\text{Nu}_D = hD/k \quad (4.11)$$

$$\text{Ra}_D = (Kg\beta h\Delta TD^2)/(k\nu\kappa) \quad (4.12)$$

where  $h$  is the heat transfer coefficient,  $D$  is the thickness of the permeable layer,  $k$  is the bulk thermal conductivity of the porous layer,  $K$  its permeability,  $g$  is gravitational acceleration,  $\beta$  is the coefficient of thermal expansion,  $\nu$  is the kinematic viscosity of the fluid (air), and  $\kappa$  is the bulk thermal diffusivity of the permeable layer. For a fractured crust 1 cm thick at 900 °C above ambient, with  $k = 1$  W/m K,  $K = 10^{-10}$  m<sup>2</sup>,  $\nu = 2 \times 10^{-2}$  m<sup>2</sup>/s, and  $\kappa = 4 \times 10^{-7}$  m<sup>2</sup>/s, I calculate an  $h$  of about 2 W/m<sup>2</sup>K. However, the Rayleigh Number has a value of only  $8 \times 10^{-5}$ , far below the range in which the above formulas are valid. This low value for the Ra suggests that no significant convection should take place in the initial thin crust of pahoehoe flow lobes. At the very least, this analysis strongly suggests that the effect of air circulating in the chill crust is small compared to the other atmospheric convective processes.

#### 4.2.3 Motion of the Lava

The motion of the molten lava within a flowing pahoehoe lobe obviously transports a large amount of heat. However, I will argue that, for the initial cooling of pahoehoe flow lobes, the net heating (*i.e.*, heat transfer) caused by this motion is negligible. The heating by the advection of lava ( $Q_{adv}$ ) is given by

$$Q_{adv} = \rho C_p \frac{\partial T}{\partial t} = \rho C_p v_x \frac{\partial T}{\partial x} \quad (4.13)$$

where  $\rho$  is the density of the lava,  $C_p$  the heat capacity,  $T$  the temperature,  $t$  is time, and  $v_x$  is the flow speed in the  $x$  direction. Upon examining equation (4.13) it should be clear that (a) large temperature gradients will only exist in the solid, stationary crust and (b) that significant fluid motion is restricted to the isothermal, molten part of the flow lobe. Thus the product of velocity and temperature gradient is zero in most of the lobe.

However, near the stretching, incandescent "lip" of a lobe, advective heat fluxes are significant. In the molten part of the lobe near the front of the lobe, flow velocities are on the order of a few cm/s and temperature gradients could be several °C/cm. In the stretching crust, temperature gradients as high as 1000 °C/cm are reasonable but flow velocities should be less than 1 mm/s. Thus in both cases  $\partial T/\partial t$  could be as high as several 100 °C/s. Such a high advective heat flux is necessary if any incandescent material is to be exposed at all. However, typically, this stretching of the crust continues for less than 10 seconds. Thus ignoring advection is appropriate except for the first few seconds around tearing sections of the crust.

Free convection is possible even within stagnant flow lobes. Using nominal values for basaltic lava ( $\rho = 2000 \text{ kg/m}^3$ ,  $C_p = 1000 \text{ J/kg K}$ ,  $\eta = 100 \text{ Pa s}$ ), it can be shown that the Rayleigh number for even small flow lobes can easily exceed the critical value of 1000 (Figure 4-6). This is true even when one recalls that the temperature difference must be the temperature difference across the molten part of the flow lobe. The free convective heat flux can be computed, as for the atmospheric free convection, using equations (4.2) - (4.5). The convective heat flux within the lobes will only a few  $\text{W/m}^2$ . Recall that the heat flux out of the lobe is on the order of tens of  $\text{kW/m}^2$ . Thus free convection is completely negligible. The excellent fit between a simple conductive cooling model achieves and field data from thick sheet flows suggests that convection is not important even in larger pahoehoe sheets [Hon *et al.*, 1994a]

The flow of lava also causes heating in the form of viscous dissipation. Viscous dissipation is governed by the equation

$$q_{\text{visc}} = \eta (\partial v_x / \partial z)^2 \quad (4.14)$$

where  $\eta$  is the viscosity of the lava and  $\partial v_x / \partial z$  is the velocity gradient.  $\partial v_x / \partial z$  can be estimated by dividing the flow speed by the thickness of the viscous boundary layer ( $\partial z$ ).

## Free Convection Inside Flows

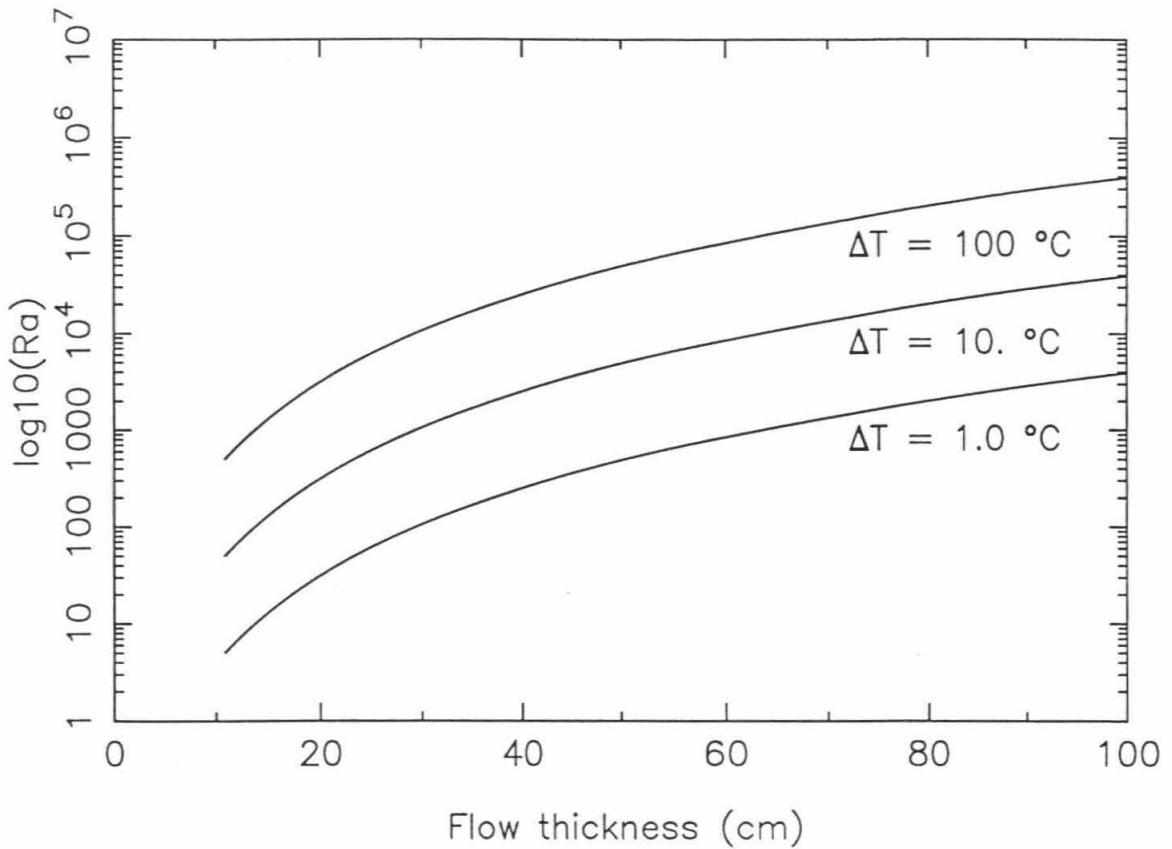


**Figure 4-6: Rayleigh Numbers inside lava flows.** Rayleigh Number is defined in equation (4.5). Inputs were  $\kappa = 7.5 \times 10^{-7} \text{ m}^2/\text{s}$ ,  $\rho = 2000 \text{ kg/m}^3$ ,  $\eta = 100 \text{ Pa s}$ , and the coefficient of thermal expansion was taken to be  $1.5 \times 10^{-5} \text{ K}^{-1}$ . Note that a layer of liquid basalt only 60 cm thick will begin to convect with only a 10 °C temperature gradient across it. This indicates that free convection should occur in even quite small pahoehoe lobes. However, the heat carried by this convection is insignificant.

For a relatively fast pahoehoe flow lobe, reasonable values are 100 Pa s for  $\eta$ , 5 cm/s for  $v_x$  and 1 cm for  $\partial z$ . The resulting  $q_{\text{visc}}$  is 2500 W/m<sup>3</sup>. Using 2000 kg/m<sup>3</sup> for  $\rho$  and 1 kJ/kgK for  $C_p$ , this translates to a heating rate of only about 10<sup>-3</sup> °C/s, which is completely negligible in this problem.

The rise of bubbles in the melt can also cause motion in the a flow lobe. Aubele *et al.* [1988] used Stoke's Law to calculate bubble speeds. They found that bubbles rise an insignificant amount in small flow pahoehoe flow lobes before such lobes freeze solid. However, they also find that bubble rise is a key process in forming the final vesicle distribution in flows that are a meters thick.

#### 4.2.4 Phase Changes

Finally, I consider phase changes that extract heat from flow lobes via latent heat. It is well known that the latent heat of crystallization is a major term in the cooling of gabbroic melts. In fact, the latent heat released during crystallization is often nearly equivalent to the heat released in cooling from the solidus to ambient temperatures. However, it can be seen in hand samples and thin sections that the outer 1-2 cm rind on pahoehoe flow lobes is extremely glassy. This has been confirmed by XRD analyses [Stroncik-Treue, written comm., 1993]. Also, in my thin sections, the glass changes from brown to black at about 1 cm depth. Such color changes in lava lake samples are caused by the onset of the crystallization of oxide minerals. Since only the top 1-2 cm of a pahoehoe flow undergoes significant cooling in the first 5 minutes, and the latent heat of vitrification is very small [*e.g.*, Stebbins *et al.*, 1984], the release of latent heat can be ignored for the initial cooling of pahoehoe flow lobes. As will be shown later, the release of the latent heat of crystallization does appear to be important over the time scale of hours.

The evaporation of water absorbs a remarkable amount of heat, potentially making rain a significant source of cooling, especially in wet climates. Assuming that all the rain evaporates on contact with the lava, cooling by rain can be expressed by

$$q_{\text{rain}} = L_w \rho_w \partial w / \partial t \quad (4.15)$$

where  $L_w$  is the latent heat of vaporization of water ( $2.5 \times 10^6$  J/kg),  $\rho_w$  is the density of water ( $1000$  kg/m<sup>3</sup>) and  $\partial w / \partial t$  is the rate of rainfall. A rain of 1 cm/hr would remove about 7 kW/m<sup>2</sup>. This is equivalent to the heat lost by thermal radiation from a surface at 300 °C. This supports the general field observation that small rain storms have no effect on active lava flows, but a heavy rain sustained for several days may have significant effect on the transport of lava through lava tubes and the "inflation zone."

Intuitively it seems that the exsolution and escape of magmatic gasses from Hawaiian basalts should not have significant thermal effects simply because the gasses make up such a small fraction of the lava (typically <0.5 wt%). As an order of magnitude check, one can calculate the cooling caused by the instantaneous exsolution and boiling off of all the dissolved water. For this crude calculation, let us take the volatiles as 0.5 wt% H<sub>2</sub>O and assume that the latent heat of boiling from lava is the same as boiling pure water. This boiling would result in about 10 °C of cooling. Thus even the instantaneous boiling off of all the dissolved gasses is only a 1% temperature effect. The escape of these gasses after boiling will remove some heat but will not change the temperature of the remaining lava. Based on these arguments I have ignored the exsolution and escape of volatiles.

To briefly summarize the above discussion of physical phenomena, I find only thermal radiation and atmospheric convection to be significant cooling processes at the top of a pahoehoe flow. I shown that radiative heat transfer within lava, radiative heat loss from cracks, convection inside the fractured chill crust, and gas exsolution are negligible. I also argue that rain, the motion of the lava, and the latent heat of crystallization are not important during the initial few minutes of cooling. However, on the time scale of tens of minutes to hours, these latter processes may be significant.

### 4.3 Thermal model

The above analysis of the physical processes acting on pahoehoe flows leads us to approximate real pahoehoe flow lobes with a stagnant, level, lava surface that cools to an unfractured glass. I also assume that the temperature does not vary horizontally, reducing the problem to one spatial variable. This assumption is appropriate on short time scales where the thermal boundary layer is much thinner than the horizontal scale of the flow lobe.

#### 4.3.1 Basic Equations

The cooling of a slab of lava can be modeled by the one-dimensional heat equation with the upper boundary condition reflecting the heat loss from the top of the lava by both thermal radiation and atmospheric convection. The temperature and vesicle dependence of the thermal properties are included. The lobe is assumed to be sufficiently thick to ignore cooling from the bottom during the model run. Mathematically, the problem being solved is

$$\rho(\phi, T) C_p(\phi, T) \frac{\partial T}{\partial t} = \frac{\partial}{\partial z} \left( \kappa_{\text{eff}}(\phi, \rho, T) \frac{\partial T}{\partial z} \right) \quad (4.16)$$

$$q_{\text{top}} = q_{\text{rad}} + q_{\text{conv}} = k_{\text{eff}}(z = 0, t) \frac{\partial T}{\partial z} \Big|_{z=0} \quad (4.17)$$

$$\frac{\partial T}{\partial z}(z = Z, t) = 0 \quad (4.18)$$

$$T(z, t = 0) = T_0 \quad (4.19)$$

where  $T$  is temperature;  $z$  depth;  $t$  time;  $\rho$ ,  $C_p$ , and  $k_{\text{eff}}$  are the temperature and porosity dependent density, heat capacity, and effective thermal conductivity of the lava;  $\phi$  is the porosity of the lava;  $r$  the mean radius of the vesicles;  $q_{\text{top}}$  is the heat flux at the surface;  $q_{\text{rad}}$  is the radiative heat flux;  $q_{\text{conv}}$  is the atmospheric convective heat flux;  $Z$  is the depth to the bottom of the model; and  $T_0$  is the initial temperature.  $q_{\text{rad}}$  and  $q_{\text{conv}}$  are calculated

using equations (4.1) and (4.2) respectively. The expressions used to describe the temperature and porosity dependence of  $\rho$ ,  $C_p$ , and  $k_{\text{eff}}$  are described in Chapter 3.

#### 4.3.2 Numerical Methods

Because of the non-linearity of the upper boundary condition, the equations making up the thermal model must be solved numerically. A simple, fully explicit, finite difference algorithm is used with 500 grid points spaced 0.1 mm apart and time steps of 1 millisecond. Small time steps are necessary because of the rapidly changing surface temperature. This drives the grid spacing to small values in order to maintain numerical stability. This in turn requires that all computations be done in 8-byte arithmetic to keep round-off errors negligible. The temperature dependent properties must be evaluated at each time step and grid point. The resulting program is simple but also very CPU intensive.

The numerical model was checked by two runs with upper boundary conditions where analytical solutions exist:  $T(z=0,t) = T_a$  and  $q_{\text{top}} = h(T_s - T_a)$  (Carslaw and Jaeger, 1959). The numerical solutions converged to the analytical solution in less than 100 time steps. Other tests confirmed that the numerical model conserves energy. Both the code and test runs for the numerical model are described in more detail in Appendix B.

#### **4.4 Comparison to field measurements**

The test that the numerical model contains all the relevant physical processes and properly solves the appropriate equation is its comparison with field measurements. The gentle, slow moving character of pahoehoe flows makes obtaining field measurements from them relatively easy, so a significant volume of data is available. I used three sets of field measurements from the Pu'u 'O'o - Kupaianaha eruption of Kilauea Volcano. One data set is published in Hon *et al.*, [1994b], the second was collected by Roger Denlinger (USGS) in 1989, and the third was collected by myself in 1993.

The data of Hon *et al.*, [1994b] include simultaneous measurements at several different depths over a period of days. These measurements were made on large sheet flows in and around the town of Kalapana in the Spring of 1990. Surface temperatures were measured with a radiometer while temperatures within the flows were measured by Cromel-Alumel (K-type) thermocouples. The reported depth of the thermocouples assumes that the probes were not bent during insertion. The thermocouples ranged from 1/16" to 1/4" in diameter, with the larger ones used to penetrate to the greater depths. Temperature data from the initial cooling of 3 separate sheet flows are presented in Figure 4-7a.

Two other sets of measurements were collected specifically for understanding the cooling of small flow lobes (Fig. 4-7b). The first data set was collected March 1-9, 1989 about 5 km downslope from the Kupaianaha vent by Roger Denlinger. These data consist of temperature measurements made 1-2 mm below the surface of 4 separate artificially induced pahoehoe flow lobes. The lobes were created by breaking open a larger flow lobe with a shovel. A fine gauge unsheathed K-type thermocouple was hooked just below the skin and allowed to freeze into the lobe. The data was recorded by videotaping the readings from a thermocouple transducer. The lobes were collected after they had cooled in order to determine the depth to which the thermocouples had been inserted and the vesicularity of the lava. Overall, the vesicularity of the lobes is about 50% with vesicle distributions identical to what Walker [1989] terms spongy pahoehoe.

My own measurements were made May 17-19, 1993 on the Kamoamoia flow field near the end of the Chain of Craters Highway. Temperatures were measured using a 1/16" stainless steel sheathed grounded K-type thermocouple inserted 2-3 mm into 3 active flow lobes. The temperatures were read off of a thermocouple reader at 10-15 second intervals and recorded in a notebook. These flows were only slightly more sluggish and dense than the flows measured in the earlier experiments.

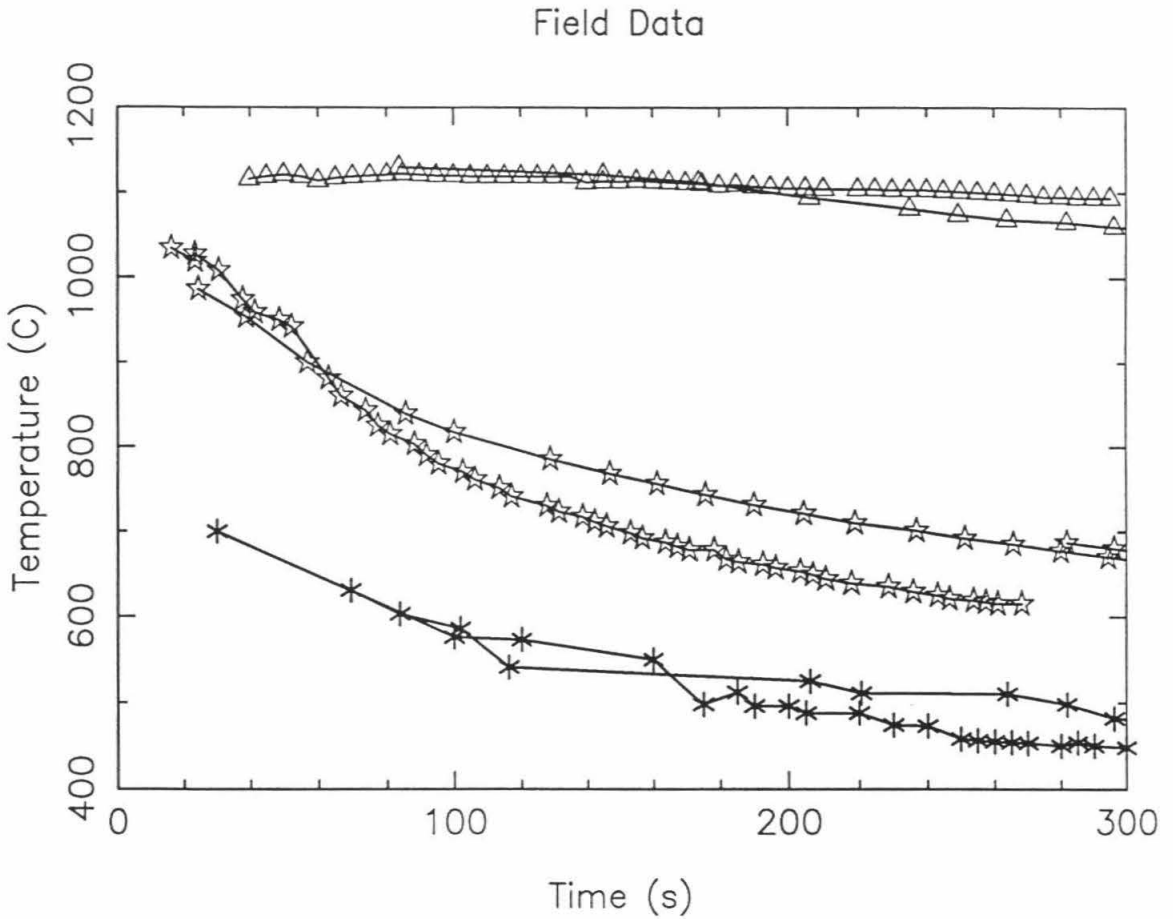


**Figure 4-7a: Field measurements from cooling pahoehoe flow lobes.** Data from Hon *et al.*, [1994b]. These cooling curves were collected from large sheet flows in the Kalapana area in the Spring of 1990. Surface temperature (asterisks) was measured with a radiometer. Measurements at 1 mm (stars) and 2 cm (triangles) depth were made with sheathed K-type thermocouples.

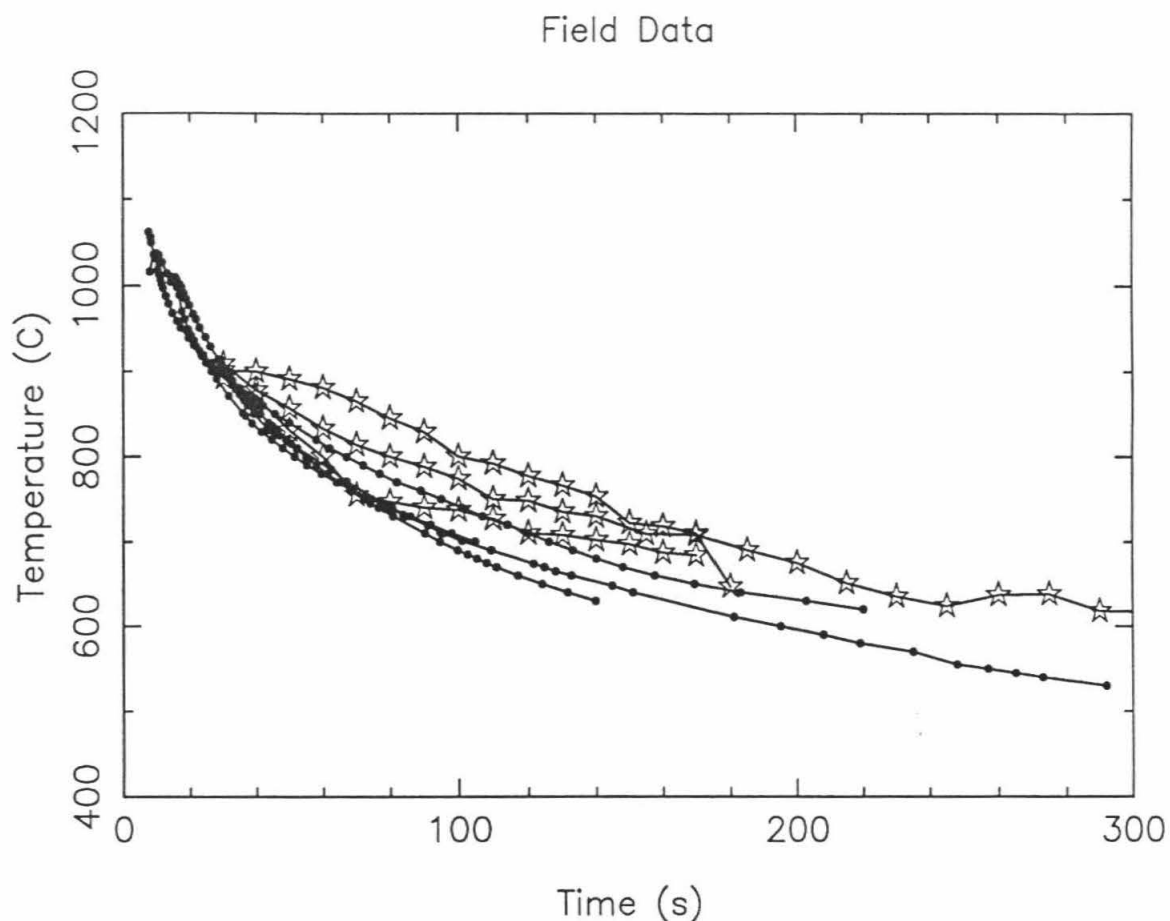


**Figure 4-7b: Field measurements from cooling pahoehoe flow lobes.** Data collected from small pahoehoe flow lobes by the authors. 1989 measurements by Denlinger (solid dots) were made on the Kupaianaha flow field about 5 km from the lava pond. 1993 data (stars) was collected by myself near the coast from the Kamoamoa flow field. 1989 measurements used fine gauge bare thermocouples (response time < 10 seconds) inserted a little more than 1 mm below the surface. 1993 data used 1/16" sheathed K-type thermocouple (response time about 40 seconds) inserted 2-3 mm below the surface.

## Comparison of Model Output and Field Data

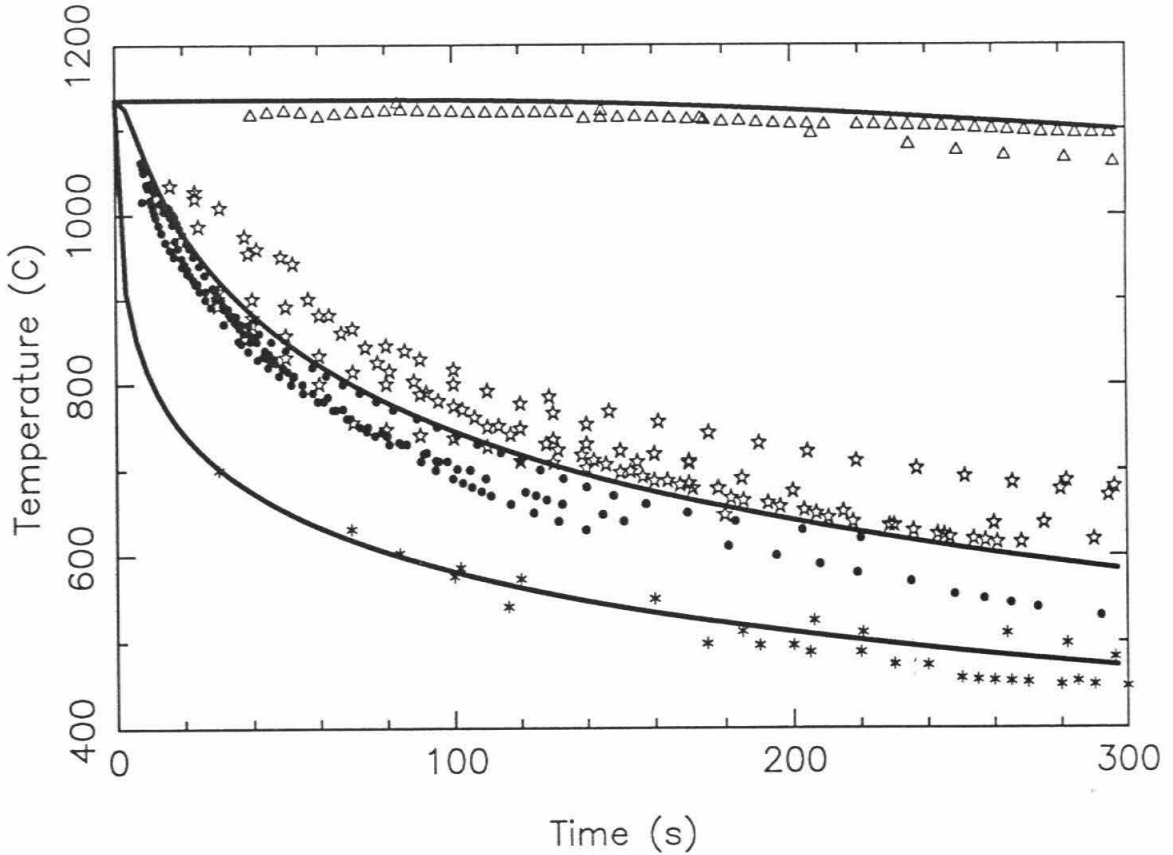


**Figure 4-8: Comparison of field data with model results.** This figure overlays model cooling curves (solid lines) over all the field data. The different symbols represent data points at different depths: asterisks = surface temperatures [Hon *et al.*, 1994b], solid dots = 1-2 mm depth [Denlinger, 1989], stars = 2-3 mm depth [Keszthelyi, 1993], triangles = 2 cm depth [Hon *et al.*, 1994b]. Model cooling curves are plotted for the surface, 1mm depth, and 2 cm depth. The thermal model was run with  $T_0 = 1135 \text{ }^\circ\text{C}$ ,  $T_a = 30 \text{ }^\circ\text{C}$ ,  $\phi = 50\%$ ,  $r = 1 \text{ mm}$ ,  $h = 40 \text{ W/m}^2\text{K}$ ,  $\epsilon = 0.95$ , and included temperature and vesicle dependent thermal properties. The correspondence between the model and measured temperatures is quite remarkable. This makes us confident that the model accurately represents the major physical processes involved in the initial cooling of small, slow-moving, pahoehoe lava flows.

In order to accurately model these Hawaiian flow lobes, reasonable input values had to be selected. Based on the deepest thermocouple data from Hon *et al.* [1994b], an initial lava temperature of 1135 °C was selected. The porosity for all of these flows was estimated to be approximately 50% and other studies [Hon *et al.*, 1994a; Mangan *et al.*, 1993; Wilmoth and Walker, 1993] have shown that vesicles in pahoehoe flow lobes are typically about 1 mm in diameter. I have not included the variation of vesicularity with depth in this model run. The other input parameters were 30 °C for the ambient temperature, 40 W/m<sup>2</sup>K for the atmospheric convective heat transfer coefficient, and 0.95 for the emissivity of the lava.

The correspondence between the model output and the field data is excellent (Fig. 4-8). The scatter in the field data can be explained by small errors in measuring the depth of the thermocouple insertion, especially since pahoehoe surfaces have millimeter scale topography making depth measurements to better than  $\pm 0.5$  mm meaningless. Measurement errors, as well as minor variations in lava porosity, vesicle sizes, initial lava temperature, and ambient conditions may also have contributed to the discrepancy between the model output and field measurements.

#### **4.5 Comparison with other cooling models**

The next question is whether my model represents the initial cooling of pahoehoe lava flows more accurately than earlier cooling models. As previously noted, most of the earlier thermal models for lava flows cannot be applied to pahoehoe lava flows. Thus I will compare my model results with two extremely simple analytical models, the cooling model presented by Head and Wilson [1986], and the empirical fit to field data presented by Hon *et al.* [1994a].

#### 4.5.1 Simple Conductive Cooling Model

The simplest problem which resembles a cooling pahoehoe flow lobe is a slab of lava cooling by conduction as its surface is held at ambient temperature. This model should overestimate the cooling rate since the surface of a flow lobe does not instantaneously reach ambient temperatures. However, simple model also has the virtue of the error function solution that has often been used for order of magnitude discussions about the cooling of dikes and lava flows:

$$T(z,t) = T_a + (T_0 - T_a) \operatorname{erf}(z/\sqrt{4\kappa t}) \quad (4.20)$$

where  $T_a$  is the ambient and surface temperature,  $T_0$  is the initial lava temperature,  $z$  is depth,  $\kappa$  is thermal diffusivity, and  $t$  is time [Carslaw and Jaeger, 1959]. This solution produces the well known square root of time dependence for the growth of a chill crust. When one compares this analytic solution to my numerical model (Fig. 4-9) it is clear how grossly it overestimates the initial cooling of a pahoehoe flow lobe. However, the square root of time dependence still holds (Fig. 4-10). Also, with the inclusion of the latent heat of crystallization a simple conductive cooling model works well on the time scale of hours to days, when the surface temperature is close to ambient [Hon *et al.*, 1994a].

#### 4.5.2 Simple Radiative Cooling Model

The next model I examined is that of a slab of finite thickness cooling by radiation. In the case that the entire slab remains isothermal, a simple analytical solution exists:

$$t = \rho C_p H (T^{-3} - T_0^{-3}) / (3 \epsilon \sigma_b) \quad (4.21)$$

where  $t$  is time,  $H$  is the thickness of the slab, and the other terms are defined as earlier. Several workers have used this solution to build thermal models for lava flows [*e.g.*,

## Model Cooling Curves

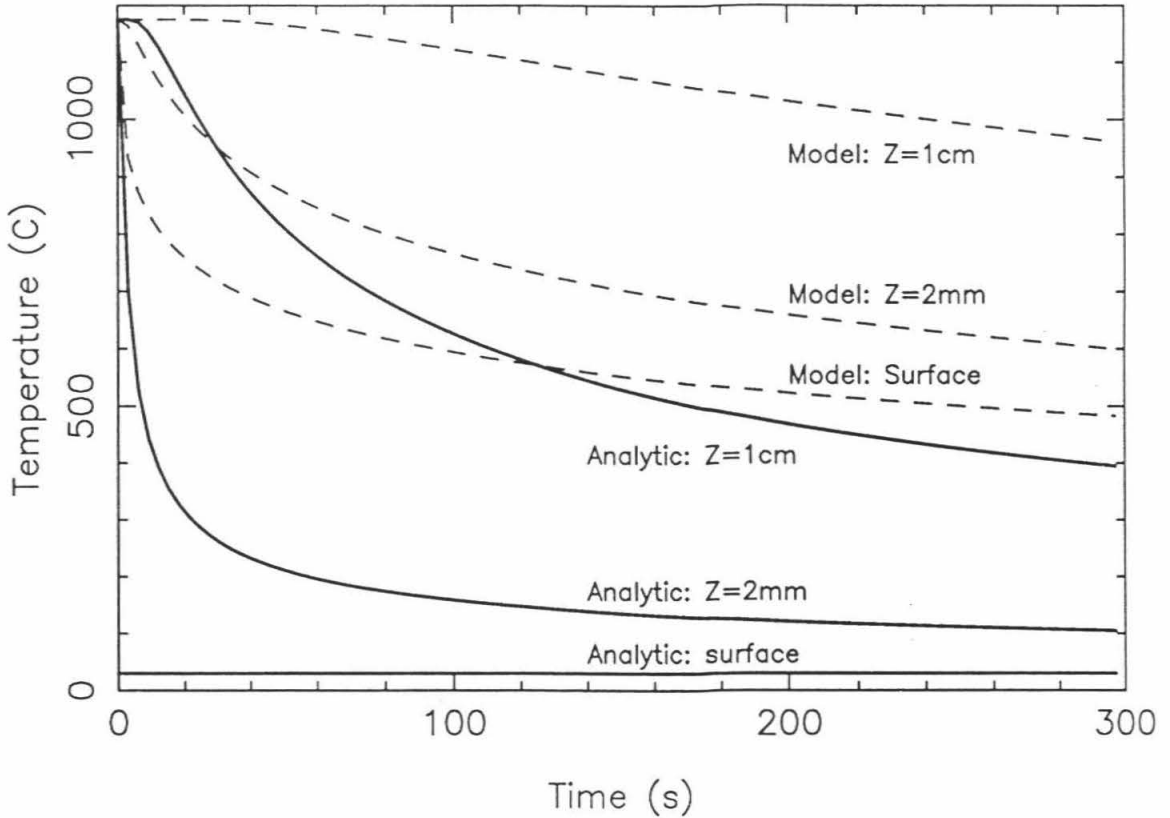


**Figure 4-9: Comparison of numerical cooling model to simple analytic model.** Analytic model is a conductively cooling slab with a fixed surface temperature and is shown with solid lines. My cooling model output is shown with dashed lines. Temperatures are shown for the surface, 2 mm depth, and 1 cm depth. The initial lava of 1175 °C, a surface temperature of 30 °C, and a thermal diffusivity of  $1 \times 10^{-6} \text{ m}^2/\text{s}$  was used in the analytic model. As expected the analytic cooling model grossly overestimates the cooling rate. This is because the surface does not actually reach ambient temperatures instantaneously.

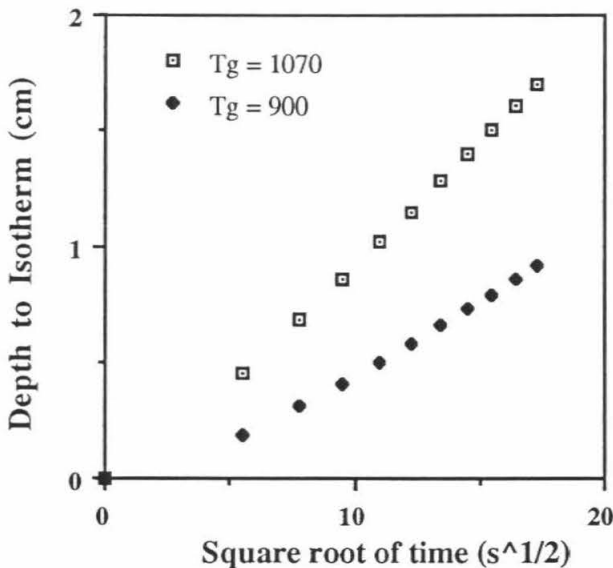


**Figure 4-10: Model predictions for depths of isotherms.** The two curves are for two different isotherms (1070 °C and 900 °C). Note that the depth of the isotherms increases linearly with the square root of time.

Danes, 1972; Park and Iverson, 1984; Pieri and Baloga, 1986]. Clearly, these models can only be valid if the lava flow is well stirred and isothermal. Figure 4-11 plots cooling curves for various slab thicknesses. This figure shows that the assumption that the entire 30 cm thick lobe is isothermal seriously underestimates the surface cooling rate. However, this same figure shows that one can roughly approximate the initial cooling of a pahoehoe lobe with a 1 cm thick isothermal chill crust that cools radiatively. As the chill crust grows with time and as atmospheric cooling becomes more important, this approximation quickly breaks down.

There are more sophisticated thermal models that expand upon this simple radiative cooling model [*e.g.*, Crisp and Baloga, 1990; Gregg and Greeley, 1993; Crisp and Baloga, in press] that I will only briefly discuss. For example, Crisp and Baloga [1990] divide a

## Model Surface Cooling Curves

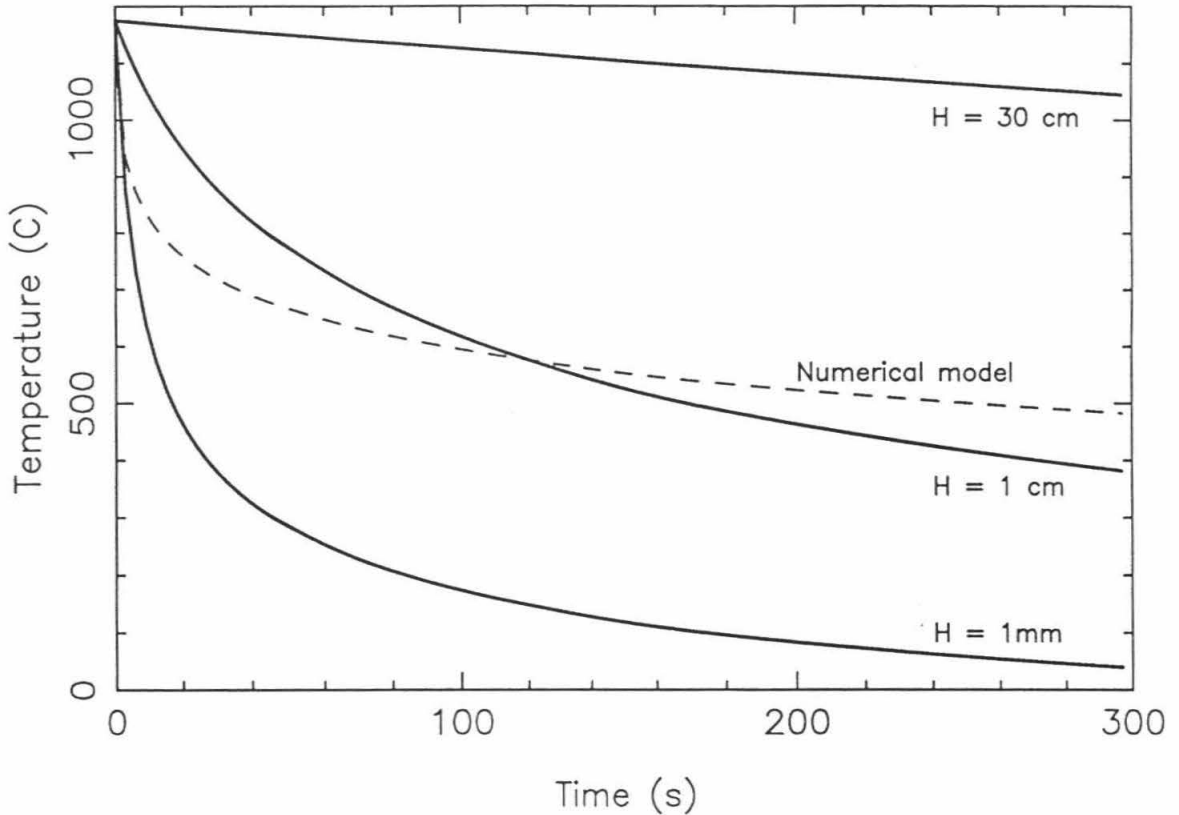


**Figure 4-11: Comparison of numerical cooling model to simple radiative cooling model:** Radiative model is based on an isothermal slab that cools by radiation from the surface. The interior of a lava flow would conceivably be nearly isothermal if it were well-mixed. Model surface temperatures are shown for different slab thicknesses. (solid lines). Other inputs are 0.95 for  $\epsilon$ , 1350 kg/m<sup>3</sup> for  $\rho$ , and 1100 kJ/kg K for  $C_p$ . This plot shows the magnitude of the error caused by assuming that small pahoehoe lobes are well-mixed. The initial cooling of a lobe can be roughly approximated by the radiative cooling of just the outer 1 cm crust.

lava flow into a colder, fractured crust and an isothermal hot interior. This and other more complex models can theoretically achieve improved fits to the field data because they have more free parameters. However, none of these models are truly applicable to pahoehoe flows because they retain the assumption of a well-mixed interior, which is not valid for small flow lobes. Furthermore, it is important to note that all of the models discussed to this point have ignored cooling by the wind.

#### 4.5.3 Cooling Model of Head and Wilson [1986]

The third model I wish to investigate in detail is that of Head and Wilson [1986]. Head and Wilson attempt to solve nearly exactly the problem same I have: a lava flow cooling at its top by both radiation and atmospheric convection and heat transport in its interior by conduction. They differ from my model only in that they include latent heat but ignore the temperature and porosity dependence of thermal properties. Unfortunately, they make mathematically unjustifiable steps in deriving their model surface temperature. They start with the analytical solution to a conduction problem with a fixed surface temperature and a phase change (Stefan Problem). This solution is then used to compute the heat flux out the top of the lava flow. Then a hypothetical surface temperature is found that could produce this heat flux via radiative and conductive cooling. However, since they are still using the solution to the problem with a fixed surface temperature, this hypothetical surface temperature has no mathematical relevance. Furthermore, the hypothetical surface temperature does not even approximate the field measurements. The technique of Head and Wilson [1986] would suggest that the surface of a Hawaiian pahoehoe flow would reach 470 °C only after 8.5 hours of cooling. In reality it takes about 5 minutes (see Fig. 4-8).

#### 4.5.4 Empirical Fit of Hon *et al.* [1994a]

The last model I wish to discuss is the purely empirical fit to field measurements presented in Hon *et al.* [1994a]. They find that the measured cooling curves are very

linear when plotted on a log-normal graph. For the surface temperature, their best fit line is given by

$$T(t) = 330 \log_{10}(t) - 140 \quad (4.22)$$

where  $t$  is expressed in hours and  $T$  in  $^{\circ}\text{C}$ .

Since I have already shown that my model accurately reproduces the field measurements of Hon *et al.* [1994a], it is natural that there is good correspondence between my numerical model and their empirical fit (Fig. 4.12). The interesting points derive from the subtle discrepancies between the two curves. Since the empirical fit is made to temperature data covering many hours of cooling, I expect it to reflect the influence of the release of the latent heat of crystallization and perhaps other physical phenomena not included in my thermal model. In fact, after about the first minute, the empirical cooling curve is significantly more shallow than my model cooling curve. Extrapolating from Figure 4-12, one can see that after some tens of minutes the empirical fit will be significantly warmer than my model output. This demonstrates that ignoring latent heat is not justified on the time scale of hours. However, it should be noted that my cooling curves match the field data significantly better than the empirical fit in the first 5 minutes.

#### **4.6 Model predictions:**

Given that a good empirical fit to the field data exists, one might ask what is gained by producing a (somewhat) complex numerical model. The key is that a model allows one to set up controlled experiments in which parameters can be changed one at a time. These parameters can also be changed to conditions under which no field data have been collected, such as for extra-terrestrial or submarine lava flows. In this section I examine the sensitivity of the model predictions of the cooling of pahoehoe flows to (1) the initial temperature of the lava, (2) lava porosity, (3) and the atmospheric heat transfer coefficient.

## Surface Cooling Curves

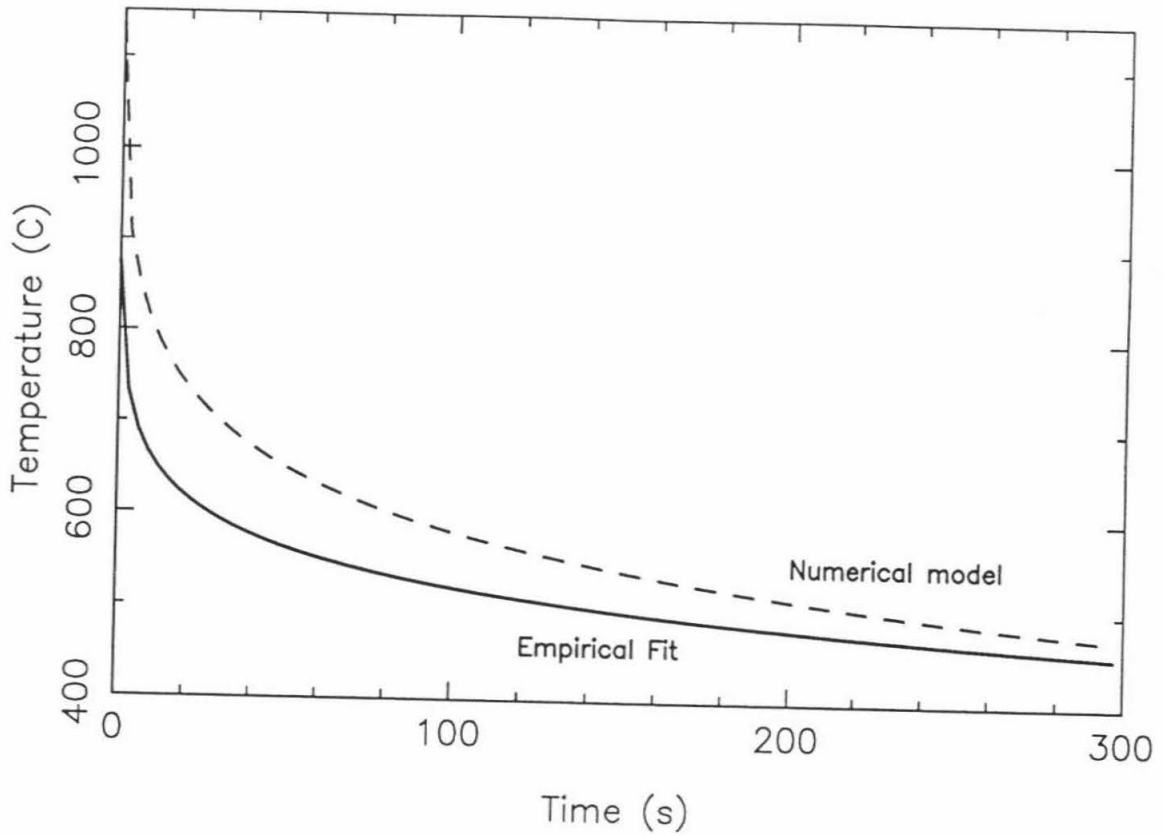


**Figure 4-12: Comparison of numerical cooling model to empirical fit.**

Empirical fit is for the surface temperature as reported in Hon *et al.* [1994a] and is shown in solid line. Since my numerical model (dashed line) fits the data of Hon *et al.*, very well, it is similar to the empirical fit. Note that while the empirical fit is cooler over the first few minutes, it is cooling more slowly than my numerical model. I interpret this to show the effect of latent heat over longer time scales.

Varying the other input parameters, such as emissivity and ambient temperature, within reasonable bounds has no significant effect.

#### 4.6.1 Initial Lava Temperature

Figure 4-13 shows the effect of varying the initial lava temperature between 1200 and 1000 °C. Note that, after about a minute, a 100 °C difference in initial lava temperature only produces a 30 °C difference in the surface temperature and that the cooling curves are essentially parallel. The fact that the changes in surface temperature are smaller than the changes in lava temperature is not difficult to explain. If the lava is initially hotter, the heat loss at the surface will be greater. Therefore there must be a steeper temperature gradient in the outer crust. Thus the  $\Delta T$  across the crust of the initially hotter flow will be larger than the  $\Delta T$  across the crust of the initially cooler flow. Therefore, if the thicknesses of the crusts do not change significantly, the difference in the surface temperatures will be smaller than the difference in the temperatures at depth.

What is somewhat more surprising is that the cooling curves are remarkably parallel. Given the  $T^4$  dependence of radiative cooling, relatively small changes in surface temperature should have significant effect on the cooling rates of a flow lobe. I suggest that thermal radiation is so effective that it will drop the surface temperature to about 600 °C in a little over a minute, irrespective of the exact initial temperature. Figure 4-13 shows that increasing the initial temperature by 100 °C merely delays the lobe reaching 600 °C by about 20 seconds. Once a flow cools below about 600 °C, atmospheric convection becomes an important process (Fig. 4-3) and heat loss becomes linear with surface temperature. Thus below a surface temperature of 600 °C the model flow lobes follow parallel cooling curves.

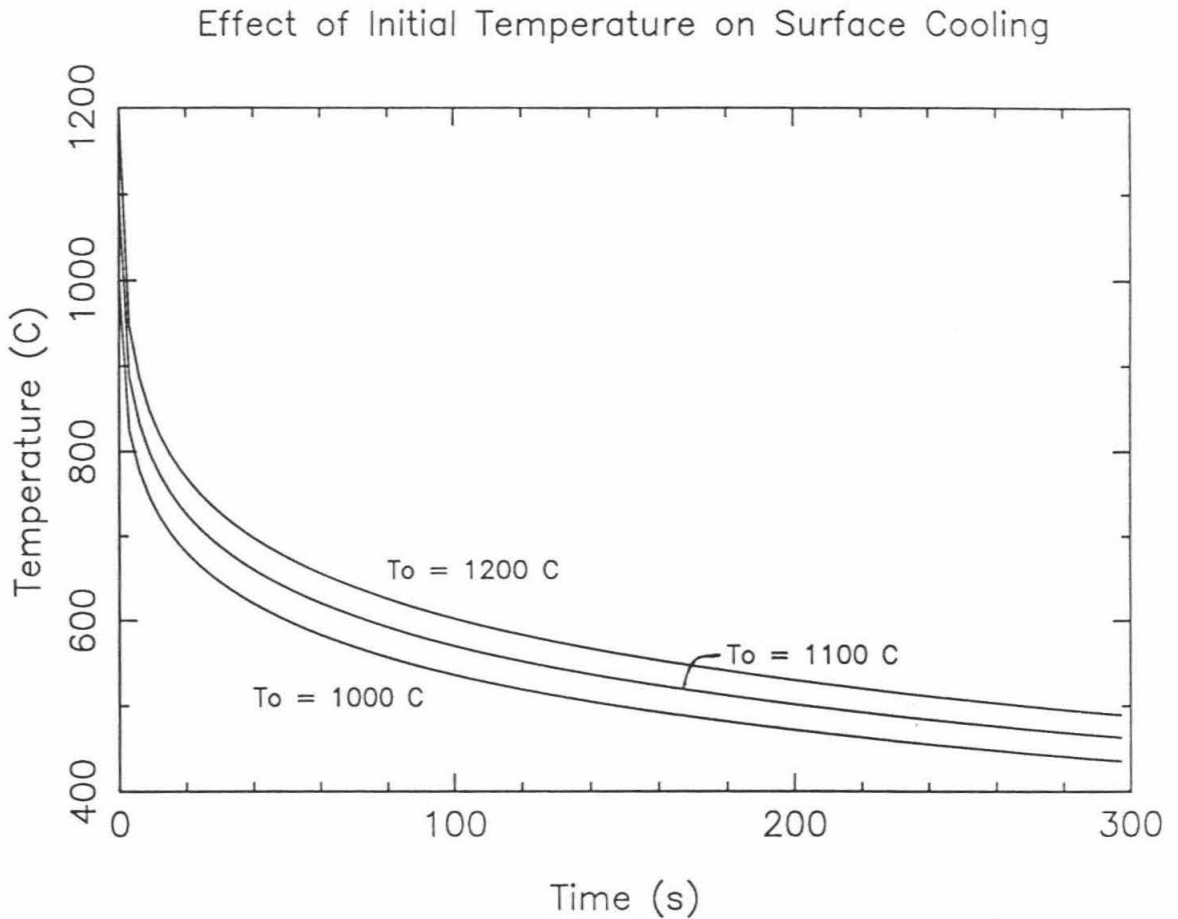


**Figure 4-13: Predicted effect of changing the initial lava temperature.** Model surface cooling curves for initial lava temperatures of 1200 °C, 1100 °C, and 1000 °C. Note that the difference in surface temperatures is nearly instantly reduced to about a third of the initial temperature difference. Also note that the cooling curves remain very parallel.

#### 4.6.2 Porosity

Figure 4-14 show the effect of varying the porosity of the lava from 0 to 75%. After about a minute, the surface of a lobe with 75% vesicularity will be about 100 °C cooler than that of a lobe with 25% vesicles, if all other parameters are held constant. This temperature difference between the surfaces of dense lobes and vesicular lobes continues to grow slowly with time.

This type of dependence of surface cooling rate on porosity has actually been observed [Jones 1992, 1993] and was discussed at length in Chapter 3. In Chapter 3, I suggested that the differences in surface cooling rate could be explained by examining thermal inertia. Since porosity can greatly reduce thermal inertia, a porous flow will have a thin chill crust that is cooled greatly while a dense flow will have a thicker layer cooled less. This is precisely what the model temperature profiles show (Fig. 4-15). The model run at 75% porosity has a thermal boundary layer about 1.5 cm thick and a surface temperature of 440 °C while the run at 0% porosity has a 2.5 cm thick boundary layer and a 550 °C surface temperature. This quantitatively supports the qualitative arguments in Chapter 3.

However, the values from the plot of Jones [1992] do not precisely match my model output (compare Fig. 3-1 and Fig. 4-14). In particular, the difference in cooling rate reported between the lobes with 23% and 28% porosity is far greater than the model predictions. Even the difference between the 28% and 54% porosity is greater than my model predictions. I speculate that the differences can be explained by the difficulty Jones has in determining the point in time where the lobes first broke out. Sliding his data along the time axis could produce much better correspondence between his observations and my model predictions. It is also possible that unmeasured environmental factors (especially wind speed) might be affecting the Jones' measurements.

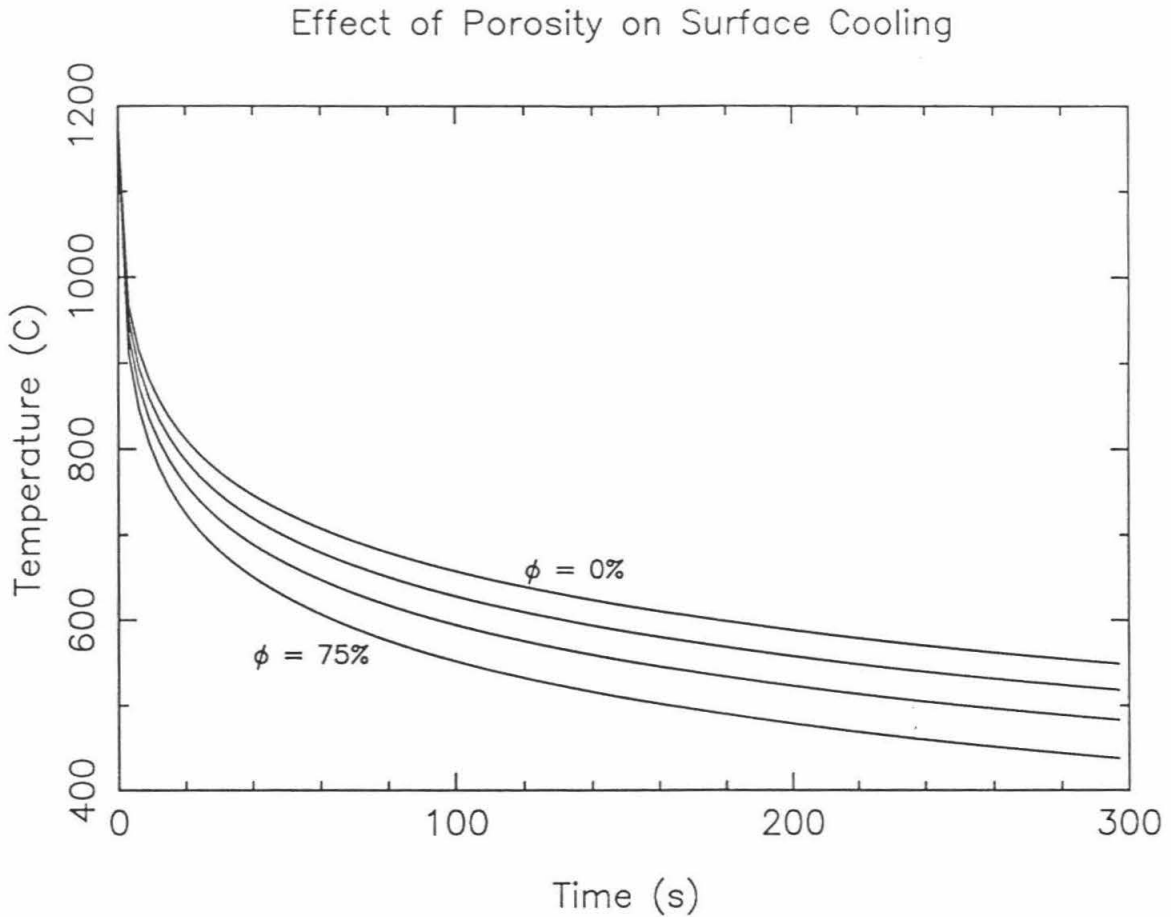


**Figure 4-14: Predicted effect of changing porosity.** Model predictions for the surface cooling of lobes with porosities of 0%, 25%, 50%, and 75%. Only the 0% and 75% curves have been labeled, but the effect of porosity on cooling rate is monotonic. Note that the predicted difference for surface temperatures of lobes with 25% and 50% porosity is about 30 °C after 5 minutes of cooling. This is less than observed by Jones [1992] (see Fig. 3-1). Also note that the temperature differences continue to grow with time.

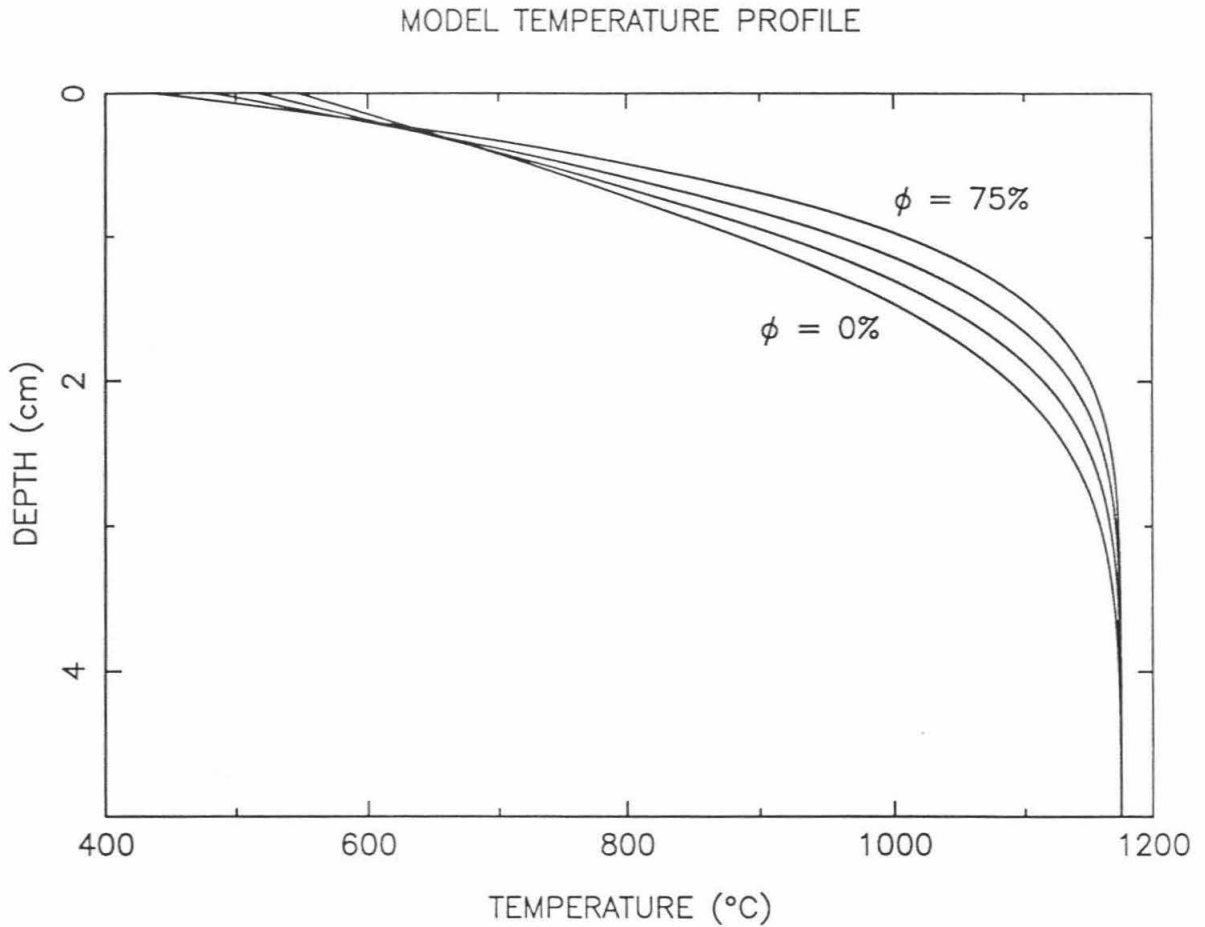


**Figure 4-15: Predicted temperature profiles through flow lobes of different porosities.** Temperature profiles after 5 minutes of cooling for model lobes with porosities of 0%, 25%, 50%, and 75%. Again, only the 0% and 75% curves are labeled, but the effect of porosity is monotonic. Observe that increasing porosity both reduces the thickness of the thermal boundary layer and makes the surface cooler. This is exactly as was qualitatively predicted in Chapter 3.

#### 4.6.3 Atmospheric Convective Cooling:

The other parameter to which the model is highly sensitive is the atmospheric convective heat transfer coefficient ( $h$ ). Figure 4-16 shows the cooling curves for  $h = 0$ , 15, 40, and 70 W/m<sup>2</sup>K. The  $h = 0$  run demonstrates the effect of completely ignoring atmospheric convection,  $h = 15$  W/m<sup>2</sup>K is my minimum estimate (*i.e.*, for convective cooling with no wind),  $h = 40$  W/m<sup>2</sup>K is my best estimate, and  $h = 70$  W/m<sup>2</sup>K is about the largest value permitted by my simple field experiment.

From Figure 4-16 one can see that ignoring atmospheric convection in the first five minutes is a significant, but not overwhelming error. However, ignoring atmospheric convective cooling is completely unacceptable on a time scale of hours, especially if there is a wind. This is made clearer by referring back to Figure 4-3. Forced convection (with  $h = 40$  W/m<sup>2</sup>K) becomes more important than thermal radiation at 500 °C. The surfaces of pahoehoe flow lobes reach 500 °C after about 4-5 minutes. However, if there is no wind, atmospheric convection may not match thermal radiation until the surface drops below 200 °C. The model predicts that, after 5 minutes of cooling, a flow lobe in stagnant air should be about 70 °C hotter than one cooling in a wind.

### **4.7 Future applications for my model**

#### 4.7.1 Field Measurements

I expect that my cooling model will be useful in planning future field observations. For example, the 70 °C difference in the surface temperatures predicted for cooling in stagnant versus moving air should be easily observed. In fact, I speculate that this may resolve some of the discrepancy between the data of Jones [1992] and my model results. Still, it is an interesting question as to why a dependence of lava cooling rate on wind speed has not been previously reported. It is possible that the rather constant weather conditions during field work on the Pu'u 'O'o - Kupaianaha flow field has allowed the effect of wind to be overlooked in earlier field studies. While collecting my measurements, it was noted

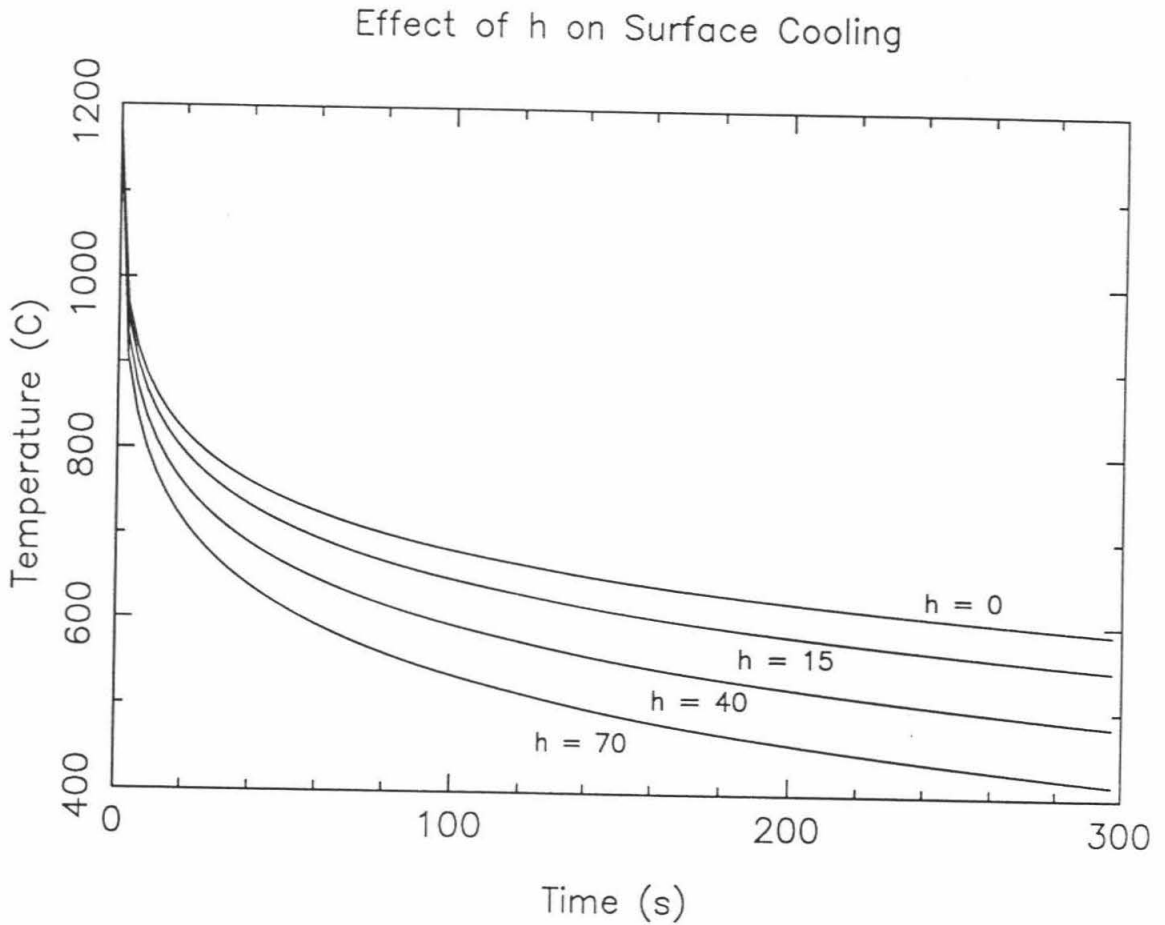


**Figure 4-16: Predicted effect of changing the atmospheric convective heat transfer coefficient.** Model surface cooling curves for  $h = 0, 15, 40,$  and  $70 \text{ W/m}^2\text{K}$ . My model predicts that there could be a  $70 \text{ }^\circ\text{C}$  temperature difference between lobes cooling in stagnant air ( $h = 15 \text{ W/m}^2\text{K}$ ) and in a wind ( $h = 40 \text{ W/m}^2\text{K}$ ). This also shows that if  $h$  is actually as high as  $70 \text{ W/m}^2\text{K}$ , then my model would not fit the field data very well.

that the temperature appeared to drop more quickly when a gust of wind came up.

I suggest that it would be a very worthwhile, and rather simple, experiment to measure the cooling rate of pahoehoe lobes versus wind speed. It would also be important to conduct more controlled experiments with an artificially heated plate. In any case, it is now clear that modeling the cooling of pahoehoe flows on the time scale of hours requires a better characterization of the convective heat transfer coefficient between the atmosphere and the lava surface.

#### 4.7.2 Chill Crust Formation

My model should help understand the formation of the 1-2 cm thick glassy rind on pahoehoe flow lobes. Since most of the distinctive centimeter scale surface morphology of pahoehoe flows forms in the first few minutes, differences in this rind may explain certain forms of pahoehoe (*e.g.*, shelly pahoehoe and blue-glassy (P-type) pahoehoe). For example, there has been some discussion about the origin of the thick, blue, glassy rind on dense (P-type) pahoehoe lobes. Based on my modeling I would suggest that the thick glassy layer is the consequence of a thicker thermal boundary layer in denser lava. However, understanding the conditions for glass formation in these lavas is challenging.

In principle, it should be possible to predict the crystallinity as a function of depth from my model outputs. The volume fraction of melt converted to crystals ( $\phi_{xtl}$ ) is given by

$$\phi_{xtl} = 1 - \exp(-ct^m) \quad (4.23)$$

where  $c$  is a function of crystal shape and the nucleation and growth rates.  $t$  is time and  $m$  is a constant that varies between 4 for pure heterogeneous nucleation and 3 for homogenous nucleation [*e.g.*, Kirkpatrick, 1981; Cashman, 1993]. For homogenous nucleation of generally spherical crystals,

$$c = (\pi/3) N G^3 \quad (4.24)$$

where  $N$  is the nucleation rate ( $\#/cm^3 s$ ) and  $G$  is the growth rate ( $cm/s$ ) [*e.g.*, Uhlmann, 1972]. Both the nucleation and growth rates for crystals can be considered functions of either undercooling or cooling rate. In multi-component systems, cooling rate is the more natural parameter to use. These functions for nucleation and growth rates have been measured for relatively few geologically interesting materials. However, there are data on the growth of plagioclase crystals in Makaopuhi lava lake [Cashman and Marsh, 1988]. If one inserts these estimates of cooling rate dependent growth rate and nucleation rate into equations (4.24) and (4.23), one predicts that significant crystallization occurs at cooling rates of only  $0.3 \text{ }^\circ\text{C/hr}$  and that increasing cooling rate increases the crystal fraction. It is almost certain that the problem with this calculation is that the data from Makaopuhi lava lake cannot be simply extrapolated to cooling rates many orders of magnitudes higher than what the interior of the lava lake experienced.

There are other techniques to determine the critical quench rate to produce a glass [*e.g.*, Uhlmann and Onorato, 1979]. This technique uses assumptions that strictly apply to single component melts undergoing homogeneous nucleation. However, it has been successfully applied to lunar samples [*e.g.*, Hopper *et al.*, 1974; Uhlmann *et al.*, 1974]. In general, the critical cooling rates were found to be between  $2$  and  $20 \text{ }^\circ\text{C/s}$  for lunar basalts. Figure 4-17 shows the predicted average cooling rates through the glass transition temperature, as a function of depth, using my cooling model. I predict an average cooling rate of  $1\text{-}0.5 \text{ }^\circ\text{C/s}$  at a depth of  $8\text{-}10 \text{ mm}$ . Thus the thickness of the observed glass rind is in at least order of magnitude accord with my predictions.

Future work should be able to more accurately calculate the critical cooling rate for the Kilauea composition. Combined with my cooling model, this will allow us to predict  $\phi_{xtl}$  as a function of depth. Comparing the predicted effect of vesicles on the thickness of the glass rind to actual flow lobes should make a very interesting study.

## Predicted Cooling Rates

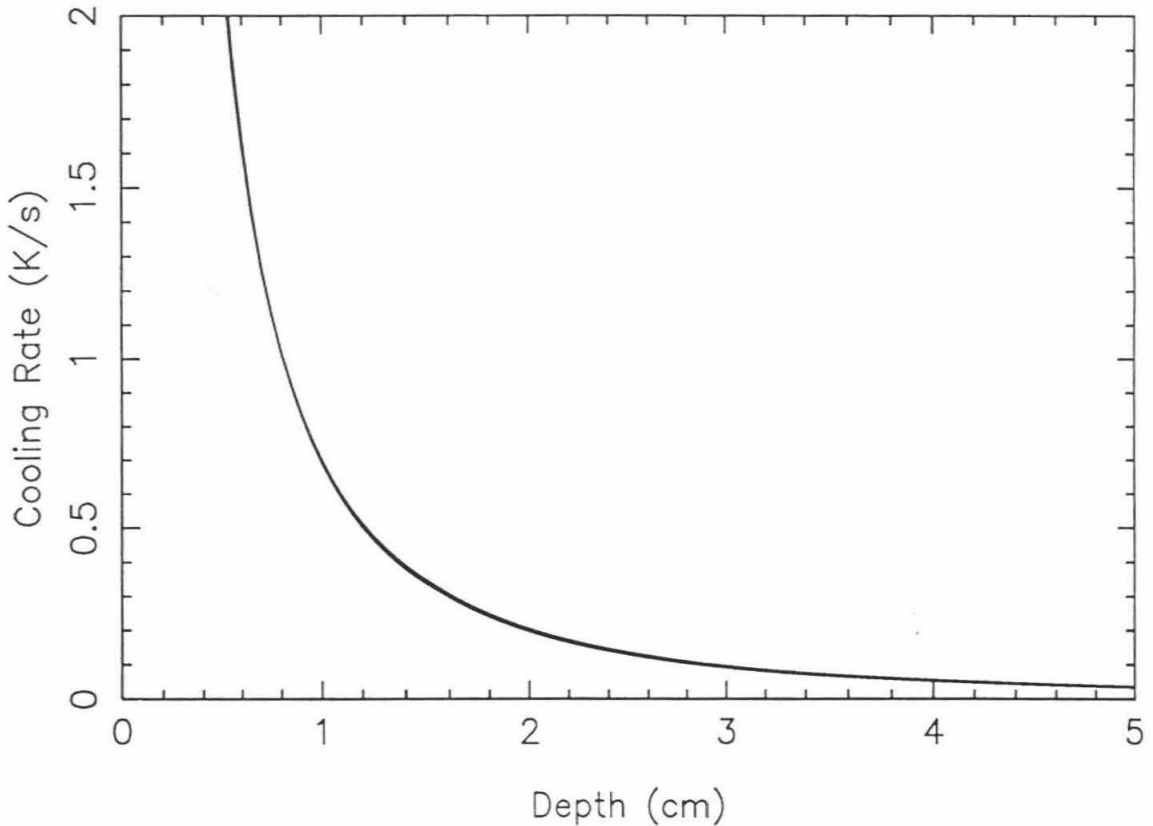


**Figure 4-17: Predicted average cooling rates through the glass transition.**

Curves are plotted for glass transition temperatures of 1070 °C and 900 °C. The two curves are indistinguishable. Average cooling rates at each depth were calculated by dividing the temperature difference between the initial lava temperature and the glass transition temperature by the time at which the point cooled through the glass transition temperature. See Figure 4-10 for the time to cool through the glass transition temperature. Note that the cooling rate at a depth of about 1 cm is close to the critical cooling rate to produce glasses in lunar basalts.

My cooling model may also shed some insight into the formation of shelly pahoehoe. Shelly pahoehoe is usually found near vents and (consequently) has a very porous crust. I suggest that the highly porous lava forms a thin chill crust that is so cold and rigid that it mechanically separates from the underlying fluid lava. This could form the 5-15 cm tall, air-filled, void under a 1-2 cm thick fragile crust that is characteristic of shelly pahoehoe. This suggestion needs to be evaluated against other possible genetic scenarios such as drainback of the molten lava after stagnation of the lobe or the massive coalescence of bubbles in the volatile rich lava.

#### 4.7.3 Future Modeling

The model can also be used to investigate the relative cooling rates for pahoehoe flows that may have erupted on the other terrestrial planetary bodies (Mercury, Venus, the Moon, and Mars). It simply requires feeding the appropriate input parameters into the model. It is clear that cooling should be significantly slower on the bodies with very thin atmospheres. The case of Venus, with a dense, hot atmosphere, is particularly intriguing. The results of a preliminary investigation of the relative cooling rates of extra-terrestrial flow lobes is presented in Chapter 6.

With minor modifications, this model should be applicable to subaqueous pillow basalts. The upper boundary condition needs to be rewritten to include the effect of boiling water at the lava-water interface. With more major improvements, the model could be extended to look at the cooling of pahoehoe flows on the time scale of hours and days. This would require including the effects of the latent heat of crystallization, the motion of the lava, and perhaps rain. And, as previously stated, atmospheric convective cooling needs to be better quantified.

However, it is important to recall that Hon *et al.* [1994a] have produced both a simple conductive cooling model and empirical expressions which fit their cooling data from Hawaiian pahoehoe sheet flows very well over these longer time scales. It will be

interesting to investigate why a simple conductive cooling model seems to suffice when my analysis suggests that processes such as rain and the motion of the lava are important. In any case, the model of Hon *et al.* [1994a] is already a valuable tool in study the formation and evolution of large sheet flows and lava tubes.

#### 4.8 Conclusions

I present a new thermal model for the first five minutes of the cooling of pahoehoe lava flows. The model includes cooling by thermal radiation and atmospheric convection at the surface and conduction with temperature and porosity dependent thermal properties in its interior. This model is able to accurately reproduce field measurements collected by ourselves and others. The fidelity of my model to the observations is significantly better than earlier models, most of which were not designed to be applied to pahoehoe lava flows.

I use the model to make some predictions about the cooling rates of pahoehoe flows under different conditions. I find that, while thermal radiation is the dominant initial heat loss mechanism, atmospheric convective cooling should not be ignored, even in the first five minutes of cooling. By the end of five minutes, the cooling by wind should actually dominate radiative cooling. However, forced atmospheric convective cooling is poorly constrained. It was necessary to conduct a field experiment in order to produce a rough estimate for the forced atmospheric convective heat transfer coefficient. More research, especially in the form of field experiments, is needed to better quantify this important parameter.

The model also predicts that the cooling rate of the surface of pahoehoe flows is relatively insensitive to initial lava temperature but is quite sensitive to the lava porosity. This latter dependence of surface cooling rate on lava porosity has been observed [Jones 1992, 1993]. The model supports the explanation for this dependence that was presented in Chapter 3.

I also use the model to make a preliminary study of the formation of blue-glassy (P-type) pahoehoe and shelly pahoehoe. The dependence of cooling rate on porosity provides the possibility that these pahoehoe textures are explained by different cooling rates. Future work with this model will involve both submarine and extra-terrestrial lava flows. With significant improvements, this model could be used to study the cooling of pahoehoe lava flows over the time scale of hours and days. This improved model would be a key tool in better understanding the inflation process and tube formation. It may also be useful in testing the hypothesis that the continental flood basalts may have been emplaced as pahoehoe sheet flows.

## CHAPTER 5: THERMAL BUDGET OF LAVA TUBES

### 5.0 Abstract

Since Hon *et al.* [1994a] cover the "inflation zone" and the time scale of hours to days, I now move on to the thermal budget of mature lava tubes and the time scale of months to years. My preliminary results were presented at the 1992 AGU Fall Meeting in San Francisco in a talk entitled "Lava Tubes are Air-Cooled."

The thermal budget presented here is the first attempt to quantify the heat transfer in and out of lava tubes. My thermal budget is based on a wide variety of observations of the lava tubes in the Pu'u 'O'o - Kupaianaha flow field on Kilauea Volcano. The thermal budget balances heat loss by: (1) conductive cooling of the tube, (2) convection of air in the wallrocks of the tube, (3) vaporization of rain water, and (4) radiation out of skylights against: (1) viscous dissipation, (2) latent heat of crystallization, and (3) the cooling of the lava. Other processes are shown to be negligible.

When I apply this analysis to the Wahaula tube in the Kupaianaha flow field, I am able to reproduce the approximately 1 °C/km cooling of the lava inside the tube. However, the uncertainties in some of the key input parameters (especially the permeability of the wallrocks) lead to significant uncertainties in the calculated thermal budget. My work does suggest that: (1) the latent heat of crystallization is, by a modest margin, the largest term in the thermal budget of the Wahaula tube, (2) radiation out of skylights is negligible, and (3) the other terms are all roughly of the same magnitude.

I also compare the insulating ability of model lava tubes on Kilauea, in a flood basalt setting, on the ocean floor, on Venus, on the Moon, and on Mars. While this investigation is not meant to precisely define the thermal budget of lava tubes in each of those settings, it does point out some interesting generalities. First, it demonstrates the effect of removing rainfall and/or atmospheric convection. Second it shows the importance of the volumetric flux of lava through the tube. Third, I show that compositional (*i.e.*,

rheological) differences in the lava can be of overwhelming importance.

This work also suggests that tube-fed flows several hundred kilometers long can be produced by eruptions with effusion rates of several tens of  $\text{m}^3/\text{s}$ . Eruptions with such effusion rates are not uncommon on the Earth. This in turn suggests that the longest lava flows observed in our solar system are probably not cooling-limited, if they are tube-fed.

## 5.1 Introduction

Until now, I have only discussed the thermal budget of the cm-scale skin on meter-scale pahoehoe flow lobes. While this work is the essential first step in understanding the thermal budget of pahoehoe flows, it says nothing about what controls the km-scale features of entire flow fields. The emplacement of large pahoehoe flow fields is controlled by lava tubes.

Lava tubes may be the single most important structure in producing very long pahoehoe lava flows. This is because lava tubes provide efficient thermal insulation as the lava is transported away from the vent area. The efficiency of this insulation is one of the main constraints on the length of long-lived tube-fed lava flows. Of course, the total erupted volume or topographic barriers can also limit the length of any given tube-fed flow. Since lava cools as it flows, in no case can a lava flow extend beyond the distance at which it would freeze (*i.e.*, the "cooling limit"). The objective of this chapter is to produce a quantitative description of each heat transfer mechanism operating on lava tubes. By quantifying the heat loss from lava tubes, it should be possible to estimate the maximum possible length for tube-fed lava flows. I also intend to describe the conditions that favor longer tube-fed lava flows.

Given the obvious importance of lava tubes in the formation of many long lava flows (see Chapter 2), the lack of any previous study of their thermal budgets is surprising. At best, it might be argued that some of the work on the formation of lunar sinuous rilles [*e.g.*, Hulme, 1973] or Venusian canali [*e.g.*, Gregg and Greeley, 1993] is partially

applicable to lava tubes. While the quantitative study of heat loss from tubes is nearly non-existent, there is a large selection of papers describing the formation of lava tubes [*e.g.*, Greeley, 1972; Greeley, 1973; Peterson and Swanson, 1974; Greeley, 1987; Kauahikaua *et al.*, 1990; Hon *et al.*, 1994a]. The formation of tubes is not the focus of this chapter but it is worthwhile to briefly cover this subject before discussing the thermal budget of established lava tubes.

There are two relatively common ways in which lava tubes form in Hawai'i: (1) roofing over of lava channels and (2) locally concentrated flow inside a flow lobe [*e.g.*, Greeley, 1987]. Channels can roof over in several ways. Perhaps the most common is the gradual "zippering shut" of the channel, from the distal end to the vent, as the crust grows inward from the margins of the channel. Channels can also roof over by a "log-jam." Pieces of crust rafting in the channel can pile up at some constriction in the channel. The formation of a lava tube in a flow lobe is described in some detail in Chapter 1 (see Fig. 1-9 in particular). Basically, a lava tube will form inside a flow lobe if the heat advected into the partially solidified lobe balances the heat flux out of the lobe. If this situation is in steady state (at least thermally), it should produce a stable lava tube. It is the balance of the heat influx and heat loss in mature lava tubes that is the focus of this chapter.

## 5.2 Observations from Kilauea lava tubes

While this work attempts to describe lava tubes in general, all the observational data come from the Pu'u 'O'o - Kupaianaha flow field on Kilauea, Hawai'i. In particular, I will later use the Wahaula tube to test my estimates for the thermal budget of lava tubes. This particular tube formed between 1986 and 1990, with the upper part of the tube system forming in the early part of the Kupaianaha eruption. This stable upper section of the tube system fed a series of lava tubes downslope. I was able to observe the last two of these tubes, the Wahaula and Woodchip lava tubes. The Wahaula tube proper formed in 1990, and began to decay in mid-1991, and finally died in early 1992. (see Chapter 1 for a more

complete description of the history of the entire eruption). The Wahaula tube started from the Kupaianaha lava lake and ended 11 kilometers downslope at the coast near the Wahaula Heiau (Fig. 5-1).

This long-lived mature tube system allowed the staff of the Hawaiian Volcano Observatory to collect a unique data set. I was fortunate to be able to assist HVO in this endeavor during the time I spent with them. The monitoring included visual observations, sample collection, and electromagnetic and magnetic surveys. These data were collected both along the length of the tube and through its life time (Fig. 5-2). The visual surveys documented the variations of the lava level within the tube, flow velocities, formation of skylights as well as the general location of the lava tube. The samples of lava were used to monitor the geochemical changes in the eruption, the degassing of lava within the tube [Mangan *et al.*, 1991], and the temperature of the lava [Helz *et al.*, 1991].

The geophysical monitoring consisted of weekly to bi-weekly re-occupation of survey lines placed across the lava tube. The data were collected using a VLF instrument and a proton-precession magnetometer. The locations for the lines were selected to optimize the geometry between the tube flow direction, the orientation of the Earth's magnetic field, and the location of VLF stations in Oahu and Seattle. The VLF instrument observes the local distortion of VLF radio waves used by the US Navy to communicate with its submarine force. These distortions of the radio waves are caused by variations in conductivity in the near surface. The contrast in electrical conductivity between solid basalt and its melt is sufficiently large to produce a very clear signal. By using a simple box model, the data could be used to calculate the cross-sectional area of the melt within the tube [Kauahikaua *et al.*, 1990; Hon and Kauahikaua, 1991]. This, combined with an estimate of flow velocity, produced the only reliable method to monitor the effusion rate for the eruption.

The magnetometer data were collected along the same survey lines as the VLF data. The proton-precession magnetometer measures the total magnetic field strength at the

## Location map for Wahaula Lava Tube

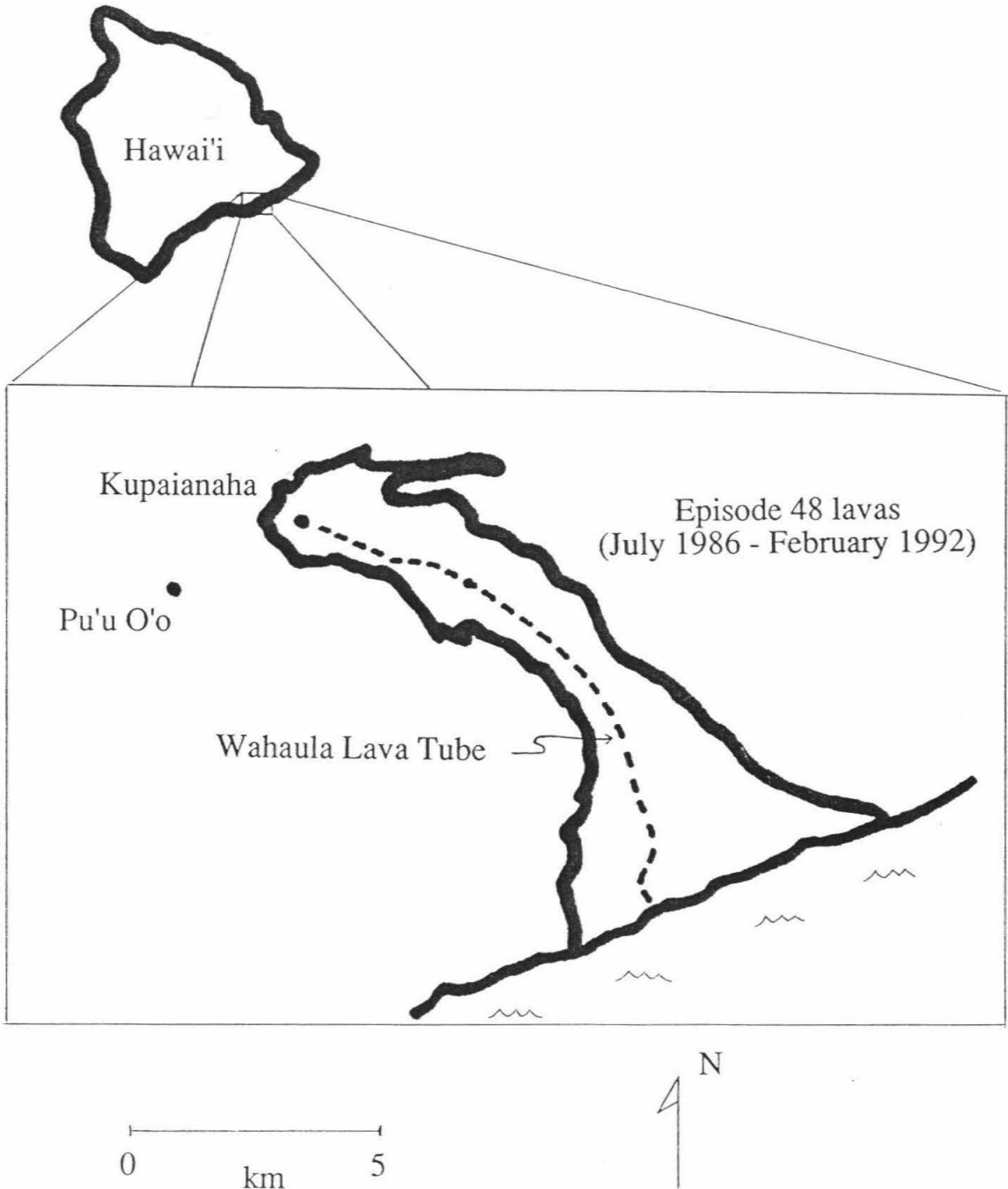


Figure 5-1: Location of the Wahaula lava tube, Kilauea Volcano, Hawai'i.



**Figure 5-2a: Photograph of lava tube monitoring.** This photograph shows HVO staff members collecting a lava sample out of a skylight on the Wahaula lava tube. A cable with a hammer head attached to its end is dropped into the skylight. It is pulled out after the hammer head has been immersed in the lava stream. Note the incandescent lava coated hammer head in mid-air. Also note the helicopter. Usually helicopters were not available and all gear was man-ported to (and from) the skylights.



**Figure 5-2b: Photograph of lava tube hunting.** Photo of HVO staff and volunteers locating the lava tubes near the Kamoamoa coast. The instrument on the tripod is a theodolite with built in laser rangefinder which was used to locate survey lines. The long white pole on the ground is an EM-31 active electromagnetic sounder. This instrument was typically only used to locate tubes and was not part of the regular tube monitoring effort. Note the tourist helicopter headed for the plumes at the coastal lava entries. As an aside, the pH inside the plumes is typically between 0 and 1.

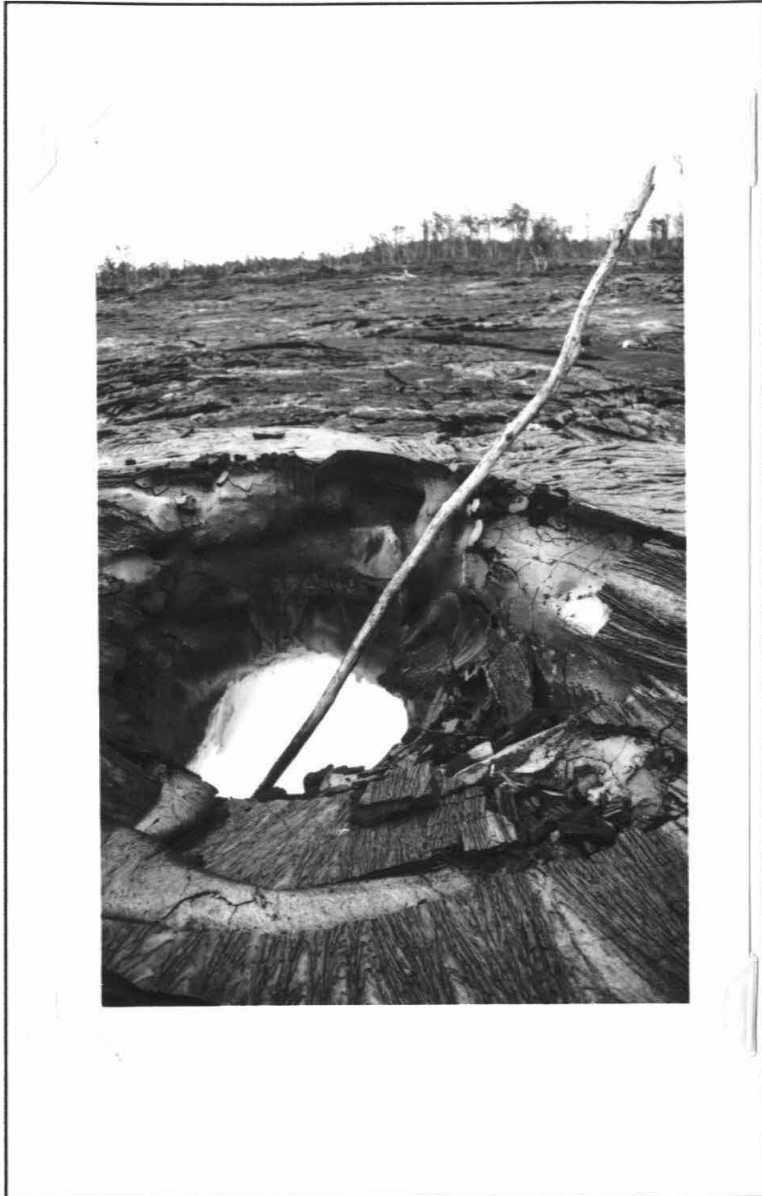


**Figure 5-2c: Photograph of lava tube monitoring.** Photo shows one method used to verifying the geophysical measurements on the Kamoamo tube. On this occasion logs were inserted into skylights to confirm that the melt in the tubes was only about 50 cm deep, as was calculated from the VLF instrument. All photographs courtesy of the USGS.

instrument. Basalt picks up a strong remnant magnetic signal as it cools below the Curie temperature (between 550 - 600 °C for basalts). When working over lava tubes, the data show the absence of this remnant magnetic field where the rock is above the Curie temperature. These data are particularly useful in monitoring the cooling of a lava tube after its source of lava is cut off.

Further data from this lava tube are available from a 1990 overflight by the NASA C-130 aircraft. The plane was carrying the Thermal Infrared Multi-spectral Scanner (TIMS) and the NS-001 Landsat Simulator as well as photogrammetric cameras and video cameras. The most useful data for the purpose of this study were collected at night when the solar heating of the surface was negligible. The TIMS instrument was able to map out the lava tubes by detecting a 10-15 °C surface temperature anomaly directly over the tubes. The instrument also detected geochemical alteration over inactive tubes and zones of active breakouts [Realmuto *et al.*, 1992].

The TIMS instrument, operating in the thermal infrared, becomes saturated by surface temperatures more than a few tens of degrees above ambient. However, the NS-001 instrument has 2 channels in the near infrared that can be used to identify surfaces at several hundred degrees above ambient. These data show that there were on the order of a dozen "hot spots" along the length of the lava tube. Visual observations at the same time showed only 2-3 skylights. The remaining "hot spots" are interpreted to be areas where the roof of the lava tube was unusually thin.

These data were supplemented by helicopter-borne IR video imaging by myself in collaboration with JPL (May, 1993) and HVO (September, 1993). The single channel thermal IR video systems were also able to identify all the interesting types of thermal features observed earlier with the large multi-spectral instruments. The single greatest short-coming of these video images is the difficulty in correlating the observed features with map locations [Keszthelyi *et al.*, 1993].

Overall, the remote sensing data showed a surprisingly complicated picture for the

morphology of the lava tube system. For most of its length, the Wahaula tube is actually a braided pair of tubes. The tubes are also far from straight. Their tortuous path means that the lava must actually traverse considerably more than the 11 km straight line distance between the vent area and the ocean entries. It also will be shown later that the variable thickness of the roof of the lava tube has significant impact on the thermal budget of this tube system.

### **5.3 Terms in the thermal budget of lava tubes**

In this section, I wish to describe how I quantified the various terms in the thermal budget of lava tubes. Specific values for the Wahaula tube will be computed in the next section. But before delving into the details, some general assumptions need to be explained. I have assumed that the lava in the tube and the interior surface of the lava tube are isothermal. Clearly, if there is any net heat loss from the lava tube, some temperature gradient within the lava and between the lava and the walls of the tube must exist. However, I argue that this gradient is negligible. It will be shown in the following that the net heat flux out of the lava tube is on the order of a  $\text{kW/m}^2$ . This heat flux can be furnished by having the ceiling of the lava tube  $1.5\text{ }^\circ\text{C}$  cooler than the lava. This difference is negligible compared to the temperature of the lava. This means that even though (Hawaiian) lava tubes typically run only partially full, the entire interior of the tube is essentially held at lava temperatures.

Another key assumption I have made is that the tube has achieved a steady state temperature distribution. This may be a bad assumption for transient phenomena such as rain. However, it should be usually valid for mature lava tubes. The assumption of steady state eliminates the time variable and makes the calculations immeasurably simpler. I have also assumed that temperatures vary slowly in the down flow direction. This assumption breaks down only around features such as skylights or bifurcations of the tube. This reduces the following calculations by another variable. Thus the analysis of the thermal

budget will be made for a generic control volume which is a cross-section of the lava tube.

One more repeated assumption is that the lava tube has an essentially circular cross-section. Lava tubes are often somewhat rectangular in shape. Crack bounded blocks can drop from the ceiling and thermal erosion may cut sharp channels into the floor. This particular geometric detail should not significantly affect the results.

### 5.3.1 Conduction through the Walls

There are published approximations to the steady state solution for the problem of a hot pipe buried in an infinite half-space. These solutions can be directly applied to lava tubes if one assumes a constant surface temperature. This means ignoring the fascinating thermal signature that lava tubes make at the surface. However, since the temperature contrast between the lava and the surface is on the order of 1000 °C, surface temperature variations on the order of 10 °C should be negligible.

The approximate solution to the aforementioned conduction problem is

$$Q_{\text{cond}} = 2\pi \Delta T k / \cosh^{-1}(2h_0/D+1) \quad (5.1)$$

where  $\Delta T$  is the temperature contrast between the lava and the surface,  $k$  is the thermal conductivity of the wall rock,  $h_0$  is the thickness of the roof of the tube, and  $D$  is the diameter of the tube [Incropera and DeWitt, 1990]. Figure 5-3 shows the sensitivity of  $Q_{\text{conv}}$  to the size and depth of the lava tube.

### 5.3.2 Radiation out of Skylights

Heat loss by thermal radiation out of a skylight is trivial to calculate. The minor subtlety is to correct for the fact that skylights make up only a (small) fraction of the surface area of the tube system. Thus

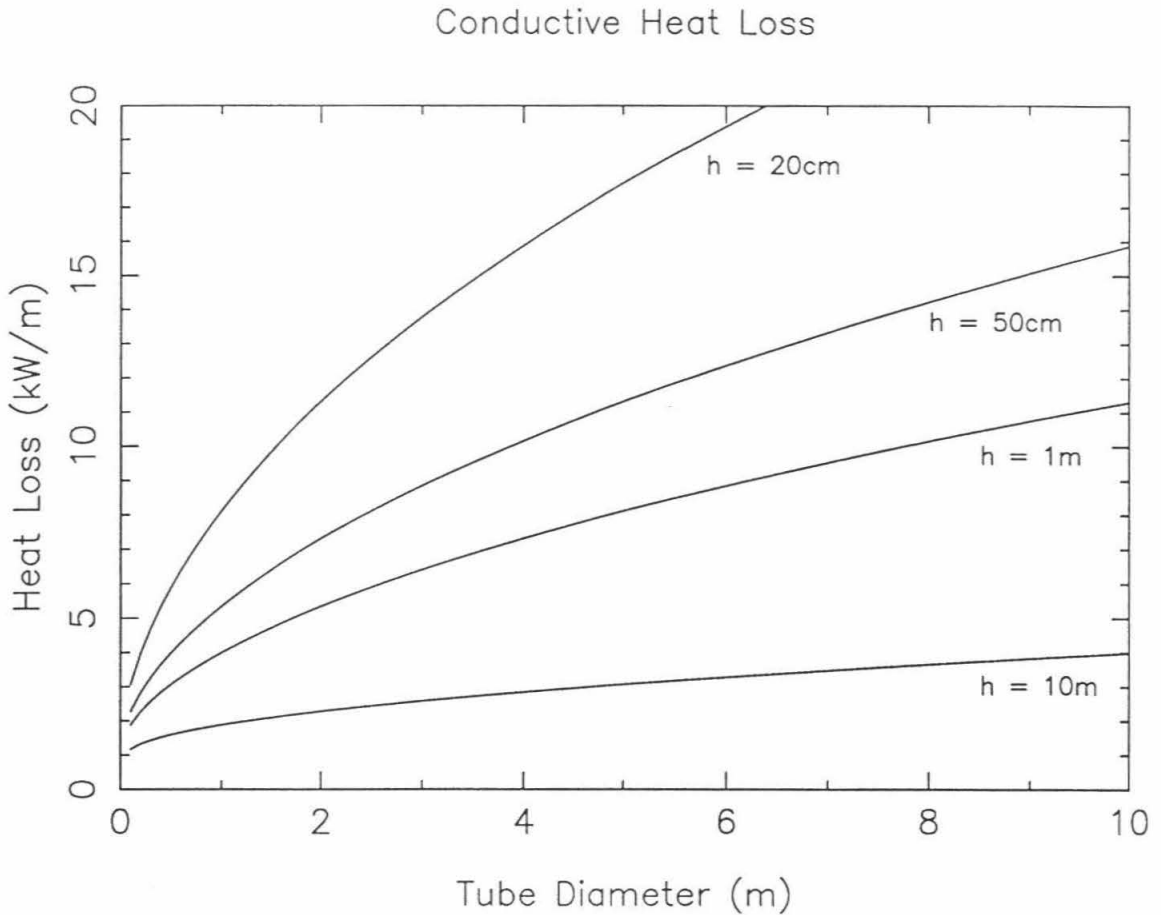


**Figure 5-3: Conductive heat losses as a function of tube diameter and roof thickness.** The curves were calculated using equation (5.1) with  $\Delta T$  equal to 1120 °C and a thermal conductivity of the wall rocks of 1 W/mK. I have considered conductive heat losses as the benchmark against which to compare other terms in the thermal budget of lava tubes. Thus significant processes must involve heat fluxes on the order of 1-10 kW/m. Note that for a roof thickness greater than 1 m, the heat loss is relatively insensitive to the dimensions of the lava tube.

$$Q_{\text{rad}} = F \epsilon \sigma_b (T_l^4 - T_a^4) (2\pi r^2) (n_{\text{sky}}/L) \quad (5.2)$$

where  $F$  is the geometric viewing function (taken to be 1),  $\epsilon$  is emissivity (also taken to be 1),  $\sigma_b$  the Stefan Boltzmann constant,  $T_l$  the lava temperature,  $T_a$  the ambient temperature,  $r$  the radius of the skylight (taken to be the radius of the tube),  $n_{\text{sky}}$  is the number of skylights along the lava tube, and  $L$  is the length of the tube. It should be noted that taking  $F = 1$  is rather generous. Many skylights allow only an oblique view into the tube. Also, skylights are rarely quite as large as the cross-section of the tube. Figure 5-4 shows this upper estimate of  $Q_{\text{rad}}$  as a function of tube diameter and density of skylights. This plot shows that radiation out of skylights can be very important if there are many skylights (more than 1/km of tube).

### 5.3.3 Rain

The heat lost by evaporation of rain was calculated in a rather simplistic fashion. It was assumed that all rain falling above the 100 °C isotherm would percolate down to the isotherm, flash to steam, and escape. In this simple picture

$$Q_{\text{rain}} = \partial r / \partial t D^* \rho^* L^* \quad (5.3)$$

where  $\partial r / \partial t$  is the rate of rain fall (in m/s),  $D^*$  is the diameter of the 100 °C isotherm,  $\rho^*$  is the density of water, and  $L^*$  is the latent heat of vaporization of water (2.5 MJ/kg). Figure 5-5 plots  $Q_{\text{rain}}$  for various  $D^*$  and rainfall rates. A large degree of uncertainty is introduced into  $Q_{\text{rain}}$  because  $D^*$  is not easily determined. The diameter of the 100 °C isotherm is bounded by the 100 °C isotherm determined from the 2-D steady state conduction problem. However, as can be seen by comparing Figures 5-3 and 5-5, the heat lost by evaporating rain is of the same order as conductive heat losses. Thus rainfall should be able to significantly perturb the temperature field around a lava tube. This implies that  $D^*$  should

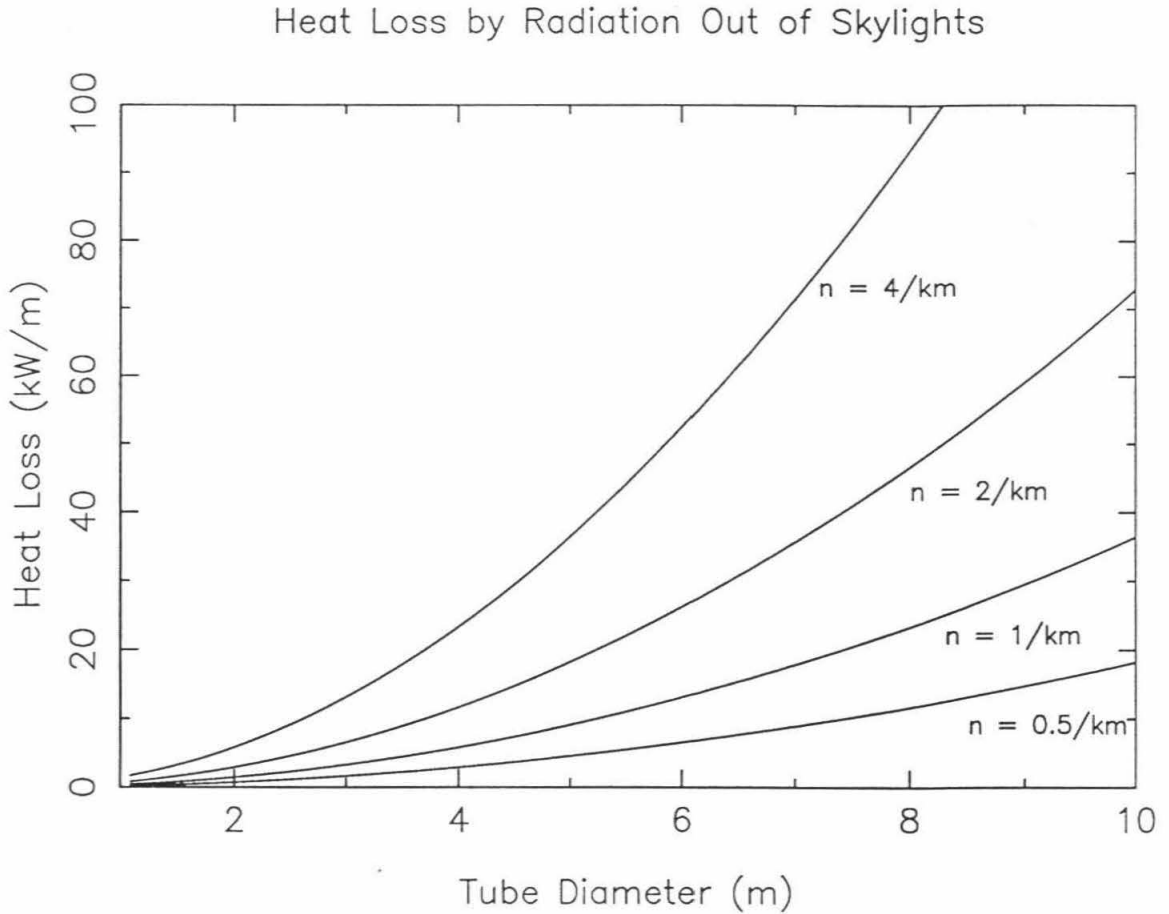


**Figure 5-4: Radiative heat losses out of skylights.** The curves are calculated using equation (5.2).  $n$  is density of skylights, expressed in number per kilometer. Lava temperature is taken to be  $1150\text{ }^{\circ}\text{C}$  and ambient temperature as  $30\text{ }^{\circ}\text{C}$ . Note that the heat flux is very sensitive to the diameter of the tube (*i.e.*, size of the skylights). This plot shows that a large number of large skylights can have a very profound effect on the thermal budget of a lava tube.

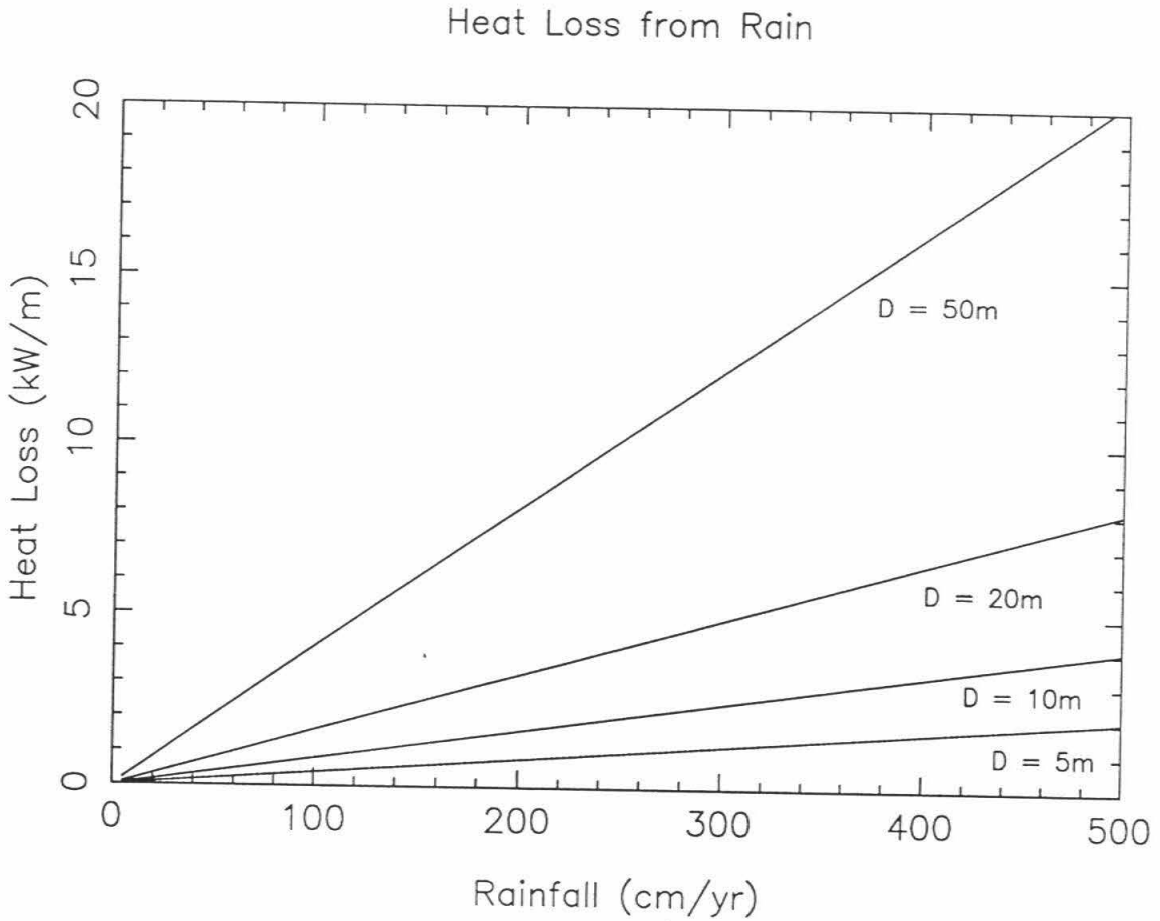


**Figure 5-5: Estimated heat loss from rainfall.** These curves are calculated using the simplistic model behind equation (5.3).  $D$  is the diameter of the  $100\text{ }^\circ\text{C}$  isotherm. Observe that rainfall is always non-negligible, but is truly important only in areas with high rainfall ( $>200\text{ cm/yr}$ ).

be much smaller than suggested by a simple conductive model. I have not produced a thermal model that simultaneously calculates the effect of rain and conduction. I have also ignored the possibility of two phase convection above the lava tube in which the steam recondenses before it can escape.

#### 5.3.4 Air Circulation

One of the interesting results from observing the cooling of Kilauea Iki lava lake was the demonstration that two phase convection was important in the thick crust on the lava lake [*e.g.*, Hardee, 1982]. Figure 5-6 shows a idealized temperature profile taken from Kilauea Iki. The large section of the crust that is held at 100 °C is explained by having steam convecting in that region. As mentioned above, I have not incorporated 2-phase convection in my study of lava tubes. In part this is because such convection requires detailed numerical simulation. The other reason is that the lava lake lessons suggest that the crust has to be a few meters thick before 2-phase convection becomes important [*c.f.* Wright and Okamura, 1977; Peck *et al.*, 1977; Peck, 1978; Hardee, 1980; and Hardee, 1982].

However, I have investigated the possibility that air may be convecting in the cracked lava surrounding the lava tube. Experiments have been done on the cooling of a hot wire embedded in a permeable medium [Cheng, 1985]. These experiments lead to the following empirical expressions:

$$Q_{\text{conv}} = \pi \text{Nu} \Delta T k \quad (5.4)$$

where Nu is the Nusselt number,  $\Delta T$  is the temperature difference between the lava and the surface, and k is the thermal conductivity of the rock.

$$\text{Nu} = 0.565 \text{Ra}^{1/2} \quad \text{for Ra} > 10 \quad (5.5)$$

### Idealized Lava Lake Temperature Profile

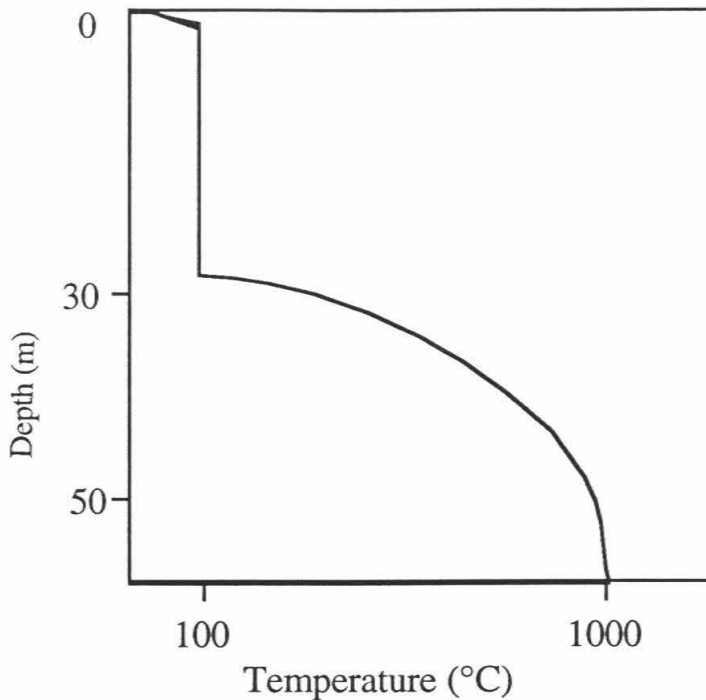


**Figure 5-6: Idealized lava lake temperature profile.** After data from Kilauea Iki, Hawaii and Heimay, Iceland [Hardee, 1982]. Note the large section at 100 °C where convection of water vapor is the main heat transport mechanism.

where  $Ra$  is the Rayleigh number.

$$Ra = \rho_{\text{air}} \beta g K \Delta T D / (\eta \alpha) \quad (5.6)$$

where  $\rho_{\text{air}}$  is the density of the air,  $\beta$  the coefficient of thermal expansion of air,  $K$  the permeability of the rocks,  $D$  the diameter of the tube,  $\Delta T$  the temperature difference

between the lava and the surface,  $\mu$  the viscosity of air, and  $\alpha$  the thermal diffusivity of the rock. Figure 5-7 plots  $Q_{\text{conv}}$  as a function of tube diameter and the permeability of the rock. Note that the permeability of basaltic lava can vary over many orders of magnitude. One important point to remember is that at permeabilities below  $1 \times 10^{-11} \text{ m}^2$ , the Rayleigh number is less than 10, which is the lower limit where the expression from Cheng [1985] is valid.

There is another convective process involving air that can transport heat away from the lava tubes. Typically, there is a plume of hot air blowing out of skylights. The effect is sometimes like a roaring chimney. It is possible to describe the heat carried by this hot plume in a fashion analogous to the expression for heat loss from skylights by radiation

$$Q_{\text{wind}} = U(T_1 - T_a)\rho_{\text{air}} C_{p_{\text{air}}} (2\pi r^2)(n_{\text{sky}}/L) \quad (5.7)$$

where  $U$  is the wind velocity,  $C_{p_{\text{air}}}$  is the heat capacity of air, and the other terms are defined as before. Figure 5-8 plots  $Q_{\text{wind}}$  as a function of  $U$  and skylight density and shows that this process is completely negligible.

### 5.3.5 Volcanic Gasses

This discussion of heat loss by the circulation of air raises the questions about the effect of the exsolution and escape of volcanic gasses. The simple escape of the volcanic gasses does not change the temperature of the lava. The heat released by the exsolution (boiling off) of the gas from the lava is potentially much more significant. The latent heat of exsolution should not be exceeded the latent heat of vaporization of the water. The boiling of 1 wt.% water would knock down the temperature of a basalt about 25 °C. Kilauea lavas actually contain about 0.3 wt.%  $\text{H}_2\text{O}$  [Greenland, 1987]. Thus even the complete boiling off of the dissolved water is only a few % effect and I will ignore it.

## Heat Loss by Air Convecting in Wallrocks

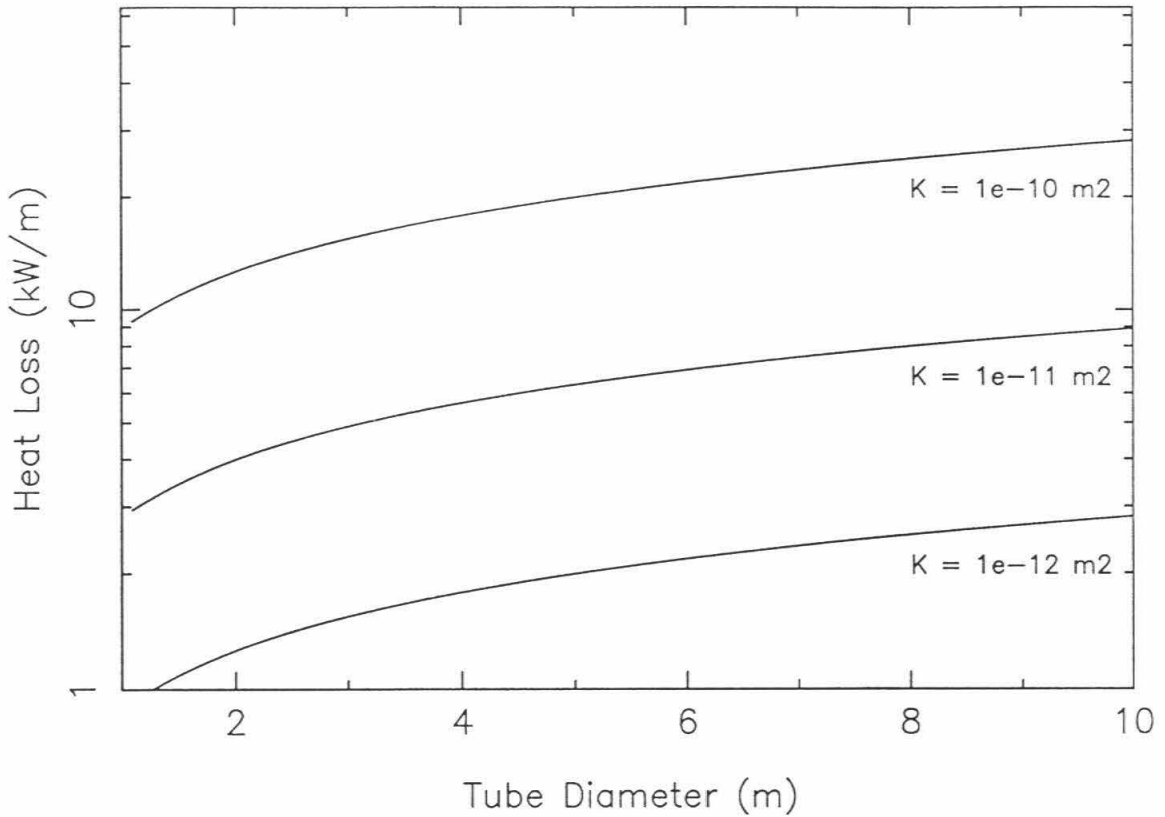


**Figure 5-7: Heat loss by air convecting in the wall rocks.** These curves are calculated using equations (5.4) - (5.6) and the full temperature dependent properties for air as described in chapter 3 of this thesis. The diameter of the lava tube was taken to be 5 m. Note that the permeability of basaltic lava can vary over many orders of magnitude, potentially even outside the range of values shown here ( $10^{-10} \text{ m}^2$  -  $10^{-12} \text{ m}^2$ ). This results in a similar range of possible heat fluxes carried by air convecting around the lava tubes. However, I argue that the permeability around active lava tubes is probably very close to  $10^{-11} \text{ m}^2$ .

## Heat Loss by Wind Out of Skylights

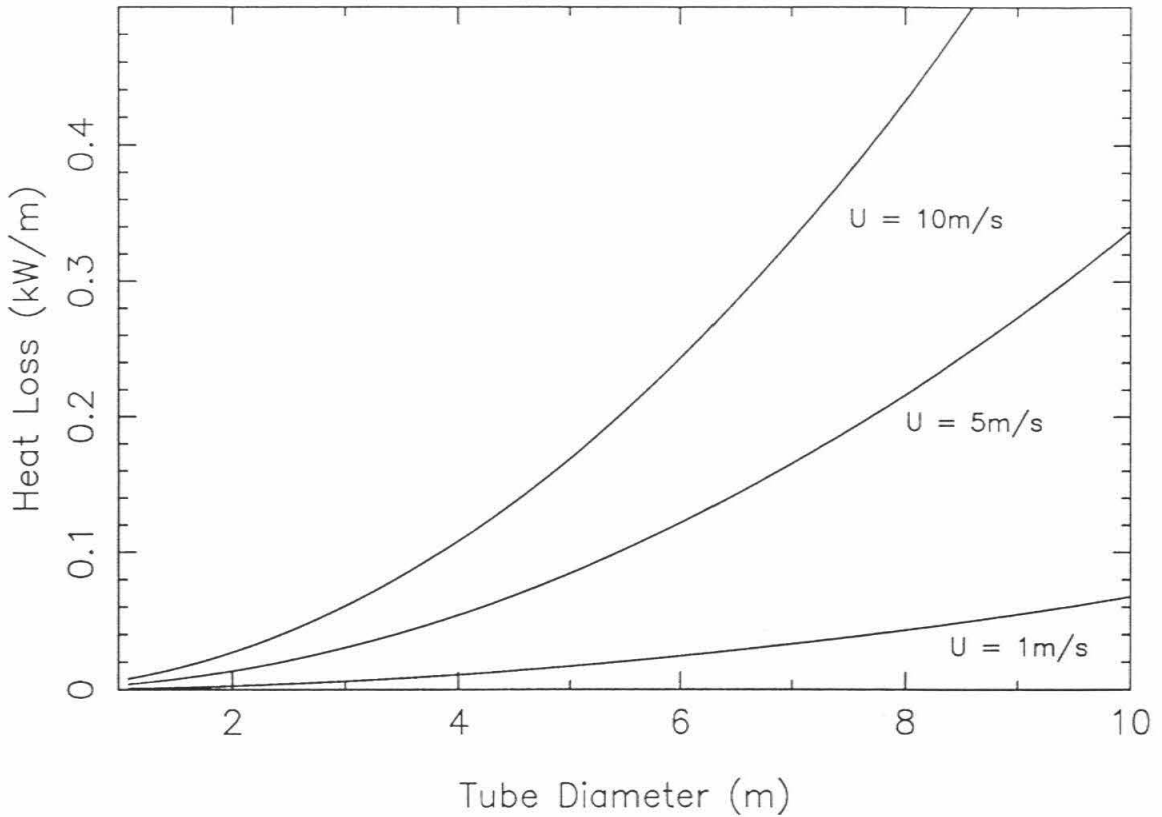


**Figure 5-8: Heat loss by the air blowing out of skylights.** These curves were calculated from equation (5.7) which estimates the heat carried by hot air escaping out of skylights. The density of skylights in these calculations was  $1/\text{km}$ . Note that this heat transport mechanism is essentially negligible.

### 5.3.6 Release of the Latent Heat of Crystallization

As noted earlier in this thesis, the release of the latent heat of crystallization can be a very significant term in the thermal budget of a basaltic lava flow. If one were following a control volume of lava down the tube, the heat input from crystallization could be written as

$$Q_{xtl} = \partial X_C / \partial t \rho_{xtl} L \quad (5.8)$$

where  $\partial X_C / \partial t$  is the increase in vol.% crystals with time,  $\rho_{xtl}$  is the density of the crystals (about 3300 kg/m<sup>3</sup>), and  $L$  is the latent heat of crystallization (400 kJ/kg). However, we are interested in the heat released in a control cross-section of the tube.  $\partial X_C / \partial t$  can be converted into crystallization rate per unit length ( $\partial X_C / \partial x$ ) by multiplying  $\partial X_C / \partial t$  by the flow velocity. The cross-sectional area of the flowing lava must also be taken into account. We finally arrive at

$$Q_{xtl} = \partial X_C / \partial x \Psi \rho L \quad (5.9)$$

where  $\Psi$  is the effusion rate. Figure 5-9 plots  $Q_{xtl}$  as a function of crystallization rate and effusion rate. There is another, possibly more useful, way to describe the release of latent heat. That is to include latent heat as an additional term in the heat capacity of the lava (see section 5.3.9).

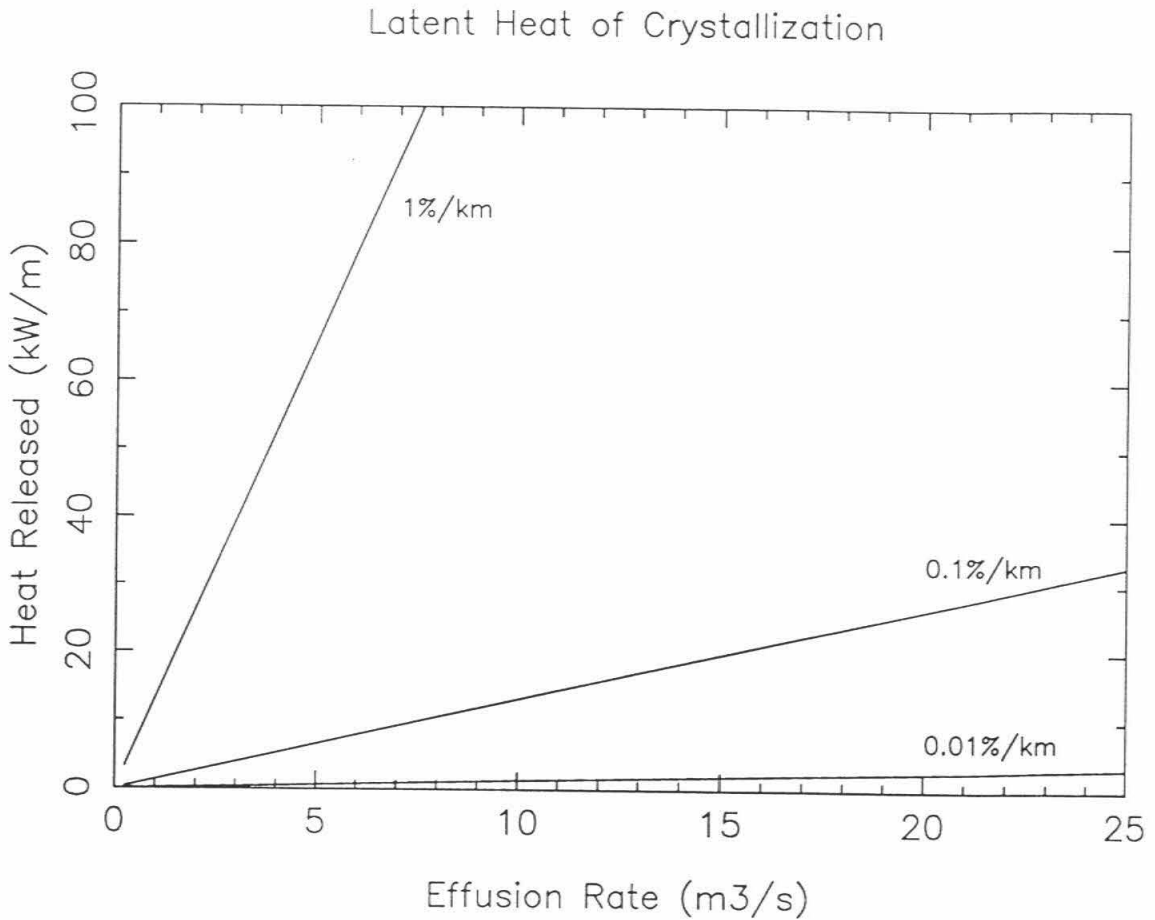


**Figure 5-9: Heat released by the latent heat of crystallization.** Curves calculated using equation (5.9). Since the rate of crystallization ( $\partial X_c/\partial x$ ) should be a function of the cooling of the lava tube ( $\partial T/\partial x$ ), this plot is not directly applicable to problems of interest. However, it does demonstrate how significant the latent heat of crystallization is in the thermal budget of freezing basalt.

### 5.3.7 Viscous Dissipation

In principle, computing viscous dissipation could be rather tricky. However, with the assumption of a steady state flow, the lava should not be accelerating. Thus all the potential energy lost by flowing downhill must be converted into heat via viscous dissipation. Thus,

$$Q_{\text{visc}} = mg \partial z / \partial t = \Psi \rho g \partial z / \partial x \quad (5.10)$$

where  $\partial z / \partial x$  is the slope. Figure 5-10 plots  $Q_{\text{visc}}$  as a function of slope and effusion rate and shows that viscous dissipation is a significant process for slopes of a few degrees or greater.

### 5.3.8 Thermal Erosion

Thermal erosion directly affects the thermal budget of a lava tube by requiring the extraction of the latent heat of fusion to melt the floor of the tube. This heat loss can be computed as

$$Q_{\text{erod}} = \rho D L \partial h / \partial t \quad (5.11)$$

where  $\partial h / \partial t$  is the rate of down cutting. It is obvious that for any reasonable erosion rate, (*i.e.*,  $\partial h / \partial t \ll 1$  m/day), the direct heat loss through thermal erosion is negligible. However, it should be noted that the diameter of the lava tube can also be increased by mechanical erosion of the floor and by collapse of the roof. An increase in the diameter of the lava tube also enhances heat loss by other processes such as conduction. The slow increase in the diameter of the tube and the resulting increase in heat loss from the tube with time may provide some constraints on the life span of a stable lava tube.

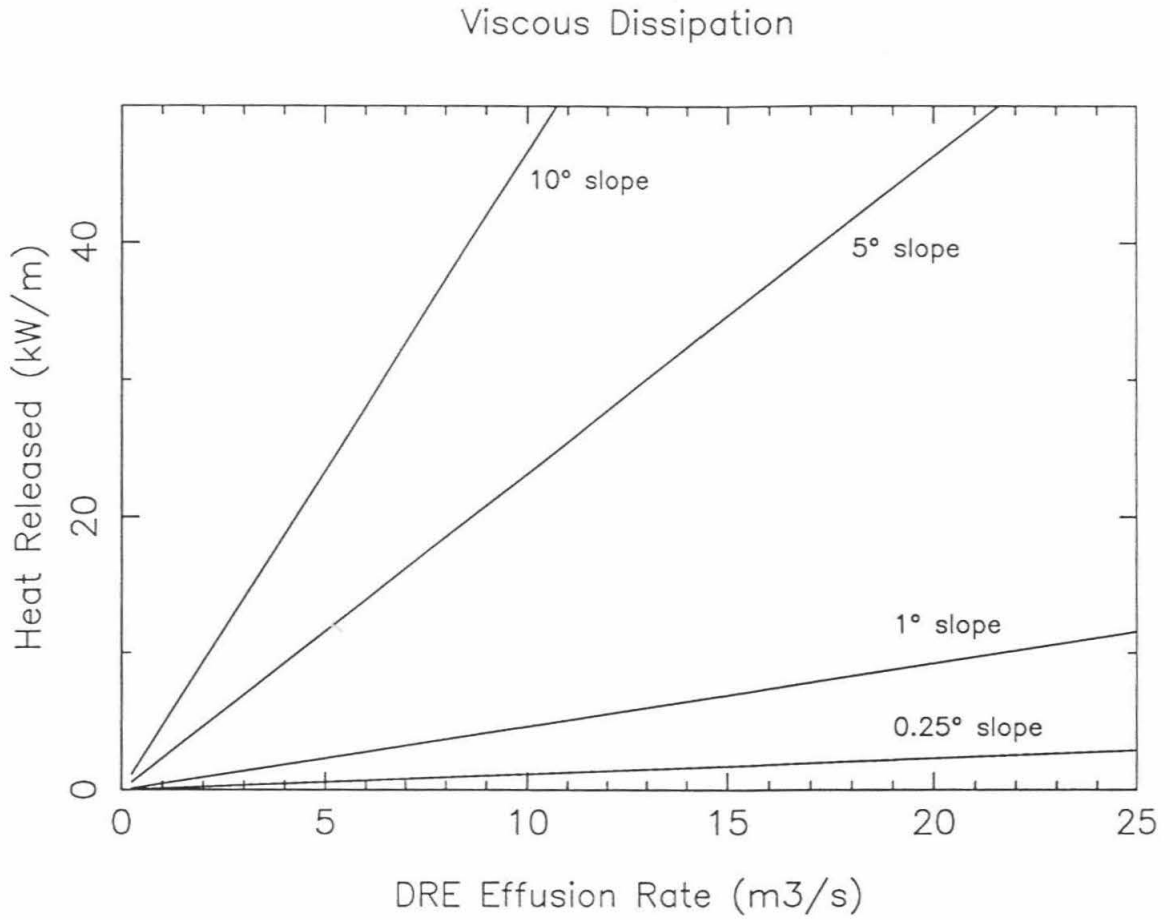


**Figure 5-10: Heat input from viscous dissipation.** Curves show heat released as a function of slope and Dense Rock Equivalent (DRE) effusion rate. Note that viscous dissipation can be rather important even on a 1° slope.

### 5.3.9 Cooling of the lava inside the tube

Any net imbalance in the thermal budget of the lava tube will be manifest through the cooling of the lava inside the tube. This cooling can be written as

$$Q_{\text{cool}} = \partial T / \partial x \Psi \rho C_p \quad (5.12)$$

where  $\partial T / \partial x$  is the cooling rate in the flow direction. As mentioned earlier, equation (5.12) can also be reformulated to include the release of the latent heat of crystallization:

$$Q_{\text{cool+latent}} = \partial T / \partial x \Psi \rho (C_p + \partial X_c / \partial T) \quad (5.13)$$

where  $\partial X_c / \partial T$  is the increase in volume fraction of crystals per degree of cooling.  $\partial X_c / \partial T$  is well known for lava lakes that have weeks or months for the lava to reach equilibrium [e.g., Wright and Okamura, 1977; Peck 1978]. It is not clear that the lava in lava tubes follows the same  $\partial X_c / \partial T$ , but it seems to be a reasonable first approximation.

To summarize this section, I suggest that the thermal budget for lava tubes can be written as

$$Q_{\text{cool+latent}} + Q_{\text{visc}} - Q_{\text{cond}} - Q_{\text{rad}} - Q_{\text{conv}} - Q_{\text{rain}} = 0. \quad (5.14)$$

## 5.4 Application to the Wahaula lava tube

The Wahaula lava tube offers a specific example to test my estimates of the thermal budget of lava tubes. Sufficient observations are available from the Wahaula tube to constrain the key parameters needed to compute every term in equation (5.14). This allows  $Q_{\text{cool}}$  to be calculated both from direct measurements and by balancing it against the other terms in equation (5.14).

To allow more accurate estimates of the input parameters, I have divided the Wahaula tube into 5 segments. These segments are labeled A-E in Figure 5-11. The bifurcations and other details in Figure 5-11 are not precisely known. They are instead based on the earlier data from the Kapa'ahu tube [Realmuto *et al.*, 1992] and my own observations while at HVO and should be considered as only schematic. The uppermost section (segment A) is the oldest. Thus, in segment A, the tube diameter is large and skylights are quite abundant. Rainfall is also highest upslope on this part of Kilauea. Segments C and D cover the steep descent down Pulama Pali and segment E represents the tube system within the coastal flats. Work on the lava tubes in the Kamoamoia area in 1993 has influenced my estimates in segment E.

My estimates for the key parameters for each segment are listed in Table 5-1. Again, let me emphasize that, other than slope, none of the values in Table 5-1 were directly measured along the entire length of the tube. They are only my best guesses based on many different sources of information. The range of values in Table 5-1 is based on my personal 90% confidence interval. To be somewhat conservative, I have taken these limits to be one standard deviation ( $\sigma$ ) in the following analysis.

Two important parameters are not listed in Table 5-1: effusion rate and the permeability of the wallrocks. The dense rock equivalent (DRE) volumetric flux through the Wahaula tube was about  $3 \pm 0.6 \text{ m}^3/\text{s}$ , based on the VLF monitoring [Kauahikaua *et al.*, 1990; Hon and Kauahikaua, 1991]. The permeability of basalt can range from  $10^{-10} \text{ m}^2$  to  $10^{-20} \text{ m}^2$  [Brace, 1984]. On Kilauea, permeabilities over  $10^{-12}$  are often encountered down to a depth of 500 m during drilling [Zablocki *et al.*, 1974]. The permeability of the crust on Kilauea Iki was measured at  $3.2 \times 10^{-13} \text{ m}^2$  [Hardee, 1982]. Clearly, surface flows make up the most permeable end member for basalt. Thus I argue that the most appropriate value for the permeability of the wallrocks around the Wahaula lava tube is about  $10^{-11 \pm 1} \text{ m}^2$ .

## Improved Tube Model

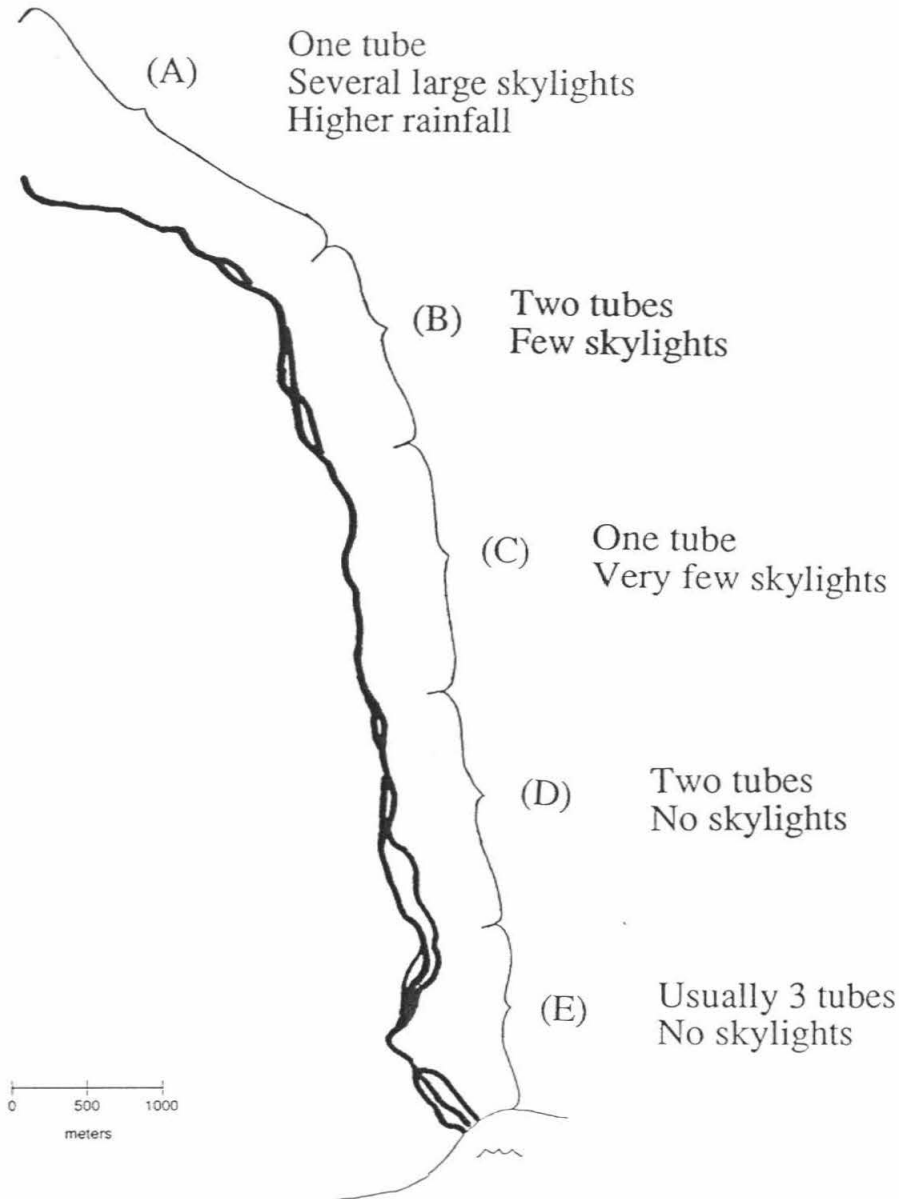


**Figure 5-11: Detailed breakdown of the Wahaula tube into 5 segments.** This division of the Wahaula tube is only schematic. However, it is based on thermal imaging [Realmuto et al., 1992] and extensive field work. Note that the number of strands of the tube changes, generally increasing toward the flow front. Also, the number of skylights increases with the age of the tube (*i.e.*, are most common near the vent).

**Table 5-1: Estimates for the input parameters for the Wahaula lava tube.**

	<b>L</b>	<b>D</b>	<b>h<sub>o</sub></b>	<b>n<sub>sky</sub></b>	<b>∂z/∂x</b>	<b>∂r/dt</b>	<b>D*</b>
	(km)	(m)	(m)	(#/km)	(%)	(cm/yr)	(m)
<b>A (1)</b>	5	4±1	1±0.5	0.6±0.2	5.1	300±50	30±10
<b>B (2)</b>	1.5	2±1	1±0.5	0.5±0.2	6.1	250±50	20±5
<b>C (1)</b>	2	3±1	1.5±0.5	0.05±0.05	10.7	225±50	30±10
<b>D (2)</b>	1.5	2±1	2±1	0±0	7.7	225±50	20±5
<b>E (3)</b>	2	1±0.5	3±1	0±0	1.8	200±50	15±5

Best guesses and estimated ranges for each of the 5 segments of the Wahaula tube. The number in parentheses by the segment label is the number of strands of the tube in that segment and L is the length of the segment. Other quantities are as defined earlier.

Using the inputs in Table 5-1 and equation (5.14) it is possible to calculate  $Q_{\text{cool+latent}}$  for each of the 5 segments of the Wahaula tube. From these values of  $Q_{\text{cool+latent}}$  it is trivial to compute  $\partial T/\partial x$  using equation (5.13). Table 5-2 lists predicted cooling of the lava along the length of the Wahaula tube. The nominal value of 11 °C of cooling for the entire length of the tube compares excellently with field measurements. Using a glass geothermometer, Helz *et al.* [1991] were able to constrain cooling in the tube to 8-10 °C. As an aside, this glass geothermometer is rather remarkable. By measuring just the CaO or MgO in a glass sample it is now possible to determine the quench temperature of a Kilauea lava to better than ±5 °C [Helz and Thornber, 1987]. This accuracy is slightly superior to Chromel-Alumel thermocouple measurements. The limitation is that this geothermometer has only been calibrated for lavas from Kilauea.

**Table 5-2: Predicted cooling inside the Wahalula lava tube.**

tube segment	$\partial T/\partial x$	$\sigma$	$\Delta T$ (cum.)	$\sigma_{cum}$
A	0.92 °C/km	0.58 °C/km	4.6 °C	2.9 °C
B	1.2 °C/km	0.81 °C/km	6.4 °C	3.1 °C
C	0.44 °C/km	0.48 °C/km	7.3 °C	3.3 °C
D	0.93 °C/km	0.78 °C/km	8.7 °C	3.5 °C
E	1.2 °C/km	0.82 °C/km	11 °C	3.9 °C

Predicted cooling using values in Table 5-1 and equation (5.14) to compute  $Q_{cool+latent}$ . The computed  $Q_{cool+latent}$  is then used to calculate  $\partial T/\partial x$  using equation (5.13). Uncertainties computed using questionable assumptions. In particular, it may not be correct to assume that errors are uncorrelated between tube segments. Note that uncertainties in  $\partial T/\partial x$  for each segment are nearly the same magnitude as the estimated values.

Some comment needs to be made about the estimated uncertainties in Table 5-2. As noted earlier, I have provided (subjective) estimates of the range of the input values. The standard deviation for  $\partial T/\partial x$  shown in Table 5-2 was computed by

$$\sigma^2 = \sum(\sigma_i^2)(\partial(\partial T/\partial x)/\partial i)^2 \quad (5.15)$$

where  $\sigma_i$  is the standard deviation for input  $i$  and  $\partial(\partial T/\partial x)/\partial i$  is the measure of sensitivity of  $\partial T/\partial x$  to input  $i$ . There are two critical assumptions in equation (5.15). First, the errors for each input are uncorrelated. Second, the change in  $\partial T/\partial x$  with input  $i$  is adequately described by a first-order differential. While the first assumption is partially defensible, the second can be shown to be violated by effusion rate, thickness of the tube's roof ( $h_0$ ), and permeability. The problem is that due to non-linearities in the relevant equations,

symmetrical changes in these input parameters cause grossly asymmetrical changes in  $\partial T/\partial x$ . For example, increasing  $h_0$  by 50% decreases  $\partial T/\partial x$  by about 10% while decreasing  $h_0$  by the same amount increases  $\partial T/\partial x$  by about 20%. Still, given the extremely crude nature of the initial error estimates, these problems may be excusable.

There is another problem in calculating the uncertainty in the predicted cumulative cooling of the lava in the tube. In computing  $\sigma_{\text{cum}}$ , I have assumed that the errors are uncorrelated between tube segments. It is reasonable to suggest that if I have the wrong value for effusion rate in segment A then I must similarly have the wrong value in all tube segments. Thus  $\sigma_{\text{cum}}$  may be somewhat understated. However, I again argue that given the highly schematic and subjective nature of the initial inputs, more formal error estimation will probably not be useful. Instead, the more productive approach is to break down the model for the Wahaula tube and examine the relative importance of the different physical parameters and processes in more detail.

The first step is to separate the effects of each physical process in equation (5.14). Figure 5-12 plots each term individually. The large uncertainty in the convective cooling of the lava tube ( $Q_{\text{conv}}$ ) is driven by the two order of magnitude range I have allowed for permeability. The large uncertainties in  $Q_{\text{cool}}$  and  $Q_{\text{latent}}$  are purely in response to the large uncertainty in  $Q_{\text{conv}}$ . Recall that in this calculation  $Q_{\text{cool}}$  and  $Q_{\text{latent}}$  are calculated by balancing them against the other heat transfer processes.

I take this as evidence that a permeability of  $10^{-10} \text{ m}^2$  for the wallrocks is excessive.  $10^{-10} \text{ m}^2$  is essentially the highest permeability measured in basalt (or any rock, for that matter). Thus it is reasonable to suggest that the warm wallrocks surrounding an active lava tube cannot achieve this limit. My "nominal" value of  $10^{-11} \text{ m}^2$  may actually be a reasonable upper bound on the permeability of the wallrocks.

There are several other interesting points in Figure 5-12. First, latent heat is the single largest term resisting the cooling of the lava. Using the lava lake data as I have, one would expect that the crystallinity of the lava in the tube to increase by 4-5 vol.% along

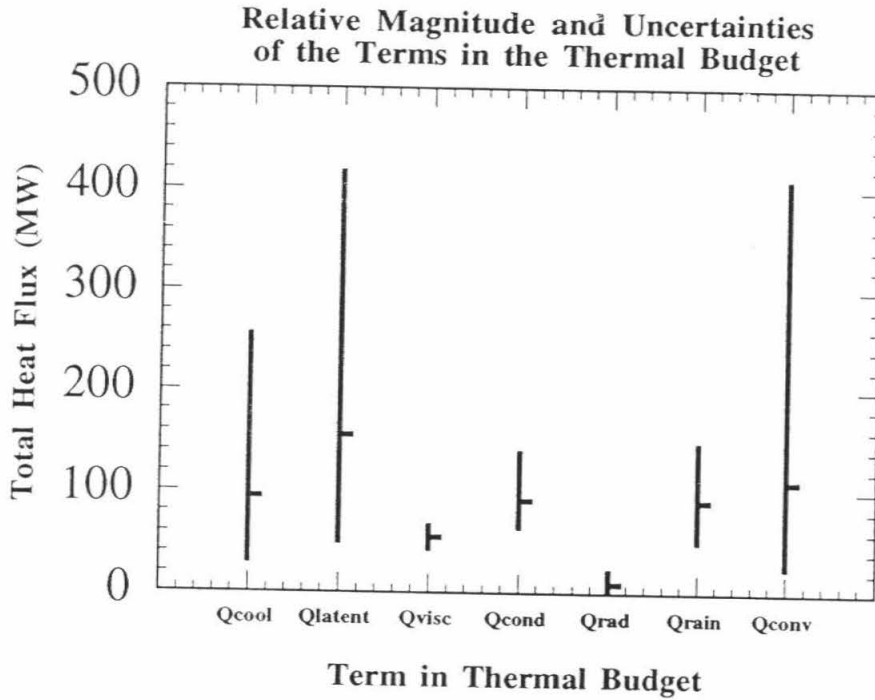


**Figure 5-12: Relative magnitudes and uncertainties of the terms in the thermal budget of the Wahaula lava tube.** Ticks mark the computed heat flux using the nominal values and the bar shows the uncertainties. These uncertainties were computed assuming that errors were correlated between tube segments. This produces larger uncertainties than in Table 5-2. Note that the uncertainties are dominated by the  $\pm 1$  order of magnitude range allowed for permeability.

the length of the Wahaula tube. However, no significant increase in crystallinity is observed in samples collected at various points along the tube [M. Mangan, HVO, USGS, *pers. comm.*]. This suggests that significant amounts of crystals (primarily olivine) may be settling out of the tube system. Where this huge volume of "dunite" might be accumulating is a mystery. It is also possible that the lava in the tube is being super-cooled and that essentially no crystals are growing. Then my estimate for  $Q_{\text{latent}}$  would be too large and my estimate for the cooling of the lava too low.

Another point to notice in Figure 5-12 is that radiation out of skylights is negligible. This is despite my rather generous characterization of this heat loss mechanism. Also, viscous heating is a small, but non-negligible term. Finally, note that the heat loss by conduction and rain are very similar.

Some more insights can be gained by examining each segment of the Wahaula tube. Figure 5-13 shows the heat fluxes for the "nominal" case. Segment C has the lowest cooling rate because in this section the lava flows down a single, relatively small, tube. Conversely, the higher cooling rate in segment B can be explained by having two relatively shallow, large, tubes in that section. Having said this, it is rather remarkable how similar the (estimated) heat fluxes are in each section of the tube. It appears that dividing the flux of lava into 2 or more tubes does not significantly increase the cooling rate, especially if the bifurcation is accompanied by a reduction in the size of the tube.

This breakdown of the heat fluxes by section also shows that the relative magnitudes of the different terms in Figure 5-12 are consistent across the entire tube. Skylights are essentially negligible even in section A, where they are most common. Latent heat is always the single largest term in the estimated thermal budget. Cooling of the lava, viscous dissipation, conduction, rain, and convecting air contribute roughly comparable heat fluxes.

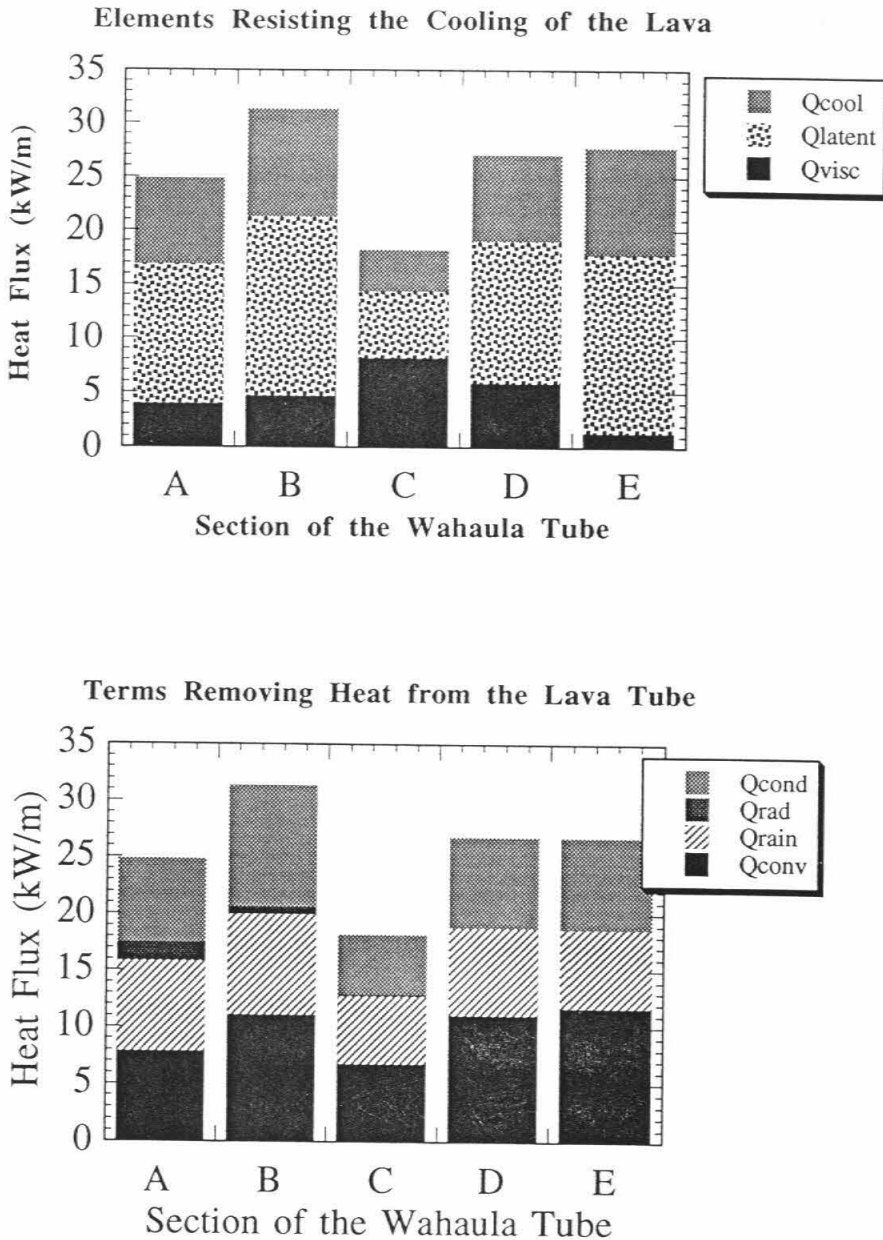


**Figure 5-13: Relative magnitudes of the heat transfer mechanisms plotted by tube segment.** Only the values using the nominal input values are shown. (a) shows the three terms that resist the cooling of the lava. Note that the three terms are roughly comparable but latent heat is the largest. (b) plots the 4 terms that remove heat from the tube. Note that radiation out of skylights is negligible, even in segment A. Other terms are again roughly comparable.

## 5.5 Application to the length of tube-fed lava flows

Both the field data [Peterson and Swanson, 1974; Helz et al., 1991] and the above calculations show that Hawaiian lava tubes typically cool at about 1 °C/km. Since Hawaiian basalts are rarely erupted much more than 100 °C above their solidus, the cooling limit for a Hawaiian tube-fed flow should be about 50 km. This puts into question the possibility of tube-fed flows hundreds of kilometers long. Does this mean that it is impossible for the long extra-terrestrial flows or flood basalts to have been tube-fed? I think not. Instead, I suggest that those very long flows formed under conditions significantly different from Hawai'i. In this section I would like to briefly explore the maximum length of tube-fed flows under different conditions.

I will examine 6 different (hypothetical) tube-fed flows. The first will be essentially a Hawaiian flow that will be used as a baseline. The next two are intended to simulate a continental flood basalt and a submarine sheet flow. I also look at flows on Venus, the Moon, and Mars. Table 5-3 lists the key parameters for each of these cases. Note that since most of the very long flows occur on nearly flat surfaces, the slope selected is very low. The lower rainfall on the flood basalt is arbitrary. Most of the other planet-scale values are hopefully familiar to the reader.

Some additional comments need to be made about the lavas on the different planetary bodies. In particular, the varying compositions of the different basalts should affect viscosity, eruption temperature, crystallization rate, latent heat, and other parameters. I have only investigated compositional effects on viscosity. As done in Keszthelyi and Pieri [1993], the major element chemistry can be used to calculate the viscosity of a lava. I have used the technique of Shaw [1972]. Table 5-4 lists the bulk compositions I have used. Note that there is very little known about the chemistry of the Martian and Venusian lavas. The data from Venus come from the Venera 13 and 14 landers. The Mars compositions are the calculated parent magmas for some of the SNC meteorites. I have also only selected one example from the Columbia River Basalts, even though flood basalts

**Table 5-3: Input for the 6 hypothetical tube-fed flows.****Variable Parameters**

<b>Setting</b>	<b>g(m/s<sup>2</sup>)</b>	<b>T<sub>a</sub> (K)</b>	<b>atmosphere</b>	<b>rainfall</b>	<b>viscosity</b>
Kilauea	9.8	300	air (1 bar)	300 cm/yr	100 Pa s
Cont. Flood Basalt	9.8	300	air (1 bar)	100 cm/yr	300 Pa s
Submarine	9.8	275	water (200 bar)	N/A	100 Pa s
Venus	8.8	750	CO <sub>2</sub> (92 bar)	none	100 Pa s
Moon	1.7	250	none	none	10 Pa s
Mars	3.9	240	CO <sub>2</sub> (6 mbar)	none	100 Pa s

**Fixed Parameters**

<b>slope</b>	<b>permeability</b>	<b>T<sub>initial</sub></b>	<b>∂X<sub>c</sub>/dT</b>	<b>L</b>	<b>C<sub>p</sub></b>
0.25°	1x10 <sup>-11</sup> m <sup>2</sup>	1150 °C	0.45 wt%/°C	400 kJ/kg	1100 J/kg K

The Kilauea flow is used as a baseline and is identical in most respects to the Wahaula tube. The continental flood basalt has reduced rainfall and is marginally more viscous than the Kilauea lava. For the submarine flow rainfall is not used but water replaces air as the medium convecting in the wallrocks. For the extra-terrestrial examples the differences in gravity and atmospheres are taken into account. The lunar viscosity compensates for known differences in bulk composition. The limited data from Venus and Mars do not justify using a viscosity different from the baseline case (see Fig. 5-14).

**Table 5-4: Bulk compositions for different basalts.**

	<b>Kilauea</b>	<b>CRB</b>	<b>V-13</b>	<b>V-14</b>	<b>Nakhla</b>	<b>Shergotty</b>	<b>hi-Ti</b>	<b>lo-Ti</b>
<b>SiO<sub>2</sub></b>	50.4	53.8	45.	49.	46.8	50.1	40.6	43.6
<b>TiO<sub>2</sub></b>	2.43	1.80	1.6	1.2	4.24	1.08	10.8	2.60
<b>Al<sub>2</sub>O<sub>3</sub></b>	12.9	14.5	16.	18.	8.14	9.45	9.70	7.90
<b>FeO</b>	11.5	11.4	9.0	9.0	23.3	19.7	18.0	21.7
<b>MgO</b>	8.92	5.30	11.	8.	5.14	5.11	7.10	14.9
<b>CaO</b>	10.9	9.10	7.	10.	9.65	10.0	12.4	8.30
<b>Na<sub>2</sub>O</b>	2.17	2.80	N/A	N/A	2.08	1.84	0.43	0.23
<b>K<sub>2</sub>O</b>	0.40	1.10	4.	0.2	1.05	0.24	0.08	0.05
<b>MnO</b>	0.17	N/A	0.20	0.16	N/A	N/A	N/A	N/A
<b>H<sub>2</sub>O</b>	0.3	0.5	0.0	0.0	0.0	0.0	0.0	0.0

Kilauea sample was collected from the Wahaula tube [M. Mangan, HVO, USGS, *pers. comm.*]. CRB sample is from the Grande Ronde member of the Columbia River plateau basalts [Hess, 1989]. V-13 and V-14 are the x-ray fluorescence results from the Venera 13 and Venera 14 landers [McGill *et al.*, 1983]. The Nakhla and Shergotty samples are the calculated parent magmas for Gobernador Valadares and Shergotty meteorites [Harvey and McSween, 1992]. It is argued that these meteorites are samples of Mars. The hi-Ti and lo-Ti are lunar basalt samples 75055 and 12002, respectively [BVSP, 1981].

show a significant range in bulk composition.

Figure 5-14 shows the computed viscosities of the different lavas. These computed viscosities do not include the effects of bubbles or crystals. Thus these values should only be used to compare the relative viscosities of the lavas. From Figure 5-14 it can be seen why the viscosity of the lunar lava in Table 5-3 is an order of magnitude lower than the Kilauea lava. The two Martian lavas and one of the Venusian lavas fall close to the Kilauea

viscosity. The flood basalt and the other Venusian lava are significantly more viscous. This explains my choice for the different viscosities in Table 5-3. Also note by comparing with Table 5-4 that these variations in viscosity correlate with silica content.

The parameters not listed in Table 5-3 have been made into functions of the tube diameter. If one assumes that the tube is completely full, then the volumetric flux through the tube is given by

$$\Psi = \pi r^4 \rho g \sin(\alpha) / 8\eta \quad (5.16)$$

where  $\Sigma$  is the effusion rate,  $r$  is the radius of the tube,  $\rho$  is the density (including vesicles),  $g$  is the gravitational acceleration,  $\alpha$  is the slope, and  $\eta$  is the viscosity. The assumption that the tube is full is a poor one. Because of thermal and mechanical erosion of the tube floor, the diameter will increase with time. Also, effusion rates typically decrease as an eruption progresses. I have arbitrarily divided effusion rate given by equation (5.16) by a factor of three in the following calculations. I have also fixed the thickness of the roof as 20% of the tube diameter and the diameter of the 100 °C isotherm as 10 times the tube diameter.

Figure 5-15 plots the magnitudes of the different terms in the thermal budgets of each of the six model tubes. There are many striking features in this figure. Let us start with the simplest points and progressively move toward the more profound. First, note that viscous dissipation is negligible on these extremely shallow slopes. Second, with the exception of Venus, conductive heat loss is essentially the same in all cases. The high ambient temperature on Venus reduces conductive heat loss by about a third. Next, note how significant rain is in the Kilauea example. In fact, the differences in the cooling of the terrestrial tubes can be totally explained by the different rainfalls in the Kilauea, Columbia River, and submarine settings.

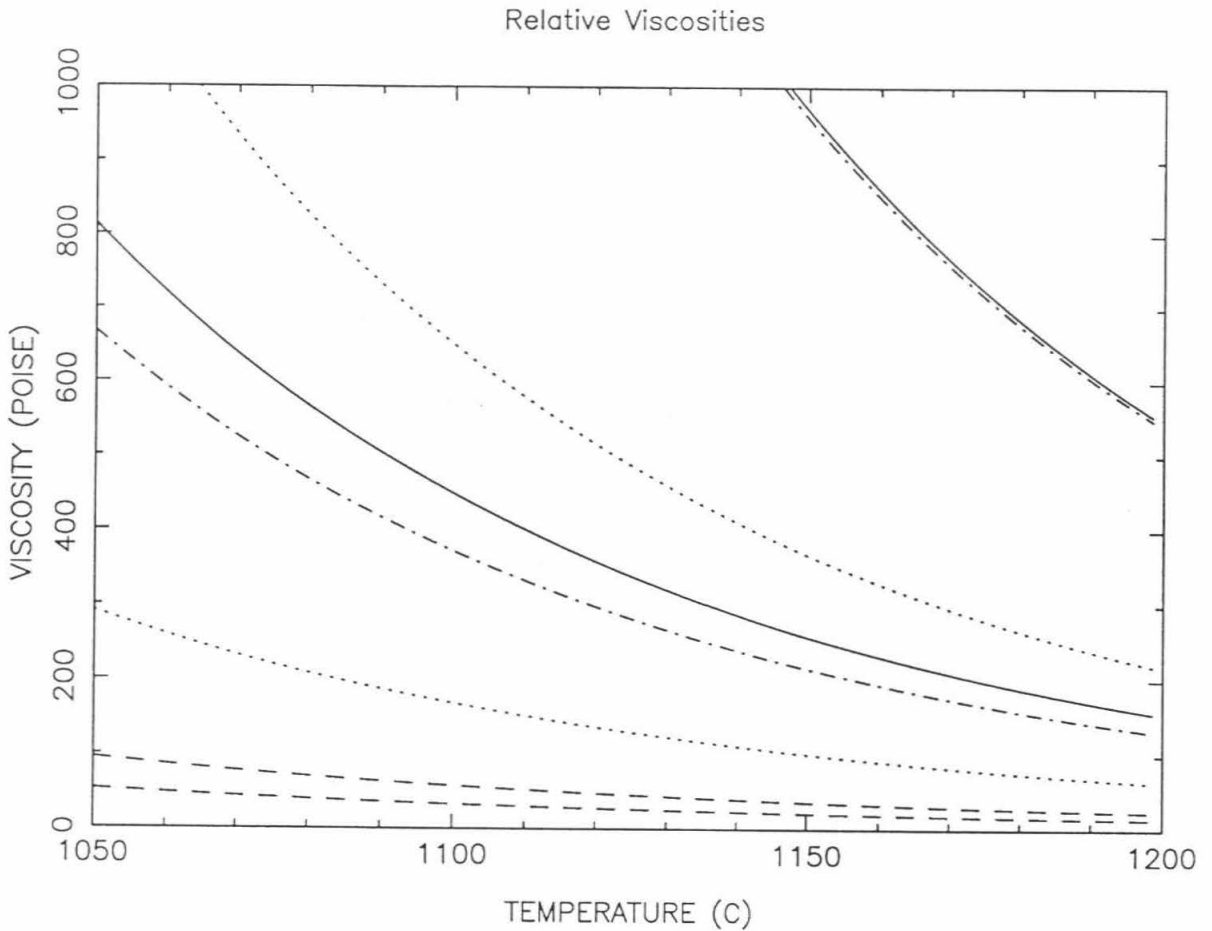


**Figure 5-14: Computed relative viscosities.** Viscosities computed using the technique of Shaw [1972] and bulk compositions in Table 5-4. Because this calculation does not account for vesicles or crystals, the viscosities should only be considered as relative viscosities. Solid lines are terrestrial lavas, dashed lines: lunar lavas, dotted lines: inferred Martian lavas, dot-dash line: Venusian lavas. The Columbia River basalt and the Venera 14 lavas make up the most viscous end members. Note that the Venera 13 lava is close to the Kilauea example and that the Martian lavas bracket the Kilauea values. Also note that the lunar lavas are typically about 1 order of magnitude less viscous than the Kilauea lava. I have based my choices for the viscosities in Table 5-3 on this plot.

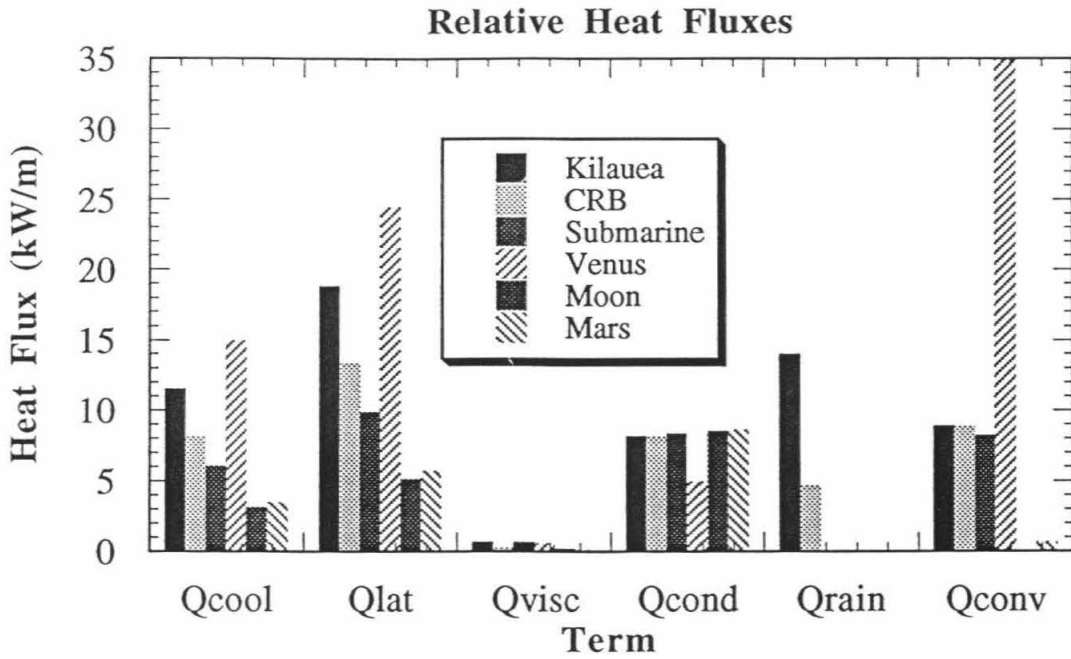


**Figure 5-15: Relative magnitudes of each term in the thermal budgets of the six model lava tubes.** Note in particular the relative magnitudes of  $Q_{cond}$ ,  $Q_{rain}$ , and  $Q_{conv}$  in each case. Those terms explain the variations in  $Q_{cool}$  (and  $Q_{latent}$ ).

It is a rather amazing coincidence that the  $Q_{\text{conv}}$  is essentially identical for the subaerial and submarine flows. The changes in density and viscosity almost precisely offset when calculating the Rayleigh number (see equation 5.6). I should note that I have not included all the complex temperature dependent behavior of water. Essentially no thermal property of water is well-behaved with temperature and pressure. The salinity of sea water only complicates matters. I have also ignored possible two phase convection in which steam could convect in the wallrocks. Still, since the boiling point for water at 2 km depth in the ocean is well over 350 °C, two-phase convection should be less important than experience with subaerial flows would suggest.

The other remarkable aspect of  $Q_{\text{conv}}$  is its value at Venus. Because of the dense Venusian atmosphere, convective cooling is more than three times as potent at Venus than on the Earth. This effect completely overwhelms the reduced Venusian  $Q_{\text{cond}}$ . The overall heat loss from Venusian lava tubes (and lava flows in general) should be far higher than on the Earth. However, it can be argued that the higher ambient temperature at Venus leads to less fractures and less permeability in the wallrocks surrounding Venusian lava tubes. Finally, because both  $Q_{\text{rain}}$  and  $Q_{\text{conv}}$  are essentially zero both on the Moon and Mars, lava tubes on those bodies should be more thermally efficient than terrestrial lava tubes.

One might very reasonably expect that Figure 5-15 (and the values of  $Q_{\text{cool}}$  in particular) should be a good measure of the relative maximum lengths of lava tubes. This is not the case. The key parameter is actually  $\partial T/\partial x$  (or perhaps  $\partial X_c/\partial x$ ). Physically,  $Q_{\text{cool}}$  is the heat flux out of the tube. But it does not measure how much lava this heat is being extracted from. One must also factor in the effusion rate to determine how quickly the lava is being cooled (see equation 5.13). In this analysis I have made effusion rate a function of tube diameter, lava viscosity, and gravity (see equation 5.16).

Figure 5-16 shows the maximum length for the 6 model lava tubes. This "cooling-limit" was taken as the distance at which the lava would cool 50 °C in the tube. This value of 50 °C is arbitrary to within a factor of two. Kilauea lava lakes would form about 20-

25% crystals after 50 °C of cooling and the viscosity of a lava would rise dramatically if more crystals would be added. To repeat, the maximum lengths in Figure 5-16 should not be taken to be more accurate than a factor of two, at best. However, the relative cooling-limited lengths of the tube fed flows should be quite accurate.

The terrestrial examples (Fig 5-16a) form a simple trend with the submarine tube being the longest and the Columbia River example being the shortest. This is despite the fact that  $Q_{cool}$  is largest for the Kilauea tube. The factor of three increase in viscosity for this particular CRB flow unit decreased flow rate to the point that its cooling limit is reached sooner than in the Kilauea case.

The extra-terrestrial flows (Fig. 5-16b) show both the effect of changing gravity and viscosity. Note that the Venusian flow is only marginally shorter than the Kilauea example. The lack of rain has nearly compensated for the more efficient atmospheric convective cooling. On Mars, with both rain and convection essentially turned off, one would expect the tubes to be as efficient as the model submarine tubes. However, the lower gravity on Mars leads to significantly lower flow rates through the tube. Thus the Martian lava tube is only slightly more efficient than the Kilauea example. Finally, the lower viscosity of the lunar basalts more than compensates for the lower lunar gravity. Lunar tube-fed flows have by far the longest cooling-limits.

Given all this discussion about the relative efficiencies of these lava tubes, it must not be overlooked that Figure 5-16 indicates that producing a 1000 km long tube-fed flow seems plausible in each and every setting. A 10 m diameter tube, even on a very shallow slope and running at 1/3 capacity, can always produce a flow well over a 100 km in length. 10 m diameter tubes are readily found on Hawai'i and elsewhere on the Earth. And some sinuous rilles are a few kilometers in width!

We, of course, should check to see if the effusion rates in these hypothetical 10 m diameter lava tubes are reasonable. Figure 5-17 plots the effusion rate calculated for the tube-fed flows on each planet. At a diameter of 10 m the effusion rate is calculated at

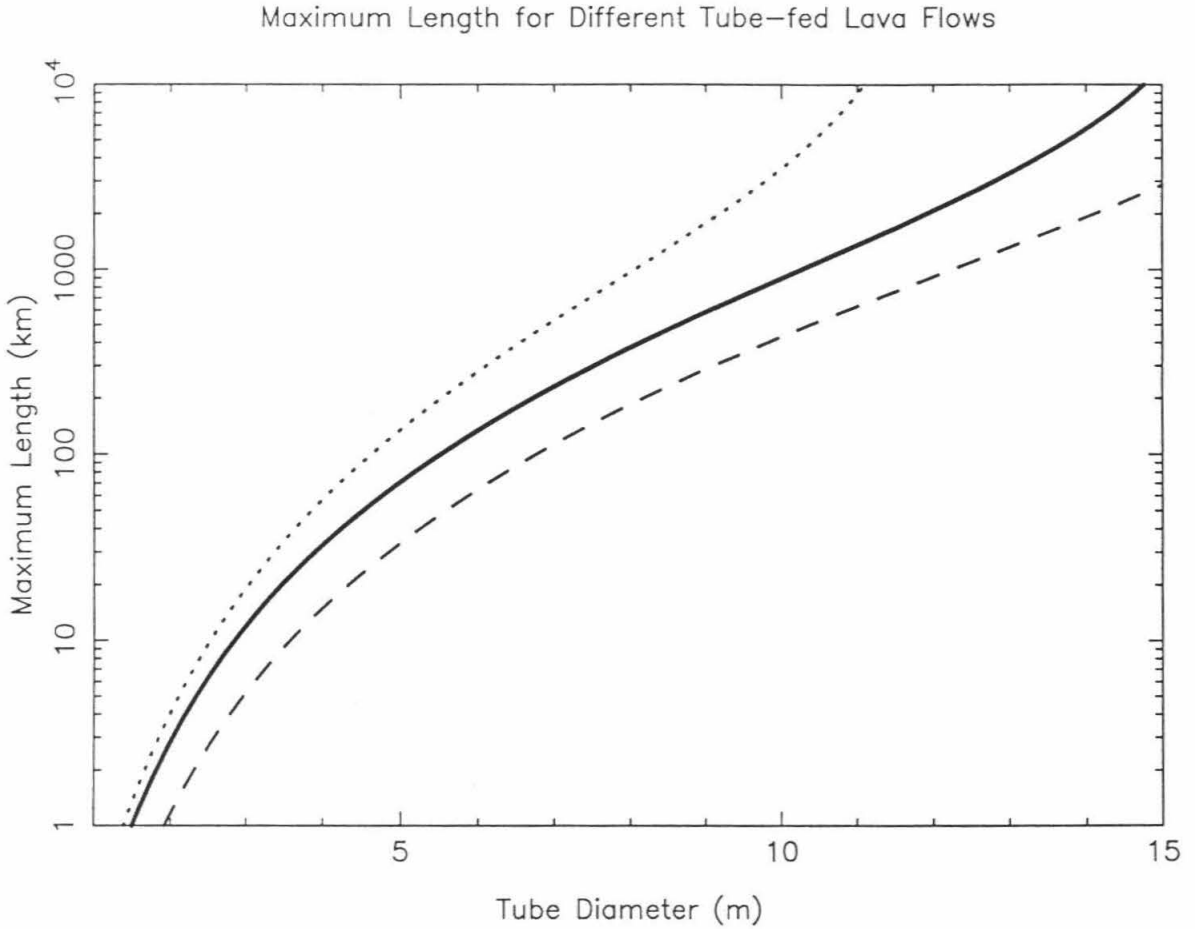


**Figure 5-16a: Relative cooling-limited lengths of the three terrestrial model lava tubes.** Solid line: Kilauea, dashed line: Columbia River basalt, and dotted line: submarine flow. Note that the Columbia River tube is the most cooling limited and that at a 10 m diameter, a lava tube could reach a few hundred kilometers in length.

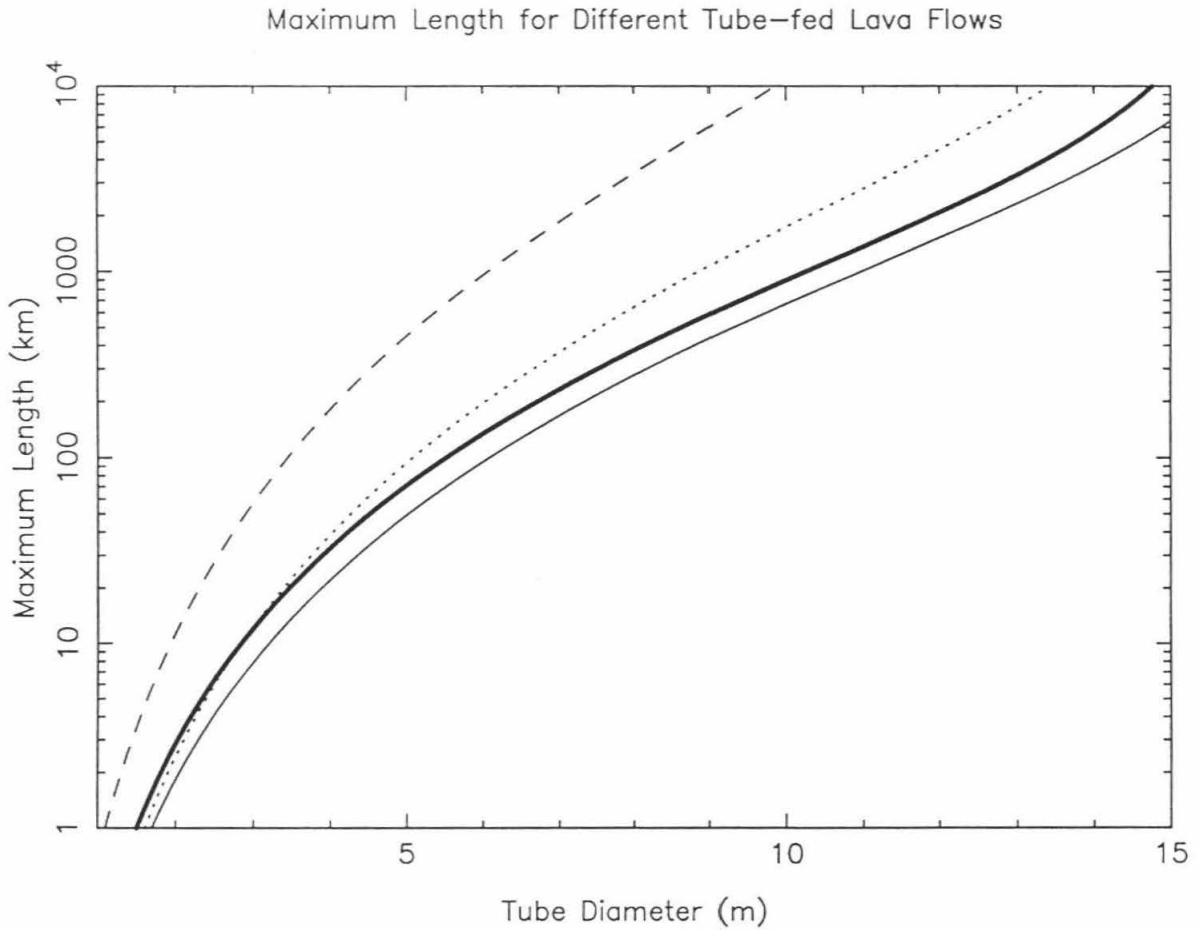


**Figure 5-16b: Relative cooling-limited lengths of model lava tubes of the different planets.** Dark solid line: Kilauea, thin solid line: Venus, dotted line: Mars, dashed line: the Moon. Note that the cooling limits of the Kilauea, Venusian, and Martian tubes are quite similar. The lunar flows, on the other hand, can be much longer.

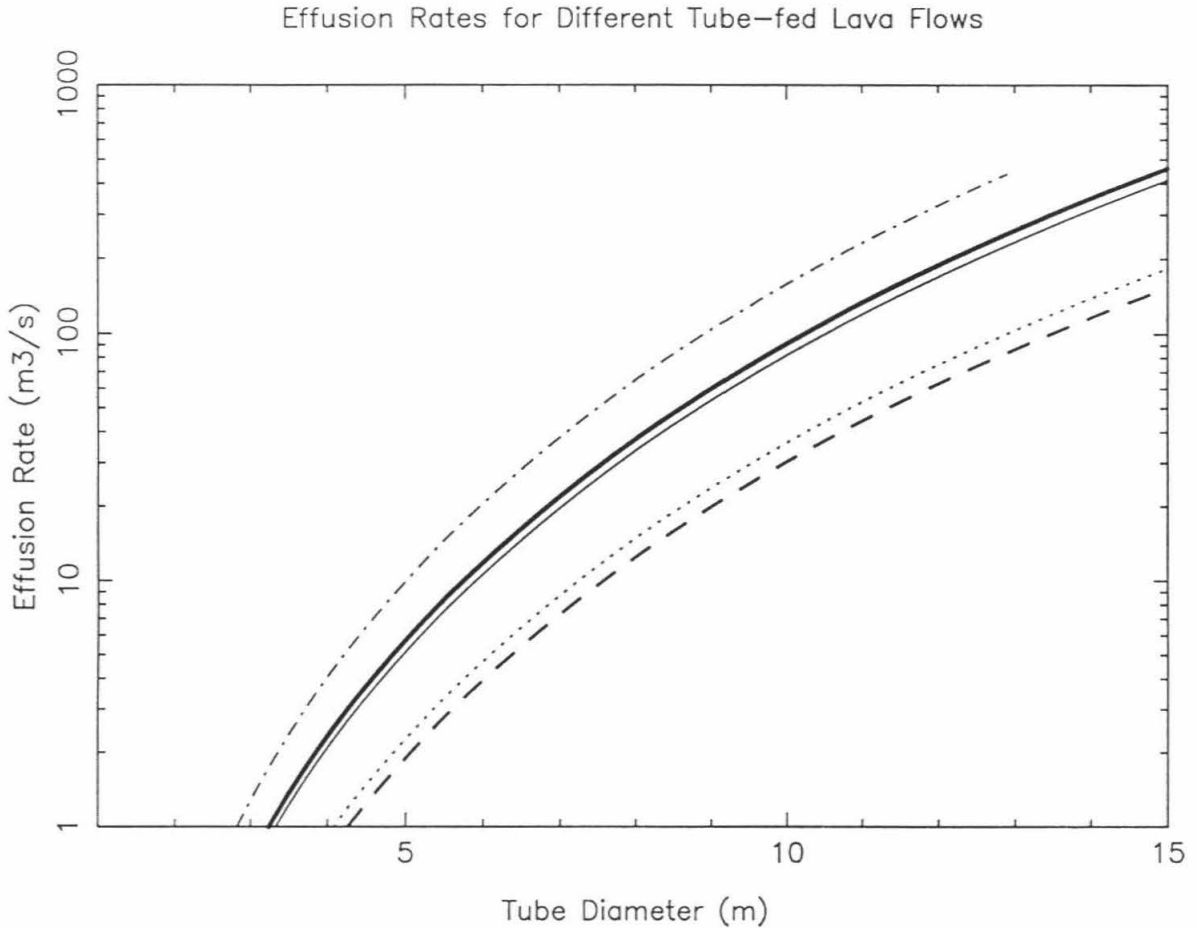


**Figure 5-17: Calculated effusion rates for the model lava tubes.** Effusion rates calculated using equation (5.16) and inputs from Table 5-3. Dark solid line: Kilauea and submarine tubes, thin solid line: Venus, dark dashed line: Columbia River basalt, dotted line: Mars, dot-dash line: Moon. Note that for a tube diameter of 10 m, effusion rates in my calculations have been on the order of several tens of  $\text{m}^3/\text{s}$ . Recall from Figure 5-16 that tube-lengths of about 1000 km are allowed for a 10 m diameter tube.

several tens of  $\text{m}^3/\text{s}$ . While this is high for Hawaiian pahoehoe flows (see Chapter 2), such effusion rates are common on the Earth. This suggests that even the longest flows we see in our solar system indeed need not be cooling-limited, if they are tube-fed.

## 5.6 Conclusions

The thermal budget I have constructed appears consistent with field observations from Kilauea. It suggests that the latent heat of crystallization is the single largest term in the thermal budget. Rain, conduction, convection of air in the wallrocks, and viscous dissipation all produce similar heat fluxes. I also find that skylights can be safely ignored. However, uncertainties in some key parameters, especially permeability of the wallrocks, remains large.

Given that lava in Kilauea tubes typically cools at about  $1\text{ }^\circ\text{C}$  per kilometer of tube length, it would seem plausible that some of the very long lava flows seen on the Earth and elsewhere might be cooling-limited, even if they were tube-fed. However, a more careful analysis shows that tube-fed flows several hundred kilometers long can easily be produced if effusion rates are on the order of  $30\text{-}100\text{ m}^3/\text{s}$ . Such effusion rates are reasonably common on the Earth. This further supports the suggestion that very long lava flows do not require very high effusion rates, if the flows are tube-fed pahoehoe flows.

## CHAPTER 6: CONCLUSIONS AND DISCUSSION

### 6.0 Executive summary

The main objective of this thesis has been to quantify the thermal budgets of pahoehoe lava flows. Combined with the work of Hon *et al.* [1994a] the thermal budget for pahoehoe lava flows has been completely described. The motivation behind my work was to better understand the emplacement of very long lava flows on the Earth and elsewhere. In particular, I have examined parts of the hypothesis that these very long lava flows might be pahoehoe lava flows fed by long-lived, low effusion rate eruptions. I have found that this hypothesis is reasonable (at least from a thermal point of view) for tube-fed pahoehoe flows. I have also laid the groundwork to study large pahoehoe sheet flows with my examination of the cooling of small pahoehoe flow lobes.

The remainder of this chapter first reviews the main conclusions from each of the previous chapters of the thesis, then draws some more general conclusions and discusses future research areas that this work has opened up. In particular, I discuss distinguishing between pahoehoe and 'a'a, better constraining atmospheric convection, and applications of my work to extra-terrestrial lava flows and flood basalts.

### 6.1 Summary of conclusions

#### Chapter 2: The Emplacement of the 75-km-Long Carrizozo Flow Field, South Central New Mexico

The tube-fed, pahoehoe, Carrizozo flow field provides a counter example to the notion that long lava flows require high effusion rates. The single most important factor in the length of this flow field appears to have been a long, undisturbed eruption duration. Present models for lava flows and empirical correlations between flow dimensions and effusion rate are only reliable when applied to simple 'a'a flows. This suggests caution in

the use of these techniques where it is not possible to determine whether a lava flow is pahoehoe or 'a'a.

### Chapter 3: Calculated Effect of Vesicles on the Thermal Properties of Basaltic Lava Flows

Based on available laboratory data and some simple calculations, the following conclusions are drawn about the effect of vesicles on the thermal properties of pahoehoe flow lobes: (1) convection of the gas phase within vesicles does not occur, (2) radiation across vesicles can transport significant heat only at very high temperatures, (3) porosity significantly reduces the bulk thermal conductivity and density of lava, (4) thermal diffusivity is relatively insensitive to porosity except in the limit of high temperature ( $T > 800$  °C) and high vesicularity ( $\phi > 40\%$ ) where radiation across vesicles may boost the thermal diffusivity, and (5) thermal inertia is significantly depressed by porosity for all temperatures. This last conclusion provides a qualitative explanation to the observation of Jones [1992, 1993] that the surfaces of porous pahoehoe lobes cool faster than the surfaces of dense lobes.

### Chapter 4: Modeling the Cooling of Pahoehoe Flow Lobes: the First Five Minutes

In this chapter I show that the problem of the initial cooling of a pahoehoe flow lobe can be reduced to a slab of lava cooling by conduction with heat loss at its top by radiation and atmospheric convection. All other processes can be neglected for the first several minutes of cooling. The conduction problem, including temperature and porosity dependent thermal properties, is solved numerically. The numerical model reproduces field measurements very accurately. The model indicates that the cooling of pahoehoe flow lobes is most strongly influenced by porosity and wind. A porosity dependence similar to that predicted by the model has been observed [Jones, 1992, 1993]. However, the dependence on wind has yet to be observed. The model also suggests an explanation for some of the different pahoehoe surface textures.

## Chapter 5: Thermal Budget of Lava Tubes

The thermal budget of lava tubes is dominated by (1) latent heat of crystallization, (2) rain, (3) conduction through the wallrocks, (4) convection of air in the wallrocks, and (5) viscous dissipation. The thermal budget I have constructed reproduces the  $\sim 1$  °C/km cooling observed in lava tubes on Kilauea. The thermal budget also indicates that tube-fed pahoehoe flows hundreds of kilometers long are possible in both subaerial and submarine terrestrial settings, on Venus, on the Moon, and on Mars given only moderate effusion rates (30-100 m<sup>3</sup>/s).

## Appendix C: Field Measurements of the Rheology of Pahoehoe Lobes, October 1991, Kilauea, Hawai'i

A penetrator was built and used in October, 1991 to measure the strength of the crust on pahoehoe flow lobes. Despite many technical difficulties, the instrument was able to provide some interesting data on the elastic nature of the crust. The strength of this crust increased from about 0.1 to 1.0 MPa over the first 2-3 minutes of cooling. This increase in strength with time appeared exponential. This suggests that the flow lobes were being driven by a hydrostatic head of several meters. Also, the exponential growth of strength was probably caused by the exponential dependence of the strength of basalt on temperature, and not by the square root of time growth of the thickness of the chill crust. Vesicles and microfractures may explain the fact that the measured crust is orders of magnitude weaker than predicted directly from laboratory data.

### **6.2 Pahoehoe vs. 'a'a**

One of the main points of this thesis is the importance of distinguishing between pahoehoe and 'a'a flows before attempting to decipher the emplacement history of a lava flow. 'A'a flows appear to be amenable to modeling with simple (Bingham) fluid models and cooling models dominated by thermal radiation [*e.g.*, Crisp and Baloga, 1990; Dragoni

and Tallarico, 1994]. The process of inflation and the essentially continuous crust on pahoehoe flows invalidates such simple models. Hence the need for my research.

On the Earth, it is almost trivial to distinguish between subaerial pahoehoe and 'a'a flows. Even with submarine flows, direct observations using manned submersibles and remotely operated vehicles are not uncommon. The real difficulties arise when studying extra-terrestrial flows using only images with no better than 10 m/pixel resolution. Two questions arise immediately: (1) is there a reason to expect pahoehoe flows on the other terrestrial planets and (2) can one identify the flow morphology from 100m - km scale features?

Pahoehoe can be expected on the other planets simply because it is so common on the Earth. But let us briefly examine the processes controlling the pahoehoe to 'a'a transition and how these processes might be different on the other terrestrial planets. The pahoehoe to 'a'a transition is controlled by some product of lava viscosity and the strain rate [Peterson and Tilling, 1980]. As was calculated in Chapter 5, the viscosities of basalts on the other terrestrial planets are not expected to be dramatically higher than on the Earth. This is despite that fact that most extra-terrestrial basalts may be drier than their terrestrial counterparts. The lower viscosity of the lunar basalts would suggest that forming 'a'a on the Moon would be particularly difficult.

The strain rate the lava encounters is directly proportional to the stress in encounters. This stress is given by

$$\sigma = \rho g H \sin(\alpha) \quad (6.1)$$

where  $\rho$  is the bulk density of the lava,  $g$  is the acceleration of gravity,  $H$  is the thickness of the flow and  $\alpha$  is the slope. Density is not expected to be dramatically different for the extra-terrestrial lavas. Gravity is weaker on the other planets and especially on the Moon. Slopes are not observed to be significantly steeper on volcanic edifices on the other planets

[*e.g.*, Pike, 1978]. The thickness of many flows, however, is known to be significantly greater on Mars and the Moon [*e.g.*, Moore *et al.*, 1978]. Identifiable lava flows often have scarps several tens of meters high. Such flow thicknesses could have formed as either large, high effusion rate, 'a'a flows or by slowly inflating pahoehoe flows. Thus, there is no *a priori* reason to rule out the existence of pahoehoe lava flows on the other planets.

The question now is how to distinguish 'a'a and pahoehoe flows using only remote sensing data. There is an interesting suggestion that, at least on the Earth, the margins of pahoehoe and 'a'a flows have different fractal dimensions [Bruno *et al.*, 1992]. The difficulty with this technique is that it has not been established that the same fractal dimensions should apply to the margins of extra-terrestrial flows. Since we do not know what physical processes control the fractal nature of the terrestrial flows, we have no way of determining how changing the environmental conditions might change the fractal nature of extra-terrestrial flows.

In the case of Mars, I hold out more hope for using high resolution images to identify 10-100 m scale inflation features. Such features have already been identified using the best of the Viking Orbiter images [Theilig and Greeley, 1986]. Should the Mars Observer Camera, with its 1.5 m/pixel resolution, make it to Mars on the Mars Surveyor Orbiter (or some other spacecraft), it should be easy to identify such features as tumuli and lava rise pits. My experience with aerial photos from lava flows in the Southwest United States gives me confidence in being able to identify these features even after considerable eolian cover has accumulated on the flows.

On the Moon, I suspect that impacts have obliterated most of the 10-m scale flow features. However, if the lunar sinuous rilles can be positively identified as collapsed lava tubes, then my work to date would have some immediate applications. If they are found to be open lava channels, it would suggest high effusion rates [*e.g.*, Hulme, 1973]. I suspect that significant additional surface and shallow subsurface exploration will be needed to

truly understand sinuous rilles. While such exploration does not seem likely at the present time, one can still dream.

Venus is a particularly troubling case. The 100 m/pixel resolution of Magellan is not nearly enough to identify the morphologic features that distinguish terrestrial pahoehoe and 'a'a flows. There is some hope that using multiple wavelengths, polarizations, and look angles one can reliably separate pahoehoe from 'a'a [*e.g.*, Arvidson *et al.*, 1993; Gaddis, 1993; Campbell and Campbell, 1992]. However, the diversity of (apparently) volcanic landforms on Venus seems to suggest a variety in lava compositions and/or emplacement styles surpassed only on Earth. There is a desperate need for a mobile vehicle to explore the surface of Venus. The most sensible design for Venus would be a buoyant vehicle. If such a balloon/submersible could spend most of its time at altitude (where the temperatures are bearable) it should be able to dive down for repeated snapshots (and perhaps chemical analyses) of the surface. Such a vehicle would naturally require an instrumented guiderope.

### **6.3 Atmospheric convection**

To me, the most unexpected result from this thesis is the repeated indication that the atmosphere plays a crucial role in the cooling of (Hawaiian) lava flows. That lava tubes appear to be significantly cooled by air circulating in the wallrocks still astounds me. I feel that further field work is needed to verify both my estimate of the atmospheric convective heat transfer coefficient and the flux of air circulating around lava tubes.

My simple experiment to constrain the atmospheric convective heat transfer coefficient (**h**) reported in Chapter 4 needs to be improved upon. In 1993 I did attempt to more carefully measure both the viscous and thermal boundary layers over lava flows. This involved deploying a 3-m tower with three anemometers and four thermometers downwind of active flow lobes. However, due to a combination of poor calibration and unreliable instrumentation, the data were completely unusable. I am certain that given more

funding and time I will be able to correctly measure the cooling effect as a function of wind speed.

However, applying those future Hawaiian field measurements more generally will be difficult. Some controlled laboratory studies or perhaps even numerical simulations may be necessary. In particular, for application to other planets, the effects of atmospheric density and ambient temperature need to be quantified. Also, it was noted in Chapter 4 that the radiative heating of the atmosphere is an important effect on the Earth. This can be properly modeled with atmospheric radiative transfer codes, such as are available at JPL.

My own confidence in the suggestion that air circulating in the wall rocks of lava tubes is a significant heat transport mechanism would be far greater if I had direct measurements of this phenomenon. I do have indirect evidence from IR video images taken in May of 1993. I observed hot cracks several tens of meters to either side of the lava tubes. The flows were old enough that the heat at depth was not from the initial cooling of the flows. The heat must have been provided by hot gasses transporting heat from the active lava tube laterally and vertically. While I have shown that air does convect around lava tubes, I have yet to show that this is really a significant heat transport mechanism.

I am presently considering several small field experiments to quantify this heat transport mechanism. One simple test would be to inject some tracer gas at one location and track its concentration through time at several other points. The permeability of the lava could also be measured using a flow test. Such tests are commonly done in hydrology using water in saturated reservoirs. The same measurement techniques could also use air. Good SCUBA diving regulators and air tanks could provide most of the needed hardware. It is not clear how much theoretical work would have to be done to use a compressible gas instead of an incompressible liquid in these flow tests. Again, to apply such results more generally, it will be necessary to tie the observations into models. In particular, I will need a model for the growth of fractures and a model for fracture permeability to extrapolate to other flows. Such models do exist but involve many subtleties.

## 6.4 Planetary applications

This indication that the atmosphere plays a key role in the thermal budget of pahoehoe lava flows should lead to some interesting insight into lava flows on the other terrestrial planets. As noted earlier, I do not at this time have a reliable way to estimate the cooling effect of the wind on the other planets. However, there are simple theoretical expressions for free convection (see Chapter 4).

Using the parameters listed in Table 5-3 for the different planets and equations (4.3) - (4.5) produces the values for the free convective heat transfer coefficient plotted in Figure 6-1. The free convection of the atmosphere should be about one order of magnitude more effective on Venus than on the Earth. On Mars, it is well over an order of magnitude weaker, making atmospheric convection an unimportant process. This suggests that the cooling rates of flows on the Moon and Mars should have been similar (assuming the lavas were similar). On Venus, atmospheric convective cooling will be frightfully efficient. In fact, there may be significant differences in the cooling rates on the lowlands versus the highlands. Venus has major topographic features that reach over 10 km above the mean planetary radius. The scale height in the atmosphere of Venus near the surface is also about 10 km.

The cooling model presented in Chapter 4 was run to examine the relative cooling rates of pahoehoe flow lobes on the Earth, Venus, Mars, and the Moon. Table 6-1 lists the input parameters to the model for each run. In addition to the nominal cases for each of the planets, I include 3 special cases: (1) a Venusian flow at 10 km altitude, (2) a lunar flow in full insolation, (3) and a lunar flow radiating to deep space.

Figure 6-2 plots the model results for each of these cases. The first conclusion from Figure 6-2a is that lava flows on all the planets cool at similar rates for the first 5 minutes. This is obviously because thermal radiation dominates over free atmospheric convection for the first few minutes of cooling. Recall that forced atmospheric convection is significantly more efficient than free convection. Therefore it is worthwhile to examine

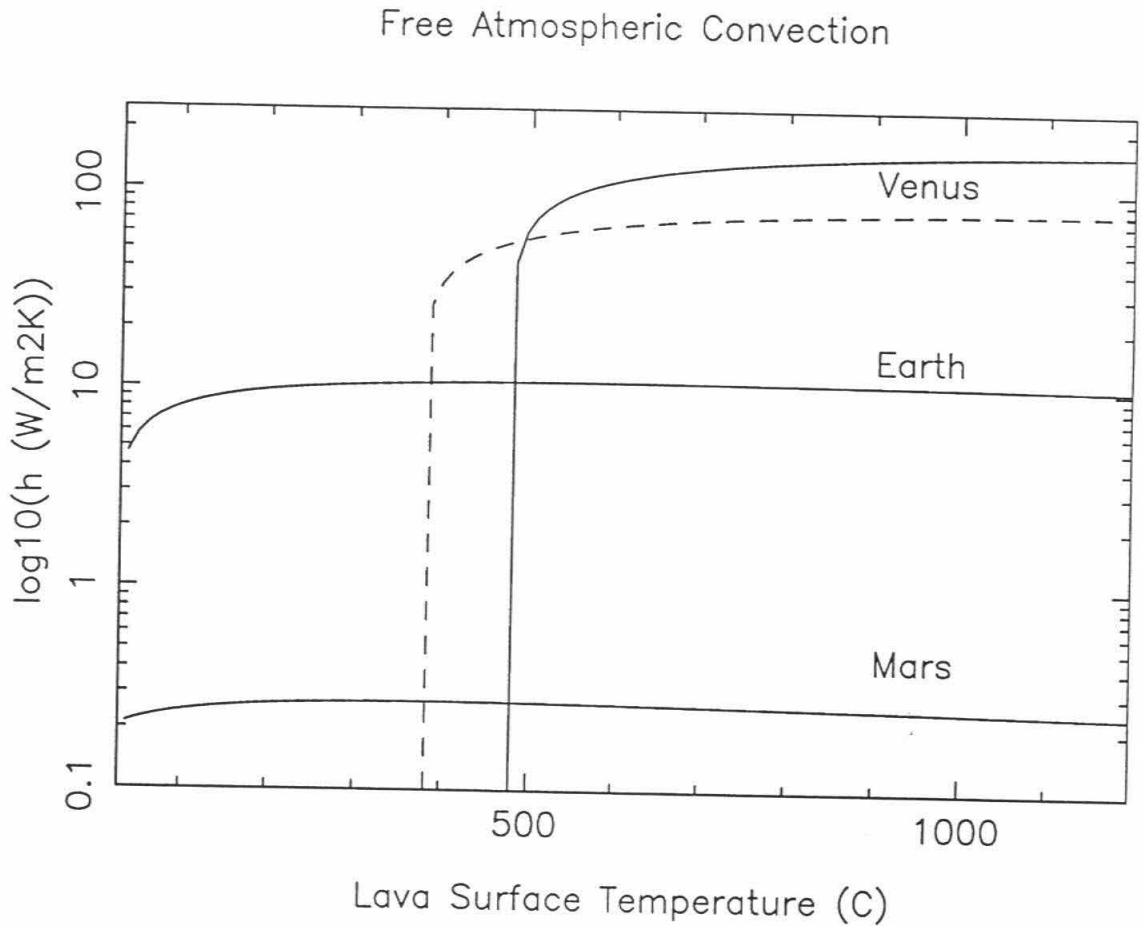


**Figure 6-1: Free convective heat transfer coefficients for Venus, Earth, and Mars.** Dashed line for Venus is at 10 km altitude (about 1 scale height). Note the log scale. Free convection is about 15 times more efficient on Venus and 50 times less efficient on Mars than on the Earth. As in Figure 4-4, the free convective heat transfer coefficient is quite insensitive to surface temperature.

**Table 6-1: Input parameters for cooling model.**

	Earth	Venus	Venus (hi-alt.)	Mars	Lunar	Lunar (noon)	Lunar (night)
$T_a$ (K)	300	750	650	240	250	390	4
$h$ (W/m <sup>2</sup> K)	11	150	78	0.27	0	0	0

Other input parameters are 50% for porosity, 1175 °C for  $T_0$ , 0.95 for emissivity and 1 mm for mean vesicle diameter. Temperature dependent thermal properties were also included as in Chapter 4 and Appendix A . Venus (hi-alt.) models flows on Maxwell Montes which has an elevation of more than 10 km. Note that the ambient temperature is thought to be significantly lower at this altitude. For the Moon, in order to investigate the effect of the large diurnal temperature variations, I ran two models. One has maximal insolation (equatorial noon) with 1350 W/m<sup>2</sup> of incoming solar radiation and the other radiates to deep space (night).

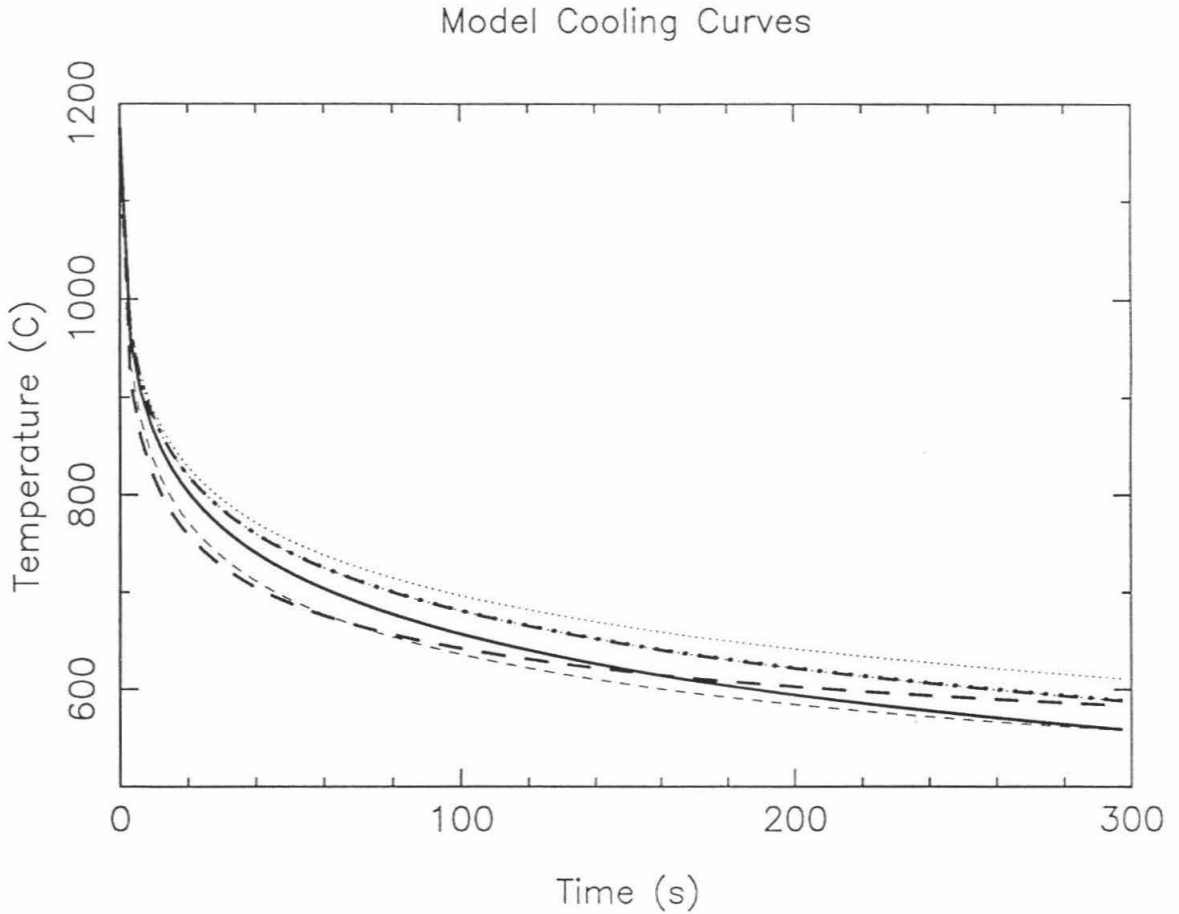
the relatively subtle effects of free convection in some detail in order to estimate the effects of forced convection.

Figure 6-2b expands the temperature scale to more clearly distinguish the surface cooling curves. The first point to notice is that the Martian, Lunar, and Lunar night curves are essentially indistinguishable. This means that free convective cooling by the Martian atmosphere is negligible. This is probably also true of forced convection on Mars. The model Venusian flows initially cool significantly faster than the terrestrial flow. This is because even free convection is an extremely efficient heat transfer mechanism on Venus. However, because of the high ambient temperature of Venus, the cooling curves level off at quite high temperatures. By the end of 5 minutes, the surface of the model Venusian flow is about 35 °C hotter than the terrestrial example. As might be expected, the high altitude Venusian flow initially cools a little slower but cools further than the baseline Venus model.

Extrapolated to a time scale of hours or days, the differences in cooling rate with altitude could be very significant on Venus.

Another interesting point is that the Lunar noon cooling curve cools significantly slower than the other lunar cases. Since only a tiny fraction of the surface of the moon actually experiences this maximal insolation, this is an extreme example. However, it does introduce an interesting, non-negligible, complication to understanding the cooling of lunar lava flows. This effect will be far more pronounced on Mercury.

Finally, observe that on the time scale of hours or days, terrestrial lava flows will cool significantly faster than lava flows on any other planet. Add in the effect of rain and it is reasonable to hypothesize that cooling rates may at least partially explain why lava flows over 100 km in length seem far rarer on the Earth than on any other of the terrestrial planets. However, this last suggestion is contrary to the results in Chapter 5 on tube-fed lava flows. For tube-fed lava flows, I suggest that the cooling for Martian, Venusian, and terrestrial flows is not very different. In fact, Venusian flows should undergo the most cooling. The difference in the results from the cooling model in Chapter 4 and the thermal analysis in Chapter 5 stem from the effect of atmospheric convection inside the frozen lava. This process is negligible in the first 5 minutes of cooling, but I suggest that it may be very important on the time scale of days to years.



**Figure 6-2a: Model surface cooling curves for pahoehoe flow lobes on different planets.** Model described in Chapter 4 and inputs listed in Table 6-2. The main conclusion from this plot is that lava flows on all the terrestrial planets will initially cool at similar rates. Earth: dark solid line; Venus: dark dashed line; Venus (hi-alt.): thin dashed line; Mars: dark dash-dot line; Lunar: dark dotted line; Lunar (night) and Lunar (noon) light dotted lines.

## Model Cooling Curves

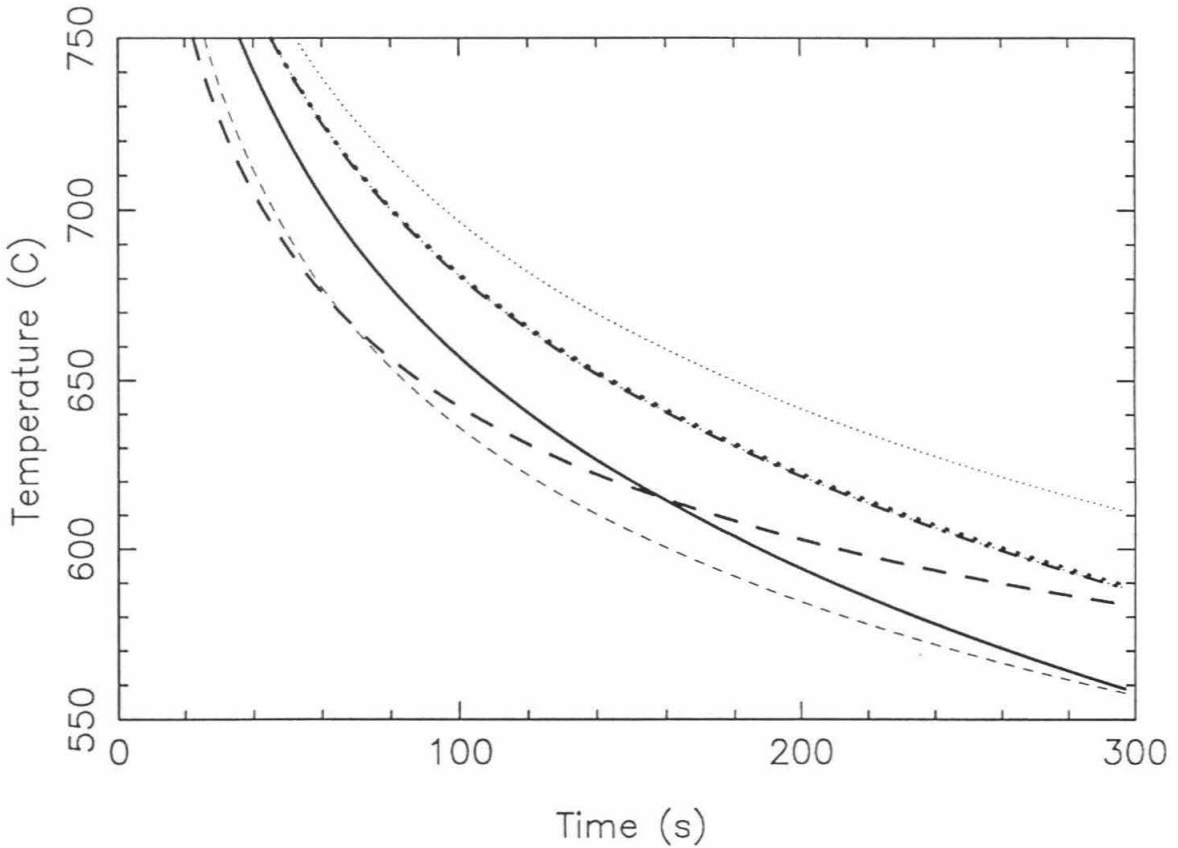


**Figure 6-2b: Blow-up of model surface cooling curves for pahoehoe flow lobes on different planets.** The temperature scale in Figure 6-2a is expanded to more clearly show the minor differences in the cooling rates of the different model flows. These differences will grow with time and will be larger if forced atmospheric convection were taken into account. Lunar (dark dotted line), Lunar night (light dotted line) and Martian cooling curves are still essentially indistinguishable. However, lunar noon (light dotted line) does stay significantly warmer. Venus (dark dashed line) and Venus high altitude (light dashed line) initially cool faster than the terrestrial example, but then level out at much higher temperatures. By the end of just 5 minutes, the terrestrial flow surface (dark solid line) is predicted to be the coldest.

## 6.5 Continental flood basalts

To conclude this thesis, I would like to discuss continental flood basalt eruptions and my plans for the next few years to produce an initial estimate of their climatic effect. Continental flood basalts are exciting for a number of reasons. They are enormous land forms, each covering over a hundred thousand square kilometers with often more than a kilometer of lava. There is continued interest in the genesis of these melts and their possible relation to mantle dynamics and geochemistry [*e.g.*, BVSP, 1981; Kent *et al.*, 1992; Gallagher and Hawksworth, 1992; Basu *et al.*, 1993]. There is also a very curious coincidence between the dates for the formation of continental flood basalt provinces and mass extinctions [Rampino and Stothers, 1988; Stothers, 1993]. There are, of course, explanations that do not involve volcanism for each of the mass extinctions. Still, the coincidence between mass extinctions and continental flood basalts deserves serious attention. Perhaps it can be shown that massive basaltic eruptions can prolong or magnify the environmental stress caused by another agent such as a meteorite impact.

The environmental impact of a volcanic eruption depends on the style of the eruption. There are two possible end members for the style of eruption that may have fed the continental flood basalts: (1) a short-lived, cataclysmic fissure eruption that suddenly dumped massive amounts of heat and volatiles high into the atmosphere and (2) a long-lived, steady eruption that led to sustained loading of the lower atmosphere with volcanic gasses. Effusion rate is probably the most useful parameter to distinguish these styles of eruption. Therefore I will concentrate my research on constraining the effusion rates that fed the continental flood basalts.

Radiometric age dating indicates that the bulk of each continental flood basalt province was emplaced in under 1 million years [*e.g.*, Renne and Basu, 1991; Renne *et al.*, 1992]. This requires minimum lava production rates of about  $1.5 \text{ km}^3/\text{yr}$ , only one order of magnitude higher than the average lava production rate at Hawai'i. In the case of the Columbia River flood basalts, it appears that the flow units were emplaced as large inflating

pahoehoe sheet flows [*e.g.*, Reidel and Tolan, 1992; Finnemore *et al.*, 1993]. Thus, quantifying the pahoehoe to 'a'a transition is one way to place a broad upper bound on flow velocities and effusion rates.

I plan to place tighter constraints on the effusion rate by examining the thermal budgets of these large sheet flows. It is important to note that no evidence for lava tubes has yet been found in the Columbia River flood basalts. Since sheet flows are far less thermally efficient than lava tubes, it is still possible that the flood basalts are cooling limited. By applying the same sort of analysis as I applied to lava tubes, it should be possible to determine a minimum effusion rate. I plan to be somewhat more ambitious and also construct a model for the dynamics of the inflation process. This potentially could place quite narrow constraints on the flux of lava that produces specific morphologic features (*i.e.*, tumuli vs. flat inflated sheets vs. new breakouts). This model could be made applicable to all inflated lava flows, not just flood basalts.

The ultimate aim of this work will be to produce an estimate of the effect of flood basalt eruptions on global climate. Using reasonable estimates of the volatile content and composition for flood basalt lavas and given the eruption duration, it is a simple exercise to roughly estimate the rate at which different volcanic products ( $\text{SO}_2$ ,  $\text{CO}_2$ ,  $\text{H}_2\text{O}$ , Cl, F, etc.) are injected into the atmosphere. However, to directly affect global climate, these volcanic products must be transported into the stratosphere.

Most work to date on the environmental impact of volcanism has concentrated on explosive eruptions which can inject matter directly into the stratosphere. In contrast, the products of basaltic eruptions are usually confined to the lower troposphere and are capable of causing only local climate change. However, observations of the large basaltic fissure eruptions in Iceland suggest that significant quantities of ash were transported hundreds of kilometers [Thordarson and Self, 1993]. These volcanic products were carried high into the troposphere by the plume of air heated by the eruption. The key control on the plume height is the rate at which heat is added at the base of the atmosphere [Wilson *et al.*, 1978;

Stothers, 1989]. This heat flux is, in turn, controlled by the rate at which hot lava is erupted and the rate at which this lava cools. These are parameters I should be able to constrain rather well.

After producing these estimates for the rates at which volcanic products might be injected into the stratosphere over a flood basalt eruption, I will try to estimate the climatic impact of the eruption. For an initial, order of magnitude type of estimate, the injection rate can be compared to historical explosive eruptions. At present we do not even know if a flood basalt eruption is more similar to a single Mauna Loa eruption or to 10,000 Toba mega-eruptions. For more precise predictions for climate impact of the eruption, my estimates of injection rates and altitudes need to be turned over to the climate modeling community.

ALL PAU.

## APPENDIX A: TEMPERATURE DEPENDENCE OF THERMAL AND PHYSICAL PROPERTIES

### A.1 Properties of basalt

#### A.1.1 Thermal Conductivity

The following fit to laboratory data on the thermal conductivity of basalt from Touloukian, *et al.* [1989] was used throughout this thesis:

$$k_{\text{bas}}(T) = 0.427 + (772/T) - (8.72 \times 10^4/T^2) \quad [\text{W/m K}].$$

However, as noted in Chapter 3, there are some studies suggesting that the thermal conductivity of basalt increases with temperature. As an example of these studies I have used the data from Birch and Clark [1940] for diabase glass:

$$k_{\text{bas}}(T) = 0.848 + 1.1 \times 10^{-3} T \quad [\text{W/m K}].$$

#### A.1.2 Heat Capacity

I used a two part fit to the heat capacity data in Touloukian *et al.* [1989]:

$$C_{\text{pbas}}(T) = \begin{array}{ll} 1100 \quad [\text{J/kg K}] & \text{for } T > 1010 \text{ K} \\ 1211 - (1.12 \times 10^5/T) & \text{for } T \leq 1010 \text{ K}. \end{array}$$

The resulting values for heat capacity are within about 15% of other published expressions for the heat capacity of basalt [*e.g.*, Birch and Clark, 1940; Peck *et al.*, 1977; Robertson, 1988]. There is often a very clear (but small) change in  $C_p$  and other thermodynamic parameters at the melt to glass transition [*e.g.*, Stebbins *et al.*, 1984; Richet and Bottinga, 1986; Knoche *et al.*, 1992; Lange and Navrtosky, 1993]. However, I have ignored this.

### A.1.3 Density

I used the following expression to describe density:

$$\rho_{\text{bas}}(T) = \rho_0 / (1 + \beta(T - 1450))$$

where  $\rho_0$  is the initial melt density (2600 kg/m<sup>3</sup>) and  $\beta$  is the volumetric coefficient of thermal expansion. Touloukian *et al.* [1989] gives a value of  $1.5 \times 10^{-5} \text{ K}^{-1}$  for  $\beta$  for vesicular basalt. This is as much as a factor of 3 less than the value for dense crystalline basalt.

## **A.2 Properties of gasses**

### A.2.1 Viscosity

The following expressions from the American Institute for Physics Handbook were used. The Keyes' Equation is recommended to describe the temperature dependence of the viscosity of gasses [Kestin, 1957]:

$$\eta_{\text{air}}(T) = \frac{a_0 \sqrt{T}}{1 + \frac{a_1}{T} 10^{-a/T}} \quad [\text{Pa s}]$$

<b>Gas</b>	<b>Temperature Range</b>	<b><math>a_0</math> (Pa s K<sup>-1/2</sup>)</b>	<b><math>a</math> (K<sup>-1</sup>)</b>	<b><math>a_1</math></b>
<b>Air</b>	79 K < T < 1845 K	$1.488 \times 10^{-6}$	122.1	5
<b>H<sub>2</sub>O</b>	373 K < T < 873 K	$1.501 \times 10^{-6}$	446.8	0
<b>CO<sub>2</sub></b>	198 K < T < 1686 K	$1.554 \times 10^{-6}$	246.0	3

Only H<sub>2</sub>O vapor was extrapolated out of the temperature range for which these fits are strictly valid.

### A.2.2 Density

From the Ideal Gas Law, it is clear that the density of gasses is essentially inversely proportional to temperature. I have used the following estimates for density (temperature in Kelvins):

$$\rho_{\text{H}_2\text{O}}(T) \cong 222.7/T \quad [\text{kg/m}^3]$$

$$\rho_{\text{air}}(T) \cong 352.6/T \quad [\text{kg/m}^3]$$

$$\rho_{\text{CO}_2}(T) \cong 540.0/T \quad [\text{kg/m}^3]$$

The resulting values are very close to actual laboratory measured values [Hilsenrath, 1957].

### A.2.3 Heat Capacity

For heat capacity, the following fits were calculated to the data from [Hilsenrath, 1957]:

$$C_{\text{P,H}_2\text{O}}(T) \cong 1860 + 1.32 \times 10^{-2} T + 4.36 \times 10^{-4} T^2 \quad [\text{J/kg K}]$$

$$C_{\text{P,air}}(T) \cong 947 + 0.191 T \quad [\text{J/kg K}]$$

### A.2.4 Thermal Conductivity

Thermal conductivity was not tabulated in the American Institute for Physics Handbook. Instead, it was calculated using a formula for ideal polyatomic gasses [Bird *et al.*, 1960]:

$$k_{\text{gas}}(T) = \eta_{\text{gas}}(T) (C_{\text{p,gas}}(T) + 5R/4M)$$

where R is the ideal gas constant and M is the mean atomic mass of the gas .

## APPENDIX B: CODE FOR, AND TESTING OF, NUMERICAL COOLING MODEL FOR THE INITIAL COOLING OF PAHOEHOE FLOW LOBES

### B.0 Executive summary

This appendix lists the code for the numerical cooling model presented in Chapter 4. It also describes some of the tests and exploratory runs done on the model. Unless the reader wishes to examine the details of this cooling model, there is little of interest in this appendix. The one point I would like to make is that the numerical model is extremely simple (by today's standards). The meat of the program lies in less than 50 lines of code. There are more sophisticated programs for thermal analysis available commercially. Creating this numerical model was essentially just a learning experience for myself. The tests I have run, as listed in Chapter 4, are (1) conservation of energy, (2) comparison to analytical solution with fixed surface temperature, and (3) comparison to analytical solution for fixed heat transfer coefficient. I also discuss stability and round-off error issues.

### B.1 Code

#### B.1.1 General Comments:

The final version of the cooling model was named COOL6A and is written in VAXFORTRAN. The numerical technique used is pure, brute-force, fully-explicit, finite differencing. The original code is very sparse on comments, so I have interspersed some additional explanations (*italicized*) in the following listing of the code. For the curious, the code was in capital letters till about version 4B when I started using lowercase. Calls to subroutines beginning with PG refer to the PGPLOT plotting package used by the Caltech Division of Geological and Planetary Sciences.

#### B.1.2 Code:

IMPLICIT NONE

real krad,ksol,kgas,kcond,beta,ro,romelt,cp

*thermal conductivities, coefficient of thermal expansion, densities, heat capacity*

real intu(100),topu(100),utime(100),iu

*internal heat, heat lost from the top surface, counters*

REAL TO,TA,TE,EMMIS,SIGMA,H,K(500),PHI,RCP(500)

*initial, ambient, and surface temperature; emissivity, Stefan-Boltzmann constant, heat transfer coefficient, effective thermal conductivity, porosity, heat capacity per unit volume*

REAL Q,DIAM,Z(500),pt(500)

*heat flux, vesicle diameter, depth, temperature for plotting routines*

REAL TOTTIME,OUTTIME,DATTIME,CROSTIME,XTIME

*time counters*

DOUBLE PRECISION T(500),NT(500),u,uu,dt,dx,time

*temperatures, heats, timestep, grid spacing, time*

INTEGER N,J,m

*counters*

*First set of constants*

DT=1.0000000000E-3

DX=1.0000000000E-4

SIGMA=5.67E-8

c DIAM=6E-3 !mean diameter of vesicles (Mangan, 1991)

c diam=1.1e-3 !mean diameter of vesicles (Hon et al., 199?)

diam=1e-3 !mean diameter (Keszthelyi and Denlinger)

beta=1.45e-5 !coefficient of volumetric thermal expansion

romelt=2600. !pure melt density

set time counters to zero

TIME=0.

OUTTIME=0.

CROSTIME=0.

*ask for variable inputs*

WRITE(\*,\*)'what is the surface emissivity?'

WRITE(\*,\*)'JPL-ers like about 0.98 for basalt'

READ(\*,\*)EMMIS

WRITE(\*,\*)'What is the initial lava temperature [C]'

```

READ(*,*)TO
TO=TO+273.16
WRITE(*,*)'What is the ambient temperature [C]'
READ(*,*)TA
TA=TA+273.16
WRITE(*,*)'What is the vesicularity?'
READ(*,*)PHI
WRITE(*,*)'What is the convective h? Baseline is 50.'
READ(*,*)H
WRITE(*,*)'how long do you want this run to go [sec]'
READ(*,*)TOTTIME
DATTIME=TOTTIME/99.
WRITE(*,*)'How often do you want a cross-section? [sec]'
READ(*,*)XTIME

```

*set initial temperature and time dependent properties (see Appendix A)*

```

krad=phi*2*diam*sigma*(To**3)
ksol=0.427+(772/To)-(8.72e4/(To**2))
kgas=-3.3969e-3+(9.7337e-5*To)

```

c for spheres

```

kcond=ksol*(2*(1-phi)*ksol+(1+2*phi)*kgas)/((2+phi)*ksol+(1-phi)*kgas)
ro=romelt*(1/(1+(To-1450.)*beta))
Cp=1100.
m=1
iu=0.

```

*set variables that vary with depth, calculate initial heat content*

```

DO 10 N=1,500
T(N)=TO
k(n)=krad+kcond
rcp(n)=ro*Cp
Z(N)=(N-1)*DX*100
iu=iu+rcp(n)*T(n)*dx
intu(m)=0.

```

10 CONTINUE

*output initial temperature values*

```
write(7,*)time,t(1),t(11),t(21),t(101),t(201)
```

*The meat of the program starts here. Advance time counters*

```
105  TIME=TIME+DT
      OUTTIME=OUTTIME+DT
      CROSTIME=CROSTIME+DT
```

*Calculate surface flux and temperature*

```
Q=EMMIS*SIGMA*(TA**4-T(1)**4)+H*(TA-T(1))
U=U-(q*dt)
TE=T(1)+Q*DX/K(1)
```

*calculate new surface temperature*

```
NT(1)=T(1)+DT*K(1)*(T(2)+TE-2*T(1))/(rcp(1)*DX**2)
```

*calculate new internal temperatures*

```
DO 110 N=2,499
  NT(N)=T(N)+((K(N-1)+K(N))*(T(N-1)-T(N))+K(N+1)+K(N))*(T(N+1)-
  T(N)))/DT/(2*rcp(n)*DX**2)
110  CONTINUE
```

*no heat flux out the bottom*

```
NT(500)=NT(499)
```

*rename new temperatures as old temperatures. recalculate temperature dependent properties at each gridpoint*

```
DO 180 N=1,500
  T(N)=NT(N)
  krad=phi**2*diam*sigma*(T(n)**3)
  ksol=0.427+(772/T(n))-(8.72e4/(T(n)**2))
  kgas=-3.3969e-3+(9.7337e-5*T(n))
c   for spheres
  kcond=ksol*(2*(1-phi)*ksol+(1+2*phi)*kgas)/((2+phi)*ksol+(1-phi)*kgas)
  k(n)=krad+kcond
```

```

ro=romelt*(1/(1+(T(n)-1450.)*beta))
if(T(n).ge.1011.) then
    Cp=1100.
else
    Cp=1211.-(1.1218e5/T(n))
endif
rcp(n)=ro*cp
NT(N)=0.
180 CONTINUE

```

*if the time is right, output temperatures at 5 depths (surface, 1mm, 2mm, 1cm, 2cm) and ...*

```

IF(DATTIME.LE.OUTTIME) THEN
M=M+1
write(7,*)time,t(1),t(11),t(21),t(101),t(201)

```

*... output the integrated heat flux out the top and the internal heat lost.*

```

topu(m)=u
uu=0.
do 181 n=1,500
181 uu=uu+rcp(n)*t(n)*dx
intu(m)=iu-uu
utime(m)=time
c write(8,*)utime(m),topu(m),intu(m)
OUTTIME=OUTTIME-DATTIME reset timecounter
ENDIF

```

*if the time is right, output a temperature profile*

```

IF(XTIME.LE.CROSTIME) THEN
DO 202 N=1,500
202 PT(N)=T(N)-273.16
write(9,*)time,z,pt
CROSTIME=CROSTIME-XTIME
ENDIF

```

*if we are not done yet, go back and do this again.*

```

IF(TIME.LE.TOTTIME) GOTO 105

```

*this ends the meat of the program*

*make plot comparing integrated heat flux out the top and the internal heat lost*

```

CALL PGBEGIN(0,'COOLUPLOT.LAS/PS',1,1)
CALL PGENV(0.,TOTTIME,0.,2E7,0,1)
CALL PGLABEL('TIME (s)','TOTAL HEAL LOST (J)','COOLING MODEL RESULTS')
call pgslw(2)
CALL PGLINE(M,UTIME,topu)
call pgsls(2)
call pglime(m,utime,intu)
CALL PGEND
write(8,*)m,utime,topu,intu

```

*plot temperature profiles*

```

DO 802 N=1,500
802  PT(N)=T(N)-273.16
CALL PGBEGIN(0,'COOLXPLOT.LAS/PS',1,1)
CALL PGENV(0.,Z(500),0.,1200.,0,1)
call pglabel('DEPTH (cm)','TEMPERATURE (C)','TEMPERATURE PROFILE')
CALL PGLINE(500,Z,PT)
CALL PGEND
write(9,*)time,z,pt

```

*make sure we did not try to cool the bottom of the model (too much)*

```

write(*,*)'final bottom temp = ',t(500)

```

END

*Nothing to it, huh?*

## B.2 Testing

It is a legitimate question to ask if this simple brute of a program can actually do what it is supposed to. As mentioned in Chapter 4, I went to very small time steps because the surface temperature changes very quickly. It is possible to make a stable program with larger time steps, but it will not be as accurate, especially early in the run. Even initially, the surface temperature will not change by much more than 10 K during a single 1 millisecond time step. Given this ridiculously small time step, two problems arise. First, in order to maintain numerical stability, the gridspacing must be very small. The 100  $\mu\text{m}$  gridspacing will be stable, even at nearly unreasonably low thermal diffusivities. The second problem is that of round-off errors. Using single precision variables, round-off errors became significant in on the order of 10,000 time steps (10 seconds of model time). By going to double precision this problem has been completely eliminated.

There is also an issue of how best to numerically implement the upper boundary condition. I have tried many variations and there is no detectable difference between any of the reasonable schemes. The lower boundary condition is that of no heat flux. A fixed lower temperature is another option. But since I am trying to model an infinite half-space, there should be no temperature changes or heat fluxes at the bottom. Bottom temperatures change by less than 1K in realistic model runs.

That leaves tests of my implementation of the finite differencing. To test the basic algorithm, I commented out the temperature dependent properties and changed the upper boundary condition to one that has an analytic solution. The two tests were done for a fixed surface temperature and for a fixed heat transfer coefficient [Carslaw and Jaeger, 1959]. For the first analytic solution is described in Chapter 4. When the same (fixed temperature) boundary condition is applied to the numerical model, the temperatures agree to better than 0.1K throughout the run (Fig. B-1). The temperature differences for the fixed  $h$  case were less than about 1K (Fig. B-2). This larger discrepancy can be best

explained by round-off errors caused by the repeated estimates of error functions in the analytic solution rather than any problem with the numerical model.

Finally, during each run of the numerical model, the integrated heat flux out the top was compared to the total internal heat loss. In the first few seconds these numbers agree to only about 1%. The values then converge to within a few tenths of a percent of each other but then very slowly drift apart (Fig. B-3). These discrepancies are explained by the extremely crude numerical integration technique I used. My conclusion is that my model is numerically accurate to at least the 1% level and probably to the 0.1% level. As noted in Chapter 4, in making this thermal model I have already ignored several physical processes that should affect temperatures at the 1% level.

### **B.3 Additional model runs**

I have made several exploratory runs of the cooling model that were not presented in Chapter 4. One involves using a thermal conductivity that increases with temperature and the other looks at the effect of microfractures. Figure B-4 compares these model runs. For the case that thermal conductivity increases with temperature, values from Birch and Clark [1940] for a diabase glass were used (see Chapter 3 and Appendix A). Note that the model results change very significantly with this type of thermal conductivity. In fact, I would not be able to match the field data using these values.

The fractured case uses an extremely crude model for the generation of cracks. Horai [1991] found that the best fit to thermal conductivity as a function of porosity was given by the Fricke-Zimmerman's Formula for spheroidal inclusions. The best fit for the aspect ratio of the spheroid ( $\alpha$ ) was 0.1 which is consistent with microfractures playing an important role in lowering the thermal conductivity of porous basalt. For an  $\alpha$  of 1, the Fricke-Zimmerman's Formula reduces to Maxwell's Formula which I have used everywhere else in the model (see Chapter 3). In order to maximize the effect of fractures in the model, I have set  $\alpha$  to 0.1 for all temperatures below 740 °C. Even with this extremely

generous fracturing model, the cooling curves are not significantly changed. Perhaps this is only because very little of the lobe is cooled under 740 °C in the first 5 minutes.

I have also found that using thermal properties fixed at their values at 1000 K was able to closely reproduce my runs with the fully temperature dependent thermal properties. As the lobes continue to cool, the temperature dependence of the thermal properties may become more apparent.

## Model Cooling Curves

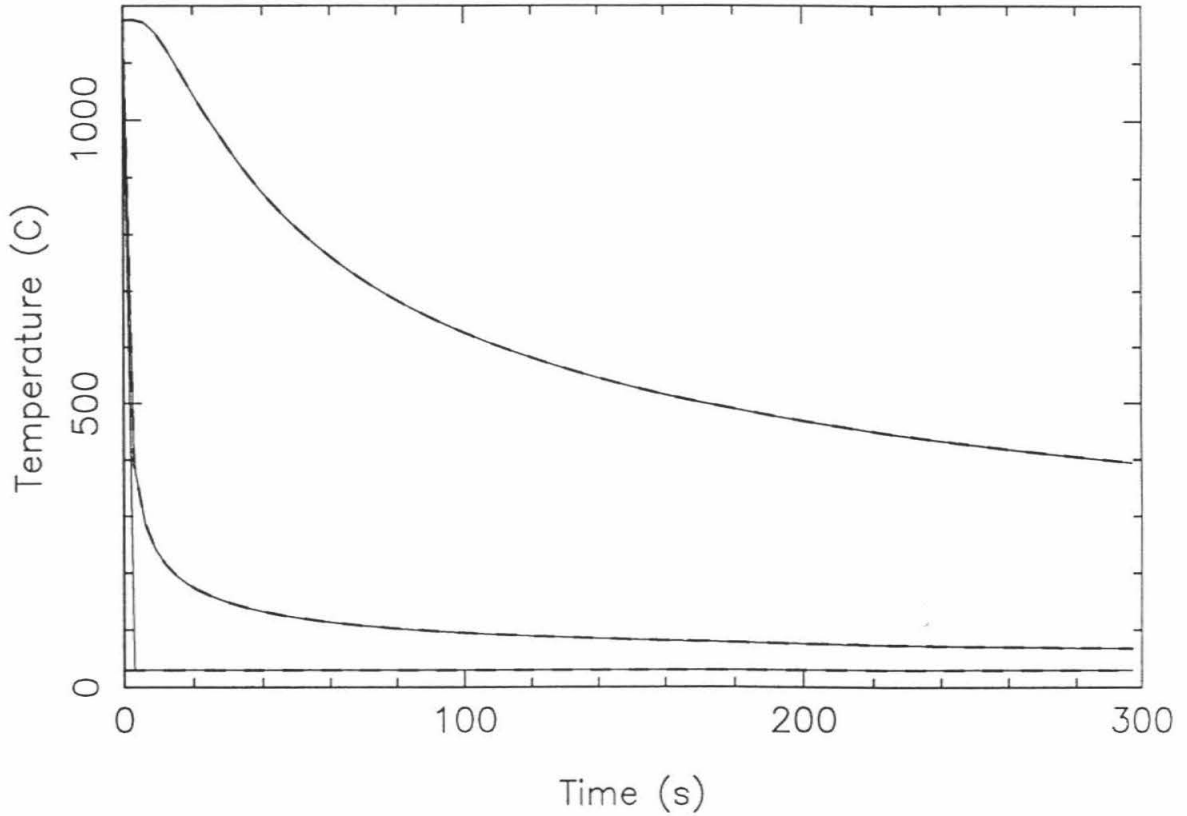


**Figure B-1: Analytic and numerical solutions for fixed temperature conductive cooling problem.** Curves plotted for the surface, 1mm depth, and 1 cm depth. Analytic solution in dashed line, numerical solution in solid line. Initial temperature set at 1175 °C, surface temperature fixed at 30 °C. Note that the curves are indistinguishable.

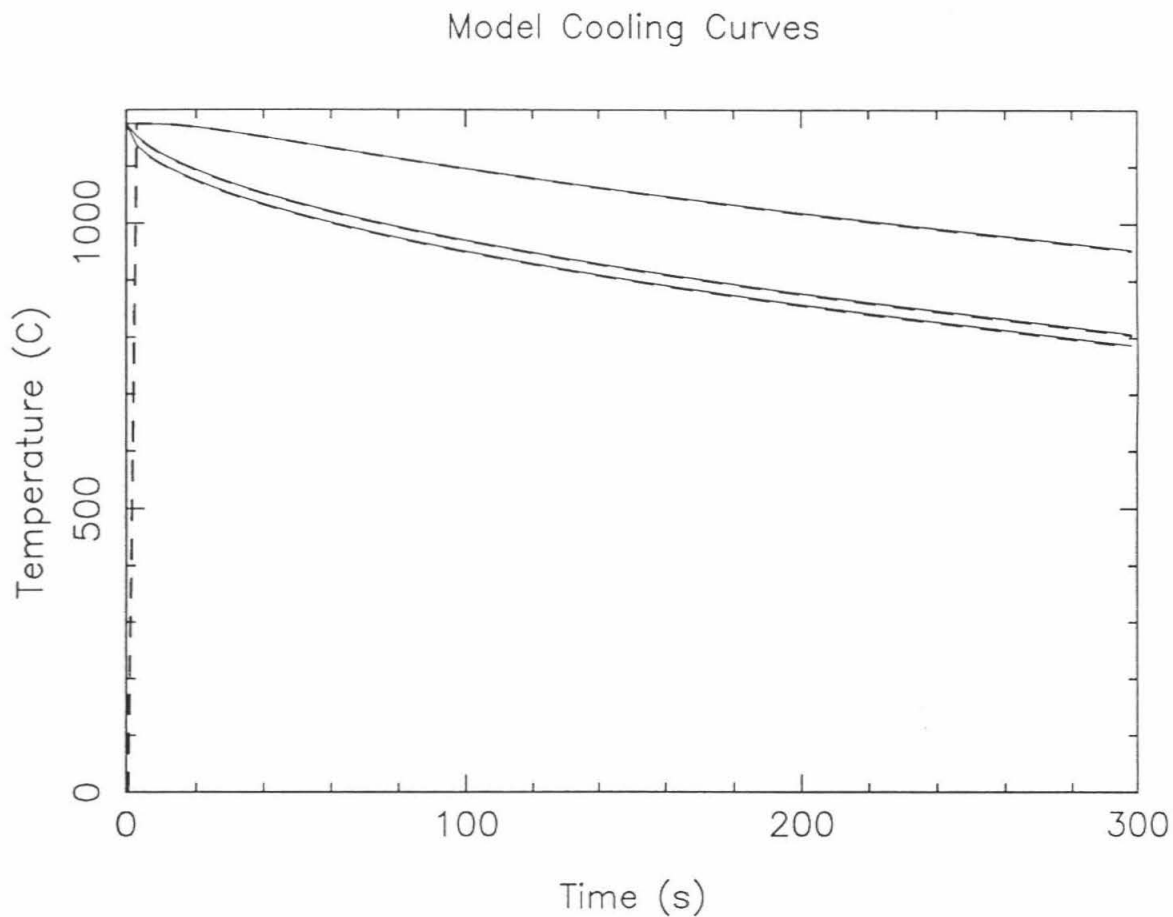


**Figure B-2: Analytic and numerical solutions to fixed heat transfer coefficient conductive cooling problem.** Curves plotted for the surface, 1mm depth, and 1 cm depth. Analytic solution in dashed line, numerical solution in solid line. Initial temperature set at 1175 °C,  $h$  fixed at 100 W/m<sup>2</sup>K. Note that the curves are indistinguishable. Dashed line to the origin is a plotting artifact.

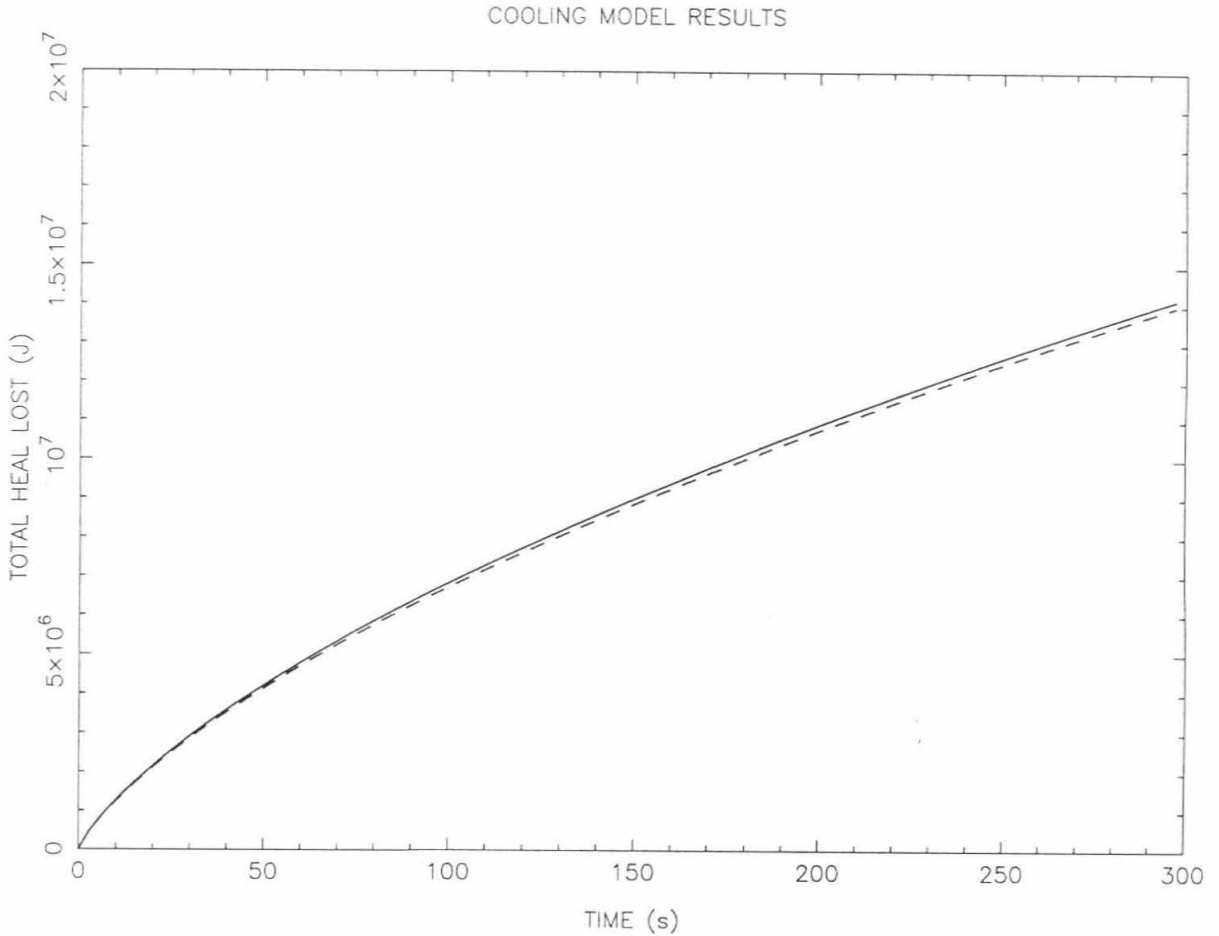


**Figure B-3: Conservation of energy test of numerical model.** Plot of total heat loss calculated by two independent methods. This run is with  $T_o = 1135$  °C,  $T_a = 30$  °C,  $f = 50\%$ ,  $r = 1$  mm, and  $h = 11$  W/m<sup>2</sup>K. All other runs look identical in form. The discrepancy between the two curves can be completely explained by the crude numerical technique used for this test.

## Model Cooling Curves

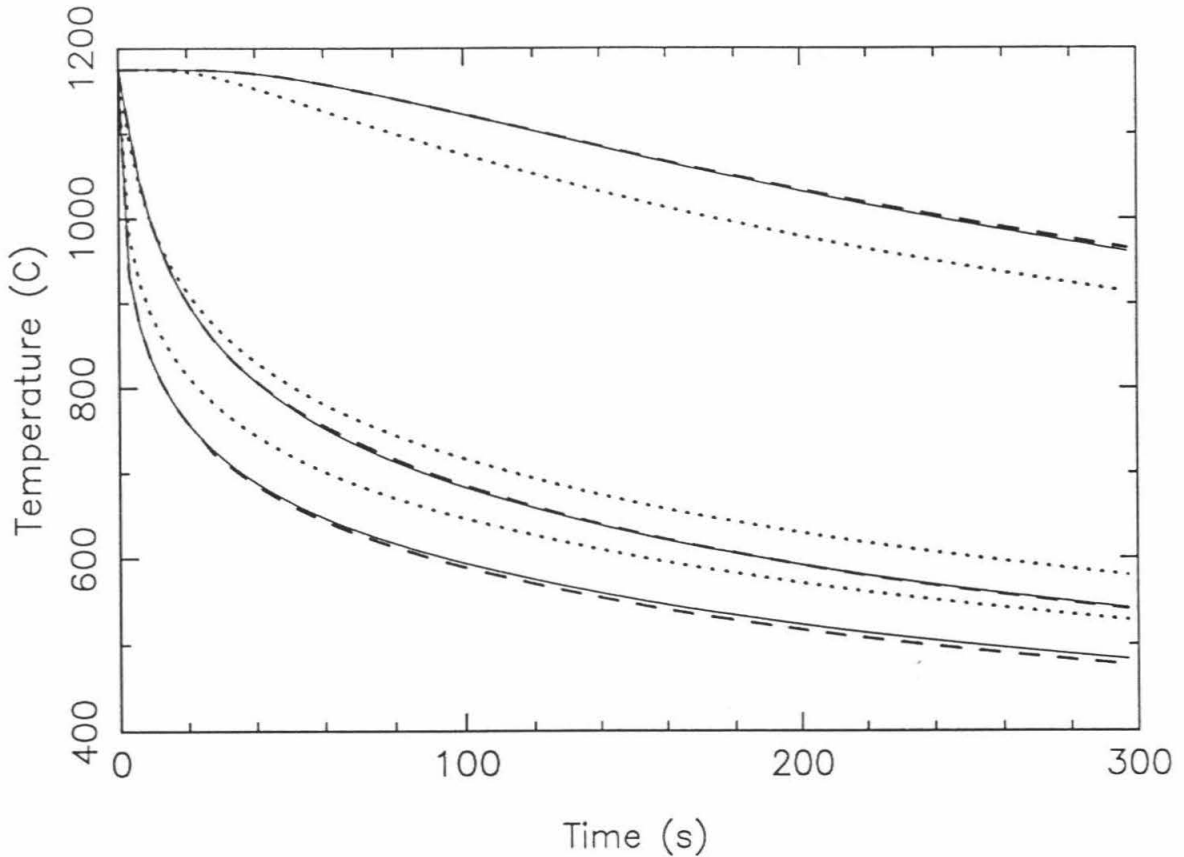


**Figure B-4: Comparison of model runs with different expressions for thermal conductivity.** Cooling curves are plotted for the surface and for depths of 1 mm and 1 cm. The light solid lines are the results from the baseline run in Chapter 4 ( $T_0 = 1175\text{ }^\circ\text{C}$ ,  $T_a = 30\text{ }^\circ\text{C}$ ,  $\epsilon = 0.95$ ,  $\phi = 50\%$ ,  $h = 40\text{ W/m}^2\text{K}$ ). The dashed lines are for a thermal conductivity including the effect of fractures at a temperature below  $740\text{ }^\circ\text{C}$  using Fricke-Zimmerman's Formula [Horai, 1991]. Note that this is not significantly different from the baseline model. The dotted lines are for a thermal conductivity that increases with temperature [Birch and Clark, 1940]. Note that these results are significantly different from the baseline model. The higher average thermal conductivity as effectively reduced the thermal inertia in this case.

## **APPENDIX C: FIELD MEASUREMENTS OF THE RHEOLOGY OF PAHOEHOE LOBES, OCTOBER 1991, KILAUEA, HAWAI'I**

### **C.0 Abstract:**

Rheological measurements of pahoehoe lobes were conducted with a penetrometer in October 1991 on the Pu'u 'O'o-Kupaianaha Flow Field in Hawai'i. This experiment was undertaken to gain insights into both the behavior of pahoehoe flows and to gain experience in conducting field experiments on lava flows. The field data suggest that (1) these Hawaiian pahoehoe flows were driven by a hydrostatic head of several meters, (2) the strength of the chill crust is controlled by the temperature dependence of the material properties of basaltic glass, (3) the rheology of pahoehoe flow lobes contains a significant component of elastic behavior. As for field operations, conducting in situ experiments on pahoehoe flow lobes with relatively sophisticated instruments was found to be feasible. However, we demonstrated that a great deal of flexibility and simplicity need to be incorporated into the design of such experiments. In practice, we also found that our extreme cost reduction resulted in significant degradation in the reliability of the instrument.

### **C.1 Introduction:**

This chapter describes the attempt by George Powell (then an Electrical Engineering student at Utah State University) and myself to measure the rheology of pahoehoe flow lobes. The project started in May 1991 with the selection of a design for an instrument to collect field measurements of the rheology of pahoehoe flow lobes. Fabrication and simultaneous testing of the instrument was begun in August 1991. It was shipped to Hawai'i, with spares and support gear, in late September with the project on schedule and under its \$1K budget. Data were collected over the first three weeks of October from the active flows on the Pu'u 'O'o - Kupaianaha Flow Field.

I felt that even the experience of attempting to operate instrumentation in close proximity to active lava flows would be worth the effort, time, and money, despite the obvious lack of development of the instrument. To our pleasant surprise, the instrument returned a significant volume of usable data which appears to show some of the complex temperature dependent rheology of pahoehoe flows.

### C.1.1 Previous Work

Previous attempts to measure the rheology of lava flows can be divided into three categories: (1) laboratory measurements, (2) "remote sensing" observations of moving or frozen flows, and (3) *in situ* field measurements.

Early laboratory measurements of magma rheology had difficulties when working below the liquidus. However, these works did show important systematics with temperature and composition [Bottinga and Wiell, 1972; Shaw, 1969; Shaw, 1972; Murase and McBirney, 1973]. More recently, experiments have been made to examine the non-Newtonian nature of the sub-liquidus melts [McBirney and Murase, 1984; Ryerson *et al.*, 1988; Webb and Dingwell, 1990]. These measurements have been supported by purely theoretical calculations such as Pinkerton and Stevenson [1992]. These experiments show that crystal and vesicle free basaltic melts are nearly Newtonian at moderate strain rates. It is not clear how best to characterize the non-Newtonian behavior of lava, but pseudoplastic and Bingham plastic models are usually invoked. For tholeiitic basalts at about 1100 °C (*i.e.*, typical Hawaiian flows) values of  $10^2$ - $10^4$  Pa for yield strength and  $10^2$ - $10^3$  Pa s for viscosity are predicted [Shaw, 1972; Pinkerton and Stevenson, 1992].

The "remote sensing" techniques combine observations of the motion and/or final dimensions of a lava flow with an assumed rheological model for the lava to estimate values for the bulk rheologic properties of the lava flow. The most common rheological model is the Bingham plastic model which was described in Chapter 2 of this thesis. The most basic version of this model is derived from the observation that the slope on which

flows stop is directly proportional to the silica content [Hulme, 1974]. Hulme [1974] proposed that a yield strength, which increases with silica content, was responsible for this. Further refinements of this technique have used the ratio of the height and width of a flow lobe or the size of levees on channelized flows to calculate yield strength [Moore *et al.*, 1978; Schaber, 1978]. Hulme's relationship between yield strength and SiO<sub>2</sub> content has been used extensively to infer the composition of flows on Mars [Zimbelman, 1985; Cattermole, 1987; Fink and Zimbelman, 1988]. To determine viscosity, it is necessary to measure the speed of advance of an active lava flow [Heslop *et al.*, 1989; Fink and Zimbelman, 1986]. Values obtained via these "remote sensing" techniques for Hawaiian basalts range from 300 to 50,000 Pa for yield strength and from 85 Pa s to  $7 \times 10^6$  Pa s for viscosity. 'A'a flows make up the high end of the range for both yield strength and viscosity. These techniques have not been successfully applied to small pahoehoe lobes in part because small flow lobes do not simply flow downhill (flow lobes have been observed climbing over topographic obstacles). This is a manifestation of the fact that pahoehoe lobes advance with a significant hydrostatic head behind them. And, as was pointed out in Keszthelyi and Pieri [1993], the simple Bingham plastic flow model cannot be applied to inflating pahoehoe flows.

*In situ* field measurements have been the most difficult to carry out. There is only one published paper that deals primarily with this subject [Pinkerton and Sparks, 1978]. Elsewhere, data from field instruments only appear as footnotes corroborating other techniques of deriving the flow rheology [*e.g.*, Dawson *et al.*, 1990]. Despite this dearth of publications, I am aware of programs using field viscometers at the University of Lancaster, University of Catania, and at the University of Hawaii at Manoa. It has been found that rotating vane viscometers are the most effective devices for measuring the viscosity of the lava inside a flow while penetrometer designs are more suited to the study of the properties of the outer crust.

## C.2 Instrument design

### C.2.0 Introduction

In this study, we decided to concentrate on the properties of the outer rind of chilled lava on pahoehoe flows because I hypothesized that it is this rind that controls the growth of pahoehoe toes. We therefore selected the penetrometer design over the more conventional rotating vane viscometer. Other more radical designs were rejected due to time and budgetary constraints.

The operating principle of a penetrometer is to measure the force required to push a rod, at a certain speed, to a given depth. This allows stress-strain and stress-strain rate diagrams to be constructed and rheological parameters to be determined. Our penetrometer basically consisted of a rod that moved inside a stationary cylinder. This design introduces forces in addition to those provided by the lava and the operator (Fig. C-1). These forces include friction between the inner rod and outer pipe and the force of gravity on the inner rod. These additional forces depend on the angle at which the device is held. There also needs to be a correction made for the acceleration of the inner rod. In order to sort out these forces, three instruments were placed on the penetrometer: a load cell to measure total force, a pair of linear potentiometers to measure the position of the inner rod with respect to the outer cylinder, and an inclinometer to measure dip (Fig. C-2).

### C.2.1 Structure

The design of the structural elements was strongly constrained by the available technical expertise as well as funds. It was not feasible to use custom machined parts. Thus the penetrometer was built exclusively from components obtained from plumbing stores and commercial electronics shops. This produced a design that was extremely cheap, modular, and easy to modify.

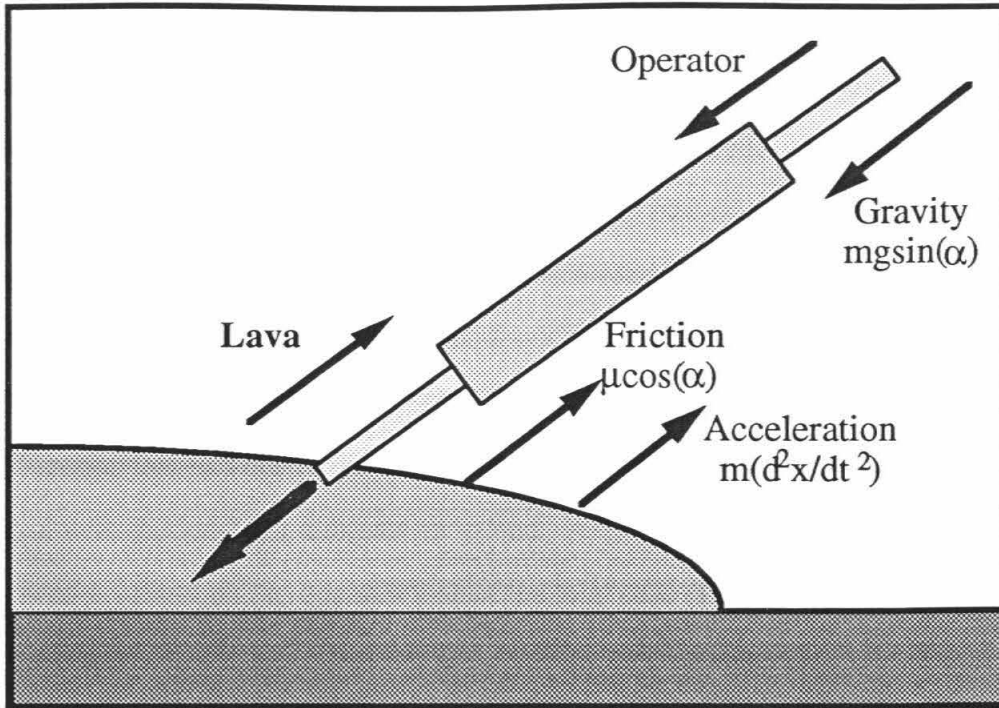


Figure C-1: Balance of Forces on Penetrometer. Both the operator and gravity push the inner rod into the lava. Friction between the pipes and acceleration can act in either direction. The crust on the flow lobe and viscous forces in the melt resist the forward motion of the inner rod.

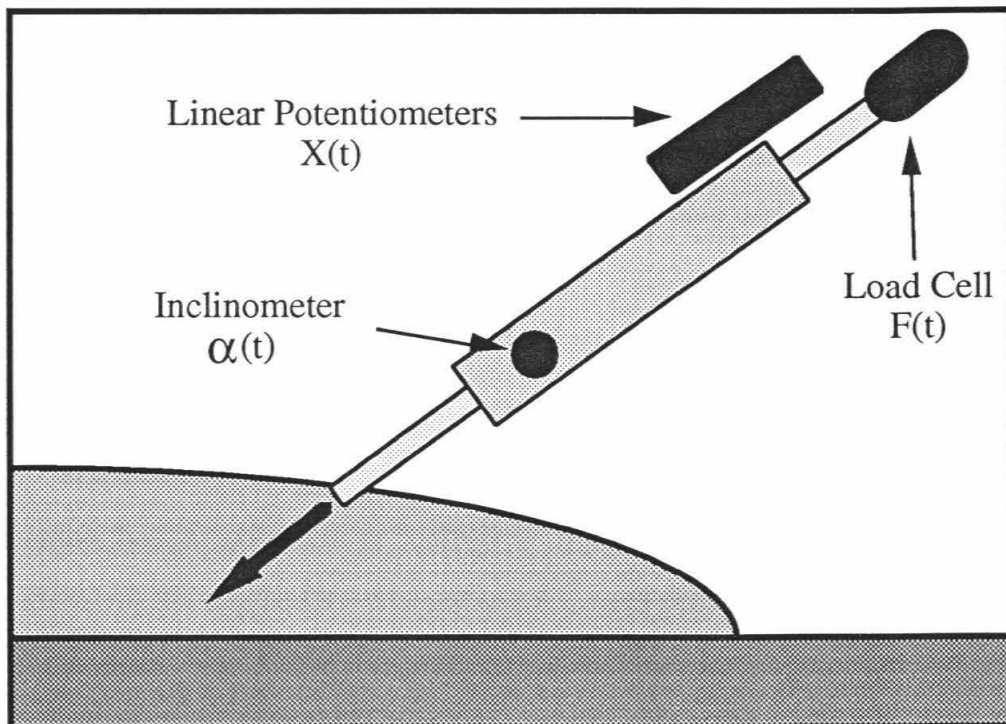


Figure C-2: Instruments on the Lava Lance: Three instruments were installed on the Lava Lance penetrometer. A ring load cell was used to measure force, a pair of linear potentiometers for position, and an inclinometer to determine the angle.

The inner rod consisted of sections of 1/4 inch (inner diameter) stainless steel water pipe connected with standard couplings. The front (*i.e.*, lava) end of the piping was sealed with a cap which had a hexagonal face with a surface area of  $\sim 4 \text{ cm}^2$ . The forward most section of the rod was a 12" pipe which was the only part of the instrument that was to be immersed in lava. This section was considered expendable should it somehow become damaged by the lava. It was followed by a 36" section and then several short (2"-6") pieces of pipe which were used to adjust the length of the inner rod. This was followed by a 12" section that had one of the linear potentiometers mounted to it and finally another 12" section with the load cell mounted to its end. A handle, made from a cut down sprinkler key, was mounted on the operator end of the load cell. This handle was used to push on the inner rod.

The outer pipe was built from 3/4" water pipe. It consisted of one 12" and one 24" section connected by a cross. The 12" section was mounted closer to the lava and had 21 holes drilled into it to allow the inner rod to cool radiatively even while it was retracted inside the outer pipe. The inclinometer was housed inside one of the unused arms of the cross.

Initially, a tripod and heat shields were included on the penetrometer. The initial field deployment showed these to be detrimental and they were immediately eliminated from the design.

### C.2.2 Instruments

The instrument selection was extremely constrained by the budget. All instruments were either bought as surplus or "borrowed" from other projects. Our connections with The Planetary Society and the Mars SNAKE project proved to be invaluable in holding down the costs. The SNAKE is an instrumented, metal-clad guiderope which is to be dragged along the surface behind the French built Mars Balloon as part of what was then the Soviet Mars 96 mission.

The load cell was originally built in 1990 by the Utah State University Space Dynamics Laboratory for use within the Engineering Test Model of the SNAKE. The load cell was of a ring design with 4 strain gages. Associated power control and amplification chips were located on a board mounted onto the load cell. Calibration was done with commercial fish scales. Calibration curves (Fig. C-3) obtained shortly before shipment to Hawai'i were linear and reproducible. However, the instrument did occasionally suffer from short circuits, so a small dial voltmeter was added in order to allow the operator to confirm that the load cell was operating properly before approaching the lava flow.

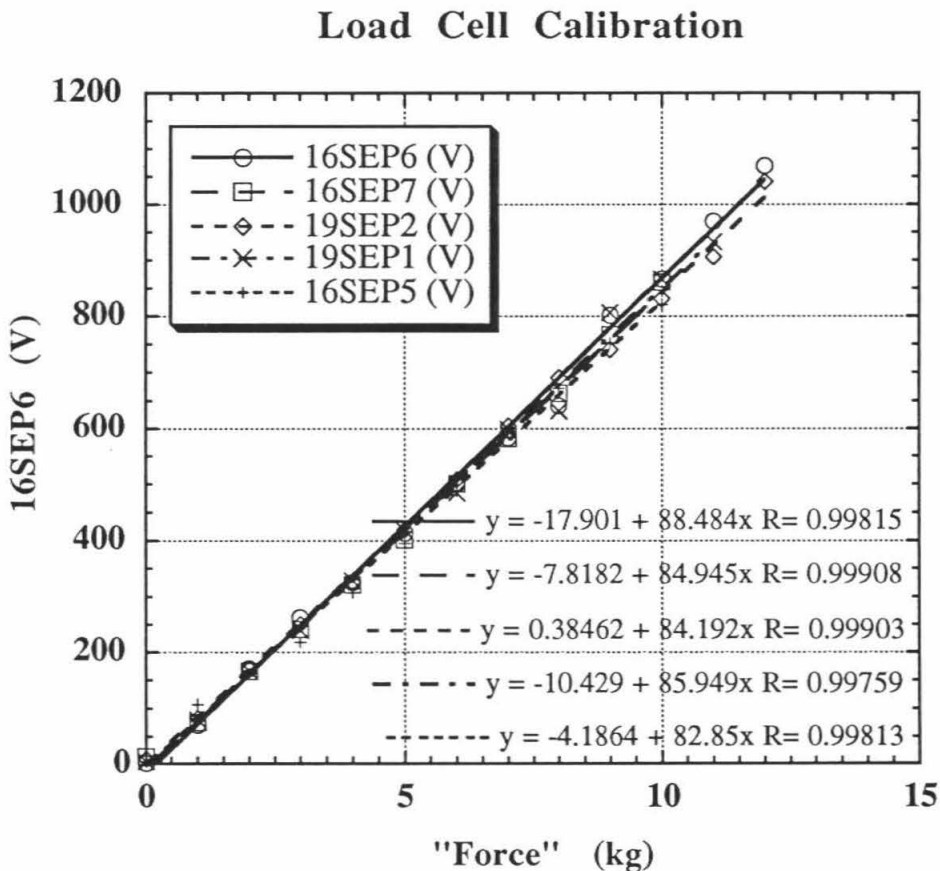


**Figure C-3: Calibration curves for the load cell.** Data from calibration runs done by pulling on the load cell with a fish scale. It is believed that the errors in the fish scale were larger than the errors in the load cell. We estimate the errors in the load cell to be less than 1%.

The linear potentiometers were bought from C&H Surplus in Pasadena and each had a usable throw of about 10 cm. It was necessary to use two of these linear potentiometers, connected end to end, to allow the inner rod to move the desired 20 cm. Calibrations showed that when connected in series, the response of the instrument was not linear. The calibration curves actually consist of several line segments but are modeled sufficiently accurately by a parabola (Fig. C-4). The linear potentiometers and the load cell were provided protection from impacts and rain by aluminum electronic boxes.

### Linear Potentiometer Calibrations

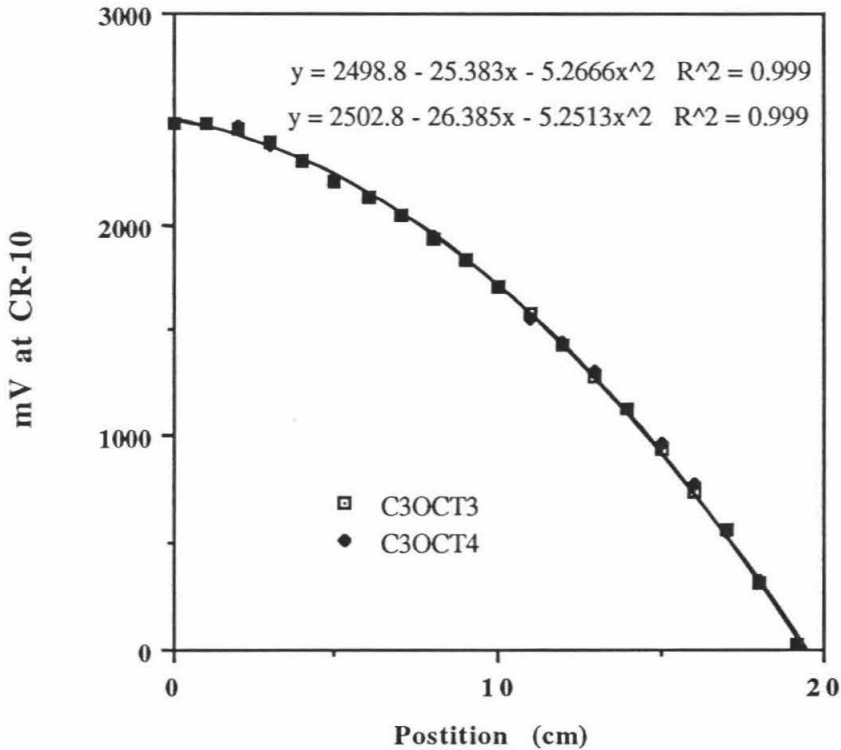


**Figure C-4: Calibration curves for linear potentiometers.** Plot shows voltage recorded at the CR-10 data logger after the current passed through the variable resistance of the linear potentiometers. Most of the non-linearity of the calibration curve is caused by the mechanical connection between the two linear potentiometers. Errors are estimated to be  $\pm 3$  mm with the largest errors at small displacements.

The inclinometer was a last minute addition after it was decided that video documentation would not provide reliable data on the angle at which the penetrometer was held. It consisted of a pendulum (a butterknife) and a rotating potentiometer. Calibrations were not as steady as would have been desired, but the instrument was deemed adequate over the range of angles it was required to operate over (Fig. C-5).

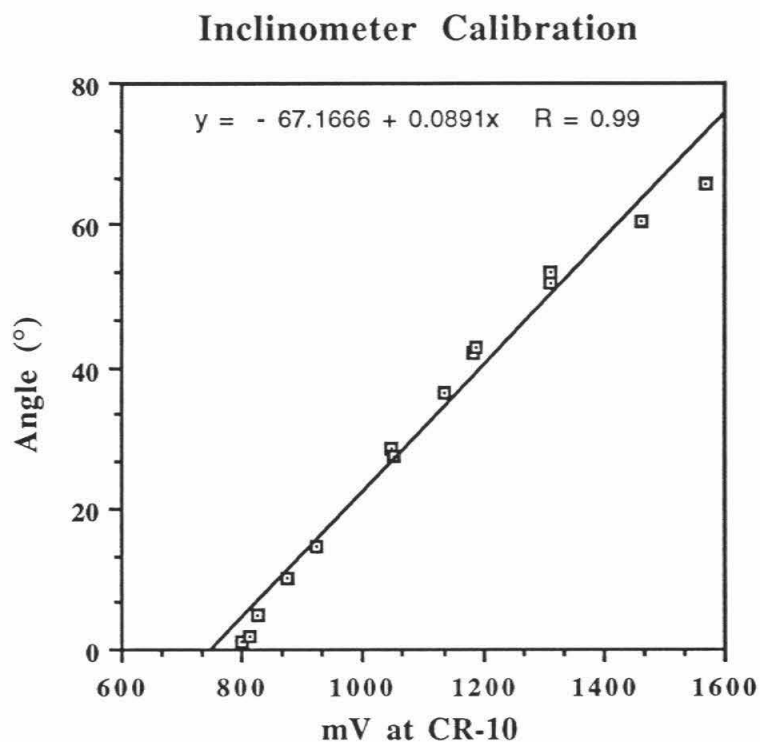


**Figure C-5: Calibration curve for the inclinometer.** Combined data from two calibration runs conducted on October 8, 1991. Note that the October 4 data used a less satisfactory inclinometer and thus the data from that day is marginally poorer than those from October 10 and 11. Also note that, though the rotating potentiometer did not have a perfectly linear response, a linear fit appears adequate over the range of 30-60°, where the penetrometer was operated, especially since errors of  $\pm 5^\circ$  were deemed acceptable.

In an attempt to collect temperatures to correlate with the rheological data, a Chromel-Alumel (K-type) thermocouple was inserted into the inner rod and jammed against the end cap. It was found that the response time from this location was far longer than the time of the rheological measurement. A hole was drilled in the end of the cap and the thermocouple was exposed to the lava in an attempt to bring down the response time. Unfortunately we discovered that the thermocouple junction was not able to withstand the severe mechanical and chemical environment at the front of the penetrometer. No useful temperature data were collected.

### C.2.3 Instrument Mounts

Most of the technical difficulties in constructing the penetrometer were in devising mounts for the instruments which were selected primarily based on cost considerations.

The lava end of the load cell was epoxied into its 12" section of 1/4" pipe. It was necessary to mill out the inside of this pipe in order to allow the load cell to be inserted. This increased diameter went down only as far as the load cell was to be inserted, providing a strong mechanical connection between the load cell and the inner rod while it was being forced into the lava. The epoxy was strong enough to hold during retraction from the lava. The handle was milled down until it fit inside the operator end of the load cell. It was held in place by a set screw.

One linear potentiometer was attached to the outer pipe and the other linear potentiometer was attached to the inner rod. The first linear potentiometer was held in place with three hose clamps. The attachment to the 1/4" inner pipe was more difficult. A tee was attached to either end of the 12" piece that the linear potentiometer was to be mounted to. 1/4" to 1/2" expanders were used as bolts to attach the electronics box housing the linear potentiometer to the tees.

#### C.2.4 Power Systems

Compared to the structure, the power systems were quite elegant. The load cell required a +12V, +5V and a -12V source. The linear potentiometers and the inclinometer were put across the +5V source. Switches were provided to allow each of the instruments and the load cell voltmeter to be powered independently. The wiring had to be modified repeatedly in the field in order to remove ground loops. The result is that there is no documentation of the final, operational, circuitry.

Power was provided by a pair of 12V NiCd 12 Ahr rechargeable batteries. These were large enough that they were never recharged in the 3 weeks of operations in Hawai'i. The batteries were connected into a power box which contained fuses and voltage dividers and the central power switch.  $\pm 12, +5V$ , and ground connections were available from the power box. A surplus 12V power source was used during tests where 120V AC power was available.

#### C.2.5 Data Collection

Data were collected with USU's Campbell Scientific CR-10 datalogger. The voltage from each instrument and the battery were recorded at 16 Hz. One design constraint on the instrumentation was the 0V - 2.5V range acceptable to the datalogger input ports. A push-button switch (data trigger) was mounted onto the penetrometer's handle to engage the data collection. The data was then transferred, in the field, in ASCII format, to a Toshiba laptop computer via Campbell's EDLOG software.

#### C.2.6 Total System

The instrument had a total length of about 2 m and a mass of about 8 kg. It could be broken down for transport so that no piece exceeded 1m in length. The power system and data logger fit in a small backpack and had a mass of 5 kg. A tool kit was assembled to

allow modifications and repairs to be conducted in the field. All instruments and key structural elements had spares.

### **C.3 Field procedure**

#### **C.3.1 Standard Operating Procedure**

A major objective of our design was to provide an instrument that was simple to operate in the field. Field operations would start by loading the instrument, data logger, power supply, laptop computer, tool box, and video camera along with the normal field attire and thermal protection into the rental vehicle. The drive from the summit of Kilauea to the end of the road near the ruins of the Wahaula Visitor Center would take less than an hour. The gear was then man-ported into the field. It would usually take approximately one hour to locate and approach the active pahoehoe flows.

A "base camp" would be set up as close to the activity as was deemed prudent. We attempted to find an area that was not likely to be approached by lava for at least a few hours, where the surface temperature was below about 100°C, was upwind from the heat sources, was flat enough to lay out the electronics, and was high enough to observe the lava. A silvered car windshield sunshade and a straw mat provided a relatively soft, clean, and cool surface to work on. The instrument, data logger, and power supply were connected and checked out at this location (see Fig. C-6). The data logger would also be programmed from the laptop at this time. The instrument would be powered up and the data logger and power system were placed in a shoulder bag or small backpack before leaving the base camp.

The data collection was done by a single person. The operator would approach the target flow lobe and set up for the measurement. This was done by fully retracting the inner tube with the right hand while holding the outer pipe, near the center of gravity, with the left. It was found that one could brace the left elbow against the hip, providing an acceptably stable platform during the measurement. The entire device would be moved

forward until it was just barely in contact with the lava. Then the inner rod would be rammed into the lava while the thumb of the right hand depressed the data collection trigger. The rod would then be pulled back, with data still being collected. The operator would then release the data collection switch and take several steps away from the lava. The entire procedure rarely exceeded 5 seconds.

In most cases loose fitting clothes (Desert BDU's) and work gloves provided sufficient protection for this quick work. In some cases it was necessary to use a face shield which we fabricated from a plastic Halloween mask with aluminum foil glued to its exterior. This device's only shortcoming was inadequate protection of the ears.

Typically, what would happen during a penetration is that the operator would push harder and harder until the crust started to move perceptibly. This initial motion was



**Figure C-6: Photograph of Lava Lance in the field.** The data logger and power systems are in the small backpack and the laptop and repair kit are in the large backpack.

in the form of bending the outer black chill crust inward. The operator would continue to push hard until the crust suddenly gave way. At this point, the inner rod would race forward, hitting its mechanical stops at full (20 cm) extension. A few attempts were made to gather data from the incandescent portion of lobes, before any significant crust could form. This was only possible in small (about 10 cm wide) channels. It was found that, in the absence of a crust, the forces attributable to the lava were in the noise level.

When the crust failed, it was common for a small piece, roughly 1.5 times the diameter of the inner rod, to be pushed into the lava. This produced a variable surface area over which the measured force was applied to the interior of the lobe. We were not able to properly quantify this surface area. In a few exceptional cases, a large (+10 cm) piece of the crust would simply fold itself around the advancing rod. When the crust became very hard and brittle, the penetrometer would punch neat holes barely larger than its own diameter.

Each penetration would leave a scar on the surface of the lobe after retraction. This allowed us to follow that section of the crust as the lobe continued to inflate. In order to study the hardening of the crust, data were collected from the same general area (within a 15 cm diameter) at about 30 second intervals. On occasion some lava would remain on the end of the inner rod after extraction. This was easily removed with a hammer, but did make it difficult to maintain the 30 second turn around time.

It was discovered that it was usually not (humanly) possible to penetrate the crust after about 2-3 minutes. The heat and physical exertion would render the operator useless after about half an hour (once tired, the operator would not be able to provide a sufficiently stable platform for the measurement). After the flow or the operator petered out, the instrument would be taken back to the base camp. The data would be downloaded to the laptop and systems would be powered down to conserve battery power. After a few such cycles the base camp would be packed up and the return trip would begin.

### C.3.2 Log of actual operations

31 SEP Depart Pasadena, arrive Hilo.

01 OCT Re-assemble penetrometer, run calibrations

02 OCT First field measurements. Tripod and heat shields removed in the field. No usable data.

03 OCT Modified penetrometer to reduce mass, added an inclinometer, increased the data acquisition rate from 4 Hz to 16 Hz.

04 OCT Second set of field measurements. Discovered the need for a face shield. Inclinometer design found to be inadequate.

06-07 OCT Conducted a different experiment.

08 OCT Purchased parts for and fabricated the face shield and improved inclinometer.

10 OCT Third set of field measurements. Very successful.

11 OCT Fourth set of field measurements. Quite successful.

12-14 OCT Conducted a different experiment.

15 OCT Fifth set of field measurements. No active lava, no data collected.

## **C.4 Data**

### C.4.1 Format

Incompatible formats between the different computer systems produced the largest difficulty in data reduction. To maximize the data rate, the CR-10 datalogger was programmed to store data in a continuous stream as long as the data trigger was depressed. This data stream was transferred and stored on the Toshiba laptop computer in ASCII format in 8 columns. These files have a "+" in front of positive values. Before becoming readable in VAX FORTRAN, the data had to be placed in 5 column rows and the "+" signs removed.

The files were named using a standardized format we had developed for the SNAKE. The filename had the format

XDDMMMLR

where X is a letter where C denotes calibration run and D denotes data run. DD are the two digits for the day of the month, MMM are three letters for the month, L is a number designating the lobe being measured, and R is a letter that increments with each penetration into the lobe.

#### C.4.2 Quality Check

Before processing, the raw data from each penetration were examined. As mentioned earlier, we encountered some nagging problems with our low cost instrumentation. The most common difficulty was an intermittent short in the load cell. This would manifest itself as surges in voltage which saturated the datalogger's A/D converter. The second most common problem was various forms of operator error. These were recorded in a notebook at the time of occurrence and include having one's thumb slip off of the trigger, bad footing, finding the lava too hot, and forgetting to turn on power to all the instruments. In all, 108 penetrations returned data, but only 67 were considered satisfactory after the quality checks. Table C-1 breaks this down in a little more detail.

**Table C-1: Results of quality check of raw data.**

<u>DATE</u>	<u>TOTAL RUNS</u>	<u>OK RUNS</u>	<u>LOAD CELL PROBLEMS</u>
04OCT91	31	14 (45%)	9 (29%)
10OCT91	21	19 (90%)	2 (10%)
11OCT91	56	34 (64%)	14 (25%)
TOTAL	108	67 (62%)	25 (23%)

Note that the majority of the unsatisfactory runs (penetrations) were caused by problems with the load cell.

The situation is actually worse than the above table suggests. The information we ultimately wish to extract from this experiment is how the strength of the crust changes with time. Lobes with only one or two successful penetrations are therefore worthless. In the end, only 7 lobes, with a total of 28 penetrations, provided enough usable data to be worth complete analysis.

### C.4.3 Processing Algorithm

The reduction of the data went through two basic steps: conversion of voltages to physical quantities and then extraction of the force exerted by the lava. The first part was very straightforward since the calibration curves were all first or second-order polynomials. The only complication was that the pendulum on the inclinometer had a tendency to oscillate. Since the instrument was held at a fixed angle, I have simply averaged over several cycles of the oscillation to obtain a single value for the inclination. Figure C-7 shows typical plots of the output from each of the instruments.

As was briefly described in the introduction, the force measured at the load cell is the sum of several effects. The operator and gravity pushed the rod downward while friction and the lava pushed upward. There was also a small force required to provide the initial acceleration of the rod. These effects are trivial to calculate given just the mass, velocity, and coefficient of friction for the moving rod. The mass was measured with the load cell by simply suspending the rod by its handle. Velocity was obtained by dividing the distance traveled between two data points by the acquisition rate of the datalogger (16 Hz). The coefficient of friction was measured in calibration runs done by sliding the inner rod back and forth inside the outer pipe while the instrument lay on a desk.

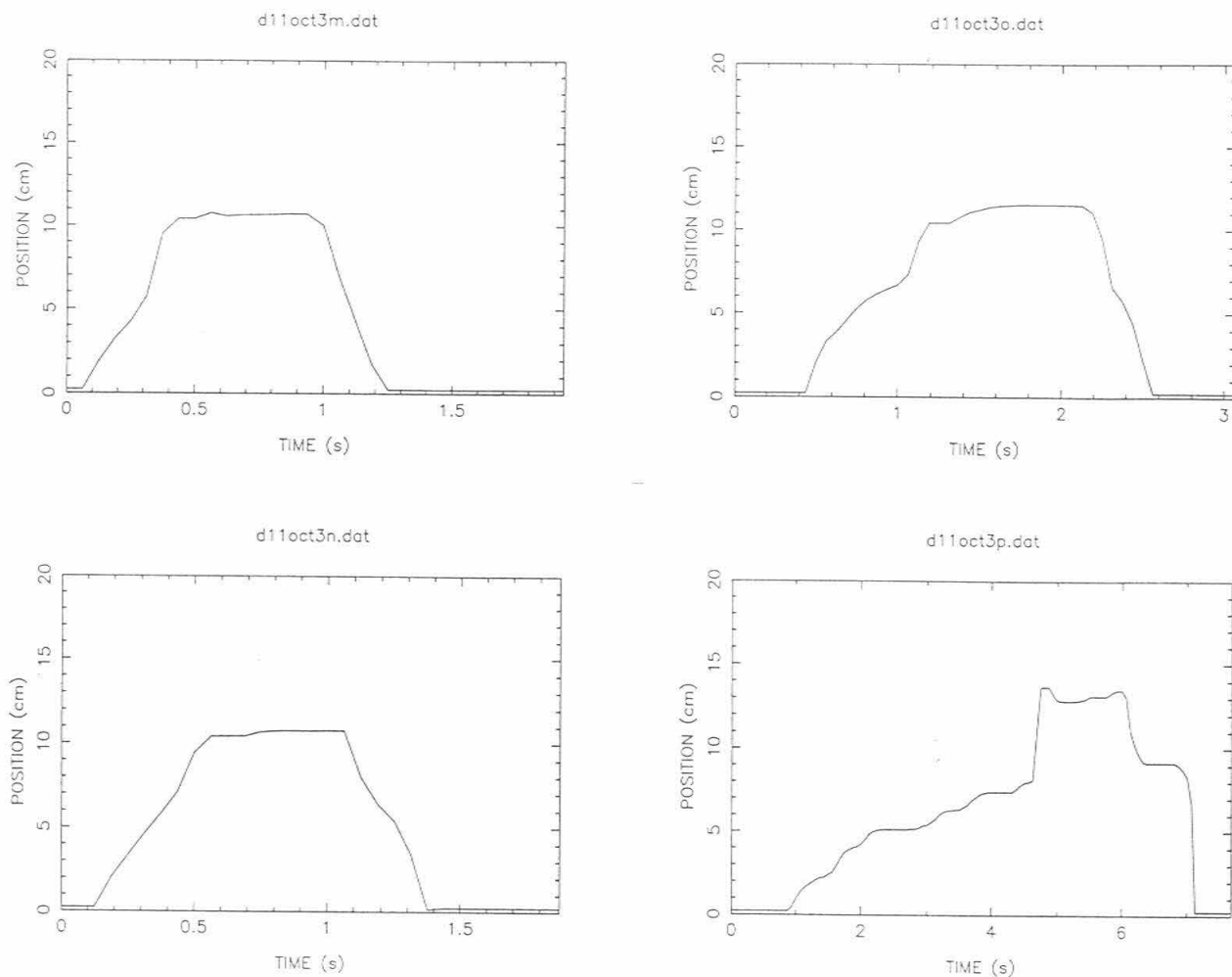


**Figure C-7a: Typical position vs. time data from Lava Lance.** Data are from the last lobe from which data was successfully returned. d11oct3m was the first penetration of the lobe, d11oct3n started 30 seconds later, d11oct3o 58 seconds after the first penetration, and d11oct3p 90 seconds after. C-7a shows the position versus time. Note how initially the penetrometer does not advance even though force is being applied and that total penetration is less than the 20 cm that the instrument is capable of. This lobe was initially only about 10 cm thick, but became over 15 cm thick by the last penetration. Also note that an attempt was made to hold a relatively constant velocity.

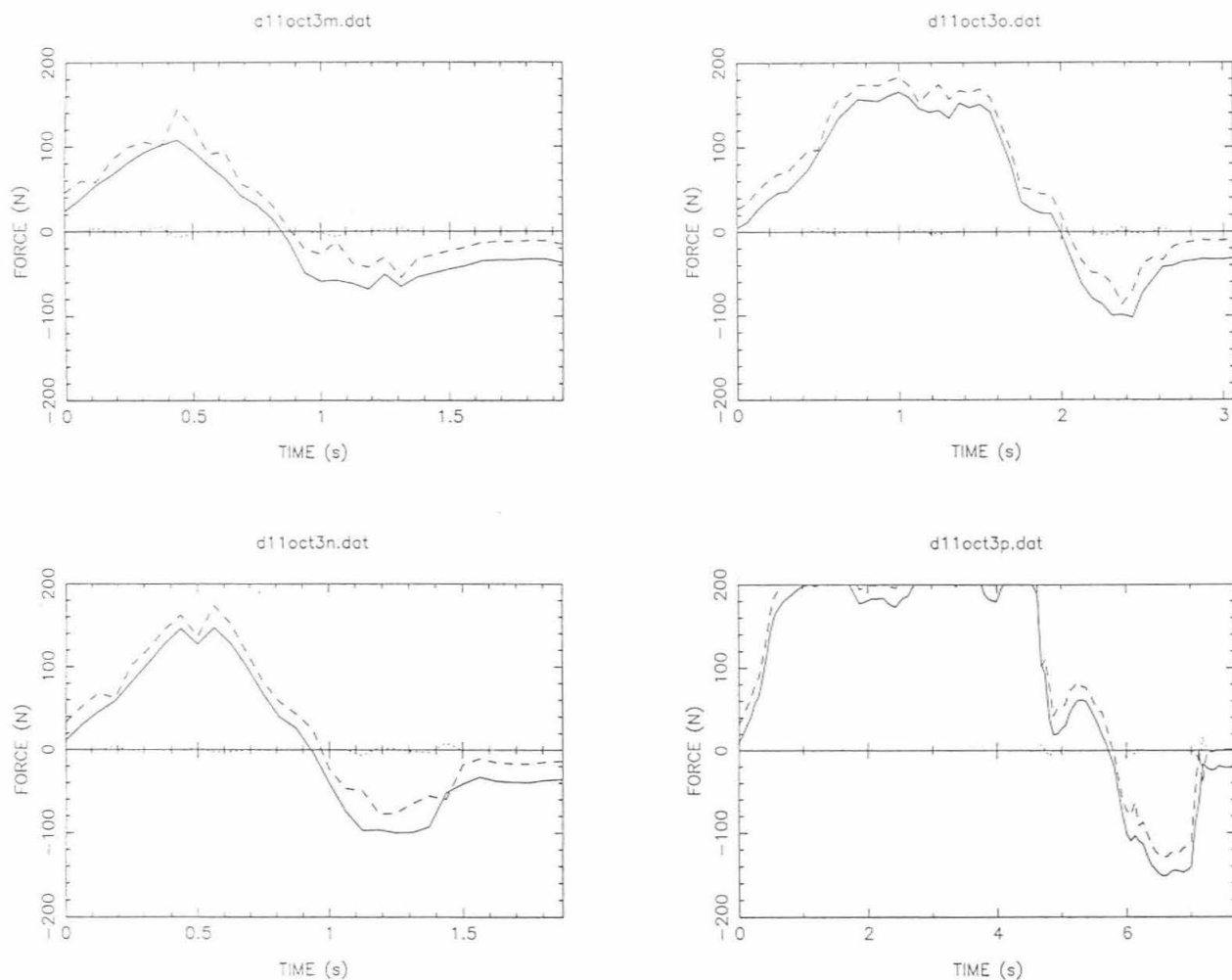


**Figure C-7b: Typical force vs. time data from Lava Lance.** The solid line is the force measured by the load cell and the dashed line is the residual force that was exerted on the lava after removing the effect of friction, gravity, and acceleration. The force at which the penetrometer begins to advance is taken as the yield or failure strength of the crust (compare figures C-7a and C-7b). Also note that repeated efforts were needed to push the rod in on the last attempt (d11oct3p).

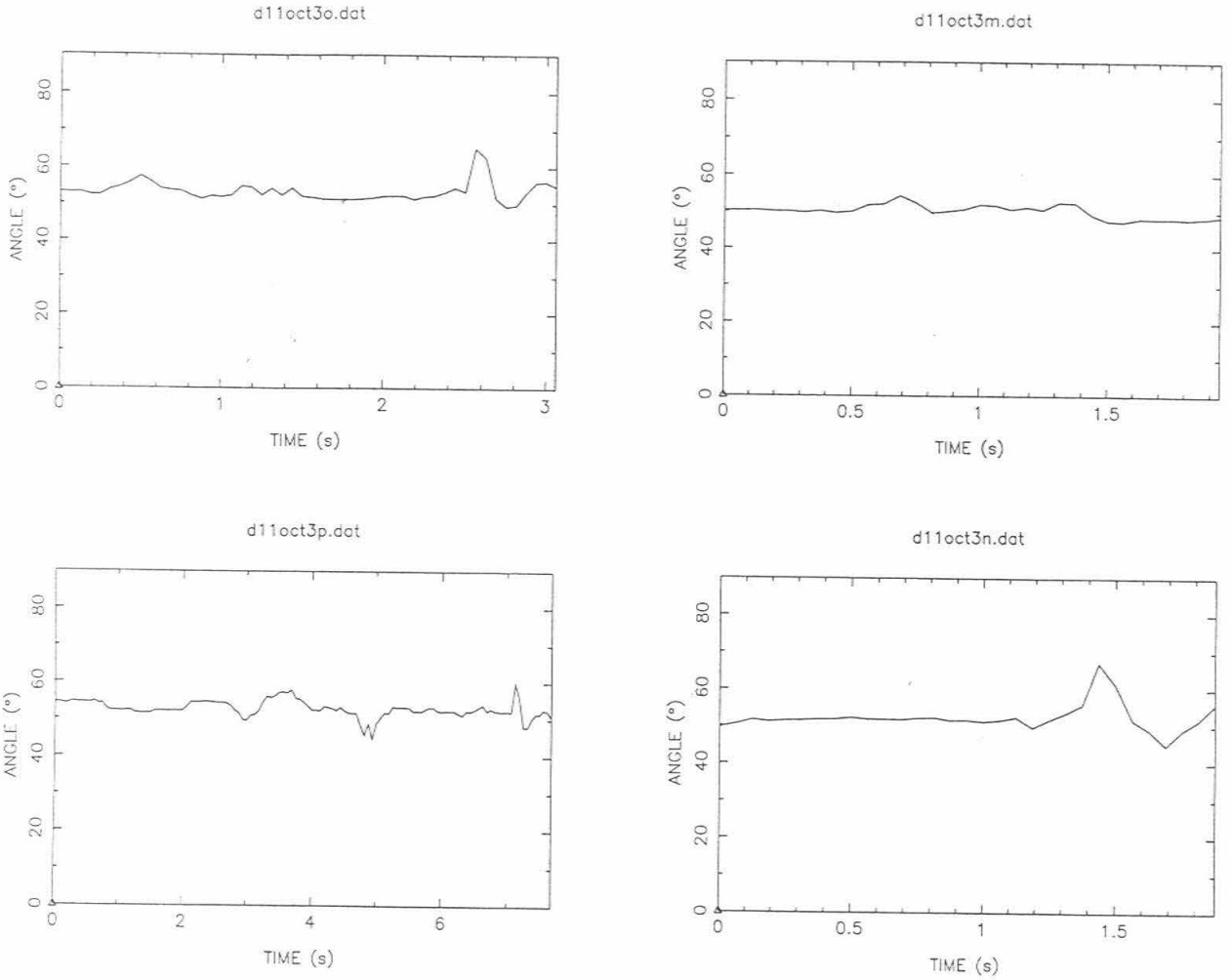


**Figure C-7c: Typical angle vs. time data from Lava Lance.** Note that the pendulum oscillates some, especially after retraction. This is overcome by using the mean value.

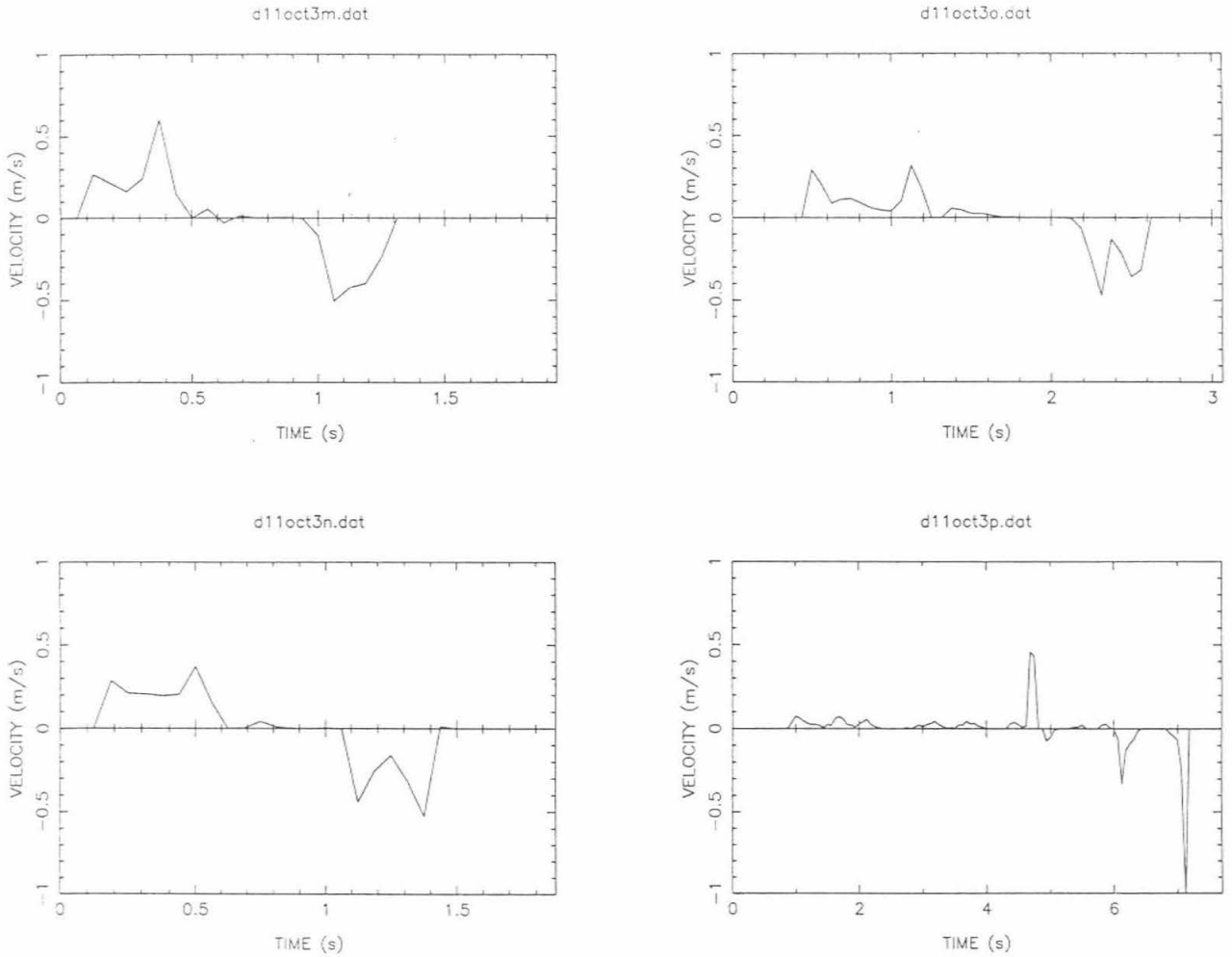


**Figure C-7d: Velocity of the inner rod vs. time data from Lava Lance.** The curves are quite noisy due to the 16 Hz data rate. Note how the velocities decrease as the lobe ages and the crust hardens.

## C.5 Interpretation

### C.5.0 Conceptual Model

Based on many hours of observation, I believe that small pahoehoe flow lobes behave much as Iverson [1990] modeled the growth of the Mount St. Helens lava dome. His model is very descriptively entitled "Lava Domes Modeled as Brittle Shells that Enclose Pressurized Magma." Mathematically, his model is identical to one that describes drop-shaped storage tanks (*e.g.*, fuel bladders) [Flügge, 1967]. In this model the shape and size of the dome are completely controlled by just 4 parameters: (1) the tensile strength of the brittle shell material, (2) the shell thickness, (3) the pressure head of the confined liquid, and (4) the density of the liquid. The first two parameters can both be described by the tensile strength of the entire crust.

### C.5.1 Strength of the Crust

The rheological parameter most easily extracted from the processed Lava Lance data is a form of yield strength for the crust of the flow lobes. This yield strength is the stress that needed to initiate forward motion of the penetrometer. This yield strength is not precisely the yield strength (in the Bingham sense) that resists the forward motion of the lava. The flow lobe grows by stretching the chill crust while the penetrometer advances by first bending, then tearing, the crust around its flat tip. The penetrometer must also overcome the hydrostatic pressure pushing against the inside of the crust. Furthermore, smaller lobes may be stronger in compression than dilatation because of the cylindrical geometry of the crust. Thus the strength that was measured is only related in some indirect fashion to the yield strength that controls the advance of flow lobes. Despite these caveats, the measured strength is at least an upper bound on the yield strength of interest. Also, since both strengths should primarily depend on the thickness and temperature of the crust, it seems very reasonable to suppose that the two quantities are directly proportional.

Figure C-8 shows the hardening of a single, typical, lobe. This failure stress is calculated from the force applied to the penetrometer that corresponds to the first non-zero velocity of the inner rod. Figure C-9 shows the entire usable data set from the 28 penetrations of 7 different lobes. One note of caution should be raised about Fig. C-9. In figure C-8 (and the six others like it for the other lobes), time is measured relative to the first penetration of that particular lobe. Thus an unknown amount of time, corresponding to the time elapsed between the initial breakout of the lobe and the first penetration, needs to be added to convert the times into the actual age of the flow lobe. In making figure C-9, these time shifts were selected to make the data group together as tightly as possible. The fact that all the data do more or less fall on the same trend suggests that this sliding of the data was perhaps appropriate.

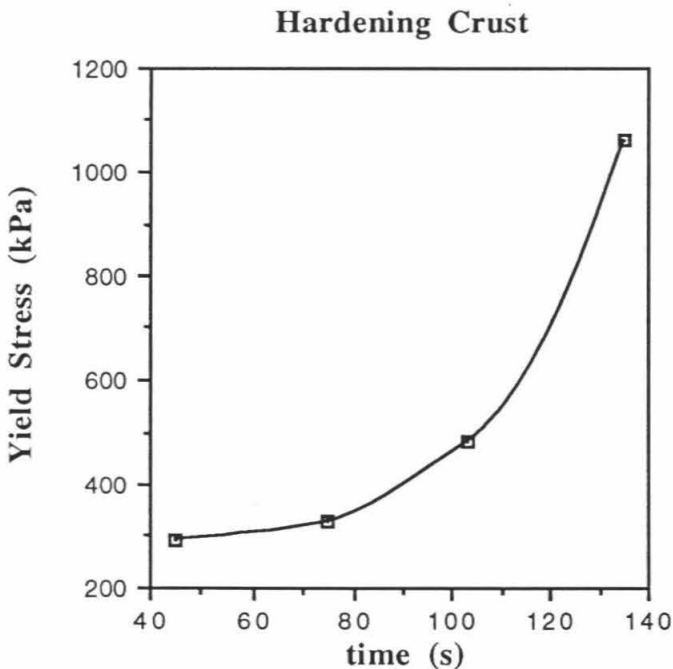


**Figure C-8: Plot of the hardening of the crust of a single lobe with time.**

These measurements were collected on the last day of successful operations (October 11, 1991) and comprise the single best data set.

Figure C-9 shows that the strength of the crust goes from about 100 kPa to over 1 MPa during the first 3-4 minutes of cooling. If we make the assumption that these strengths are indeed similar to the yield strengths of the lobes, these values can be used to estimate the hydrostatic head driving the flow. Pressures of 0.1-1 MPa correspond to the hydrostatic pressure provided by a column of lava 5-50 m high. These values are reasonable upper bounds on the hydrostatic head in the flow field, especially when one realizes that the lobes are not able to stretch the crust by the time the highest strengths were measured. This estimate for the hydrostatic head is supported by the observation that inflation features are typically 2-10 m high.

### Combined Data for Hardening of the Crust

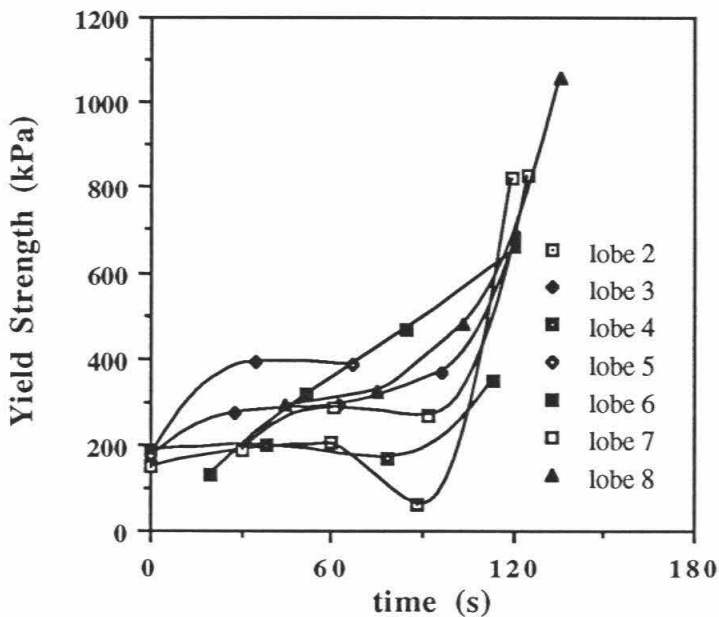


**Figure C-9: Combined data for all 7 lobes.** Lobe 2 was observed on October 4, lobes 3-6 on October 10, and lobes 7 and 8 on October 11.

### C.5.2 Growth of the Chill Crust

The form of the curve of the hardening of the crust with time in figure C-9 is also interesting. The thickness of the crust increases roughly as the square root of time [*e.g.*, Hon *et al.*, 1994a]. This can also be seen in Figure C-10 which plots the predicted growth of the crust assuming either 1070 °C or 900 °C for the glass transition temperature using the cooling model presented in Chapter 4 of this thesis. However, the strength of the crust is best fit by an exponential (Fig. C-11a) or quadratic (Fig. C-11b) equation in time. This suggests that the strength of the crust increases with time, not because it becomes thicker, but because the glass becomes stronger.

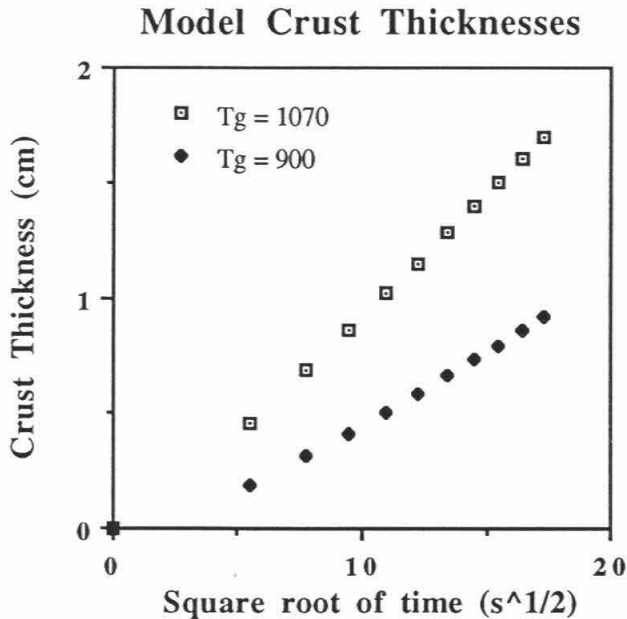


**Figure C-10: Model predictions for thickness of chill crust.** The two curves are for two different estimates of the glass transition temperature (1070 °C and 900 °C). Note that the thickness of the crust grows as the square root of time.

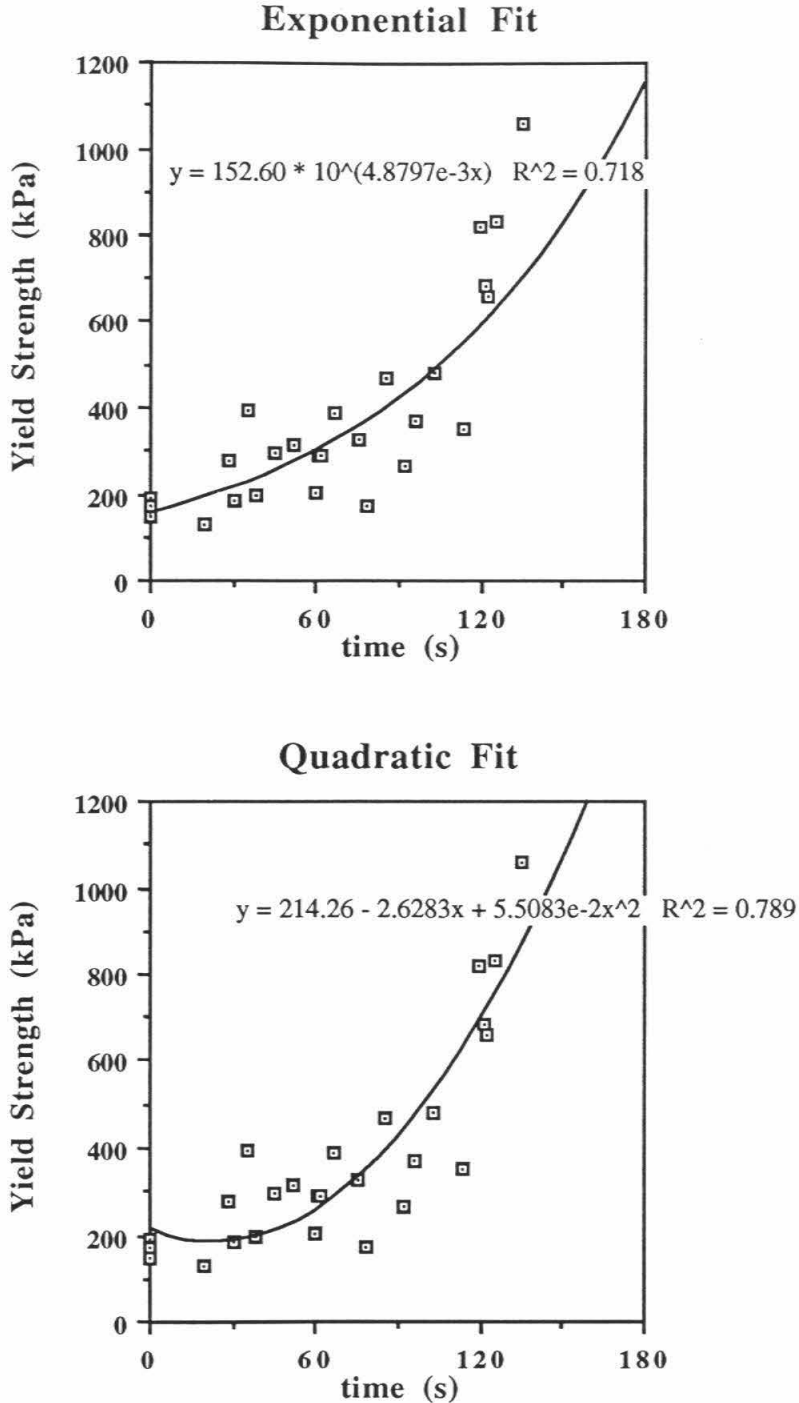


**Figure C-11: Fits to yield strength field data.** Note that the increase in strength of the crust is not a function of the square root of time. Quadratic and exponential fits provide nearly identical quality fits. The exponential fit makes more physical sense for a failure strength while a quadratic fit may be more appropriate for a bending plate model.

There is actually surprisingly little published laboratory data on the strength of basalt. Descriptions of measurement techniques are abundant [*e.g.*, Touloukian *et al.*, 1989; Carmichael, 1982; Cermak and Ryback, 1982] but actual values are not provided (at least for basalt at surface conditions). The most readily applicable published data is on the tensile strength of glass fibers of various lava compositions [Webb and Dingwell, 1990]. They find that the fibers fail at a strain rate ( $\epsilon'_{\text{fail}}$ ) that is consistently about 3 orders of magnitude below the relaxation time ( $\tau$ ) of the glass or melt. The viscosity ( $\eta$ ) of the glass is also directly proportional to the relaxation time. These observations and the Arrhenius relationship provide a way to quantify the temperature dependent tensile failure strength ( $\sigma_{\text{fail}}$ ) of basalt. This is most clearly demonstrated algebraically. From Webb and Dingwell [1990] we have that

$$\epsilon'_{\text{fail}}(T) = c_1 \tau(T) \quad (\text{C.1})$$

$$\eta(T) = c_2 \tau(T). \quad (\text{C.2})$$

But the Arrhenius relationship states that

$$\eta(T) = \eta_0 e^{(E_0/RT)} \quad (\text{C.3})$$

so that

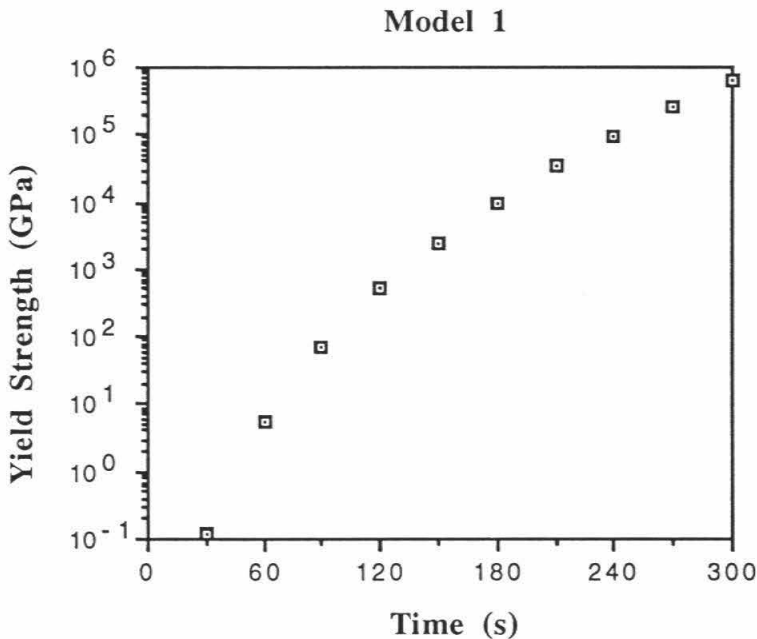
$$\tau(T) = \tau_0 e^{(E_0/RT)}. \quad (\text{C.4})$$

From the definition of viscosity,

$$\sigma_{\text{fail}}(T) = \epsilon'_{\text{fail}}(T) \eta(T) = c_1 c_2 \tau^2(T) = \sigma_0 e^{(2E_0/RT)}. \quad (\text{C.5})$$

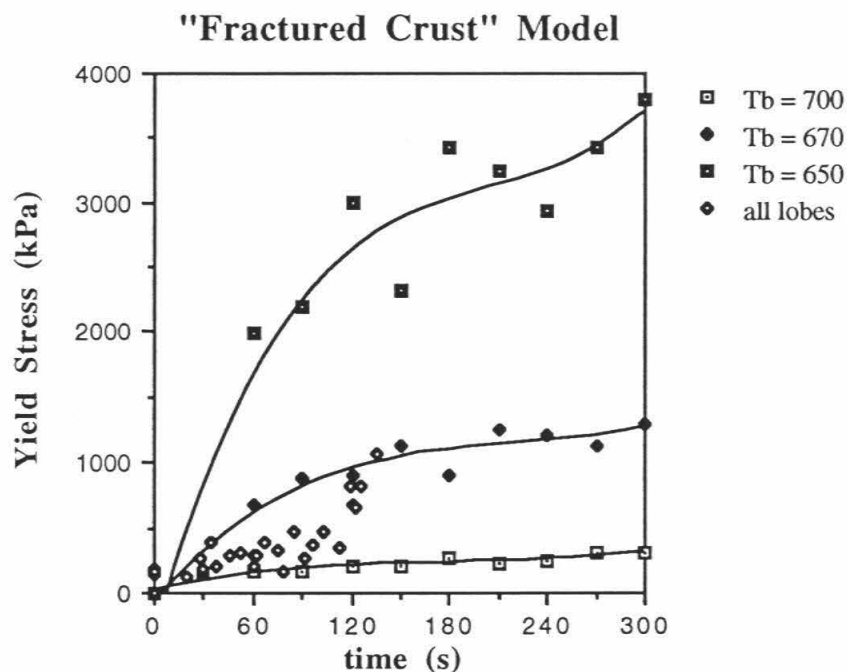
The measured activation energy ( $E_0$ ) for the viscosity of basalt is about 200 kJ/mole [Hacker and Christie, 1991].

Figure C-12 plots the predicted strength of the crust of pahoehoe lobes using equation (C.5), the growth of the crust predicted shown in figure C-10, and assuming that the melt has no inherent strength. An interesting point is that the predicted strength of the crust is totally insensitive to the choice of either 1070 °C or 900 °C as the glass transition temperature. This implies that the predicted strength of the crust is entirely due to its colder part and that the region between 1070 °C and 900 °C adds negligible strength. What is disturbing about figure C-12 is that the predicted strength of the crust, while initially similar to our field measurements, rapidly becomes many orders of magnitude larger than the observations.



**Figure C-12: Prediction of pahoehoe crust strength based on laboratory data and thermal modeling.** Note the log scale on the strength axis and that the values are in GPa. While the form of the increase in strength is similar to the observations, the values are orders of magnitude larger than those measured.

The simplest solution to this discrepancy is to hypothesize that fractures caused by thermal contraction significantly weaken the frozen crust. It has been shown that fractures in the brittle crust played an important role in the growth of the Mount St. Helens lava dome [Denlinger, 1990]. However, this weakening of the crust by fracturing is an extremely difficult process to quantify. Figure C-13 shows a crude attempt to model this secondary weakening by simply assuming that the crust has zero strength below some temperature,  $T_b$ . This crude model seems to bracket the observed yield strengths given values of  $T_b$  between 670 °C and 700 °C. These values for  $T_b$  are arbitrary model fits, but they seem to be intuitively reasonable for the brittle-ductile transition of the crust. While this model is an extreme oversimplification, it does show that the observations are not many orders of magnitude out of line with reasonably expected values.



**Figure C-13: Predicted yield strengths for a fractured crust.** This model assumes that the strength of the crust is caused by the portion of the flow between the glass transition temperature (taken to be 1070 °C) and some temperature at which fractures completely destroy the strength of the crust ( $T_b$ ). There is some similarity between the model results for  $T_b$  between 700 °C and 670 °C and the actual measured values (diamonds).

### C.5.3 Viscosity

I also attempted, and failed, to extract some estimate of the viscosity of the lava from the lava lance data. Viscosity is usually determined by examining the relationship between the stress applied to the fluid and the resulting strain rate. For example, the data from a simple Bingham fluid should form a line with the slope indicating the viscosity and the intercept of the stress axis determining the yield strength.

In the case of the Lava Lance, neither the stress nor the strain rate was directly measured. I have assumed that the entire wetted surface area of the penetrometer transmits force into the liquid. Thus the measured force is divided by a surface area that increases as the rod moves forward. Estimating strain rate is even more arbitrary. Dimensional analysis shows that the strain rate can be thought of as the velocity of the rod divided by some length scale. This length scale is taken to be the width of the viscous boundary layer around the advancing penetrometer. A value of one centimeter was selected for this boundary layer thickness based on the observation that the Lava Lance seemed to disturb the lava about that distance radially.

Figure C-14 shows 4 typical examples of the resulting plots of stress versus strain rate. No clear pattern seems to emerge. Figure C-15 shows the apparent viscosity (strain rate divided by stress) for the same penetrations as figure C-14. In general, the apparent viscosity appears to increase with depth and the values are about 2 orders of magnitude above the expected value of about 100 Pa s [see Chapter 2 of this thesis]. This increase in apparent viscosity with depth is contrary to my expectations since, as the rod penetrates farther into the hot interior, it should be encountering less viscous lava. It turns out that the most revealing plot is of stress versus depth (Fig. C-16). Here we see that, at least initially, stress seems to linearly increase with displacement. This is the kind of plot that an elastic medium, such as a spring or a rock, would produce. Again, analogous to rock mechanics, at an ultimate strength the crust fails and strain increases rapidly while stress drops. This suggests that the crust of the flow lobe is largely behaving elastically and that

the rheology of pahoehoe flow lobes indeed is best modeled as a visco-elastic fluid, much the way that silicic domes are modeled [Iverson, 1990; Denlinger, 1990].

In principle, it should be possible to determine values for the bulk modulus (*i.e.*, spring constant) for the lobes from Figure C-16. I have not done so simply because I fear that it would be pushing the data too far. The uncertainties in precisely determining the stress will also affect these values. However, I am confident in the qualitative conclusion that pahoehoe lobes behave more elastically than viscously, on the timescale of these measurements.

## **C.6 Conclusions**

### **C.6.1 Lava rheology**

Despite difficulties, the Lava Lance was able to provide some interesting data on the strength of the crust on pahoehoe lava flows. The strength of this crust goes from about 0.1 to 1.0 MPa over the first 2-3 minutes and the increase in strength with time appears exponential. This suggests that the flow lobes are being driven by a hydrostatic head of several meters. Also, the exponential growth of strength is probably caused by the exponential dependence of the strength of basalt on temperature, and not by the square root of time growth of the thickness of the chill crust. Vesicles and microfractures may explain the fact that the measured crust is orders of magnitude weaker than predicted directly from laboratory data.

It was not possible to extract the viscosity of the melt from the data in part because the penetrometer design did not allow us to directly measure stress or strain rate. Attempts to estimate the proper values of stress and strain rate did not produce results that can be readily interpreted. Instead, the data suggest that pahoehoe flow lobes should be treated as visco-elastic fluids.

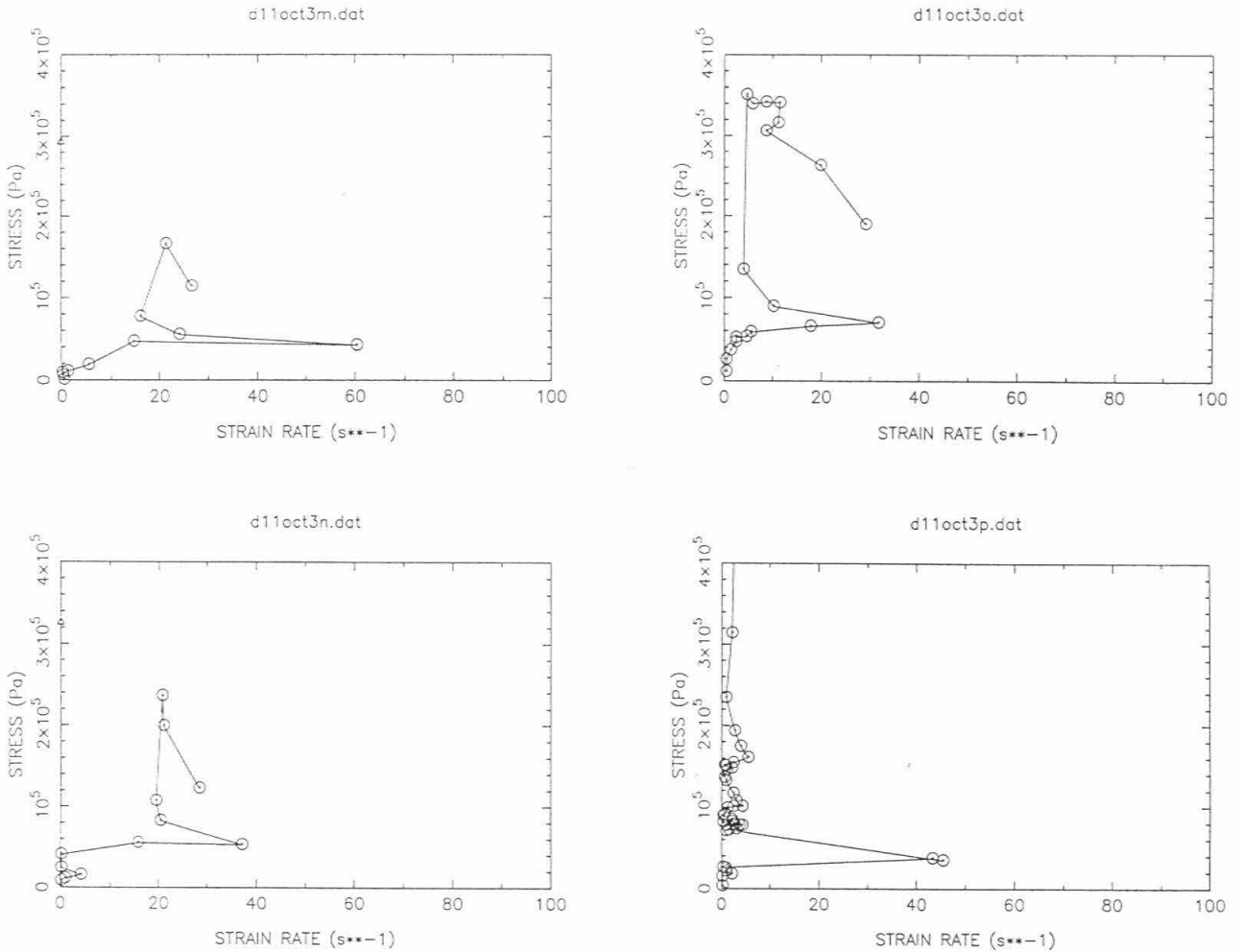


**Figure C-14: Stress vs. strain rate diagrams for lobe 7.** Plots for same four penetrations of a single lobe as shown in figure C-7a,b,c,d. Again, these data are quite representative of the entire usable data set. Observe that while there is some hint of a relationship between stress and strain rate for the first two penetrations (d11oct3m,n), no relationship is evident in the latter two (d11oct3o,p). This suggests that the crust on the pahoehoe lobes was not behaving as a simple viscous fluid.

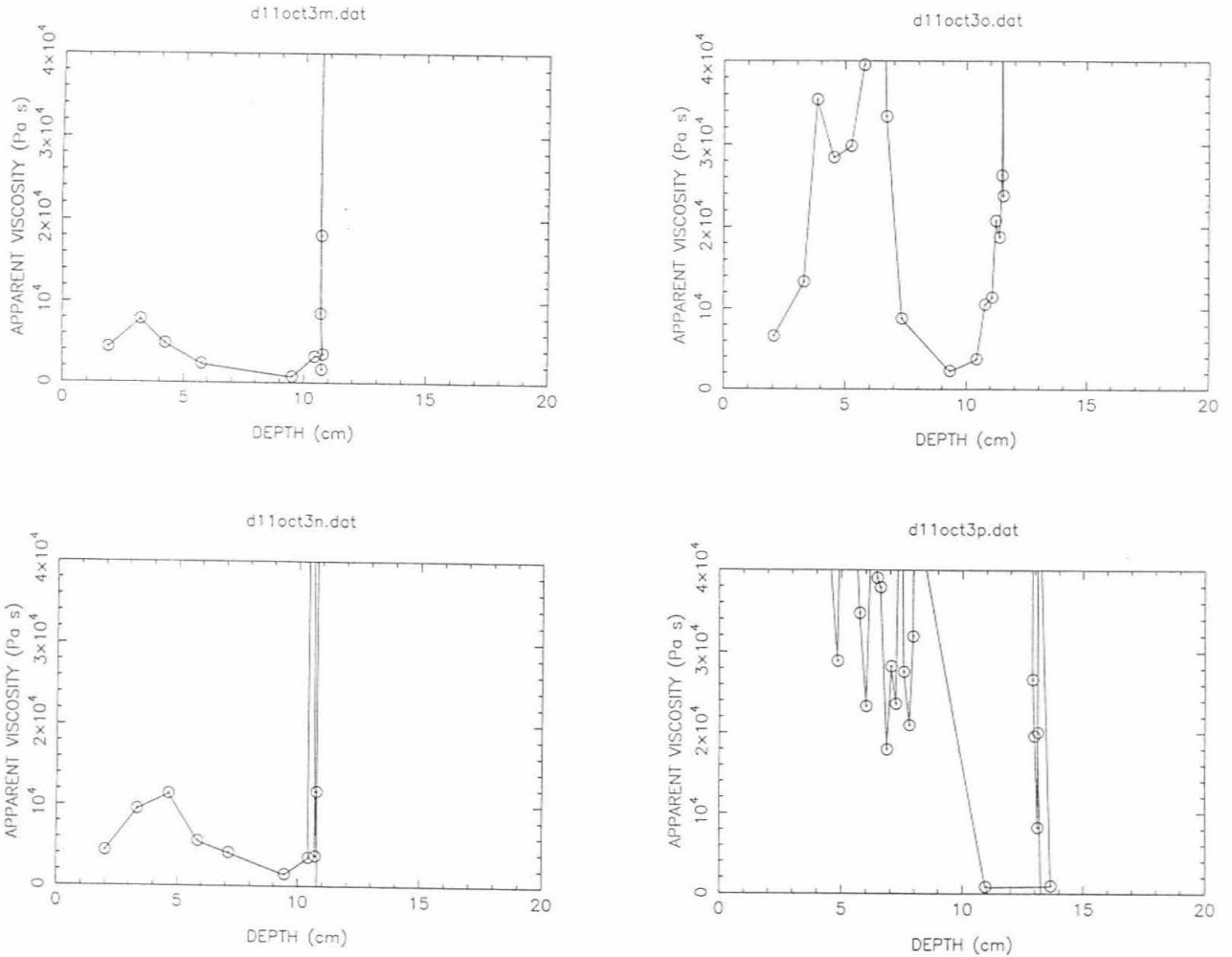


**Figure C-15: Apparent viscosity vs. depth for lobe 7.** Apparent viscosities derived by simply dividing the stress by the strain rate in figure C-14. Again, the first two penetrations into the relatively soft lobe show somewhat reasonable values with a suggestion of a melt viscosity of a few thousand Pa s. However, the latter two penetrations cannot be analyzed sensibly in this fashion.

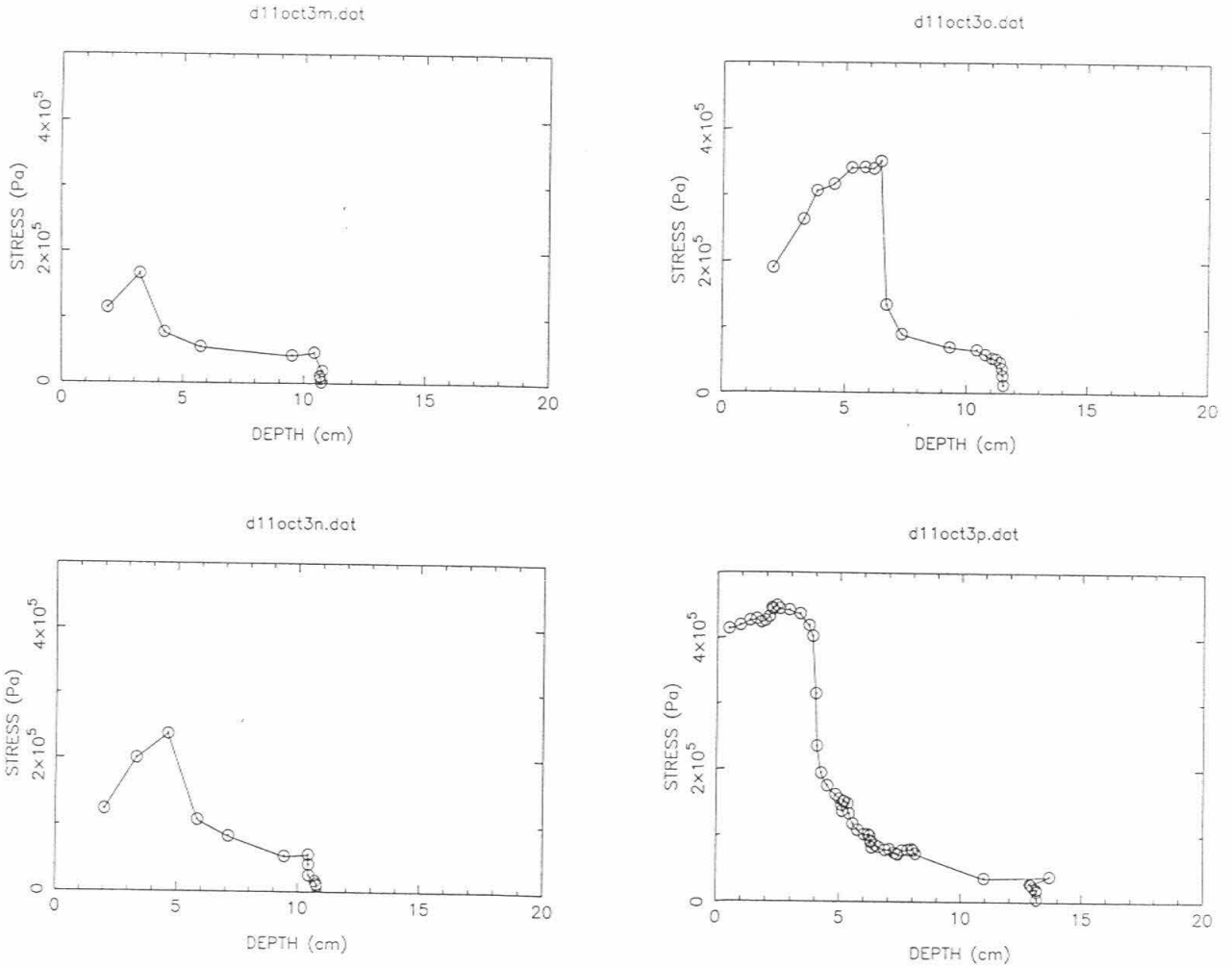


**Figure C-16: Stress vs. strain for lobe 7.** These graphs replot the data into a format common in rock mechanics experiments. Note how strain (depth of penetration) increases nearly linearly with increasing stress until the crust fails suddenly. Note also that this "ultimate strength" increases with time. These data suggest that the crust on pahoehoe flow lobes contain significant elastic behavior in their rheology and possibly that pahoehoe lobes can be best modeled by as a visco-elastic fluid.

### C.6.2 Field measurements

The main objective of this project was to gain experience in operating instrumentation near active lava flows. The most recurring lesson from this experiment was KISS (Keep It Simple, Stupid). This axiom most strongly applies to field operations. Our procedure was to step up to the flow, grab some data, and step back. While close to the lava, no time or attention was wasted on adjusting our instrument. I learned quickly that small details, such as taping wires together into neat bundles, can make life much simpler in the field.

Simplicity in the selection of materials was also a great cost saver. There is no reason to use exotic alloys when working with lava. Ordinary stainless steel retains most of its strength even at lava temperatures. The chemical environment of the lava tarnishes the steel but otherwise leaves it unaffected. Another nice feature is that because of the different coefficients of thermal expansion, lava stuck to a piece of metal will flake off as it cools.

I also found that simplicity and low cost do not always go hand in hand. My penetrometer would have been much simpler mechanically, electronically, and to operate if we had been able to afford new instruments built specifically for this experiment. The cheap (used) instruments also very significantly degraded the reliability of the overall system. As indicated earlier, less than one third of the data collected were actually usable.

Despite the above caveat, there is much to be said for modular designs made up of simple components. As Dr. Robert Sharp is fond of saying, "Madam Pele is a tempestuous lady." Any field experiment must be able to adjust to the whims of the lava flows. Because of the modular nature of our penetrometer design, we were able to effect a major re-design of the instrument, in the field, immediately after our bumbling first contact with lava.

The final point I have learned from this work is that one can never take too many notes while in the field. As shown in Chapter 4, the porosity of the lava and the ambient weather conditions can significantly affect the early cooling history of a pahoehoe flow lobe. However, I failed to take note of these variables during this field experiment. I have found that the only practical way to collect all the potentially relevant peripheral data associated with a field experiment is to have an individual, other than the instrument operator, designated as the note taker.

Overall, I have found working with active pahoehoe lava flows only marginally more difficult than operating, for example, in the Mojave Desert. I should also state for the record that in my subsequent field experiments I have not always been able to fully implement the lessons I learned during this project. Funding and man-power shortages are only partially responsible for this. Looking back, I can see that I have been sometimes over-eager to deploy hardware into the field. My colleague, George Powell's, insistence on repeated calibrations and attention to detail was perhaps the key factor that allowed this project to return any usable scientific data. In the end, I feel it safe to conclude that this experiment was an invaluable learning experience which allowed me to avoid some of the fiascoes I have witnessed on the lava flows of Kilauea.

## APPENDIX D: TERMINOLOGY AND SYMBOLS

The terminology used in this thesis follows that used, both formally and informally, at the Hawaiian Volcano Observatory (HVO). This appendix is primarily intended to help any non-volcanologists who may have stumbled onto this thesis.

### D.1 Lava Flow

The Glossary of Geology defines it as "a lateral, surficial outpouring of molten lava from a vent or fissure; *also*, the solidified rock that is so formed." The only difficulty with this definition is determining what should constitute a single "outpouring." In practice this problem is left to the observer and is rarely a point of contention. *Lava flow unit* may be used as a synonym for *lava flow* especially when one is discussing both lava flows in general as well as an individual lava flow. The term *lava flow field* is commonly used to describe an area covered by multiple lava flows from a single source area. The definition of "single source area" is again imprecise but as long as an entire volcano is not dubbed a *flow field*, few eyebrows will be raised. *Compound lava flow* is a synonym for *flow field* though one might contend that *compound lava flow* should only be used for multiple *lava flows* from precisely the same vent.

### D.2 Pahoehoe

*Pahoehoe* is a morphological and textural term taken from the Hawaiian language used to describe a class of lava flows which have relatively smooth surfaces. Pahoehoe lava flows are almost exclusively basaltic. There are many forms of pahoehoe of which the Glossary of Geology lists the following kinds: *corded*, *elephant-hide*, *entail*, *festooned*, *filamented*, *sharkskin*, *shelly*, and *slab*. HVO also uses the terms *toothpaste*, *spiny*, and *blue-glassy* to describe some types of pahoehoe. Many forms of pahoehoe are actually descriptions of the incredible variety of textures that basalt forms in the pahoehoe to 'a'a transition. Thus *slabby*, *toothpaste*, and *spiny pahoehoe* are transitional lavas which are quite different from the more classical *ropy* or *entail pahoehoe*.

Ignoring these transitional lavas, pahoehoe flows are characterized by being covered by a nearly continuous crust as they move. This crust is initially quite ductile and is capable of extensive folding and stretching. Typically, small pahoehoe flow lobes grow in a fashion similar to a large water balloon being filled by a garden hose. Ropes form when the upper crust is in motion and hits some obstacle. The surface then folds like a carpet being pushed against a wall. The infinite combinations of the basic pahoehoe morphologic features provide endless entertainment to a dedicated observer. I must apologize for not being equal to the task of conveying in words the thrill of basking in radiated heat and sulfurous fumes while watching incandescent-lipped, alligator-sized, silver-black slugs slowly creeping over the ground with their skins popping and crackling from thermal contraction.

### D.3 'A'a

'A'a is another Hawaiian term and is used to describe a lava flow with a surface covered with sharp, loose clinker. When the clinker approaches boulder size, the term *blocky* lava is usually used. The transition between 'a'a and pahoehoe is related to both the flow velocity (*i.e.*, strain rate) and lava viscosity. High viscosity and high flow velocities both favor 'a'a [*e.g.*, Peterson and Tilling, 1980; Rowland and Walker, 1990].

Since I have yet to personally witness an active 'a'a flow, I consider my understanding of 'a'a dynamics inadequate for any profound insights. 'A'a flows apparently move as a plug of melt that encases itself in a pile of loose clinker. The formation of these typically fist-sized jagged balls of lava may be caused by some shear instabilities in fast moving viscous lavas [Peterson and Tilling, 1980]. The front of an 'a'a flow is a steep wall of lava with the clinker on the top cascading down the front of the flow. The main plug of lava travels over this bed of rubble and moves in intermittent surges. From firsthand tales I have heard recounted, it seems that an 'a'a flow is much like a giant fiery runaway bulldozer, creaking and groaning its way blindly downhill.

#### D.4 Parts of Pahoehoe lava flows.

*Lava flows* are made up of smaller morphologic features such as lava tubes, channels, flow lobes, and tumuli. *Lava tubes* and *channels* are efficient conduits for transporting lava and form spontaneously within lava flows. As might be gathered from their names, *lava tubes* are covered while *lava channels* have no roof. Technically, any enclosed lava conduit could be called a *lava tube*. However, I shall restrict the term *lava tube* to tubes large enough to transport a significant portion of the lava being erupted. Views into lava tubes are afforded by *skylights*. *Skylights* form when a part of the tube's roof collapses. *Skylights* are invaluable for investigating active lava tubes, but are also relatively hazardous to approach. *Lava channels* are flanked by *levees* built up of *spill-overs* from the channel. *Spill-over* and *overflow* are also used to describe lava issuing out of a skylight. *Flow lobes* can be thought of as mini-lava flows emanating from the main lava flow. They are the smallest parcel of lava moving across the surface as a single unit. Depending on their size and shape (and personal taste), flow lobes are also called *toes*, *fingers*, and *buds* (Fig. D-1). Large, flat flow lobes are often called *sheet flows*.

*Tumuli* are 10-100 meter scale mounds of upheaved lava shaped somewhat like a loaf of bread. During the upheaval, the surface of the lava flow is broken into several large blocks, usually leaving a large axial crack running along the top of the tumulus (Fig. D-2). It is now known that the upheaval is caused by the injection of fresh lava beneath a cooled crust [Walker, 1991; Hon *et al.*, 1994a]. Before this realization, tumuli were occasionally referred to as *gas blisters*. This process of lifting the crust of a lava flow by injecting fresh lava is now called *inflation* though some at the University of Hawaii at Manoa prefer the term *lava-rise*. Inflation is apparently unique to pahoehoe. The range of morphologic features formed by inflation had generated a host of now obsolescent genetic terms such as *pressure plateaus*, *pressure ridges*, and *collapse pits*.



**Figure D-1: Photograph of some exceptionally well formed pahoehoe flow lobes, Kupaianaha flow field, Hawai'i.** [Photo courtesy of USGS]



**Figure D-2: Photograph of a typical tumulus.** Note the axial crack and breakout from inside the tumulus. Kupaianaha flow field, Hawai'i. [Courtesy of USGS]

## Symbols

$\Psi$	Volumetric effusion rate. <i>Unless otherwise noted, includes the volume of vesicles</i>	[m <sup>3</sup> /s]
$\tau$	Time scale. <i>Usually eruption duration.</i>	[s]
$\eta$	Dynamic viscosity	[Pa s]
$\eta_e$	Effective dynamic viscosity. <i>Includes effect of bubbles and crystals.</i>	
$\eta_m$	Dynamic viscosity of pure fluid (melt)	
$\epsilon'$	Strain rate	[s <sup>-1</sup> ]
$\nu$	Kinematic viscosity	[m <sup>2</sup> /s]
$\sigma_y$	Yield strength	[Pa]
$\rho$	Density. <i>Subscript often used to identify material.</i>	[kg/m <sup>3</sup> ]
$\phi$	Porosity.	[%]
$r$	Radius. <i>Usually for a vesicle or lava tube.</i>	[m]
$D$	Diameter. <i>Usually for a vesicle or lava tube.</i>	[m]
$g$	Gravitational acceleration	[m <sup>2</sup> /s]
$H$	Height. <i>Usually for a lava flow.</i>	[m]
$H_c$	Thickness of undeforming plug in Bingham model.	
$W$	Width. <i>Usually for a lava flow.</i>	[m]
$L$	Length. <i>Usually for a lava flow.</i>	[m]
$V$	Volume. <i>Usually for a lava flow.</i>	[m <sup>3</sup> ]
$\alpha$	Angle. <i>Usually slope.</i>	[°]
$\langle v \rangle$	Mean flow speed.	[m/s]
$U$	Wind speed.	[m/s]
$\kappa$	Thermal diffusivity.	[m <sup>2</sup> /s]
$\kappa_{\text{eff}}$	Effective thermal diffusivity. <i>Includes effects of vesicles.</i>	

k	Thermal conductivity	[W/m K]
$k_{\text{bas}}$	Thermal conductivity of basalt	
$k_{\text{gas}}$	Thermal conductivity of gas phase	
$k_{\text{eff}}$	Effective thermal conductivity. <i>Includes all effects of vesicles.</i>	
$k_{\text{cond}}$	Bulk thermal conductivity. <i>Includes effect of vesicles on conduction.</i>	
$k_{\text{rad}}$	Effective radiative thermal conductivity. <i>Radiative heat transfer expressed as a thermal conductivity.</i>	
$k_{\text{conv}}$	Effective convective thermal conductivity. <i>Convective heat transfer expressed as a thermal conductivity.</i>	
I	Thermal inertia	[J/m <sup>2</sup> K <sup>1/2</sup> ]
T	Temperature	[K]
$T_0$	Initial temperature.	
$T_s$	Surface temperature.	
$T_a$	Ambient temperature.	
$\Delta T$	Temperature difference	
Gz	Grätz Number. <i>Measure of conductive versus advective heat flux.</i>	[ ]
Ra	Rayleigh Number. <i>Measure of viscous versus buoyancy forces.</i>	[ ]
Nu	Nusselt Number. <i>Measure of conductive versus convective heat flux.</i>	[ ]
h	Heat transfer coefficient.	[W/m <sup>2</sup> K]
$\beta$	Coefficient of thermal expansion.	[K <sup>-1</sup> ]
$\gamma$	Adiabatic lapse rate.	[K/m]
Cp	Heat capacity. <i>Constant pressure.</i>	[J/kg K]
Q	Heat.	[J]
q	Heat flux. <i>Subscript denotes heat transport mechanism.</i>	[W/m <sup>2</sup> ]
$\epsilon$	Emissivity	[ ]
F	View factor.	[ ]
Xc	Crystallinity.	[%]

N	Nucleation rate.	[m <sup>-3</sup> s <sup>-1</sup> ]
G	Growth rate	[m/s]
E <sub>0</sub>	Activation energy.	[J/mole]
L	Latent heat.	[J/kg]
h <sub>0</sub>	Thickness of tube roof	[m]
n <sub>sky</sub>	Skylight density	[m <sup>-1</sup> ]
σ <sub>b</sub>	Stefan-Boltzmann Constant	[5.67x10 <sup>-8</sup> W/m <sup>2</sup> K <sup>4</sup> ]
π		[3.14159265... ]
R	Ideal Gas Constant	[8314 kg m <sup>2</sup> /s <sup>2</sup> K mole]
x	Generic spatial dimension. <i>Usually in flow direction.</i>	
z	Vertical dimension.	
t	time dimension	

## APPENDIX E: VHS VIDEO LOG

### E.0 Introduction

The video is intended to supplement the introduction in Chapter 1 and this log will make several references to the figures and text in Chapter 1. The video starts with an overview of the Pu'u 'O'o flow field in early to mid-1993 (see Fig. 1-5). While this portion of the video shows footage from the Episode 50-53 Pu'u 'O'o Flow Field in early-mid 1993, the it is intended to help illustrate the different portions of the idealized flow field in Fig 1-6. Aerial and ground views are shown of (1) the Pu'u 'O'o cone and lava lake, (2) the start of the Episode 53 vent on the side of the Pu'u 'O'o cone, (3) several skylights along the main lava tube(s), (4) various surface flows and inflation features, and (5) the ocean entries. This tour also shows the viewer to a few of the other research problems associated with pahoehoe lava flows. Following this first tour is a series of short clips showing various field experiments, some of which were total failures and are not mentioned anywhere else in the text of this thesis. At the end I include some additional clips of working with skylights, Mt. Etna, and life at Caltech. These latter parts may be considered an extreme scenic detour off of my thesis research.

Some general comments need to be made about the idiosyncrasies of my video-camera. All times on the screen are Pacific Standard Time (*i.e.*, California time, not local time). Subtract 2 hours for local time. The camera has problems with autofocus and auto color balance when dealing with the lava. I have tried to edit out the worst footage, but some problems are remain. In particular, I find the colors are unpleasantly garish. I have also removed most of the audio from the tape because the recordings are dominated by either wind noise or helicopter engines. One further problem is that the fumes and dust from the eruption seriously degraded my camera's ability to record and the image often "winks" out. Also, the inclusion of people in the scenes is more to provide a sense of scale rather than to embarrass my friends.

All video footage from Hawai'i was made possible by the courtesy of the USGS.

## **E.1 Tour of the Episode 50-53 Pu'u 'O'o Flow Field.**

### (0m 4s - 1m 23s) View of Pu'u 'O'o from the ground.

This clip was shot from just uprift (NW) of the Pu'u 'O'o cinder cone. The video zooms in on the Episode 50-51 fissure vents which were thought to be dormant at the time. The camera pans right (to the south), looking at the Episode 51-52 ponded flows, then pans back (to the north) across to the Episode 50 perched lava pond. As an aside, this was our primary campsite when visiting Pu'u 'O'o overnight.

### (1m 26s - 3m 7s) Approaching Pu'u 'O'o by helicopter.

This clip starts with the campsite in the center of the image. The helicopter rapidly passes over the hazardous shelly pahoehoe surrounding the fuming and collapsing Episode 50-51 fissure vents. The helicopter then makes a slow pass to view the lava pond inside Pu'u 'O'o. Note that at this time the activity in the pond seems to be concentrated at a single point. This can change on the time scale of minutes. Also note that the helicopter NEVER passes beyond the edge of the rim of Pu'u 'O'o.

### (3m 7s - 4m 17s) View of Pu'u 'O'o lava pond from the rim.

This is the view from ground level just below the point where the helicopter went into hover. This section of the rim has been unusually stable and is the sight of a time lapse 8mm camera maintained by HVO. Note that at this time the activity inside the pond is focused along a line. The surface of the pond is typically about 70-80 m below the rim of the cone. The correlation of the fluctuations of the pond level and the summit inflation data is an area of current investigations.

### (4m 17s - 4m 31s) View of Episode 53 vent hours after initial eruption.

On the day of this particular hike to Pu'u 'O'o, we were greeted by a new episode of the eruption. The clip starts by panning up the channelized pahoehoe flow. Then the we

reach the vent and the camera is unable to cope with Pele's splendor. It should be stated that our current understanding of what controls the pauses in the eruption and the start of new episodes is very poor. Even our understanding of the plumbing directly under Pu'u 'O'o is basically conjecture. It is "difficult" to set up a detailed geophysical study in an area that changes dramatically every few months.

(4m 33s - 5m 0s) View of Episode 53 vent the next day.

This clip shows the Episode 53 vent the next day. A partial spatter cone had built up, but would periodically collapse. The clip shows the beginnings of a hole in the spatter cone. The camera pans to the observers to remind the viewer that large quantities of sulfur rich gasses are exsolved at this point. The clip ends with a pan out over the flow field where our lava tubes lurk.

(5m 1s - 7m 53s) Skylights.

This clip shows a series of skylights found along the tube system inside the Episode 51-53 flow field. As well as the prominent skylights, there are occasional incandescent cracks that are indicative of being in the "inflation zone" of Fig. 1-6. Note that the HVO staff avoid standing directly over the tube. Also note that the lava continues to degas, emitting a blue haze. The clip ends with a pan out to where the flows were actively burning forest and to the sea.

(7m 53s - 8m 3s) Breakout from inflating sheet.

This (short) clip shows a small breakout from a larger inflating sheet. The camera zooms back to view the entire flow field. The entire area, up to about 100 m to front of the camera, was inflating at the time.

(8m 3s - 9m 2s) Typical small pahoehoe lobes.

This clip shows some typical small pahoehoe lobes moving at their typical snail's pace. Rock hammer for scale. Note the skin texture on the lobe.

(9m 3s - 9m 43s) End members for styles of pahoehoe lobe motion.

This clip first shows a very slow lobe that moves by peeling up its front (Fig. 1-7a) then switches to a larger, rolling flow lobe (Fig. 1-7b). Note in the first case the pieces of dark lava on top of the shiny fresh lobe. These are pieces of old lava that the lobe has picked up from in front of itself. The clip ends by zooming out to see a series of flows cascading over a small scarp.

(9m 43s - 10m 27s) Ocean entries forming.

This clip shows pahoehoe flows reaching the sea. Before the development of tubes feeding directly into the sea, strong plumes do not form. The interaction between the lava and the sea water builds the materials for black sand beaches.

(10m 27s - 10m 56s) Well developed ocean entries viewed from a helicopter.

This clip shows the discoloration of the water and the large plume associated with well developed tube-fed ocean entries. There are several efforts underway to better understand the local effects of these types of entries on both the ocean and atmosphere.

## **E.2 My field experiments**

(11m 01s - 11m 20s) Lava lance in the basement of HO.

This clip shows the Laszlo Lava Lance (LLL) Mk. II making its debut in the basement of HVO in October of 1991. The load cell (that measures force) is in the box at the operator end of the lance. The linear potentiometers (that measure position) are in the

two aluminum boxes strapped on midway down the LLL. At this point the inclinometer had not been installed. Note the 20 cm maximum range of the inner rod.

(11m 20s - 11m 36s) Lava Lance in repair in the field.

One of the best attributes of the LLL was that it could be easily modified in the field to adjust to Pele's whims. This clip shows us breaking down the LLL to shorten the inner rod. These modifications did require that we carry a substantial tool box with us into the field.

(11m 36s - 12m 30s) Testing the Lava Lance in the field.

This clip shows some of our early test penetrations into the lava to observe the interaction between the LLL and pahoehoe. Note the variety of responses of the crust depending on its strength. The clip ends with a zoom on the small (2-4 cm diameter) scars that the penetrations would leave on the flow lobes. Successive penetrations were kept in the same part of the lobe, but not so close together as to be affected by the earlier penetrations.

(12m 30s - 12m 49s) Lava Lance at work

This clip shows 4 penetrations into the same lobe. Note how each penetration becomes more difficult as the crust cools, thickens, and hardens. Also note how quickly each measurement could be taken. This allowed us to use minimal thermal protection.

(12m 50s - 13m 40s) Lava lance at work

This clip shows another 3 penetrations that were taken about 30 seconds apart and demonstrates the (leisurely) pace at which we collected data. Again note that the measurement process was quick and painless for the operator. The last penetration of this clip was done by George Powell, the engineer for this project.

(13m 41s - 16m 06s) My attempt to measure temperature profiles

The plan was to measure temperatures inside flow lobes at 4 different depths. Thermocouples were installed inside a ceramic pipe that was placed in the path of oncoming flows. Holes were drilled to allow the thermocouples contact with the lava at the designated depths. As this clip shows, this did not work well. The ceramic pipe was sufficient to divert the flow lobes and thus the device was never overrun. Eventually, successive lobes would surround the ceramic pipe. However, being in the suture between flow lobes gave very atypical measurements. Note the metal stake used to hold the wires above the lava. It is not visible from this angle, but the stake was painted at 10 cm intervals. The yellow-green powder around the pipe is olivine sand which was used to fill the pipe. This rather long clip also nicely demonstrates the dynamics of small pahoehoe flow lobes.

(16m 10s - 16m 35s) Measuring inflation

This clip shows the measurement site a few days later. The stake now works to measure the amount of inflation (only about 30-40 cm in this case). The top of the ceramic pipe is also still exposed.

(16m 35s - 16m 54s) Air flow visualization

In my attempt to measure the heat carried by the wind, it was necessary to estimate the thickness of the thermal boundary layer over the lava. Smoke was used to visualize the flow over the lava. This particular surface was a few days old and had a surface temperature of only about 110 °C. Airflow did not appear to be significantly disturbed by individual active flow lobes either. However, one of the most reliable ways of locating activity on the flow field is to search for unusually intense heat waves.

(16m 55s - 17m 33s) Boundary layer studies

This is my failed attempt to properly measure the heat carried by the wind. The tower contains 3 anemometers and 4 thermocouples. The primary problem was that the anemometers were built by myself and turned out to be completely unreliable. There was also a problem with the mounting of the thermocouples not allowing them to read true ambient temperatures. Had I spent about \$10K instead of about \$100 for this tower, there should have been no problems.

(17m 38s - 18m 33s) Helicopter-borne view of the ground above a lava tube.

To the experienced observer there are many clues of a lava tube. Fresh, golden colored spill overs from skylights and blue fumes are the key indicators. However, it is still impossible to track the tube in detail with just visible imaging. Note the trees for scale.

(18m 33s - 19m 10s) Thermal IR view of the same area.

These images were collected using JPL's Inframetrics Corporation scanning radiometer. The instrument is sensitive in the 8-13  $\mu\text{m}$  range of the thermal infrared. The temperature variations in the images are on the order of 10  $^{\circ}\text{C}$ . and lighter shades are hotter areas. The lava tube shows up as the meandering warm stripe. Observe that detailed tracking of the tube is possible with this portable instrument. Also note that there are repeated suggestions of the tube bifurcating.

(19m 11s - 19m 42s) Helicopter-borne visible view over active flows.

For the experienced observer, there are some clues that there is very fresh lava below. For example, the bright, shiny surfaces must be very young. However, it is again very difficult to map out the areas of activity.

(19m 43s - 20m 12s) Thermal IR view of the same area.

The areas of recent activity are strikingly obvious in the thermal IR images. However, the shapes of the warm areas are extremely irregular, not providing a clear indication of the breakout point or the flow direction.

(20m 13s - 21m 55s) Thermal IR of flows breaking out of a lava tube

This clip demonstrates what I believe to be one of the most useful applications of this type of airborne IR imaging. In this case the first set of flows can be clearly traced back to a breakout from an earlier flow. The higher flows are emanating directly from the lava tube. In principle, this level of knowledge of the sources feeding individual surface flows should improve predictions of their future behavior and potential hazards.

### **E.3 Some other interesting footage**

(21m 44s-22m 26s) Verifying geophysical measurements.

While these next clips are easily mistaken for playing with lava, they were a rather important experiment. The objective of this experiment was to confirm geophysical measurements indicating that the flowing, molten, lava in the tubes was only about 0.5 m thick (*i.e.*, the tube was running at about 10% of its capacity). Presumably tubes form essentially full, so a drop in level, with no slowing of the eruption, suggests significant thermal and mechanical erosion of the tube floor. Logs were marked at 1 m intervals, then lowered until they just contacted the upper surface of the lava. Then they were rammed through the lava. The logs indeed did only penetrate about 50 cm. This experiment was repeated with steel rebar on a later date.

(22m 26s - 22m 34s) Recovered log.

This shows one of the logs that was successfully removed from the lava after insertion. Lava coated the log up to about 70 cm from the end of the log. However, some of this lava coating was caused by lava splashing up in a "bow wave."

(22m 34s - 23m 45s) Pele takes her log.

Not all logs were recovered. Recall that lava is 100-1000 times more viscous than water and is about twice as dense. This exerts a remarkable force on the log. Also note how the wet ohia log catches fire just from the radiated heat. Further note that the molten lava is a good 4-5 m below the ceiling of the tube. This clip is intended to also remind the viewer of some of the potential hazards of working around skylights.

(23m 45s - 23m 55s) Measuring flow velocity in the lava tubes

The standard means by which HVO determines the flow velocity inside lava tubes is to measure the time it takes for a (small) log dropped into one skylight to appear at another one downstream. This clip shows how such a log appears at the downstream skylight.

(23m 55s - 27m 40s) Etna

In the interest of reminding the viewer that Kilauea is not the only volcano in the world, I have included some of my clips from Mt. Etna. This series of clips shows the volcano from a distance, the view from the south rim of the Valle de Bove (Etna's peculiar attempt at caldera formation) emphasizing the dike swarms, a view of the 1991-1993 flow field, an overview of the many towns and cities endangered by Etna, collecting gravity data, and the view from the north rim of the Valle de Bove emphasizing the texture of the 'a'a flows, tubes, and channels. Also appearing at random times are other volcanologists including Alun Jones who is repeatedly referenced in Chapters 3 and 4.

## REFERENCES

- Allen, J. E. (1952) The Carrizozo Malpais. Roswell Geologic Society Guidebook, 5th Field Conference, pp. 9-11.
- Appelgate, B., and R. W. Embley (1992) Submarine Tumuli and Inflated Tube-Fed Lava Flows on Axial Volcano, Juan de Fuca Ridge. Bull. Volc., 54: 477-458.
- Arndt, N. T., and U. Christensen (1992) The Role of Lithospheric Mantle in Continental Flood Volcanism: Thermal and Geochemical Constraints. J. Geoph. Res., 97: 10 967-10 981.
- Arvidson, R. E., M. K. Shepard, E. A. Guinness, S. B. Petroy, and J. J. Plaut (1993) Characterization of Lava-Flow Degradation in Pisgah and Cima Volcanic Fields, California, Using Landsat Thematic Mapper and AIRSAR Data. Geol. Soc. Am. Bull., 105: 175-188.
- Aubele, J. C., L. S. Crumpler, and W. E. Elston (1988) Vesicle Zonation and Vertical Structure of Basalt Flows, J. Volc. Geoth. Res., 35: 349-374.
- Ayra, S. P., (1988) Introduction to Micrometeorology, Academic Press, Orlando
- Basaltic Volcanism Study Project (1981), Basaltic Volcanism on the Terrestrial Planets, Pergamon Press, New York, 1286 pp.

- Basu, A. R., P. R. Renne, D. K. Dasgupta, F. Teichmann, and R. J. Poreda (1993) Early and Late Alkali Igneous Pulses and a High He<sup>3</sup> Plume Origin for the Deccan Flood Basalts. Science. 261: 902-906.
- Bejan, A. (1984) Convection Heat Transfer. John Wiley & Sons, New York, 477 pp.
- Bertagnini, A., S. Calvari, M. Coltelli, P. Landi, M. Pompilio, and V. Scribano (1990) The 1989 eruptive sequence. In: Barberi, F., A. Bertagnini, and P. Landi (editors) Mt. Etna: The 1989 Eruption. Giardini. Pisa. pp. 10-22.
- Birch, F., and H. Clark (1940) The Thermal Conductivity of Rocks and its Dependence upon Temperature and Composition. Am. J. Sci., 238: 529-558.
- Bird, R. B., W. E. Stewart, and E. N. Lightfoot (1960) Transport Phenomena. John Wiley and Sons, New York, 780 pp.
- Bottinga, Y., and D. F. Weill (1972) The Viscosity of Magmatic Silicate Liquids: a Model for Calculation. Am. J. Sci. 272: 438-475.
- Brace, W. F. (1984) Permeability of Crystalline Rocks: New in situ Measurements. J. Geoph. Res., 89: 4327-4330.
- Bruno, B. C., G. J. Taylor, S. K. Rowland, P. G. Lucey, and S. Self (1992) Lava Flows are Fractals. Geophys. Res. Lett., 19: 305-308.

- Bryan, W. B., S. E. Humphris, G. Thompson, and J. F. Casey (1994) Comparative Volcanology of Small Axial Eruptive Centers in the MARK Area. J. Geophys. Res., 99: 2973-2984.
- Campbell, B. A., and D. B. Campbell (1992) Analysis of Volcanic Surface-Morphology on Venus from Comparison of Aricebo, Magellan, and Terrestrial Airborne Radar Data. J. Geophys. Res., 97: 16 293-16 314.
- Carrigan, C. R., G. Schubert and J. G. Eichelberger (1992) Thermal and Dynamical Regimes of Single- and Two-phase Magmatic Flow in Dikes. J. Geoph. Res., 97: 17 377-17 392.
- Carslaw, H. S., and J. C. Jaeger (1959) Conduction of Heat in Solids. Oxford University Press, Oxford, 510 pp.
- Cashman, K. V. (1993) Relationship Between Plagioclase Crystallization and Cooling Rate in Basaltic Melts. Contrib. Mineral. Petrol., 113: 126-142.
- Cashman, K. V., and B. D. Marsh (1988) Crystal Size Distribution (CSD) in Rocks and the Kinetics and Dynamics of Crystallization II: Makaopuhi Lava Lake. Contrib. Mineral. Peterol., 99: 292-305.
- Cattermole, P. (1987) Sequence, Rheolgical Properties, and Effusion Rates of Volcanic Flows at Alba Patera, Mars. Proc. Lunar Planet. Sci. Conf., XVII: E553-E560.

- Cermak, V., and L. Rybach (1982) Thermal Properties in Physical Properties of Rocks, in Landolt-Bornstein Numerical Data and Functional Relationships in Science and Technology. in K. H. Hellwege (editor) Springer-Verlag, Berlin, pp. 9543-9552.
- Cheng, P. (1985) Natural Convection in a Porous Medium: External Flows, in Kakac, S., W. Aung, and R. Viskanta (editors) Natural Convection: Fundamentals and Applications. Springer-Verlag, Berlin, 1181 pp.
- Chester, D. K., A. M. Duncan, J. E. Guest, and C. R. J. Kilburn (1985) Mount Etna: The Anatomy of a Volcano. Stanford University Press, Stanford. 404 pp.
- Clark, S.P. (1957) Radiative Transfer in the Earth's Mantle. Am. Geoph. Union Trans., 38: 931-938.
- Clemons, R. E., R. W. Kelley, F. E. Kottowski and J. M. Robertson (1982) New Mexico Highway Geologic Map. Williams and Heintz Map Corp, Washington, D.C.
- Crisp, J., and S. Baloga (1990) A Model for Lava Flows with Two Thermal Components. J. Geophys. Res., 95: 1255-1270.
- Crisp, J. and S. Baloga S (in press) The Influence of Crystallization and Entrainment of Cooler Material on the Emplacement of Lava Flows. J. Geophys. Res.
- Crisp J., A. B. Kahle, and E. A. Abbott (1990) Thermal Infrared Spectral Character of Hawaiian Basaltic Glasses. J. Geoph. Res., 95: 21 657-21 669.

- Danes, Z. F. (1972) Dynamics of Lava Flows. J. Geophys. Res. 77: 1430-1432.
- Dawson, J. B., H. Pinkerton, G. E. Norton, and D. M. Pyle (1990) Physicochemical Properties of Alkali Carbonatite Lavas: Data from the 1988 Eruption of Oldoinyo Lengai, Tanzania. Geology, 18: 260-263.
- Decker, R. W., T. L. Wright, and P. H. Stauffer (editors) (1987) Volcanism in Hawaii. USGS Professional Paper 1350, United States Government Printing Office, Washington, 1667 pp.
- Delaney, P. T. (1988) Fortran-77 Programs for Conductive Cooling of Dikes with Temperature-Dependent Thermal-Properties and Heat of Crystallization. Computers and Geosciences, 14: 181-212.
- Denlinger, R. P. (1990) A Model for Dome Eruptions at Mount St. Helens, Washington, Based on Subcritical Crack Growth. in Fink, J. H. (editor) Lava Flows and Domes: Emplacement Mechanisms and Hazard Implications. Springer-Verlag, Berlin, pp. 70-87.
- Dragoni, M. (1989) A Dynamical Model of Lava Flows Cooling by Radiation. Bull. Volcanol., 51: 88-95.
- Dragoni, M., M. Bonafede and E. Boschi (1986) Downslope Flow Models of a Bingham Liquid: Implications for Lava Flows. J. Volc. Geoth. Res., 30: 305-325.
- Dragoni, M., and A. Tallarico (1994) The Effect of Crystallization on the Rheology and Dynamics of Lava Flows. J. Volcanol. Geoth. Res., 59: 241-252.

- Farris, K. B. (1980) A Geochemical Model for the Magmatic History of the Carrizozo Basalt Field, South Central New Mexico. Thesis. New Mexico Institute of Mining and Technology, Socorro. 168 pp.
- Fink, J. H., and J. R. Zimbelman (1986) Rheology of the 1983 Royal Gardens Basalt Flows, Kilauea Volcano, Hawaii. Bull. Volc., 48: 87-96.
- Fink, J. H., and J. R. Zimbelman (1988) A Comparison of Lava Flow Rheology Calculations for High-Resolution Data Sets From Hawaii and Mars. Lunar Planet. Sci. Conf. Abstr., XIX: 327-328.
- Finnemore S., S. Self, and G. P. L. Walker (1993) Inflation Features in Lava Flows of the Columbia River Basalts. AGU Fall Meeting Abstracts. EOS, 74: 555.
- Flügge, W. (1967) Stresses in Shells. Springer-Verlag, Berlin.
- Flynn, L. P., and P. J. Mougini-Mark (1992) Cooling Rate of an Active Hawaiian Lava Flow from Nighttime Spectroradiometer Measurements. Geophys. Res. Lett., 19: 1783-1786.
- Flynn, L. P., P. J. Mougini-Mark, J. C. Gradie, and P. G. Lucey (1993) Radiative Temperature Measurements at Kupaianaha Lava Lake, Kilauea Volcano, Hawaii, J. Geoph. Res., 98: 6461-6476.
- Gaddis, L. R. (1993) Lava-Flow Characterization at Pisgah Volcanic Field, California, with Multiparameter Imaging Radar. Geol. Soc. Am. Bull., 104: 695-703.

- Gallagher, K., and C. Hawksworth (1992) Dehydration Melting and the Generation of Continental Flood Basalts. Nature. 358: 57-59.
- Garratt, J.R. (1990) The Internal Boundary Layer: A Review. Boundary-Layer Meteorology, 50: 171-203.
- Gerlach, T. M. (1986) Exsolution of H<sub>2</sub>O, CO<sub>2</sub>, and S During Eruptive Episodes at Kilauea Volcano, Hawaii. J. Geoph. Res., 91: 12 177-12 185.
- Gillespie, A. R., A. B. Kahle, and F. D. Palliconi (1984) Mapping Alluvial Fans in Death Valley, California, Using Multichannel Thermal Infrared Images. Geoph. Res. Let., 11: 1153-1156.
- Greeley, R. (1972) Additional Observations of Actively Forming Lava Tubes and Associated Structures, Hawaii. Mod. Geol., 3: 157-160.
- Greeley, R. (1973) Geological Guide to the Island of Hawaii. NASA CR-152416. US Government Printing Office, Washington, 257 pp.
- Greeley, R. (1987) The Role of Lava Tubes in Hawaiian Volcanoes. In: R. W. Decker, T. L. Wright, and P. H. Stauffer (Editors), USGS Professional Paper 1350. US Government Printing Office, Washington, pp. 1584-1602.
- Greeley, R., and P. D. Spudis (1981) Volcanism on Mars. Rev. Geoph. Space Phys., 19: 13-41.

- Greenland, L. P. (1987) Hawaiian Eruptive Gases. In: R. W. Decker, T. L. Wright, and P. H. Stauffer (Editors), USGS Professional Paper 1350. US Government Printing Office, Washington, pp. 759-770.
- Gregg, T. K. P., and R. Greeley (1993) Formation of Venusian Canali: Considerations of Lava Types and Their Thermal Behaviors. J. Geoph. Res., 98: 10 873-10 882.
- Griffiths, R. W., and J. H. Fink (1992a) Solidification and Morphology of Submarine Lavas: A Dependence on Extrusion Rate. J. Geoph. Res., 97: 19 729-19 737.
- Griffiths, R. W. and J. H. Fink (1992b) The Morphology of Lava Flows in Planetary Environments: Predictions From Analog Experiments. J. Geoph. Res., 97: 19 739-19 748.
- Guest, J. E., C. R. J. Kilburn, H. Pinkerton and A. M. Duncan (1987) The Evolution of Lava Flow Fields: Observations of the 1981 and 1983 Eruptions of Mount Etna, Sicily. Bull. Volc., 49: 527-540.
- Hardee, H. C. (1980) Solidification in Kilauea Iki Lava Lake. J. Volc. Geoth. Res., 7: 211-223.
- Hardee, H. C. (1982) Permeable Convection above Magma Bodies. Tectonophysics, 84: 179-195.
- Harvey, R. P. (1992) The Parent Magma of the Nakhlite Meteorites: Clues from Melt Inclusions. Earth Planet. Sci. Lett., 111: 467-482.

- Head, J. W., D. B. Cambell, C. Elachi, J. E. Guest, D. P. McKenzie, R. S. Saunders, G. Schaber, and G. Schubert (1991) Venus Volcanism: Initial Analysis from Magellan Data. Science, 252: 276-288.
- Head, J.W., and L. Wilson (1986) Volcanic Processes and Landforms on Venus: Theory, Predictions, and Observations. J. Geophys. Res., 91: 9407-9446.
- Heliker, C., M. Mangan, T. Moulds, P. Okubo, A. Okamura, and J. Kauahikaua (1991) Kilauea Eruption Nears its Ninth Anniversary. AGU Fall Meeting Abstracts, EOS, 72: 556.
- Heliker, C., and T. Wright (1991) Lava-Flow Hazards from Kilauea's Current Eruption. Geotimes, 36: 16-19.
- Helz, R. T., C. Heliker, M. Mangan, K. Hon, C. A. Neal, and L. Simmons (1991) Thermal History of the Current Kilauean East Rift Eruption. AGU Fall Meeting Abstracts, EOS, 72: 557.
- Helz, R. T., and C. R. Thornber (1987) Geothermometry of Kilauea Iki Lava Lake, Hawaii. Bull Volc., 49: 651-668.
- Heslop, S. E., L. Wilson, H. Pinkerton, and J. W. Head (1989) Dynamics of a Confined Lava Flow on Kilauea Volcano, Hawaii. Bull. Volc., 51: 415-432.
- Hess, P. C. (1989) Origins of Igneous Rocks. Harvard University Press, Cambridge, 336 pp.

- Hilsenrath, J. (1957) Thermodynamic Properties of Gases, in American Institute of Physics Handbook. D. E. Gray (editor), McGraw-Hill Book Co., New York, pp. 4/80-4/117.
- Holcomb, R. T. (1987) Eruptive History and Long-Term Behavior of Kilauea Volcano, in Decker, R.W., T. L. Wright, and P. H. Stauffer (editors) Volcanism in Hawaii. USGS Professional Paper 1350, pp. 261-350.
- Hon, K., and J. Kauahikaua (1991) The Importance of Inflation in the Formation of Pahoehoe Sheet Flows. AGU Fall Meeting Abstracts, EOS, 72: 557.
- Hon, K., J. Kauahikaua, R. Denlinger, and K. McKay (1994a) Emplacement and Inflation of Pahoehoe Sheet Flows: Observations and Measurements of Active Lava Flows on Kilauea Volcano, Hawaii. Geol. Soc. Am. Bull., 106: 351-370.
- Hon, K., J. Kauahikaua, and K. McKay (1994b) Inflation and Cooling Data from Pahoehoe Sheet Flows on Kilauea Volcano. USGS Open-File Report 93-342B.
- Hopper, R. W., P. Onorato, and D. R. Uhlmann (1974) Thermal Histories and Crystal Distribution in Partly Devitrified Lunar Glasses Cooled by Radiation. Proc. Lunar Planet. Sci. Conf. V: 2257-2273.
- Horai, K. (1991) Thermal Conductivity of Hawaiian Basalt: A New Interpretation of Robertson and Peck's Data. J. Geoph. Res., 96: 4125-4132.
- Hulme, G. (1973) Turbulent Lava Flow and the Formation of Lunar Sinuous Rilles. Mod. Geology 4: 107-117.

- Hulme, G. (1974) The Interpretation of Lava Flow Morphology. Geoph. J. Roy. Astr. Soc. 39: 361-383.
- Incropera, F. P., and D. P. DeWitt (1990) Fundamentals of Heat and Mass Transfer, Wiley, New York, 919 pp.
- Iverson, R. M (1990) Lava Domes Modeled as Brittle Shells that Enclosed Pressurized Magma, with Application to Mount St. Helens. in Fink, J. H. (editor) Lava Flows and Domes: Emplacement Mechanisms and Hazard Implications. Springer-Verlag, Berlin, pp. 47-69.
- Jackson, D. B., J. Kauahikaua, K. Hon and C. Heliker (1988) Rate and Variation of Magma Supply to the Active Lava Lake on the Middle East Rift Zone of Kilauea Volcano, Hawai'i. Abstracts Geol. Soc. Am. Annual Meeting, p. A397.
- Jaeger, J. C., and A. F. A. Harper (1950) Nature of the Surface of the Moon. Nature, 166: 1026.
- Jones, A. C. (1992) Remote Sensing and Thermal Modelling of Active Lava Flows, Kilauea Volcano, Hawaii. Thesis, Lancaster University.
- Jones, A. C. (1993) The Cooling Rates of Pahoehoe Flows: the Importance of Lava Porosity. Lunar Planet. Sci. Conf. Abst., XXIV: 731-732.
- Kahle, A. B., A. R. Gillespie, E. A. Abbott, M. J. Abrams, R. E. Walker, G. Hoover, and J. P. Lockwood (1988) Relative Dating of Hawaiian Lava Flows Using

Multispectral Thermal Infrared Images: A New Tool for Geologic Mapping of Young Volcanic Terranes. J. Geoph. Res., 93: 15,239-15,251.

Kahle, A. B., and L. C. Rowan (1980) Evaluation of Multispectral Middle Infrared Images for Lithologic Mapping in the East Tintic Mountains, Utah. Geology. 8: 234-239.

Kauahikaua, J., R. Denlinger, J. Foster, and L. Keszthelyi (1993) Lava Delta Instability: Is it mass-wasting or is it triggered by lava flowing through tubes? AGU Fall Meeting Abstracts, EOS 74: 616.

Kauahikaua, J., T. Moulds, and K. Hon (1990) Observations of Lava Tube Formation in Kalapana, Hawai'i. AGU Abstracts, EOS 71: 1711.

Kent, R. W., M. Storey, and A. D. Saunders (1992) Large Igneous Provinces: Sites of Plume Impact or Plume Incubation. Geology. 20: 891-894.

Kestin, J. (1957) Viscosity of Gases. in American Institute of Physics Handbook. D. E. Gray (editor), pp. 2/201-2/210, McGraw-Hill Book Co., New York.

Keszthelyi, L. P. (1992) Lava Tubes are Air-Cooled. AGU Fall Meeting Abstracts, EOS 73: 648

Keszthelyi, L. (in press) Calculated Effect of Vesicles on the Thermal Properties of Cooling Basaltic Lava Flows. J. Volc. Geoth. Res.

Keszthelyi, L. P., and D. C. Pieri (1993) Emplacement of the 75-km-Long Carrizozo Lava Flow Field, South Central New Mexico. J. Volc. Geoth. Res., 59: 59-75.

Keszthelyi, L., V. Realmuto, and D. Pieri (1993) Monitoring Lava Flows with Portable IR Imaging Devices. AGU Fall Meeting Abstracts, EOS 74: 640.

Kilburn, C. R. J., and R. M. C. Lopes (1991) General Patterns of Flow Field Growth: Aa and Blocky Lavas. J. Geoph. Res., 96: 19 721-19 732.

Kirkpatrick, R. J. (1981) Kinetics of Crystallization in Igneous Rocks. in Lasaga, A. C., and R. J. Kirkpatrick (editors) Kinetics of Geochemical Processes. Rev. Mineral. 8: 321-384.

Knoche, R., D. B. Dingwell, and S. L. Webb (1992) Non-linear Temperature Dependence of Liquid volumes in the System Albite-Anorthite-Diopside. Contrib. Mineral. Petrol., 111: 61-73.

Kouchi, A., A. Tsuchiyama, and I. Sunagawa (1986) Effect of Stirring on Crystallization Kinetics of Basalt: Texture and Element Partitioning. Contr. Min. Pet. 93: 429-438.

Lang, H. R., S. L. Adams, J. E. Conel, B. A. McGuffie, E. D. Paylor, and R. E. Walker, (1987) Multispectral Remote Sensing as Stratigraphic and Structural Tool, Wind River Basin and Big Horn Basin Areas, Wyoming. Am. Assoc. Petr. Geol., Bull. 71: 389-402.

Lange, R. A., and I. S. E. Carmichael (1987) Densities of Na<sub>2</sub>O-K<sub>2</sub>O-CaO-MgO-FeO-Fe<sub>2</sub>O<sub>3</sub>-Al<sub>2</sub>O<sub>3</sub>-TiO<sub>2</sub>-SiO<sub>2</sub> Liquidus: New Measurements and Derived Partial Molar Properties. Geoch. Cosmoch. Acta, 51: 2931-2946.

- Lange, R. A., and A. Navrotsky (1993) Heat Capacities of TiO<sub>2</sub>-bearing Silicate Liquids: Evidence for Anomalous Changes in Configurational Entropy with Temperature. Geoch. Cosmoch. Acta, 57: 3001-3011.
- Lipman, P. W., D. A. Clague, J. G. Moore, and R. T. Holcomb, (1989) South Arch volcanic field: Newly identified young lava flows on the sea floor south of the Hawaiian Ridge. Geology, 17: 611-614.
- Lister, J. R., and R. C. Kerr, (1991) Fluid-Mechanical Models of Crack Propagation and Their Application to Magma Transport in Dykes. J. Geoph. Res., 96: 10 049-10 077.
- Lockwood, J.P., and P. W. Lipman (1987) Holocene Eruptive History of Mauna Loa Volcano, in Decker, R. W., T. L. Wright, and P. H. Stauffer (editors) *Volcanism in Hawaii*. USGS Professional Paper 1350, pp 509-536.
- Lofgren, G. E. (1983) Effect of Heterogeneous Nucleation on Basaltic Textures: A Dynamic Crystallization Study. J. Petrology, 24: 229-255.
- Macdonald, G. A. (1972) Volcanoes. Englewood Cliffs, Prentice-Hall, 510 pp.
- Malin, M. C. (1980) Lengths of Hawaiian Lava Flows. Geology, 8: 306-308.
- Mangan, M. T., and K. V. Cashman (1991) Vesiculation Kinetics in Magmas at Shallow Levels. EOS, 72: 557.

- Mangan, M. T., K. V. Cashman, and S. Newman (1993) Vesiculation of Basaltic Magma During Eruption. Geology, 21: 157-160.
- Mattox, T., C. Heliker, J. Kauahikaua and K. Hon (1993) Development of the 1990 Kalapana Flow Field, Kilauea Volcano, Hawaii. Bull. Volc. 55: 407-413.
- McBirney, A. R., and T. Murase (1984) Rheological Properties of Magmas. Annual Reviews in Earth and Planetary Science. 12: 337-357.
- McGill, G. E., J. L. Warner, M. C. Malin, R. E. Arvidson, E. Eliason, S. Nozette, and R. D. Reasenberg (1983) Topography, Surface Properties, and Tectonic Evolution. in Hunten, D. M., L. Colin, T. M. Donahue, and V. I. Moroz (editors) Venus. Univ. Arizona Press, Tucson, pp. 69-130.
- Moore, H., D. Arthur, and G. Shaber (1978) Yield Strengths of Flows on the Earth, Mars, and Moon. Proc. Lunar Planet. Sci. Conf. IX: 3351-3378.
- Moulds, T. N., C. Heliker, K. Hon, J. Kauahikaua, T. Wright, and W. J. Bussard, (1990) Kilauea Eruption Update. AGU Fall Meeting Abstracts EOS, 71: 1694.
- Murase, T., and A. R. McBirney (1973) Properties of Some Common Igneous Rocks and their Melts at High Temperatures. Geol. Soc. Am. Bull. 84: 3563-3592.
- NASA-Ames Res. Center, (1989) C-130 Flight Summary Report: Flight # 89-012-02. Aircraft Data Facility, Moffett Field. 7 pp.

- Ondrusek, J., P. R. Christensen, and J. H. Fink (1993) Mapping the Distribution of Vesicular Textures on Silicic Lavas Using the Thermal Infrared Multispectral Scanner. J. Geoph. Res., 98: 15,903-15,908.
- Oppenheimer, C. (1991) Lava Flow Cooling Estimated from Landsat Thematic Mapper Infrared Data: the Lonquimay Eruption, Chile, 1989. J. Geophys. Res., 96: 1865-1878.
- Palluconi, F. D., and H. H. Kieffer (1981) Thermal Inertia Mapping of Mars from 60°S to 60°N. Icarus, 45: 415-426.
- Park, S., and J. D. Iverson (1984) Dynamics of Lava Flow: Thickness Growth Characteristics of Steady Two-Dimensional Flow. Geophys. Res. Lett., 11: 641-644.
- Peck, D. L. (1978) Cooling and Vesiculation of Alae Lava Lake, Hawaii. USGS Prof. Paper 935-B, US Government Printing Office, Washington, 50 pp.
- Peck, D. L., M. S. Hamilton, and H. R. Shaw (1977) Numerical Analysis of Lava Lake Cooling Models: Part II, Application to Alae Lava Lake, Hawaii. Am. J. Sci. 277: 415-437.
- Peterson, D. W., and D. A. Swanson (1974) Observed Formation of Lava Tubes During 1970-1971 at Kilauea Volcano, Hawaii. Speleology, 2: 209-222.

- Peterson, D. W., and R. I. Tilling (1980) Transition of Basaltic Lava from Pahoehoe to Aa, Kilauea Volcano, Hawaii: Field Observations and Key Factors. J. Volc. and Geoth. Res., 7: 271-293.
- Pieri, D. C. and S. M. Baloga (1986) Eruption Rate, Area, and Length Relationships for some Hawaiian Lava Flows. J. Volc. Geoth. Res., 30: 29-45.
- Pieri, D. C., L. S. Glaze and M. J. Abrams (1990) Thermal Radiance Observations of an Active Lava Flow During the June 1984 Eruption of Mt. Etna. Geology., 18: 1018-1022.
- Pinkerton, H., and R. S. J. Sparks (1976) The 1975 Sub-terminal Lavas, Mount Etna: a Case History of the Formation of a Compound Lava Field. J. Volc. Geoth. Res., 1: 167-182.
- Pinkerton, H., and R. S. J. Sparks (1978) Field Measurements of the Rheology of Lava. Nature. 276: 383-384.
- Pinkerton, H., and R. Stevenson (1992) Methods of Determining the Rheological Properties of Lavas from their Physico-Chemical Properties. J. Volc. Geoth. Res. 53: 47-66.
- Pinkerton, H., and L. Wilson (1988) The Lengths of Lava Flows. Lunar Planet. Sci. Conf. Abstr., XIX: 937-938.
- Pinkerton, H., and L. Wilson (1992) The Dynamics of Channel-fed Lava Flows. Lunar Planet. Sci. Conf. Abstr., XXIII: 1083-1084.

- Pinkerton, H., and L. Wilson (*in press*) Factors Controlling the Lengths of Channel-fed Lava Flows. Bull. Volc.
- Realmuto, V. J., K. Hon, A. B. Kahle, E. A. Abbott, and D.C. Pieri (1992) Multispectral Thermal Infrared Mapping of the 1 October 1988 Kupaianaha flow field, Kilauea Volcano, Hawaii. Bull. Volc., 55: 33-44.
- Reidel, S. P., and T. L. Tolan (1992) Eruption and Emplacement of Flood Basalt: An Example from the Large-Volume Teepee Butte Member, Columbia River Basalt Group, Geol. Soc. Am. Bull., 104: 1650-1671.
- Renault, J. (1970) Major-Element Variations in the Potrillo, Carrizozo, and McCarty's Basalt Fields, New Mexico. New Mexico State Bureau of Mines and Mineral Resources Circular 113, Socorro, New Mexico.
- Renne, P. R., and A. R. Basu (1991) Rapid Eruption of the Siberian Traps Flood Basalts at the Permo-Triassic Boundary. Science, 253: 176-179.
- Renne, P. R., M. Ernesto, I. G. Pacca, R. S. Coe, J. M. Glen, M. Prevot, and M. Perrin (1992) The Age of Paraná Flood Volcanism, Rifting of Gondwanaland, and the Jurassic Cretaceous Boundary. Science. 258: 975-978.
- Richet, P., and Y. Bottinga (1986) Thermochemical Properties of Silicate Glasses and Liquids: A Review. Reviews of Geophysics, 24: 1-25.

- Robertson, E. C. (1988) Thermal Properties of Rocks. USGS Open File Report 88-441, 106 pp.
- Robertson, E. C., and D. L. Peck (1974) Thermal Conductivity of Vesicular Basalt from Hawaii. J. Geoph. Res. 79: 4875-4888.
- Roscoe, R. (1952) The Viscosity of Suspensions of Rigid Spheres. British J. of Applied Physics, 3: 267-269.
- Rowland, S. K., and G. P. L. Walker (1990) Pahoehoe and Aa in Hawaii: Volumetric Flow-Rate Controls the Lava Structure. Bull. Volc., 52: 615-628.
- Ryerson, F. J., H. C. Weed, and A. J. Piwinski (1988) Rheology of Subliquidus Magmas: 1. Picritic Compositions. J. Geoph. Res. 93: 3421-3436.
- Schaber, G. G., K. C. Horstman, and A. L. Dial, Jr. (1978) Lava Flow Materials in the Tharsis Region of Mars. Proc. Lunar Planet. Sci. Conf., IX: 3433-3458.
- Self, S., S. Finnemore, Th. Thordarson, and G. P. L. Walker (1991) Importance of Compound Lava and Lava-Rise Mechanisms in Emplacement of Flood Basalts. AGU Fall Meeting Abstracts, EOS, 72: 566.
- Shaw, H. R. (1969) Rheology of Basalt in the Melting Range. J. Petrology. 10: 510-535.
- Shaw, H. R. (1972) Viscosities of Magmatic Silicate Liquids: an Empirical Method of Prediction. Am. J. Sci., 272: 870-893.

- Shaw, H. R., T. L. Wright, D. L. Peck, and R. Okamura (1968) The Viscosity of Basaltic Magma: An Analysis of Field Measurements in Makaopuhi Lava Lake, Hawaii. Am. J. Sci., 266: 225-264.
- Shimozuru, D. (1978) Dynamics of Magma in a Volcanic Conduit - Special Emphasis on Viscosity of Magma with Bubbles. Bull. Volc., 41: 333-340.
- Smith, C. T. (1964) Geology of the Little Black Peak Quadrangle, Socorro and Lincoln Counties, New Mexico. New Mexico Geological Society, 15th Field Conference, pp. 92-99.
- Spence, D. A., and D. L. Turcotte (1990) Buoyancy-Driven Magma Fracture: A Mechanism for Ascent Through the Lithosphere and the Emplacement of Diamonds. J. Geoph. Res., 95: 513-5139.
- Stebbins, J. F., I. S. E. Carmichael, and L. K. Moret (1984) Heat Capacities and Entropies of Silicate Liquids and Glasses. Contrib. Min. Petr., 86: 131-148.
- Stephenson, P. J., and T. J. Griffin (1967) Some Long Basaltic Lava Flows in North Queensland. In: Volcanism in Australasia, Johnson, R. W. (editor), Elsevier. Amsterdam. pp. 41-51.
- Stothers, R. B (1989) Turbulent Atmospheric Plumes Above Line Sources with an Applicaiton to Volcanic Fissure Eruptions on the Terrestrial Planets. J. Atmos. Sci., 17: 2662-2670.

- Strom, R. G., N. J. Trask, and J. E. Guest (1975) Tectonism and Volcanism on Mercury. J. Geoph. Res., vol. 80, p. 2478-2507.
- Stunder, M., and S. Sethuraman (1985) A Comparative Evaluation of the Coastal Internal Boundary-Layer Height Equations. Boundary-Layer Meteorology, 32: 177-204.
- Swanson, D. A., T. L. Wright, and R. T. Helz (1975) Linear Vent Systems and Estimated Rates of Magma Production and Eruption for the Yakima Basalt on the Columbia Plateau. Am. J. Sci., 275: 877-905.
- Taylor, P. A. (1971) Airflow Above Changes in Surface Heat Flux, Temperature, and Roughness: an Extension to Include the Stable Case. Boundary-Layer Meteorology, 1: 474-497.
- Theilig, E. (1986) Formation of Pressure Ridges and Emplacement of Compound Basaltic Lava Flows. Thesis. Arizona State University, Tempe. 214 pp.
- Theilig, E., and R. Greeley (1986) Lava Flows on Mars: Analysis of Small Surface Features and Comparisons with Terrestrial Analogs. Proc. Lunar Planet. Sci. Conf., XVII: 193-206.
- Thordarson, Th., and S. Self (1993) The Laki (Skaftár Fires) and Grímsvötn Eruptions in 1783-1785. Bull. Volc., 55: 233-263.
- Thordarson, Th., S. Self, and G. P. L. Walker (1992) The potential influence of tropospheric aerosols from volcanic eruptions on the atmosphere and climate.

Abstracts of the American Geoph. Union Chapman Conference on Climate,  
Volcanism, and Global Change, p.18

Touloukian, Y. S., W. R. Judd, and R. F. Roy (editors) (1989) Physical Properties of  
Rocks and Minerals. Hemisphere Publishing Co., New York, 548 pp.

Turcotte, D. L., and G. Schubert (1982) Geodynamics. John Wiley and Sons, New York,  
450 pp.

Uhlmann, D. R. (1972) A Kinetic Treatment of Glass Formation. J. Non-Cryst. Sol., 7:  
337-348.

Uhlmann, D. R., L. Klein, G. Kritchevsky, and R. W. Hopper (1974) The Formation of  
Lunar Glasses. Proc. Lunar Planet. Sci. Conf. V: 2317-2331.

Uhlmann, D. R., P. I. K. Onorato, and G. W. Scherer (1979) A Simplified Model for  
Glass Formation. Proc. Lunar Planet. Sci. Conf. X: 375-381.

Walker, G. P. L. (1973) Lengths of Lava Flows. Roy. Soc. Phil. Trans., A274: 107-118.

Walker, G. P. L. (1989) Spongy pahoehoe in Hawaii: a Study of Vesicle-Distribution  
Patterns in Basalt and their Significance. Bull. Volc., 51: 199-209.

Walker, G. P. L. (1991) Structure and Origin by Injection of Lava Under Surface Crust of  
Tumuli, 'Lava Rises', 'Lava-Rise Pits', 'Lava-Inflation Clefts' in Hawaii. Bull.  
Volc., 53: 546-558.

- Webb, S. L., and D. B. Dingwell (1990) Non-Newtonian Rheology of Igneous Melts at High Stresses and Strain Rates: Experimental Results for Rhyolite, Andesite, Basalt, and Nephelinite. J. Geoph. Res., 95: 15 696-15 701.
- Weber, R. H. (1964) Geology of the Carrizozo Quadrangle, New Mexico. New Mexico Geological Society 15th Field Conference. pp. 100-109.
- Wechsler, A. E., P. E. Glaser, and J. A. Fountain (1972) Thermal Properties of Granulated Materials, in J. W. Lucas (editor) Thermal Characteristics of the Moon. MIT Press, Cambridge, pp. 215-241.
- Weisel, D., and C. Heliker (1990) Kilauea: The Newest Land on Earth, Bishop Museum Press, Honolulu, 76 pp.
- Wilhelms, D. E., (1987) The Geologic History of the Moon. USGS Professional Paper 1348, United States Government Printing Office, Washington, 326 pp.
- Wilmoth, R. A., and G. P. L. Walker (1993) P-type and S-type Pahoehoe: a Study of Vesicle Distribution Patterns in Hawaiian Lava Flows. J. Volc. Geoth. Res., 54: 129-142.
- Wilson, L., and J. W. Head III (1981) Ascent and Eruption of Basaltic Magma on the Earth and Moon. J. Geoph. Res., 86: 2971-3001.
- Wilson, L., and J. W. Head III (1983) A Comparison of Volcanic Eruption Processes on Earth, Moon, Mars, Io and Venus. Nature, 302: 663-669.

- Wilson, L., R. S. J. Sparks, and T. C. Huang (1978) The Control of Volcanic Column Heights by Eruption Energetics and Dynamics. J. Geoph. Res., 83: 1829-1836.
- Wright, T. L., and R. T. Okamura (1977) Cooling and Crystallization of Tholeiitic Basalt, 1965 Makaopuhi Lava Lake, Hawaii. USGS Prof. Paper 1004, US Government Printing Office, Washington, 59 pp.
- Wright, T. L., M. T. Mangan, and D. A. Swanson (1989) Chemical Data for Flows and Feeder Dikes on the Yakima Basalt Subgroup, Columbia River Group, Washington, Oregon, and Idaho, and their Bearing on a Petrogenetic Model. USGS Bulletin 1821, 71pp.
- Young, P., and G. Wadge (1990) FLOWFRONT: Simulation of a Lava Flow. Computers and Geosciences, 16: 1171-1191
- Zablocki, C. H., R. I. Tilling, D. W. Peterson, and R. L. Christiansen (1974) A Deep Research Drill Hole at the Summit of an Active Volcano, Kilauea, Hawaii. Geoph. Res. Lett., 1: 323-326.
- Zimbelman, J. R. (1985) Estimates of Rheological Properties for Flows on the Martian Volcano Ascaeus Mons. Proc. Lunar Planet. Sci. Conf., XVI: D157-D162.
- Zimbelman, J. R. (1986) The Role of Porosity in Thermal Inertia Variations on Basaltic Lavas, Icarus, 68: 366-369.